

NBSIR 75-828

JAN 20 1976  
RECEIVED

# SEMI-ANNUAL REPORT ON MATERIALS RESEARCH IN SUPPORT OF SUPERCONDUCTING MACHINERY

---

R. P. Reed, J. G. Hust, M. B. Kasen, H. M. Ledbetter, D.T. Read,  
E.R. Naimon, R. E. Schramm, L. L. Sparks, R. L. Tobler,  
and W. F. Weston

RECEIVED  
DATE \_\_\_\_\_  
OTW

Cryogenics Division  
Institute for Basic Standards  
National Bureau of Standards  
Boulder, Colorado 80302

January 1976

Prepared for  
Advanced Research Projects Agency  
1400 Wilson Boulevard  
Arlington, Virginia 22209



NBSIR 75-828

# SEMI-ANNUAL REPORT ON MATERIALS RESEARCH IN SUPPORT OF SUPERCONDUCTING MACHINERY

---

R. P. Reed, J. G. Hust, M. B. Kasen, H. M. Ledbetter, D.T. Read,  
E.R. Naimon, R. E. Schramm, L. L. Sparks, R. L. Tobler,  
and W. F. Weston

Cryogenics Division  
Institute for Basic Standards  
National Bureau of Standards  
Boulder, Colorado 80302

January 1976

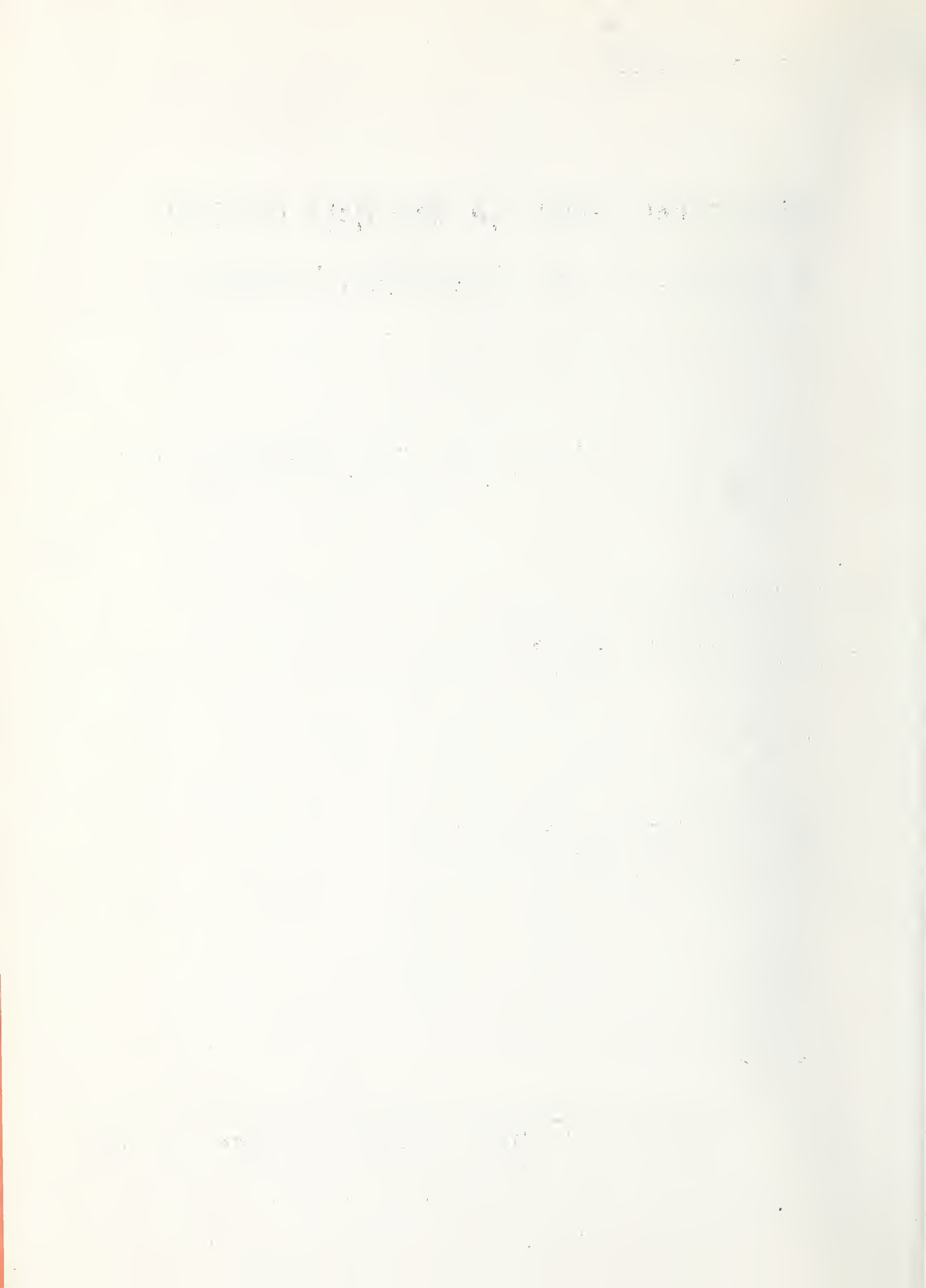
Prepared for  
Advanced Research Projects Agency  
1400 Wilson Boulevard  
Arlington, Virginia 22209



---

U.S. DEPARTMENT OF COMMERCE, Rogers C. B. Morton, Secretary  
James A. Baker, III, Under Secretary  
Dr. Betsy Ancker-Johnson, Assistant Secretary for Science and Technology

NATIONAL BUREAU OF STANDARDS, Ernest Ambler, Acting Director



SEMI-ANNUAL REPORT ON MATERIALS RESEARCH

IN SUPPORT OF SUPERCONDUCTING MACHINERY

Sponsored by  
Advanced Research Projects Agency  
ARPA Order No. 2569  
Program Code 4D10  
August 10, 1974 - August 9, 1975

Program Director  
Dr. E. C. van Reuth  
Materials Sciences  
Advanced Research Projects Agency  
1400 Wilson Boulevard  
Arlington, Virginia 22209

Program Manager  
Dr. R. P. Reed  
Cryogenics Division  
Institute for Basic Standards  
National Bureau of Standards  
Boulder, Colorado 80302

The views and conclusions contained in this document are those of the authors and should not be interpreted as necessarily representing the official policies, either expressed or implied, of the Advanced Research Projects Agency or of the U.S. Government.

## Abstract

Results are reported of a six-month study, March through August 1975, on candidate materials for superconducting machinery. The results cover five areas--advanced composites, elastic properties, fatigue resistance and fracture toughness, magnetothermal conductivity, and thermal conductivity. Material properties were studied over the temperature range 4 to 300 K. Materials studied include: oxygen-free copper; copper-nickel alloys; a precipitation-hardening copper alloy; invar; nickel-chromium-iron alloys; stainless steels; and the composite materials boron/aluminum, boron/epoxy, S-glass/epoxy, graphite/epoxy, and an organic-fiber/epoxy. Some notable results of the study are: the first 4 K fatigue data on a composite material; a ten-fold increase in the fatigue life of a uniaxial glass/epoxy composite between room temperature and liquid-helium temperature; the first 4 K fatigue fracture toughness studies on a nitrogen-strengthened chromium-nickel-manganese steel, which show this material has higher yield strength and adequate toughness compared to conventional stainless steels; room-temperature elastic properties of a copper-cadmium-chromium precipitation-hardening alloy, which are quite different from those of unalloyed copper and show a non-parallel behavior of the shear modulus and the bulk modulus; the thermal conductivity of 304 stainless steel may be reduced one third at 4 K by a 6 MA/m (80 kOe) magnetic field; the first systematic study of the tensile properties of fiber-reinforced composite materials between room temperature and liquid-helium temperature.

This work was supported by the Advanced Research Projects Agency of the U.S. Department of Defense.

Keywords: Composites; copper alloys; elastic properties; engineering materials; fatigue; fracture; iron alloys; cryogenic temperatures; mechanical properties; nickel alloys; superconducting machinery; thermal conductivity.

## Report Contents

	Page
<b>ADVANCED COMPOSITES</b>	
R. E. Schramm and M. B. Kasen . . . . .	1
Reprint: Mechanical and Thermal Properties of Filamentary-Reinforced Structural Composites at Cryogenic Temperatures. 1: Glass-Reinforced Composites; M. B. Kasen; Cryogenics <u>15</u> (1975) 327-49 . . . . .	22
Reprint: Properties of Filamentary-Reinforced Composites at Cryogenic Temperatures; <u>Composite Reliability</u> , ASTM STP 580, Am. Soc. Testing Mater., Philadelphia (1975) . . . . .	45
Preprint: Static Tensile Properties of Boron-Aluminum and Boron-Epoxy Composites at Cryogenic Temperatures; R. E. Schramm and M. B. Kasen; Proc. ICMC-CEC, Kingston, Ontario, (July 1975), forthcoming . . . . .	58
<b>ELASTIC PROPERTIES OF ENGINEERING MATERIALS AT CRYOGENIC TEMPERATURES</b>	
H. M. Ledbetter, E. R. Naimon, and W. F. Weston . . . . .	71
Low-Temperature Elastic Properties of some Copper-Nickel Alloys H. M. Ledbetter and W. F. Weston . . . . .	73
Elastic Properties of a Copper-Cadmium-Chromium Precipitation-Hardened Alloy H. M. Ledbetter . . . . .	77
Low-Temperature Elastic Properties of Invar H. M. Ledbetter, E. R. Naimon, and W. F. Weston . . . . .	81
Reprint: Dynamic Low-Temperature Elastic Properties of Two Austenitic Nickel-Chromium-Iron Alloys; W. F. Weston, H. M. Ledbetter, and E. R. Naimon; Mater. Sci. Eng. <u>20</u> (1975) 185-94 . . . . .	95
Reprint: Low-Temperature Elastic Properties of Four Austenitic Stainless Steels; H. M. Ledbetter, W. F. Weston, and E. R. Naimon; J. Appl. Phys. <u>46</u> (1975) 3855-60 . . . . .	105
<b>FATIGUE RESISTANCE AND FRACTURE TOUGHNESS OF ENGINEERING MATERIALS AT CRYOGENIC TEMPERATURES</b>	
R. L. Tobler, D. T. Read, and R. P. Reed . . . . .	111
Fatigue Resistance of a Uniaxial S-Glass/Epoxy Composite at Room and Liquid Helium Temperatures R. L. Tobler and D. T. Read . . . . .	113
Tensile and Fracture Behavior of a Nitrogen-Strengthened, Chromium-Nickel-Manganese Stainless Steel at Cryogenic Temperatures R. P. Reed and R. L. Tobler . . . . .	131
<b>MAGNETOTHERMAL CONDUCTIVITY</b>	
L. L. Sparks . . . . .	150
Preprint: Magnetothermal Conductivity of Selected Pure Metals and Alloys; L. L. Sparks; Proc. ICMC-CEC, Kingston, Ontario (July 1975), forthcoming . . . . .	160
<b>THERMAL CONDUCTIVITY</b>	
J. H. Hust . . . . .	171

### Disclaimer

Tradenames of equipment and materials are used in this report for clarity and to conform with standard usage in the scientific and engineering literature. Selection of materials for discussion and examination with regard to application in superconducting machinery is based on properties reported in the literature, and must be regarded as preliminary and tentative. In no case does such selection imply recommendation or endorsement by the National Bureau of Standards, nor does it imply that the material or equipment is necessarily the best available for the purpose.

NBSIR

SEMI-ANNUAL REPORT ON MATERIALS RESEARCH IN  
SUPPORT OF SUPERCONDUCTING MACHINERY

ADVANCED COMPOSITES

R. E. Schramm and M. B. Kasen

Cryogenics Division  
Institute for Basic Standards  
National Bureau of Standards  
Boulder, Colorado 80302

October 1975

Summary: Advanced Composites

Phase II of the experimental program is now in progress. This report contains 295 K, 76 K, and 4 K tensile measurements of elastic, plastic, and ultimate tensile properties necessary to characterize five fiber-reinforced composites selected for their potential use at 4 K: 5.6 mil boron-6061 aluminum; 5.6 mil boron-5505 epoxy; S-901 glass NASA resin 2; type A graphite-NASA resin 2; and Kevlar 49\*-NASA resin 2. Compression tests are in progress.

\*The use of trade names in this paper in no way implies endorsement or approval by NBS and is included only to define the material.

Contents: Advanced Composites

	Page
1.0 Review . . . . .	4
2.0 Phase II: Characterization of the Mechanical Properties of Uniaxial Composites at Cryogenic Temperatures . . . . .	4
2.1 Introduction . . . . .	4
2.2 Materials . . . . .	4
2.3 Procedures . . . . .	5
2.4 Results and Discussion . . . . .	6
2.5 Future Work . . . . .	7
3.0 References . . . . .	7
4.0 List of Figures . . . . .	8
5.0 List of Tables . . . . .	10
Appendix I: Symbols . . . . .	21
Appendix II: M. B. Kasen, "Mechanical and thermal properties of filamentary-reinforced structural composites at cryogenic temperatures. 1: Glass-reinforced composites," Cryogenics <u>15</u> (6), pp. 327-349 (1975) . . . . .	22
Appendix III: M. B. Kasen, "Properties of Filamentary-Reinforced Composites at Cryogenic Temperatures," <u>Composite</u> <u>Reliability</u> , ASTM STP 580, American Society for Testing and Materials, 1975 . . . . .	45
Appendix IV: R. E. Schramm and M. B. Kasen, "Static Tensile Properties of Boron-Aluminum and Boron-Epoxy Composites at Cryogenic Temperatures," Paper T3, Cryogenic Engineering Conference, Kingston, Ontario, July 22-25, 1975 (to be published) . . . . .	58

## 1.0 Review

Previous ARPA reports [1,2] included two extensive literature reviews on the cryogenic properties of glass-filament and advanced-fiber-reinforced structural composites. One has recently appeared in Cryogenics [3] and the other is now in-press for a Special Technical Publication of the American Society for Testing and Materials [4]. A reprint and preprint of these papers are Appendices II and III. This information clearly indicated the almost complete lack of 4 K data directly applicable to the design of superconducting machinery. It was possible, however, to select five candidate composites for structural use and we set out to obtain fundamental static tensile and compressive properties to make it possible to compute design values for complex, low-temperature structures by macromechanical analyses. Commercial suppliers began fabricating the following composites:

5.6 mil Boron-6061 Aluminum  
5.6 mil Boron-5505 Epoxy  
S-901 Glass-NASA Resin 2  
Type A Graphite-NASA Resin 2  
Kevlar 49-NASA Resin 2.

While awaiting material delivery, Phase I preliminary tests were begun to determine working procedures. For these tests, two commercial suppliers provided boron-epoxy and graphite-epoxy materials. With these, we developed a grip system that yielded a high fraction of satisfactory fractures and also determined that cryogenic environments changed most mechanical properties relatively little from the room temperature values for these composites. With this background, the boron-aluminum became the first material available for our Phase II characterization program. Both this preliminary data and the boron-aluminum data appeared in the last ARPA report [5]. Two previously unseen phenomena did appear among the results: a two-part elastic region in the graphite-epoxy longitudinal (0°) specimens and a serrated stress-strain curve (discontinuous yielding) in the boron-aluminum transverse (90°) and crossply (+ 45°) specimens at 295 K and 4 K but not at 76 K.

The boron-aluminum measurements and those subsequently made on boron-epoxy were recently presented in a talk at the International Cryogenic Materials Conference in Kingston, Ontario, Canada (July 22-25, 1975). The paper that will appear in the proceedings of this meeting [6] is Appendix IV.

## 2.0 Phase II: Characterization of the Mechanical Properties of Uniaxial Composites at Cryogenic Temperatures

### 2.1 Introduction

This program constitutes the first attempt to characterize fiber-reinforced composites at cryogenic temperatures and obtain the basic laminar properties needed for macromechanical analysis. The present report deals with static tensile properties; compressive tests are now in progress. Other NBS investigators under ARPA contract are making plans for dynamic mechanical tests (H.M. Ledbetter) as well as thermal measurements (J.G. Hust).

While the boron-aluminum data appeared in the last report, it will be included here again to facilitate comparison and for completeness.

### 2.2 Materials

Each of the five composites came from the suppliers as trimmed, flat sheets that were 15.2 x 55.9 cm (6 x 22 in) for the boron-aluminum, and 27.9 cm (11 in) square for all the polymer-matrix materials. Uniaxial layups were six plies thick for the longitudinal tests and 15 plies for the transverse tests; crossply plates were ten plies thick. Table 1 gives the nominal thicknesses of the various sheets.

The suppliers stated that the void content should be < 2 volume % and that NaOH extraction on two specimens of boron-aluminum indicated an average of 47.2 volume % boron. Our own radiography of all plates revealed no visible voids. The tungsten cores of the boron filaments were visible in the radiographs, thereby permitting a spot check of their axial

alignment in the finished specimens. In all cases, the filament alignment was within  $1/2^\circ$  of nominal. The boron-aluminum was tested in the F temper (as fabricated). Processing procedures and a fuller characterization of all composites are forthcoming from the manufacturers.

### 2.3 Procedures

As noted in our last report [5], all test specimens were straight-sided coupons with no tabs. The boron-aluminum specimen length was 15.2 cm (6 in) while all other specimens were 27.9 cm (11 in) long. Specimen widths were 1.3 cm (0.5 in) for longitudinal tests and 2.5 cm (1 in) for transverse and crossply tests. Cutting was done by a diamond circular saw lubricated and cooled by a stream of water soluble oil except for the Kevlar 49 composite for which a dry slitting saw was necessary. Light hand buffing with emery paper further minimized any imperfections on the already very smooth edges. The Kevlar 49 material was again an exception since this process caused fuzzy edges.

Two commercial strain gages cemented directly to the surface monitored elongation and Poisson's ratio in the longitudinal and crossply specimens. There was only one gage on the transverse specimens since the Poisson's ratio ( $\nu_{21}$ ) can be calculated from the transverse elastic modulus ( $E_{22}$ ) and the longitudinal values of elastic modulus ( $E_{11}$ ) and Poisson's ratio ( $\nu_{12}$ ) by:

$$\nu_{21} = \nu_{12} E_{22}/E_{11}.$$

Curing the strain gage cement overnight at 345 K caused softening of the NASA resin 2; thus it was necessary to support these specimens on a flat plate during this process.

Following ASTM D 3039-71T, Method of Test of Tensile Properties of Oriented-Fiber Composites, pre-test conditioning of polymer-based materials was exposure for at least two days to room temperature air at 40-60% relative humidity. The grip system developed earlier [2] was attached in a separate alignment fixture just prior to the test. Gage lengths were 15.2 cm (6 in) for the long specimens and 10.2 cm (4 in) for those of boron-aluminum. Tests were conducted in air at 295 K, in liquid nitrogen at 76 K, or in liquid helium at 4 K at a strain rate of 0.01-0.02  $\text{min}^{-1}$ .

Outputs of the load cell and strain gages were recorded continuously during the test. To check within-specimen repeatability, we cycled the load to about one third of its ultimate value (within the elastic limit) and back to no load about three times before loading to ultimate for most of the polymer-matrix specimens. In some cases, the loading was monotonic to failure: when the ultimate load was very small (e.g., graphite-NASA resin 2 transverse, and all Kevlar 49-NASA resin 2), and for the boron-aluminum which began to yield plastically early in its loading history.

As before, a "good" or acceptable fracture was one which occurred at least one specimen thickness away from the grips. The ultimate values from the unacceptable breaks (inside or too near the grips) were usually quite comparable to those of the good tests but they were not included in computing averages. This criterion of determining fracture location (at least its origin) became very difficult, usually impossible, to apply to the polymer-based longitudinal specimens due to their fracture mode (see 2.4 Results and Discussion).

The primary purpose of testing the crossply laminates here was to determine the in-plane shear modulus ( $G_{12}$ ). With the Petit technique [7], the calculation requires knowledge of the uniaxial elastic properties. With the Sims and Halpin approach [8], a shear stress-shear strain curve is constructed solely from tensile data. Because of this independence from prior test data, we've chosen to calculate  $G_{12}$  with this latter method. The values calculated by the Petit technique and listed in the last report [5] for boron-aluminum agree quite well with those listed here.

## 2.4 Results and Discussion

Numerical results from the individual tests are presented in Tables 2-6; the average values, standard deviations, and coefficients of variation are in Tables 6-10. Table 11 gives the calculated shear moduli.

Discontinuities on the stress-strain diagram of boron-aluminum in the transverse ( $90^\circ$ ) and crossply ( $\pm 45^\circ$ ) orientations were graphed and discussed in our last report [5]. We still have no explanation and have found this behavior is unfamiliar to other workers.

The two-part elastic region noted in graphite-epoxy [5] was again in evidence for the graphite-NASA resin 2. With the load along the fiber direction, the initial elastic response is followed by a second of higher modulus and higher Poisson's ratio; these are noted as primary and secondary values in Tables 5 and 10. The uncertainties in Poisson's ratio make possible the argument that there is no real difference, but the change in modulus is repeatable and usually quite distinct in the load-strain curves recorded. Again, it would appear that this increase in stiffness could be due to straightening of the graphite filaments.

In almost all instances, a minimum of three tests resulting in "good" fractures were conducted at each temperature. In the case of the Kevlar 49-NASA resin 2 composite, the initial results at 295 K and 76 K were very poor and showed that it was not worth running the full series or any 4 K tests. These low strengths and the very low interlaminar shear strength, causing delamination problems in handling, are signs of severe incompatibility between this particular fiber and resin. Component compatibility is obviously important and, before any extensive commitment, should be checked, e.g., with short beam shear tests.

Figure 1 shows typical specimens fractured at 4 K. The longitudinal boron-aluminum specimens appear similar to most normal metals while longitudinal boron-epoxy specimens fracture into discrete pieces throughout the gage length. All of the longitudinal NASA resin 2-matrix materials tend to explode between grips and produce a fuzzy, filamentary mass. All transverse fractures are defined by fiber direction and are typically brittle. There is some necking and plastic yielding in all crossply specimens; in boron-aluminum, the specimens maintain integrity while all others fail by delamination. Figure 1 shows only 4 K fractures (except for the Kevlar 49-NASA resin 2), but tests at other temperatures produced breaks of basically the same type.

Mechanical anisotropy is an outstanding characteristic of composites and all properties must be correlated with fiber direction. The high modulus of boron marks both its composites because of their stiffnesses in the longitudinal orientation ( $200-235 \times 10^9$  N/m<sup>2</sup> or  $29-34 \times 10^6$  psi). Matrix properties dominate the transverse and crossply specimens, however, and here the aluminum matrix shows a higher modulus by a factor of three or better over its polymer counterparts. The longitudinal moduli are very close to being temperature independent ( $< 5\%$  change between 295 K and 4 K) while the matrix-dependent orientations show some small effects: polymer bases show some increase with lowering temperature while the boron-aluminum generally shows a small decrease.

In most metals, the Poisson's ratio is generally about 0.3; this is roughly true for boron-aluminum in all orientations and the longitudinal specimens of the other composites. For the polymer matrices, the transverse values are very low while the crossply values are much higher.

Longitudinal ultimate strengths do show some temperature dependence -- increasing at cryogenic temperatures particularly for boron-aluminum ( $16.4 \times 10^8$  N/m<sup>2</sup> or  $238 \times 10^3$  psi) and glass-NASA resin 2 ( $19.6 \times 10^8$  N/m<sup>2</sup> or  $284 \times 10^3$  psi). In the other two orientations the metal matrix again shows a superiority.

Those composite layups in this group which do display any yielding do not have a sharp transition between elastic and plastic zones. Consequently, the determination of a proportional limit is quite difficult and hence the rather large variation in values as seen in the standard deviations. The 0.2% yield strength is a considerably less variable measure of plastic yield.

The polymer-matrix intralaminar shear moduli in Table 11 appear to agree reasonably with other room temperature determinations [9]; the boron-aluminum values are, however, quite low. This difference is probably due to the non-linear stress-strain response in the ductile matrix invalidating assumptions necessary for the indirect  $\pm 45^\circ$  method of calculating  $G_{12}$  [10]. The boron-aluminum values listed here should serve only as lower boundaries.

Composite properties are strongly dependent on fiber volume fraction and void content but, where general comparison is possible with the data reviewed in Appendix III, there is reasonable agreement with the present data with a few exceptions. In the glass-NASA resin 2 we did not see the large increase in  $E_{11}$  at 4 K that would be indicated by earlier 20 K measurements [3]. The type A graphite-NASA resin 2 here had a very low transverse tensile strength; this may indicate low filament-resin compatibility. All the Kevlar 49-NASA resin 2 properties indicate the severe compatibility mentioned above.

## 2.5 Future Work

Compression tests are in progress. We designed and built a special fixture and have now seen it through several modifications. After working with a few specimen configurations, it now appears that the major hurdles have been cleared and good compression data are possible.

Fatigue testing will begin later this fall and, for this purpose, we now have in hand boron-aluminum and boron-epoxy materials in a ( $0_2 \pm 45^\circ$ ) configuration.

## 3.0 References

1. Kasen, M. B., "Advanced Composites," Semi-Annual Technical Reports on Materials Research in Support of Superconducting Machinery, (1 Sept., 1973 to 1 March, 1974) National Bureau of Standards - Advanced Research Projects Agency.
2. Kasen, M. B. and Schramm, R. E., "Advanced Composites," Semi-Annual Technical Reports on Materials Research in Support of Superconducting Machinery - II, (1 March, 1974 to 1 Sept., 1974) National Bureau of Standards - Advanced Research Projects Agency.
3. Kasen, M. B., "Mechanical and thermal properties of filamentary-reinforced structural composites at cryogenic temperatures. 1: Glass-reinforced composites," Cryogenics 15(6), 327 (1975).
4. Kasen, M. B., "Properties of Filamentary-Reinforced Composites at Cryogenic Temperatures," Composite Reliability, ASTM STP 580, American Society for Testing and Materials, 1975 (to be published).
5. Schramm, R. E. and Kasen, M. B., "Advanced Composites," Semi-Annual Technical Reports on Materials Research in Support of Superconducting Machinery-III (1 Sept., 1974 to 1 March, 1975) National Bureau of Standards-Advanced Research Projects Agency.
6. Schramm, R. E. and Kasen, M. B., "Static Tensile Properties of Boron-Aluminum and Boron-Epoxy Composites at Cryogenic Temperatures," Paper T3, Cryogenic Engineering Conference, Kingston, Ontario, July 22-25, 1975 (to be published).
7. Petit, P. H., "A Simplified Method of Determining the In-plane Shear Stress-Strain Response of Unidirectional Composites," Composite Materials: Testing and Design, ASTM STP 460, American Society for Testing and Materials, 1969, pp. 83-93.
8. Sims, D. F. and Halpin, J. C., "Methods for Determining the Elastic and Viscoelastic Response of Composite Materials," Composite Materials: Testing and Design (Third Conference), ASTM STP 546, American Society for Testing and Materials, 1974, pp. 46-66.
9. Advanced Composite Design Guide, Third Edition, Volume IV, Materials, Air Force Materials Laboratory, Wright-Patterson Air Force Base, Ohio (1973).

10. Ramsey, J. E., Waszczak, J. P. and Klouman, F. L., "An Investigation of the Non-Linear Response of Metal-Matrix Composite Laminates," AIAA/ASME/SAE 16th Structures, Structural Dynamics and Materials Conference, Denver, Colorado (May 27, 1974):

#### 4.0 List of Figures

1. Composite tensile specimens fractured at 4 K (except for Kevlar 49-NASA resin 2) All transverse  $90^\circ$  specimens broke in the same manner while all crossply ( $\pm 45^\circ$ ) polymer matrix specimens were similar to each other in appearance.

# FIBER-REINFORCED STRUCTURAL COMPOSITES

## 4K TENSILE FRACTURES

Longitudinal (0°)

5.6 mil Boron-6061 Aluminum

5.6 mil Boron-5505 Epoxy

S-901 Glass-NASA Resin 2

Type A Graphite-NASA Resin 2

Kevlar 49-NASA Resin 2

76 K

Transverse (90°)

Type A Graphite-NASA Resin 2

Crossply ( $\pm 45^\circ$ )

5.6 mil Boron-6061 Aluminum

S-901 Glass-NASA Resin 2

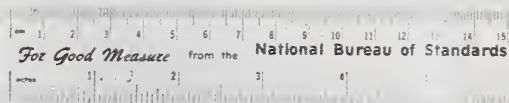


Fig. 1. Composite tensile specimens fractured at 4 K (except for Kevlar 49-NASA resin 2). All transverse (90°) specimens broke in the same manner while all crossply ( $\pm 45^\circ$ ) polymer matrix specimens were similar to each other in appearance.

5.0 List of Tables

1. Composite Plates Used for Tensile Mechanical Tests.
2. Tensile Properties of 5.6 mil Boron-6061 Aluminum Composites (Individual Specimens).
3. Tensile Properties of 5.6 mil Boron-Epoxy Composites (Individual Specimens).
4. Tensile Properties of S Glass-NASA Resin 2 Composites (Individual Specimens).
5. Tensile Properties of Type A Graphite-NASA Resin 2 Composites (Individual Specimens).
6. Tensile Properties of Kevlar 49-NASA Resin 2 Composites (Individual Specimens and Averages).
7. Tensile Properties of 5.6 mil Boron-6061 Aluminum Composites (Averages of Specimens Tested).
8. Tensile Properties of 5.6 mil Boron-Epoxy Composites (Averages of Specimens Tested).
9. Tensile Properties of S Glass-NASA Resin 2 Composites (Averages of Specimens Tested).
10. Tensile Properties of Type A Graphite-NASA Resin 2 Composites (Averages of Specimens Tested).
11. In-Plane Shear Modulus (Averages of Three Specimens).

Table 1.

Composite Plates Used for Tensile Mechanical Tests

Composite	Orientation	Nominal Thickness		Plies
		(cm)	(in)	
5.6 mil Boron 6061-Aluminum	longitudinal (0°)	0.109	0.043	6
	transverse (90°)	0.246	0.097	15
	crossply (± 45°)	0.178	0.070	10
5.6 mil Boron-5505 Epoxy	longitudinal (0°)	0.102	0.040	6
	transverse (90°)	0.257	0.101	15
	crossply (± 45°)	0.170	0.067	10
S-901 Glass - NASA Resin 2	longitudinal (0°)	0.124	0.049	6
	transverse (90°)	0.315	0.124	15
	crossply (± 45°)	0.196	0.077	10
Type A Graphite-NASA Resin 2	longitudinal (0°)	0.112	0.044	6
	transverse (90°)	0.292	0.115	15
	crossply (± 45°)	0.196	0.077	10
Kevlar 49 - NASA Resin 2	longitudinal (0°)	0.124	0.049	6
	transverse (90°)	0.356	0.140	15
	crossply (± 45°)	0.218	0.086	10

Table 2.

Tensile Properties of 5.6 mil Boron-6061 Aluminum Composites

(Individual Specimens)

Temperature (K)	Elastic Modulus, E		Poisson's Ratio <sup>a</sup> , $\nu$	Proportional Limit, $\sigma^p$		0.2% Yield Strength, $\sigma^{0.2}$		Ultimate Strength, $\sigma^{tu}$		Ultimate Elongation, $\epsilon^{tu}$ (%)
	( $10^9$ N/m <sup>2</sup> )	( $10^6$ psi)		( $10^8$ N/m <sup>2</sup> )	( $10^3$ psi)	( $10^8$ N/m <sup>2</sup> )	( $10^3$ psi)	( $10^8$ N/m <sup>2</sup> )	( $10^3$ psi)	
Longitudinal (0°)										
295	195	28.3	0.320					12.4 <sup>b</sup>	180 <sup>b</sup>	0.6 <sup>b</sup>
295	194	28.1	0.280					12.7 <sup>b</sup>	184 <sup>b</sup>	0.6 <sup>b</sup>
295	194	28.2	0.275					12.2 <sup>b</sup>	171 <sup>b</sup>	0.6 <sup>b</sup>
295	217	31.4	0.320					12.5 <sup>b</sup>	175 <sup>b</sup>	0.6 <sup>b</sup>
76	186	27.0	0.345					16.9	245	0.8
76	196	28.4	0.344					15.8	230	0.7
76	208	30.1	0.335					16.5	239	0.8
76	196	28.4	0.351					16.0 <sup>b</sup>	233 <sup>b</sup>	0.8 <sup>b</sup>
4	211	30.6	0.313					14.9	217	0.7
4	207	30.0	0.358					16.9	245	0.8
4	191	27.7	0.343					16.0	231	0.8
4	206	29.9	0.360					16.4	238	0.8
Transverse (90°)										
295	165	24.0	0.247	0.67	9.7	1.38	20.1	1.74	25.3	0.8
295	177	25.7	0.265	0.54	7.8	-	-	1.80	26.1	-
295	142	20.6	0.212	0.67	9.7	1.29	18.7	1.46	21.1	0.6
76	101	14.6	0.175	0.92	13.3	1.86	27.0	2.29 <sup>b</sup>	33.2 <sup>b</sup>	0.8 <sup>b</sup>
76	155	22.5	0.268	0.75	10.9	1.67	24.3	2.57	37.3	0.8
76	138	20.1	0.239	0.65	9.4	1.94	28.2	2.47	35.9	0.8
76	116	16.8	0.201	0.72	10.5	1.66	24.1	2.42	35.1	0.9
4	180	26.2	0.304	0.50	7.3	1.97	28.6	2.79	40.5	0.9
4	152	22.1	0.256	0.80	11.6	-2.05	29.7	2.73	39.6	0.8
4	118	17.1	0.199	0.86	12.5	1.87	27.1	2.76	40.0	0.9
Crossply (+45°)										
295	112	16.2	-	0.27	3.9	0.90	13.0	3.62	52.4	13.6
295	100	14.5	0.417	0.68	9.9	1.01	14.6	3.92	56.9	-
295	120	17.3	0.375	0.17	2.4	0.92	13.3	3.32	48.2	10.6
76	61.8	9.0	0.313	0.08	1.2	1.52	22.0	4.11	59.6	4.6
76	71.8	10.5	0.361	0.20	2.8	1.44	20.9	4.64	67.2	8.8
75	99.0	14.4	0.325	0.16	2.3	1.09	15.8	3.66	53.1	-
4	109	15.9	0.405	0.48	6.9	1.40	20.3	4.25	61.7	3.2
4	111	16.0	0.378	0.26	3.7	1.20	17.4	4.06	58.9	4.1
4	84	12.1	0.337	0.18	2.7	1.41	20.5	4.02	58.4	5.2

<sup>a</sup>Poisson's ratios for transverse (90°) specimens ( $\nu_{21}$ ) were calculated from  $E_{22}$  and the average values of  $E_{12}$  and  $E_{11}$ .

<sup>b</sup>These values resulted from an invalid fracture and were not included in the average value.

Table 3.

Tensile Properties of 5.6 mil Boron-Epoxy Composites

Temperature (K)	(Individual Specimens)							Ultimate Strength, $\sigma_{tu}$ ( $10^3$ psi)	Ultimate Elongation, $\epsilon_{tu}$ (%)
	Elastic Modulus, E ( $10^9$ N/m <sup>2</sup> )	Poisson's Ratio <sup>a</sup> , $\nu$	Proportional Limit, $\sigma^1$ ( $10^3$ psi)	0.2% Yield Strength, $\sigma^{1/2}$ ( $10^3$ psi)	Ultimate Strength, $\sigma_{tu}$ ( $10^8$ N/m <sup>2</sup> )	Ultimate Elongation, $\epsilon_{tu}$ (%)	Ultimate Elongation, $\epsilon_{tu}$ (%)		
295	235	0.261				16.3	236	0.7	
295	235	0.213				16.9	245	0.8	
295	228	0.221				17.1b	247b	0.8b	
295	230	0.221				16.4b	238b	0.7b	
295	227	0.223				15.8	229	0.7	
76	240	0.243				16.6b	241b	0.7b	
76	230	0.242				16.4	238	0.7	
76	231	0.240				16.1	234	0.8	
76	236	0.223				12.9b	187b	0.6b	
76	229	0.256				17.8	258	0.9	
4	244	0.227				18.5	268	0.8	
4	237	0.241				18.3	265	0.8	
4	234	0.262				16.2b	234b	0.7b	
4	235	0.239				17.8b	258b	0.8b	
4	238	0.227				17.7	257	0.8	
295	17.2	0.017	0.321	4.66	0.446b	0.446b	6.47b	0.3b	
295	16.3	0.016	0.348	5.04	0.472b	0.472b	6.84b	0.3b	
295	17.3	0.017	0.346	5.02	0.473	0.473	6.85	0.3	
295	17.3	0.017	0.343	4.98	0.503	0.503	7.30	0.3	
295	18.9	0.019	0.464	6.73	0.434	0.434	6.29	0.2	
295	18.0	0.018	0.242	3.50	0.419b	0.419b	6.08b	0.2b	
76	29.6	0.031			0.502	0.502	7.23	0.2	
76	28.9	0.030			0.515	0.515	7.47	0.2	
76	32.5	0.034			0.420b	0.420b	6.09b	0.1b	
76	33.9	0.035			0.452	0.452	6.56	0.1	
4	35.2	0.033			0.469	0.469	6.81	0.1	
4	33.9	0.032			0.303	0.303	4.40	0.1	
4	38.3	0.037			0.469	0.469	6.81	0.1	
295	16.8	0.856	0.421	6.11	0.939	0.939	18.5	1.8	
295	18.6	0.801	0.396	5.74	0.969	0.969	19.0	1.8	
295	18.8	0.794	0.402	5.82	0.961	0.961	18.9	2.0	
76	31.9	0.665	0.417	6.05	0.993	0.993	15.9	0.8	
76	33.0	0.624	0.388	5.63	0.940	0.940	16.4	0.9	
76	33.1	0.724	0.427	6.19	0.920	0.920	15.9	0.9	
4	32.1	0.677	0.328	4.75	0.849	0.849	14.8	0.8	
4	35.5	0.758	0.278	4.03	0.821	0.821	14.2	0.8	
4	32.2	0.664	0.282	4.09	0.821	0.821	15.0	0.9	

<sup>a</sup> Poisson's ratios for transverse (90°) specimens ( $\nu_{21}$ ) were calculated from  $E_{22}$  and the average values of  $\nu_{12}$  and  $E_{11}$  for each temperature.

<sup>b</sup> These values resulted from an invalid fracture and were not included in the average value.

Table 4.

## Tensile Properties of S Glass-NASA Resin 2 Composites

Temperature (K)	(Individual Specimens)										Ultimate Elongation, $\epsilon$ (%)				
	Elastic Modulus, E ( $10^9$ N/m <sup>2</sup> )		Poisson's Ratio, <sup>a</sup>	Proportional Limit, $\sigma^b$ ( $10^3$ psi)		0.2% Yield Strength, $\sigma^b$ ( $10^8$ N/m <sup>2</sup> )		Yield Strength, $\sigma^b$ ( $10^3$ psi)		Ultimate Strength, $\sigma^b$ ( $10^3$ psi)					
	( $10^6$ psi)	( $10^8$ N/m <sup>2</sup> )		( $10^3$ psi)	( $10^8$ N/m <sup>2</sup> )	( $10^3$ psi)	( $10^8$ N/m <sup>2</sup> )	( $10^3$ psi)	( $10^8$ N/m <sup>2</sup> )	( $10^3$ psi)		( $10^8$ N/m <sup>2</sup> )			
295	59.3	8.59	0.238	Longitudinal (0°)										216	3.1
295	57.2	8.31	0.261											173	2.7
295	55.4	8.05	0.305											204	2.7
76	58.0	8.40	0.257											276	3.4
76	58.6	8.50	0.278											280	3.3
76	58.2	8.44	0.272											295	3.2
4	62.8	9.10	0.310											276	3.0
4	57.4	8.35	0.299											314	3.4
4	60.2	8.74	0.261											253	2.7
295	11.8	1.71	0.055	Transverse (90°)										6.84	0.7
295	11.7	1.69	0.054	3.06	0.211	0.457	6.63	0.472	6.40	0.441	6.40	0.5			
295	13.7	1.99	0.064	1.66	0.114	0.396	5.74	0.489	7.09	0.489	7.09	0.7			
76	21.8	3.16	0.101	1.27	0.087	0.375	5.43	0.789	11.4	0.789	11.4	0.3			
76	18.2	2.63	0.084											11.8 <sup>b</sup>	0.4 <sup>b</sup>
76	22.2	3.21	0.102											12.2	0.4
76	21.5	3.12	0.099											16.4 <sup>b</sup>	0.5 <sup>b</sup>
76	22.4	3.25	0.105											16.0	0.5
4	19.5	2.82	0.094											9.53	0.3
4	24.8	3.60	0.120											13.4	0.4
4	21.8	3.17	0.105											11.2	0.4
295	21.4	3.10	0.509	Crossply ( $\pm 45^\circ$ )										18.7	5.2
295	19.5	2.83	0.587	2.44	0.168	0.474	6.87	1.29	20.8	1.44	20.8	5.9			
295	18.4	2.67	0.535	2.30	0.159	0.450	6.53	1.44	20.9	1.44	20.9	7.0			
76	31.1	4.51	0.396	2.16	0.149	0.462	6.70	2.42	35.2	2.42	35.2	1.5			
76	31.4	4.55	0.347	12.2	0.843	1.80	26.1	2.00	28.9	2.00	28.9	1.1			
76	32.6	4.72	0.392	14.0	0.962	1.77	25.7	2.41	35.0	2.41	35.0	1.4			
4	4.97	0.72	0.397	9.9	0.682	1.79	26.0	2.31 <sup>b</sup>	34.0 <sup>b</sup>	2.31 <sup>b</sup>	34.0 <sup>b</sup>	0.9 <sup>b</sup>			
4	35.1	5.09	0.419	17.8	1.21	2.17	31.9	2.35	34.1	2.35	34.1	1.0			
4	33.2	4.81	0.383	15.3	1.06	2.19	31.7	2.39	34.6	2.39	34.6	0.9			
4	36.0	5.21	0.349	19.9	1.37	2.29	33.1	2.31	33.5	2.31	33.5	0.9			

<sup>a</sup> Poisson's ratios for transverse (90°) specimens ( $\nu_{21}$ ) were calculated from  $E_{22}$  and the average values of  $\nu_{12}$  and  $E_{11}$  for each temperature.

<sup>b</sup> These values resulted from an invalid fracture and were not included in the average value.

Table 5.

Tensile Properties of Type A Graphite-NASA Resin 2 Composites  
(Individual Specimens)

Temperature (K)	Primary		Secondary		Proportional Limit, $\sigma_{pl}$ ( $10^3$ psi)	0.2% Yield Strength, $\sigma_{0.2}$ ( $10^6$ N/m <sup>2</sup> )	Yield Strength, $\sigma_{0.2}$ ( $10^3$ psi)	Ultimate Strength, $\sigma_{tu}$ ( $10^8$ N/m <sup>2</sup> )	Ultimate Strength, $\sigma_{tu}$ ( $10^3$ psi)	Ultimate Elongation $\epsilon_{tu}$ (%)
	Elastic Modulus, E ( $10^9$ N/m <sup>2</sup> ) ( $10^6$ psi)	Poisson's Ratio, $\nu$	Elastic Modulus, E ( $10^9$ N/m <sup>2</sup> ) ( $10^6$ psi)	Poisson's Ratio, $\nu$						
295	115	16.7	124	18.0				12.9	187	0.9
295	113	16.3	122	17.8	0.341			14.8	214	1.0
295	126	18.2	130	18.9	0.346			11.9	173	0.9
					0.354					
76	112	16.3	123	17.8	0.301			12.1	176	1.1
76	97.7	14.2	116	16.7	0.285			12.6	183	0.9
76	93.8	13.6	115	16.7	0.310			12.1	176	0.9
4	111	16.1	121	17.6	0.297			12.6	183	0.9
4	132	19.1	149	21.6	0.429			13.2	191	0.9
4	107	15.5	123	17.8	0.294			13.4	194	0.9
						Longitudinal (0°)				
						Transverse (90°)				
295	8.57	1.24			0.024			0.128	1.86	0.2
295	7.74	1.12			0.021			0.155	2.24	0.2
295	7.09	1.03			0.020			0.102	1.47	0.2
76	9.6	1.40			0.027			0.016	0.235	0.02
76	11.4	1.65			0.032			0.031	0.444	0.03
76	11.6	1.69			0.032			0.026	0.382	0.02
4	11.0	1.60			0.028			0.038	0.556	0.03
4	11.0	1.60			0.028			0.028	0.404	0.02
4	12.6	1.83			0.032			0.024	0.344	0.02
4	10.4	1.50			0.026			0.032	0.461	0.03
						Crossply ( $\pm 45^\circ$ )				
295	12.9	1.87			0.655			0.697	10.1	1.6
295	16.7	2.42			0.706			0.678	9.8	0.7
295	17.1	2.49			0.758			0.718	10.4	0.9
								0.524		
76	19.4	2.82			0.903			0.451	6.54	0.2
76	16.0	2.32			0.703			0.448	6.50	0.3
76	16.6	2.41			0.794			0.423	6.13	0.3
4	19.4	2.82			0.772			0.474	6.87	0.3
4	17.5	2.53			0.602			0.470	6.81	0.3
4	17.2	2.50			0.697			0.490	7.11	0.3

a Poisson's ratios for transverse (90°) specimens ( $\nu_{21}$ ) were computed from  $E_{22}$  and the average values of  $\nu_{12}$  and  $E_{11}$  for each temperature.

Table 6.

Tensile Properties of Kevlar 49 - NASA Resin 2 Composites  
(Individual Specimens and Averages)

Temperature (K)	Elastic Modulus, E ( $10^9$ Nm <sup>2</sup> )		Poisson's Ratio <sup>a</sup> , $\nu$	Ultimate Strength, $\sigma_{tu}$ ( $10^3$ psi)		Elongation, $\epsilon_{tu}$ (%)	
	( $10^6$ psi)	( $10^8$ N/m <sup>2</sup> )		( $10^3$ psi)	( $10^3$ psi)		
295	69.7	10.1	Longitudinal (0°)	10.1	147	1.6	
295	72.0	10.3		0.446	10.5	153	1.7
Avg 295	70.9	10.2		0.553	10.3	150	1.7
76	79.5	11.5	Transverse (90°)	9.32	135	1.1	
76	83.7	12.2		0.471	130	130	1.0
Avg 76	81.6	11.9		0.524	133	133	1.1
295	0.638	0.093	Crossply (+ 45°)	0.002	0.032	0.02	
295	0.981	0.142		0.004	0.052	0.04	
Avg 295	0.810	0.118		0.006	0.042	0.03	
76	0.794	0.115	Crossply (+ 45°)	0.001	0.017	0.01	
76	0.597	0.087		0.004	0.017	0.01	
Avg 76	0.696	0.101		0.005	0.017	0.01	
295	4.37	0.634	Crossply (+ 45°)	0.062	0.902	1.5	
295	3.27	0.475		1.078	1.12	0.2	
295	3.41	0.494		1.215	2.33	0.6	
Avg 295	3.68	0.534	1.101	1.451	0.8		
76	23.7	3.44	Crossply (+ 45°)	0.020	0.284	0.01	
76	24.8	3.59		1.131	0.207	0.01	
Avg 76	24.3	3.52		0.580	0.246	0.01	
			0.482				
			0.531				

<sup>a</sup>Poisson's ratios for transverse (90°) specimens ( $\nu_{21}$ ) were computed from  $E_{22}$  and the average values of  $\nu_{12}$  and  $E_{11}$  for each temperature.



Table 8.

Tensile Properties of 5.6 mil Boron-Epoxy Composites  
(Averages of Specimens Tested<sup>a</sup>)

Temperature (K)	Elastic Modulus, E			Poisson's Ratio <sup>b</sup> , $\nu$		Proportional Limit, $\sigma^{pl}$			0.2% Yield Strength, $\sigma^{ty}$			Number of Specimens
	( $10^9$ N/m <sup>2</sup> )	( $10^6$ psi)	CV(%)		CV(%)	( $10^8$ N/m <sup>2</sup> )	( $10^3$ psi)	CV(%)	( $10^8$ N/m <sup>2</sup> )	( $10^3$ psi)	CV(%)	
						Longitudinal (0°)						
295	231(4)	33.5(0.6)	1.6	0.228(0.019)	8.3							5
76	233(5)	33.9(0.7)	2.1	0.241(0.012)	4.8							5
4	238(6)	34.5(0.6)	2.3	0.239(0.014)	5.9							5
						Transverse (90°)						
295	17.5(0.9)	2.54(0.12)	5.0	0.017(0.001)	6.1	0.344(0.071)	4.99(1.02)	20.7				6
76	31.2(2.4)	4.53(0.34)	7.5	0.033(0.002)	7.3							4
4	35.8(2.3)	5.19(0.32)	6.3	0.034(0.003)	7.8							3
						Crossply ( $\pm 45^\circ$ )						
295	18.1(1.1)	2.62(0.17)	6.3	0.817(0.034)	4.1	0.406(0.013)	5.89(0.19)	3.3	0.956(0.016)	13.9(0.3)	1.8	3
76	32.7(0.7)	4.72(0.13)	2.8	0.671(0.050)	7.4	0.411(0.020)	5.96(0.29)	4.9	0.951(0.038)	13.8(0.5)	3.9	3
4	33.3(1.9)	4.83(0.28)	5.8	0.700(0.051)	7.2	0.296(0.028)	4.29(0.40)	9.3	0.830(0.016)	12.0(0.2)	1.9	3

Temperature (K)	Ultimate Strength, $\sigma^{tu}$			Ultimate Elongation, $\epsilon^{tu}$		Number of Specimens
	( $10^8$ N/m <sup>2</sup> )	( $10^3$ psi)	CV(%)	(%)	CV(%)	
				Longitudinal (0°)		
295	16.3(0.6)	237(8)	3.3	0.73(0.04)	5.1	3
76	16.8(0.9)	243(13)	5.4	0.77(0.07)	9.3	3
4	18.2(0.4)	263(6)	2.2	0.76(0.01)	1.5	3
				Transverse (90°)		
295	0.470(0.035)	6.81(0.51)	7.4	0.27(0.06)	21.7	3
76	0.490(0.033)	7.09(0.47)	6.7	0.15(0.03)	17.6	3
4	0.414(0.096)	6.01(1.39)	23.1	0.12(0.04)	33.6	3
				Crossply ( $\pm 45^\circ$ )		
295	1.30(0.02)	18.8(0.3)	1.4	1.88(0.14)	7.5	3
76	1.11(0.02)	16.1(0.3)	1.7	0.85(0.05)	5.3	3
4	1.01(0.03)	14.7(0.4)	2.8	0.83(0.05)	6.3	3

<sup>a</sup>Standard deviations are in parentheses. CV is coefficient of variation. Data from the specimens that broke at or in the grips are not included in the calculations of ultimate strength or elongation.

<sup>b</sup>Poisson's ratios for transverse (90°) specimens ( $\nu_{21}$ ) were calculated from  $\nu_{12}$ ,  $E_{11}$ , and  $E_{22}$ .

Table 9.

Tensile Properties of S Glass-NASA Resin 2 Composites  
(Averages of Specimens Tested<sup>a</sup>)

Temperature (K)	Elastic Modulus, E (10 <sup>9</sup> N/m <sup>2</sup> )		Poisson's Ratio, $\nu$ <sup>b</sup>		Proportional Limit, $\sigma_{pl}$ (10 <sup>8</sup> N/m <sup>2</sup> )		0.2% Yield Strength, $\sigma_y$ (10 <sup>8</sup> N/m <sup>2</sup> )		CV (%)	Number of Specimens
	(10 <sup>6</sup> psi)	CV (%)	CV (%)	CV (%)	(10 <sup>3</sup> psi)	CV (%)	(10 <sup>3</sup> psi)	CV (%)		
295	57.3(0.5)	3.2	0.268(0.034)	12.7	Longitudinal (0°)					
	58.3(0.3)	0.6	0.272(0.011)	4.0						
	60.1(2.7)	4.5	0.269(0.011)	8.9						
295	12.4(1.1)	9.3	0.058(0.006)	9.5	Transverse (90°)					
	21.2(2.4)	11.7	0.098(0.008)	8.4	0.137(0.065) 2.00(0.94) 47.6					
	22.0(2.7)	12.2	0.106(0.013)	12.3	Crossply ( $\pm 45^\circ$ )					
295	19.8(1.5)	7.7	0.544(0.040)	7.3	0.16(0.01) 2.30(0.14) 6.1					
	31.7(0.8)	2.5	0.378(0.027)	7.2	0.83(0.14) 12.0(2.1) 17.1					
	34.5(1.5)	4.5	0.387(0.036)	9.3	1.19(0.17) 17.3(2.5) 14.6					
Temperature (K)	Ultimate Strength, $\sigma_{tu}$ (10 <sup>8</sup> N/m <sup>2</sup> )		Ultimate Strength, $\sigma_{tu}$ (10 <sup>3</sup> psi)		Ultimate Elongation, $\epsilon_{tu}$ (%)		Ultimate Elongation, $\epsilon_{tu}$ CV (%)		Number of Specimens	
	CV (%)	CV (%)	CV (%)	CV (%)	CV (%)	CV (%)				
295	13.6(1.6)	11.4	198(22)	11.4	Longitudinal (0°)					
	19.6(0.6)	3.5	284(10)	3.5	2.8(0.2)					
	19.4(2.1)	11.0	281(31)	11.0	3.3(0.1)					
295	0.467(0.024)	5.2	6.8(0.4)	5.2	3.0(0.4)					
	0.936(0.234)	25.3	13.6(3.4)	25.3	0.6(0.1)					
	0.783(0.132)	17.0	11.4(1.9)	17.0	0.4(0.1)					
295	1.39(0.87)	6.2	20.1(1.2)	6.2	Crossply ( $\pm 45^\circ$ )					
	2.28(0.24)	10.9	33.0(3.6)	10.9	6.0(0.9)					
	2.34(0.05)	2.0	34.1(0.6)	2.0	1.3(0.2)					
76	6.70(0.17)	2.6	6.70(0.17)	2.6	15.6					
	25.9(0.2)	0.9	25.9(0.2)	0.9	15.1					
	31.8(1.4)	4.4	31.8(1.4)	4.4	16.0					
76	6.70(0.17)	2.6	6.70(0.17)	2.6	6.6					
	25.9(0.2)	0.9	25.9(0.2)	0.9	6.6					
	31.8(1.4)	4.4	31.8(1.4)	4.4	6.6					

<sup>a</sup> Standard deviations are in parentheses. CV is coefficient of variation. Data from the specimens that broke at or in the grips are not included in the calculations of ultimate strength or elongation.

<sup>b</sup> Poisson's ratios for transverse (90°) specimens ( $\nu_{12}$ ,  $\nu_{11}$ , and  $\nu_{22}$ ) were computed from  $\nu_{12}$ ,  $\nu_{11}$ , and  $\nu_{22}$ .



Table 11.

In-Plane Shear Modulus<sup>a</sup>  
(Averages of Three Specimens)

Temperature (K)	Shear Modulus, $G_{12}$		
	( $10^9$ N/m <sup>2</sup> )	( $10^6$ psi)	CV(%)
	Boron-Aluminum <sup>b</sup>		
295	39.7(4.0)	5.75(0.58)	10.0
76	27.5(5.5)	3.92(0.80)	20.4
4	32.6(5.5)	4.73(0.80)	16.9
	Boron-Epoxy		
295	4.72(0.44)	0.68(0.06)	9.3
76	9.19(0.38)	1.33(0.06)	4.1
4	9.28(0.19)	1.35(0.03)	2.0
	Glass - NASA Resin 2		
295	6.19(0.51)	0.90(0.07)	8.3
76	11.0(0.6)	1.60(0.09)	5.8
4	12.9(0.3)	1.87(0.05)	2.8
	Graphite - NASA Resin 2		
295	4.14(0.33)	0.600(0.047)	7.9
76	4.50(0.15)	0.652(0.022)	3.3
4	5.32(0.36)	0.772(0.053)	6.8

<sup>a</sup>These values are calculated from the crossply ( $\pm 45^\circ$ ) data using the method of Sims and Halpin. Standard deviations are in parentheses; CV is the coefficient of variation.

<sup>b</sup>The boron-aluminum moduli are only lower limits to the true values.

Appendix I: Symbols

$E_{11}$	=	longitudinal (0°) elastic modulus
$E_{22}$	=	transverse (90°) elastic modulus
$E_x$	=	crossply ( $\pm 45^\circ$ ) elastic modulus
$\nu_{12}$	=	longitudinal (0°) Poisson's ratio
$\nu_{21}$	=	transverse (90°) Poisson's ratio
$\nu_x$	=	crossply ( $\pm 45^\circ$ ) Poisson's ratio
$G_{12}$	=	intralaminar (in-plane) shear modulus
$\sigma^{pl}$	=	proportional limit; stress at which a stress-strain curve deviates from elasticity, i.e., is no longer a straight line
$\sigma^{ty}$	=	0.2% tensile yield strength; stress at the intersection of the stress-strain curve with a straight line having the same slope as the elastic modulus and offset by 0.2% along the strain scale
$\sigma^{tu}$	=	ultimate strength; highest stress attained on the stress-strain curve
$\epsilon^{tu}$	=	ultimate elongation; highest strain attained on the stress-strain curve

*This article is an extensive review of the literature on the mechanical and thermal properties of glass-reinforced structural composites at cryogenic temperatures. The objective is to provide an understanding of the general magnitude of property values obtainable within the cryogenic temperature range, to provide a feel for the relative literature ranking of specific composite types with regard to a specific property, and to impart an understanding of the temperature sensitivity of the property of interest. A bibliography and bibliography-property cross-reference is included. This is Part I of a two-part series. Part II will consider advanced composites.*

# Mechanical and thermal properties of filamentary-reinforced structural composites at cryogenic temperatures

## 1: Glass-reinforced composites

M. B. Kasen

Nomenclature			
$\sigma^{tu}$	tensile ultimate strength	$\sigma^{by}$	bearing yield strength
$E_1^t$	initial tensile modulus	$\sigma^1$	impact strength
$E_2^t$	secondary tensile modulus	$\lambda$	thermal conductivity
$\epsilon^{tu}$	tensile ultimate strength	$\Delta L/L$	thermal contraction
$n^{tu}$	tensile fatigue failure stress	$C_p$	specific heat
$\sigma^{fu}$	flexural ultimate strength	<i>Units</i>	
$E_1^f$	initial flexural modulus	lb in <sup>-2</sup>	pounds per square inch
$E_2^f$	secondary flexural modulus	k lb in <sup>-2</sup>	lb in <sup>-2</sup> x 10 <sup>3</sup>
$\sigma^{cu}$	compressive ultimate strength	N m <sup>-2</sup>	Newtons per metre squared (Pascal)
$E^c$	compressive modulus	J kg <sup>-1</sup> K <sup>-1</sup>	Joules per kilogram-Kelvin
$\sigma^{si}$	interlaminar shear strength	W m <sup>-1</sup> K <sup>-1</sup>	Watts per metre-Kelvin

The primary impetus for structural composite development arose from the need to obtain improved long-term mechanical properties at elevated temperatures or to reduce the cost of structures designed for ambient temperature use. Comparatively little effort has been expended on development of composites for use at cryogenic temperatures. A notable exception has been the rather extensive body of work sponsored by the USAF and NASA wherein a series of glass-reinforced plastics were characterized to 20 K. The other major field of cryogenic development has been concerned with composite reinforcement of pressure vessels

for aerospace use, largely exploiting the continuous-filament method of fabrication. To a large extent, the remaining published data on composite properties at cryogenic temperatures reflects work on which the generation of cryogenic property data was peripheral to the main work objective.

This relative lack of emphasis on cryogenic structural composites is perhaps understandable, as the majority of such structural applications are presently satisfied by readily available and well-characterized metals and alloys. In view of the extensive data base available on metals, it is probable that metals will continue to constitute the main body of structural materials at low temperatures.

Why then, should one consider composites? The answer lies in the increasingly stringent demands made on materials in advancing cryogenic technology, of which superconduct-

The author is with the Cryogenics Division, National Bureau of Standards, Institute for Basic Standards, Boulder, Colorado 80302, USA. This research was supported by the Advanced Research Projects Agency of the Department of Defence under ARPA Order No 2569. Received 6 January 1975.

ing machinery may serve as an example. Undoubtedly, the first generation of superconducting motors and generators will be dependent almost entirely on metals technology. However, it is highly probable that succeeding generations of such equipment will capitalize on advanced composite technology for reasons of increased reliability, reduced weight, and increased efficiency, reflecting the higher specific strengths and moduli of advanced composites coupled with a wider range of thermal and electrical properties than are obtainable with any conventional metal. In particular, the high strength of the polymeric-matrix composites combined with very low thermal conductivity will be advantageous in minimizing heat losses in critical components.

The technological problems associated with integration of composites into superconducting machinery are three-fold: (a) most designers lack a feel for the properties available with composites, (b) an adequate data base does not exist for composites at cryogenic temperatures, particularly at 4 K, and (c) most existing composites are optimized for service at room temperature and above not for cryogenic service. The current programme at NBS is aimed at these three problem areas.

Our first effort has been to initiate an extensive review of what is known about the mechanical and thermal properties of composites at cryogenic temperatures. The objectives of the review are four-fold: (a) we wish to provide the designer with a feel for the general magnitude of property values which may reasonably be expected from a given category and class of composites within the cryogenic range. (We define a composite *category* by the general reinforcement type, for example, glass-fibre or advanced fibre (graphite, boron, etc). We subdivide the category into composite *classes* by the general matrix type, for example, glass-polyester or graphite-epoxy. We further subdivide the class by referring to a composite *type* when a specific reinforcement/matrix combination is specified, for example, HT-S graphite/X-904 epoxy.] (b) we wish to provide him with a feel for the literature ranking of specific composite classes with regard to a specific property, (c) we wish to impart a feel for whether the property of interest is likely to increase, remain unaffected, or decrease with lowering of temperature, and (d) we wish to define those areas in which further data are needed and to define the direction that future work should take in optimizing composites for cryogenic service and for implementing their use in the construction of superconducting machinery. For those with more specific interests we include an extensive Bibliography and Bibliography-property cross-reference to simplify retrieval of specific documents.

It must be emphasized that, although this survey is intended to be comprehensive, the complex nature of the subject makes it unavoidable that some works worthy of inclusion have been inadvertently omitted. The author will appreciate references to any additional material which bears on the subject. It must also be emphasized that the results reported in the surveyed publications have not been experimentally confirmed by NBS and that the conclusions and evaluations presented in this paper reflect those of the cited authors and do not imply approval, endorsement, or recommendation by NBS.

The discussion of properties given below does not take into consideration the effect of variations in fibre/resin ratio of specific types of composites and test specimens, as this characteristic was not reported for all referenced works. Com-

posite properties may be strongly influenced by this ratio. The property data discussed in this paper reflects actual values and trends reported by the cited authors for specific composites. Controlled variations in many of the properties are obtainable in practice by specific variation of the fibre content of the composite.

The literature review covers 1960 to the present time, as it is within this time span that almost all of the significant work was undertaken. We include only continuous-fibre reinforced composites, as such composites are the primary structural materials. The review excluded cryogenic insulations, superconductor composites, thin films, honeycomb structures, composite-overwrapped metal, or fibre-only properties. Filled composites are also excluded. There remains the very large field of composites reinforced by a variety of fibres in a variety of lay-ups in a variety of matrix materials, and it is with this body of data that this review is concerned.

The wide variety of composite formulations and lay-ups are further complicated by lack of standard test procedures. Furthermore, as the field is relatively new, much of the earlier work was performed on relatively poorly characterized composites. We have attempted to cope with this complexity by dividing the review into two major sections: Part I treating glass-reinforced composites and Part II treating the so-called advanced composites, for example, boron, graphite, etc. The rationale for this separation is the distinctly different use of these two composite categories in engineering practice, that is, glass-reinforced composites are used in applications where stiffness is not a design limitation, while the advanced composites are used where a high modulus material is essential.

Within each of these categories, we present the reader with a series of graphs on which appear the *average* literature values of each property for each composite class from room temperature into the deep cryogenic range. Admittedly, presenting average data is in danger of being misleading, as each curve has associated with it a considerable scatter band. For this reason, we discuss the range of values associated with each curve, emphasizing those specific composite types for which the highest values were reported. It is of utmost importance, however, that the reader understands that the graphed data appearing in this review are class averages and are therefore not to be used for engineering design purposes. The reader interested in design values is referred to the specific literature references.

### Scope of the literature survey

We initially conducted a subject search using the data bases of the NBS Cryogenic Data Center (CDC), Defense Documentation Center (DDC), and the National Technical Information Service (NTIS). Additionally, a subject search was conducted through the volumes of NASA Scientific and Technical Aerospace Reports (STAR), and the ASM-AIME Metals Review. As the search progressed, a series of contract numbers were identified as being associated with studies of the cryogenic properties of composites. The DDC and NASA data bases were then searched for all reports issued under such contracts. Finally, the DDC data base and that of the Smithsonian Science Information Exchange were searched for current work in progress.

### Organization of the Bibliography

The appended Bibliography contains 148 references. As the work progressed, it became apparent that a large part of the

relevant data had been produced under a relatively few contracts sponsored either by NASA or the USAF. Eleven such contracts have been listed at the start of the Bibliography with references to the most pertinent publications issued under each contract. Only final reports are listed, as they adequately summarize the data which also appeared in numerous interim reports on each project. Journal publications are listed, as they often provide a convenient review of the subject matter contained in the comprehensive reports and are generally more readily available to the reader.

The Bibliography also contains a general section, alphabetically arranged by author, listing relevant publications sponsored by other contracts or by corporate in-house funding. A separate part of the Bibliography itemizes handbooks or reviews which will be found useful references but which do not contain original data. Finally, a miscellaneous reference section lists publications which are referenced in the text but which do not contain relevant mechanical or thermal property data.

Wherever possible, the pertinent NASA or DDC code number is included to facilitate retrieval of specific publications. Corporate reports not so identified must be obtained from the corporate source.

An extensive cross-reference relating mechanical and physical properties of specific types of composites to specific literature references is included to simplify literature retrieval by the reader. The latter includes separate references to filament-wound pressure vessels in recognition of the importance of such applications to cryogenic technology. A separate listing is also provided of reports containing information on the effect of combined cryogenic temperature and nuclear radiation.

### Glass-reinforced composites

The mechanical and thermal properties of glass-polymeric composites are summarized on Figs 1–16. Where available, data are presented for 295 K, 200 K, 77 K, and 20 K (4 K data are almost non-existent). Straight lines connect average values at each temperature. Absence of a data point for a given temperature implies that no significant data was found in the literature. An asterisk adjacent to the number identifying a curve indicates that the data for that particular composite type was minimal relative to that available for the other composite types included on the figure.

When considering the mechanical property data, the reader should be aware that there exists no universally accepted method of determining these properties for composites, although committees of the ASTM are working diligently on the problem of standardization. The data discussed in the present review were for the most part obtained in the course of comprehensive research programmes by reliable investigators who were concerned with obtaining the most valid results possible. Nevertheless, it remains a possibility that some of the scatter in the data reported in the literature, particularly for compression and interlaminar shear, reflects differing test procedures. Where this has become apparent, the data have been separated by test method.

### Static mechanical properties

#### Composite tensile strength and modulus

The reason for the widespread use of glass-reinforced composites is evident from the tensile strength data presented on Fig.1. No other type of composite can match the uniaxial

tensile strengths of 250–300 k lb in<sup>-2</sup> provided by the glass-epoxy formulations. Even in the 0°/90° crossply lay-up, the glass-epoxy strength is almost equal to that of the advanced composites in the uniaxial longitudinal configuration. Unfortunately, the moduli of glass-reinforced composites are quite low, as may be seen in Fig.2. It is this low modulus of glass that has given impetus for development of the advanced composites.

From Fig.1 we see that the tensile strength is reduced about 50% at all temperatures in a 0°/90° configuration as compared to uniaxial, for example, from about 300 k lb in<sup>-2</sup> to about 150 k lb in<sup>-2</sup> for glass-epoxies. This is expected from a 50% decrease in longitudinal fibre content, the crossply fibres contributing nothing to the overall strength when tested parallel to one fibre direction.

Approximately another 25% decrease in strength is found upon going to woven cloth reinforcement of an epoxy matrix, reflecting the decrease in load carrying capacity of fibres which are slightly bent in the weaving process.

Epoxy resins are most widely used as matrices for structural applications where maximum strength is required. This appears justified on the basis of the data of Fig.1 wherein the ultimate tensile strengths of the cloth-epoxy composites are overall higher than those of other cloth-polymeric composites at all temperatures. The polyurethane, Teflon, phenyl silane, polyimide, and silicone-matrix composites appear to have the poorest strength properties at 295 K, with phenolic, polybenzimidazole (also known as PBI or Imidite), and polyester-matrix composites being intermediate in strength. At 77 K, the polyimide, silicone, and phenyl silane-matrix composites continue their relatively poor performance, while the polyurethane, polybenzimidazole, and Teflon-matrix composites have about equalled the phenolics and polyesters.

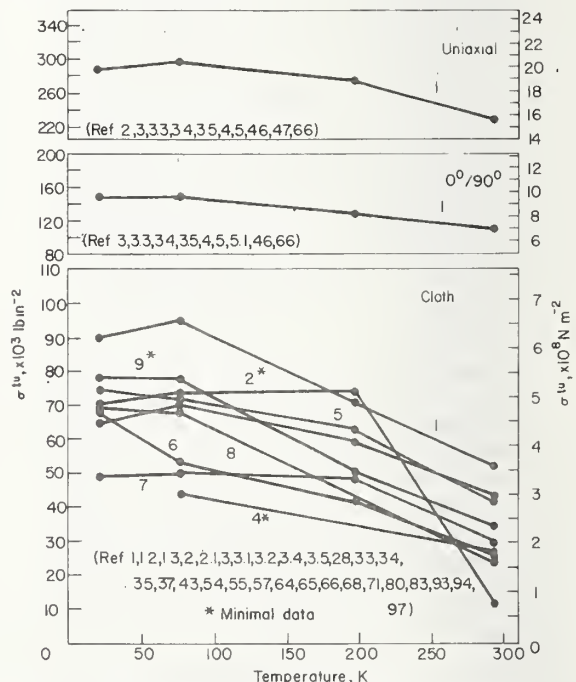


Fig.1 Ultimate tensile strength of glass-reinforced composites 1 — epoxy; 2 — polyurethane; 3 — phenolic; 4 — polyimide; 5 — polyester; 6 — silicone; 7 — phenyl silane; 8 — Teflon; 9 — polybenzimidazole

Among the uniaxial glass-epoxy composites, the highest reported strengths were about 175 k lb in<sup>-2</sup> at 77 K for NOL-ring tests with S-HTS/660 FW and S-901/ERL 2256/ZZL 0820 composites.<sup>46,47</sup> This work was directed toward filament-wound pressure vessels, which has been the incentive for much of the cryogenic composite development work. Other authors<sup>3,66</sup> have reported strengths of 315–330 k lb in<sup>-2</sup> at this temperature for S-901/E-787 and S-HTS/Epon 828/Epon 1031 filament-wound composites. About the same strength was reported for Hi-Stren glass filament-wound in a NASA Resin 2 matrix.<sup>4</sup> The overall data range was 213–375 k lb in<sup>-2</sup> at 77 K.

A comment on two of these epoxy resins is in order so as to prepare the reader for proper understanding of these and subsequent data. Resin E-787 will be referred to frequently in this paper, as it is often associated with the highest reported mechanical properties. E-787 is the US Polymeric Corporation designation for an Epon 828/Epon 1031/NMA/BDMA formulation in proportions 50/50/90/0.55 pbw. This resin is referred to as 58–68R by the Shell Chemical Company and is often referred to as the Polaris resin because of its successful use in that missile. It is a conventional type of resin, not optimized for cryogenic service. By contrast, Resin 2, consisting of Epon 828/DSA/Empol 1040/BDMA in proportions 100/115.9/20/1 pbw, is a bisphenolic. A epoxy system modified for low-temperature flexibility by means of a long-chain anhydride and a high-molecular weight tricarboxy acid. This latter resin was developed by Soffer and Molho under NASA sponsorship.<sup>5</sup> Soffer and Molho compared the Resin 2 formulation to that of 58–68R (E-787) in a series of burst tests on metal-lined, S-901 glass filament-wound pressure vessels, their results showing Resin 2 to develop equal strength at room temperature and higher longitudinal filament stresses at 77 K and 20 K. Additionally, Resin 2 was found to have relatively greater ductility and toughness at cryogenic temperatures and to be highly resistant to cracking when thermal cycled to 20 K. As the E-787 and Resin 2 epoxy formulations are likely candidates for cryogenic applications, the present report compares the property values obtained with each resin whenever such data are available. A further discussion of resins for cryogenic service is presented in the concluding part of this paper.

Continuing with the analysis of the data on Fig.1, it is found that among the 0°/90° data, the highest tensile strengths at cryogenic temperatures have been reported for S-901/E-787<sup>3</sup> and S-901/Resin 2<sup>5</sup> with values ranging from 170–200 k lb in<sup>-2</sup>. The overall range was 115–200 k lb in<sup>-2</sup>.

Among the woven-cloth composites, the highest cryogenic composite strengths were reported for the epoxy-matrix composites 181/modified Epon 828<sup>2</sup> and 1581/E-787,<sup>3</sup> having tensile strengths on the order of 125–145 k lb in<sup>-2</sup> at 77 K tested parallel to the woof or warp. The phenolic-matrix composite data showed quite consistent strengths of 60–70 k lb in<sup>-2</sup> at 77 K except for the work of Levin et al<sup>71</sup> who has reported 200 k lb in<sup>-2</sup> at 77 K in a composite based on a butvar-phenolic adhesive. The polyester-matrix data scatters from 50–80 k lb in<sup>-2</sup> at 77 K except for one report of 100–105 k lb in<sup>-2</sup> for 181 glass in Hetrion 31 or Narmco 527 resin.<sup>2</sup> The Teflon-matrix composites ranged from 50–80 k lb in<sup>-2</sup>, the highest value being reported for type 116 glass in TFE or FEP.<sup>80</sup> The silicone-matrix data showed relatively large scatter from 25–70 k lb in<sup>-2</sup> at 77 K with the highest values being reported for 181/Trevarno F-131<sup>2</sup>

and for 181/Narmco 513.<sup>3</sup> Few data were found for polyurethane, phenyl, silane, and polyimide-matrix composites. About 73 k lb in<sup>-2</sup> was reported at 77 K for 181 glass reinforced with the flexible polyurethane Adiprene L-100 and 60 k lb in<sup>-2</sup> for the same reinforcement in the phenyl silane Narmco 534.<sup>2</sup> Polyimides are relatively new matrix materials, having been developed primarily for elevated-temperature use, particularly for stability. Krause et al<sup>68</sup> reports a comparatively low value of 43 k lb in<sup>-2</sup> at 77 K for a glass-polyimide composite. On the other hand, polybenzimidazole-matrix composites, which are of the same family as the polyimides, appear to develop very high strength at 77 K and at 20 K, exceeded only by the epoxies.

All of the above comparisons were made at 77 K because, as seen on Fig.1, while the tensile strength in all cases increases between 295 K and 77 K, further cooling to 20 K produces erratic results. This is more clearly illustrated by Fig.5a, which is a histogram illustrating the frequency with which the literature reports a given change in the ultimate tensile strength of glass-epoxy composites upon cooling from room temperature to 77 K and to 20 K. The data are broken down as to lay-up type. Here it is seen that cooling of glass-epoxy composites from 295 K to 77 K can produce a strength increase of from 10–140 k lb in<sup>-2</sup> with a high probability of an increase on the order of 30–60 k lb in<sup>-2</sup>, essentially independent of the type of lay-up. However, on cooling further to 20 K, the probability is for a slight decrease in strength for cloth and 0°/90° crossply reinforced epoxies and a reasonably high probability that uniaxial glass-epoxies will suffer a strength degradation which may be as high as 80 k lb in<sup>-2</sup>. The phenolic, polyester, phenyl silane, and polyurethane-matrix composites all showed a similar erratic behaviour. An exception appeared to be the silicone-matrix composites which showed consistent moderate increases in strength at 20 K. The behaviour at 200 K offers few surprises except for the 181/Adiprene L-100 data<sup>2</sup> which indicate that the strength of this flexible polyurethane composite rapidly increases as temperature is lowered.

As with the tensile strength, the initial tensile modulus (The initial slope of the stress-strain curve in crossply and cloth-reinforced glass composites), Fig.2, shows the expected dependence on fibre orientation. Values range from about 10<sup>7</sup> lb in<sup>-2</sup> for the uniaxial longitudinal lay-ups to 5–6 x 10<sup>6</sup> lb in<sup>-2</sup> for the 0°/90° crossply to 2–5 x 10<sup>6</sup> lb in<sup>-2</sup> for the woven cloth composites. The polybenzimidazole-matrix composites developed much higher moduli than any of the other cloth-reinforced materials at cryogenic temperatures. Also, the glass-cloth phenolic composites are found to have, on the average, slightly higher moduli than glass cloth-epoxies, while glass cloth-polyesters appear as good as the epoxies. The silicone, polyurethane, and Teflon-matrix composites displayed the lowest moduli with an indication that phenyl silane-matrix composites are of intermediate modulus.

Again taking 77 K as a criterion temperature, the uniaxial glass-epoxies showed a modulus range of about 8–11 x 10<sup>6</sup> lb in<sup>-2</sup> with the higher values reflecting variants of S-HTS/Epon 828<sup>66</sup> and Hi-Stren/Resin 2.<sup>4</sup> The 0°/90° crossply data ranged from 3–7 x 10<sup>6</sup> lb in<sup>-2</sup> with values of 5.5–7 x 10<sup>6</sup> lb in<sup>-2</sup> being reported for S-901 glass with a series of epoxy resin formulations.<sup>3</sup> The cloth-reinforced

epoxies yielded moduli from  $2-5 \times 10^6 \text{ lb in}^{-2}$  with the comparatively highest values being reported for 181 glass/Epon 828 formulations.<sup>2</sup>

Although the average moduli of the glass cloth-phenolic composites was higher than that of the epoxies, literature values ranged from  $3-4.7 \times 10^6 \text{ lb in}^{-2}$  which suggests that no significant difference in moduli should be expected for good composites made with either epoxy or phenolic matrices. A detailed look at the glass-cloth polyester data, however, shows a relatively narrow modulus range of about  $3.5-4 \times 10^6 \text{ lb in}^{-2}$  suggesting that the strongest composites made with this polymeric matrix are probably weaker in modulus than the strongest epoxies or phenolics by about  $10^6 \text{ lb in}^{-2}$ . In a similar way, the glass cloth-silicone matrix composites are still weaker having moduli which vary from  $2.5-2.9 \times 10^6 \text{ lb in}^{-2}$  at 77 K. Somewhat fewer moduli data are available for polybenzimidazole, Teflon, polyurethane, and phenyl silane-matrix composites, but that which is available suggests that the Teflon matrix produces moduli of only  $1.6-3 \times 10^6 \text{ lb in}^{-2}$  with  $3.3 \times 10^6 \text{ lb in}^{-2}$  and  $3.6 \times 10^6 \text{ lb in}^{-2}$  for the polyurethane and phenyl silane matrices, respectively. The polybenzimidazole data were obtained with a 181/polybenzimidazole composite<sup>2</sup> and are noteworthy not only for the high average value of  $4.38 \times 10^6 \text{ lb in}^{-2}$  developed at 77 K, but also for the indication of a substantial increase to  $4.9 \times 10^6 \text{ lb in}^{-2}$  at 20 K.

As with the ultimate tensile strength, Fig.2 indicates that the moduli become erratic below 77 K. Reference to Fig.5b shows that, with the exception of a few crossply data, the literature indicates that cooling from 295 K to 77 K will produce a modulus increase of about  $0.3-1.2 \times 10^6 \text{ lb in}^{-2}$  with about  $0.7-0.8 \times 10^6 \text{ lb in}^{-2}$  being most likely. There does not appear to be a strong dependence on lay-up. Results of further cooling to 20 K are more difficult to interpret. In general, the data seem to cluster around a small increase in modulus up to  $0.6 \times 10^6 \text{ lb in}^{-2}$  for cloth reinforcement and suggests that a somewhat larger increase on the order of  $0.6-1.3 \times 10^6 \text{ lb in}^{-2}$  could be expected for crossply and uniaxial composites. Nevertheless, the scatter from  $-0.8 \times 10^6 \text{ lb in}^{-2}$  to  $+3.2 \times 10^6 \text{ lb in}^{-2}$  modulus change is indicative of something erratic occurring below 77 K.

Again, the only surprises in the 200 K data of Fig.2 are the high value of the modulus of the flexible polyurethane Adiprene L-100 compared to the room temperature modulus and the almost equally large increase in the polybenzimidazole data.

### Composite flexure strength and modulus

Flexural tests are frequently used for screening a large number of composites during development studies, as such tests are simple and relatively inexpensive compared to tensile testing. In this application, flexure tests have the added advantage of testing the matrix as well as the reinforcement fibre. Unfortunately, the state of stress is continuously changing throughout the flexure specimen as the test proceeds, which makes engineering interpretation of the data difficult. Consequently, data on flexural strength and moduli are generally considered valid only for establishing relative performance ranking.

Fig.3 shows the flexural strengths of the glass-epoxies to be higher than that observed in tension by approximately

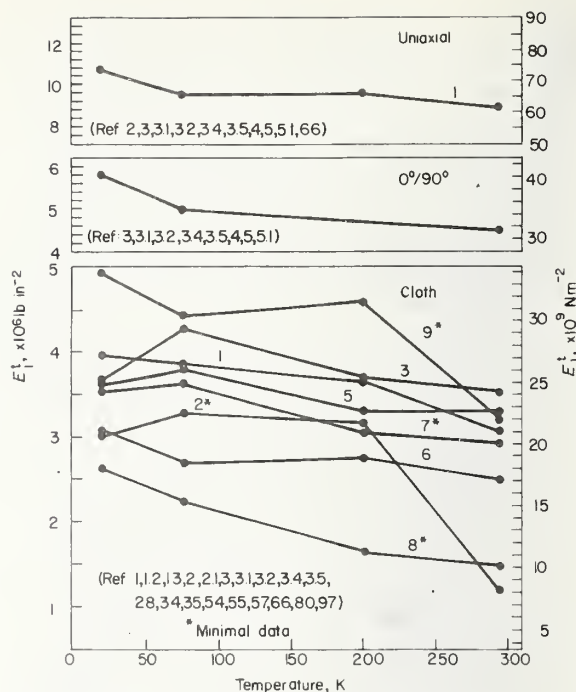


Fig.2 Initial tensile modulus of glass-reinforced composites 1 - epoxy; 2 - polyurethane; 3 - phenolic; 4 - polyimide; 5 - polyester; 6 - silicone; 7 - phenyl silane; 8 - Teflon; 9 - polybenzimidazole

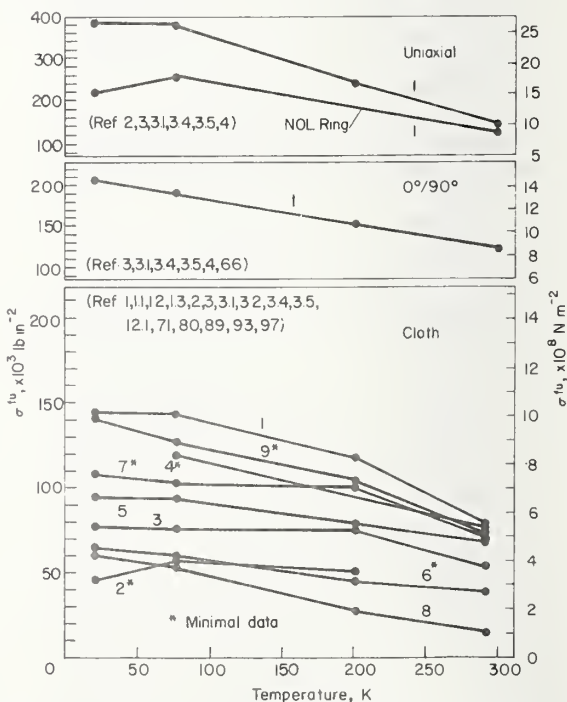


Fig.3 Ultimate flexural strength of glass-reinforced composites 1 - epoxy; 2 - polyurethane; 3 - phenolic; 4 - polyimide; 5 - polyester; 6 - silicone; 7 - phenyl silane; 8 - Teflon; 9 - polybenzimidazole

100 k lb in<sup>-2</sup> k lb in<sup>-2</sup> in the uniaxial specimens and by about 50 in the 0°/90° or cloth lay-ups (verified by comparison of  $\sigma^{tu}$  and  $\sigma^{fu}$  data from the same authors testing the same composites.)

As in the tensile results, the data show the epoxy-matrix composites to be superior in flexural strength at all temperatures, although the polybenzimidazole-matrix composites are almost as good. Among the other matrix types, the agreement with the tensile data is less clear. For those composites for which there are a reasonable number of data, for examples, the polyester, phenolic, and Teflon-matrix types, the strength order is the same at 77 K as it is in tension; however, the relative strength difference bear little relationship to the tensile data. The polyimide and phenyl silane-matrix composites rank near the top in flexural strength, while appearing near the bottom in tension. Conversely, the polyurethane-matrix composite appears good in flexure but poor in tension. However, as the data on the former two composites are based on only one or two references and on a comparison between composites of different authors, caution is necessary in interpreting the results. The polyurethane-matrix data does reflect the same composite tested both in tension and in flexure.<sup>2</sup>

Within the uniaxial data, a separation has been made between data generated from flat flexural specimens and those obtained from curved segments of NOL rings because flexural properties obtained from each type of specimen are distinctly different.

Examining the available flexural strength data in more detail, we find that the flat-specimen uniaxial strength of the glass-epoxies ranged from 325–470 k lb in<sup>-2</sup> at 77 K with the highest values reported for S-901/E-787.<sup>3</sup> A value of 375 k lb in<sup>-2</sup> was reported for S-901/Resin 2.<sup>4</sup> The NOL specimen data were significantly lower, ranging from 200–270 lb in<sup>-2</sup> at 77 K.<sup>4</sup> Flexural strengths varied among the 0°/90° epoxy data from 145–260 k lb in<sup>-2</sup> at 77 K with the highest values again reported in S-901 glass using either E-787 or an experimental epoxy formulation.<sup>3</sup> Data for the cloth-reinforced epoxies showed a spread of 95–175 k lb in<sup>-2</sup>. The highest values were obtained with 1581/E-787, with almost as high values reported for 181 glass in a variation of Epon 826 resin.<sup>2</sup> These were the same composites for which high tensile values were reported.

The glass-phenolic composites ranged from 70–110 k lb in<sup>-2</sup> at 77 K. The highest values were reported for 181/CTL-91-LD.<sup>1</sup> Glass-polybenzimidazole data reflect only the average data with 181 glass reinforcement.<sup>2</sup> The glass-polyesters showed a slightly higher range, 80–127 k lb in<sup>-2</sup> with the highest value reported for 181/Hetron 31.<sup>2</sup> Reported flexural strengths of cloth-reinforced Teflon-matrix composites varied from 30–70 k lb in<sup>-2</sup>, the highest values being developed with 181/FEP.<sup>2</sup>

Following a pattern which is found to repeat itself in all strength properties of glass-polymeric composites, the flexural strengths all initially increased upon cooling from 295 K to 77 K; however, they then changed in erratic ways upon additional cooling to 20 K. Changes in flexural strength during cooling as reported in the literature are summarized on Fig.5c, which shows that the expected strength increase from 295 K to 77 K is about 50–80 k lb in<sup>-2</sup> for crossply and woven-cloth lay-ups. However, strength increases of up to 250 k lb in<sup>-2</sup> have been reported for uniaxial composites, suggesting that the magnitude of the increase is lay-up dependent in flexural strength testing.

A comparison of Fig.5c with that of 5a shows a much greater scatter in the flexural data as compared to the tensile data on cooling to 77 K.

Upon cooling further to 20 K, Fig.5c indicates that one may obtain strength changes varying from –50 k lb in<sup>-2</sup> to +150 k lb in<sup>-2</sup> with a higher probability of a decrease than an increase. The data do not appear to be lay-up sensitive at 20 K.

The flexural modulus data, Fig.4, show a value of about  $8.5 \times 10^6$  lb in<sup>-2</sup> for uniaxial glass-epoxy. This is lower than the average moduli in tension; however, these data reflect only data for a flat specimen of S-901/E-787.<sup>3</sup> A check of the data shows that this specific composite had an initial tensile modulus of only about  $8.8 \times 10^6$  lb in<sup>-2</sup>, which suggests that the two methods are giving about the same answers for the uniaxial case. The same is true for the 0°/90° case, about  $5 \times 10^6$  lb in<sup>-2</sup> being obtained in both the flexural and tensile modes of testing. The cloth-reinforced polymer flexural modulus data range of  $2.3 \times 10^6$  lb in<sup>-2</sup> to about  $5 \times 10^6$  lb in<sup>-2</sup> is also similar to that of the tensile modulus.

Except for the Teflon-matrix showing the lowest modulus, the silicone-matrix showing next lowest, and the polybenzimidazole matrix showing one of the highest, in both tests there appears to be little correlation between the relative modulus ranking in flexure and in tension for the same series of composite types. This is not a condemnation of the flexural test – it may equally well indicate that average data from the literature cannot be used to predict tensile behaviour from flexural data with any degree of reliability.

Examining the flexural modulus data in more detail, we find that the reported 0°/90° crossply glass-epoxy data

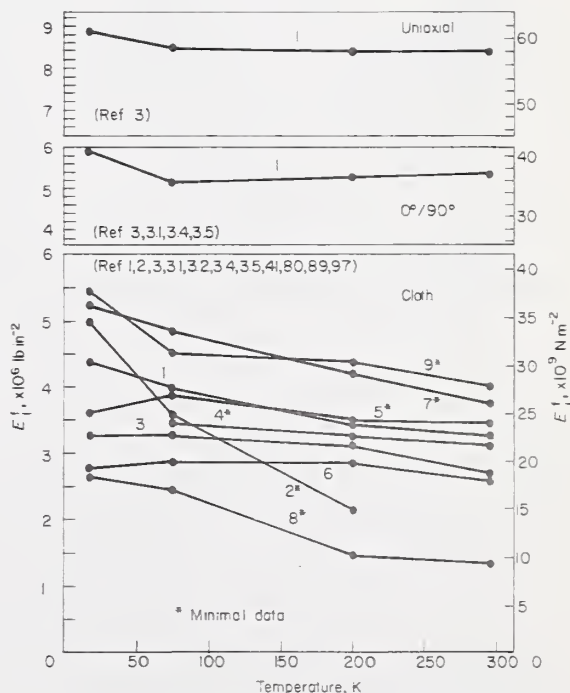


Fig.4 Initial tensile modulus of glass-reinforced composites 1 — epoxy; 2 — polyurethane; 3 — phenolic; 4 — polyimide; 5 — polyester; 6 — silicone; 7 — phenyl silane; 8 — Teflon; 9 — polybenzimidazole

ranged from  $4.6\text{--}5.8 \times 10^6 \text{ lb in}^{-2}$  at 77 K with the highest values appearing for S-901/E-787.<sup>3</sup> Among the cloth-reinforced composites, the epoxy-matrix data varied from  $2.6\text{--}5 \times 10^6 \text{ lb in}^{-2}$  with maximum values reported in 181/Epon 828<sup>1</sup> and in 181 glass with modified Epon 828 resin.<sup>2</sup>

The phenolic-matrix data encompassed  $1.2\text{--}5.3 \times 10^6 \text{ lb in}^{-2}$  at 77 K, the highest values being reported for in Conolon 516.<sup>41,97</sup> The silicone-matrix type composites showed a relatively small spread of  $2.6\text{--}3.2 \times 10^6 \text{ lb in}^{-2}$  at 77 K, the highest value being reported for 181 glass/Trevarno F-131.<sup>2</sup> Among the composites for which fewer data were available, a comparatively high flexural modulus was reported by Chamberlain, et al.<sup>2</sup> for the phenyl silane-matrix composite Narmco 534. These data again show high moduli at all temperatures for 181/polybenzimidazole composites.<sup>2</sup> The polyurethane and polyimide-matrix flexural modulus data reflect only one reference each.<sup>89,2</sup> Again, cooling below 77 K causes the data to become erratic. Fig. 5d summarizes the glass-epoxy flexural modulus data and shows that, while on the average one would expect an increase of about  $0.4 \times 10^6 \text{ lb in}^{-2}$  on cooling to 77 K and a like increase in further cooling to 20 K, one may find changes ranging from  $-0.8$  to  $+2 \times 10^6 \text{ lb in}^{-2}$ . The data suggest that the crossply might be more adversely affected by cooling to 77 K than the cloth-reinforced specimens; however, there are not sufficient data to verify this indication.

### Composite compressive strength and modulus

The compressive strength data discussed herein were obtained by compressing in the fibre direction or, in the case of cloth-reinforced materials, in the plane of the cloth. As most composites are used in fairly thin sheet form, the major problem is one of avoiding failure by column buckling during the test. Problems are further accentuated in the uniaxial longitudinal case, where slight misorientation of the fibres can substantially reduce the compressive strength.

One observes from Fig. 6 that the average of the data reported in the literature for the compressive strength of uniaxial glass-epoxy composites is less than half of the ultimate tensile strength average for the same type composites. Yet, the  $0^\circ/90^\circ$  compressive strength is but slightly lower than its tensile strength, while the cloth-reinforced data span about the same range in compression and in tension. Consideration should thus be given to the possibility that the uniaxial data, and to a lesser extent the  $0^\circ/90^\circ$  data, are lower than the true value due to testing problems.

Among the cloth-reinforced polymers, the epoxy-matrix composites continue to show superiority over all others. Once again, as in the tensile case, the polyurethane-matrix materials indicate a remarkable transformation from an extremely low strength at 295 K to one of the strongest of the group at 77 K. The glass-phenolics continue their reasonably good performance previously noted in the tensile results. The glass-polybenzimidazole appears to rank about average in compressive strength, similar to its performance in tension. The glass-phenyl silanes appear to rank somewhat better in compression than in tension, although few data are available. The glass-polyesters appear to have relatively low compressive strengths, although they were ranked among the top in tension. Finally, the Teflon and silicone-matrix composites display consistently the lowest compressive strengths of all materials surveyed.

Considering the uniaxial compressive strength data in more detail, we found the reported data at 77 K to vary widely from  $100\text{--}240 \text{ k lb in}^{-2}$  with about equal scatter at the other temperatures. This is almost twice the percentage variation found in the uniaxial tensile data even though the latter data were much more extensive. This large scatter very likely reflects the aforementioned problems inherent in compression testing. The highest value reported at 77 K for uniaxial compression was  $237 \text{ k lb in}^{-2}$  in S-901/E-787.<sup>3</sup>

The  $0^\circ/90^\circ$  data showed much less scatter, ranging from  $106\text{--}130 \text{ k lb in}^{-2}$  at 77 K, the highest value reported in biaxially filament-wound S-901 glass in DER 332 epoxy.<sup>3</sup>

Among the glass-reinforced composites, the epoxy-matrix data varied from  $90\text{--}138 \text{ k lb in}^{-2}$  at 77 K with the highest value reported for a modified 181/Epon 828 composite.<sup>2</sup> Glass-phenolic properties covered a range of  $60\text{--}100 \text{ k lb in}^{-2}$  at 77 K, distinctly lower than those of the epoxies. The highest value was reported for 181/Narmco 506.<sup>1</sup> The polyester-matrix composites were by comparison, still another notch down in strength with a  $35\text{--}68 \text{ k lb in}^{-2}$  showing at 77 K, the highest compressive strengths being reported for 181 glass with Hetron 31 or Narmco 527 resin.<sup>2</sup> The  $19\text{--}40 \text{ k lb in}^{-2}$  range of the glass-silicones and the  $25\text{--}40 \text{ k lb in}^{-2}$  range of the glass-Teflons at 77 K leaves little doubt of the weakness of the latter composite types in compression. The data for polyurethane, polybenzimidazole, and phenyl silane-matrix composites reflect the work of Chamberlain et al.<sup>2</sup>

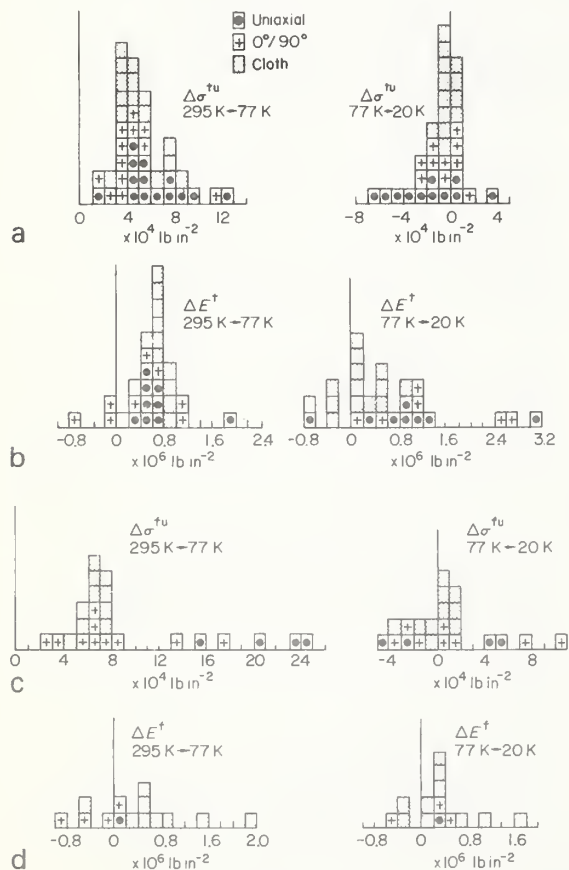


Fig. 5 Histogram illustrating changes in tensile and flexural properties of glass-epoxy composites upon cooling

As with tensile and flexural properties, cooling below 77 K produces somewhat erratic results in compression. The 200 K data appear to be in line except for the glass-Teflon composite for which cooling to 200 K had no apparent effect.

No uniaxial or 0°/90° data were available at cryogenic temperatures for compressive moduli. In theory, compressive modulus of any perfectly elastic body should equal the tensile modulus. Thus, we find that the average values among the cloth-reinforced polymers which appear in Fig. 7 bear a striking resemblance to the tensile modulus data. Again, the phenolic-matrix composites had highest values with the epoxy-matrix next highest. Teflon-matrices were clearly the weakest with the polyurethanes starting out equally low in modulus but again rapidly increasing its value to the middle of the group. The silicone-matrices were again on the low modulus side. The only significant change from the tensile modulus ranking is the somewhat lower value of the polyester and polybenzimidazole-matrix composites in compression.

The phenolic composites ranged from 4–8.4 × 10<sup>6</sup> lb in<sup>-2</sup> in compression modulus at 77 K, maximum value being reported for 181/CTL-91-LD.<sup>1</sup> The glass-epoxy data showed much less scatter at 77 K ranging from 4–5.15 × 10<sup>6</sup> lb in<sup>-2</sup>. The highest reported value for 181 glass/modified Epon 826 composite.<sup>2</sup> The phenyl silane and polyurethane data reflects only the values for Narmco 534 and 181/Adiprene L-100, respectively.<sup>2</sup> Somewhat more compressive moduli data were available for glass-polyester composites, values ranging from 2.5–4.3 × 10<sup>6</sup> lb in<sup>-2</sup> at 77 K with highest values for 181/Polyester C.<sup>66</sup> The silicones not only averaged about like the polyesters but had about the same spread in 77 K values at 2.3–4.6 × 10<sup>6</sup> lb in<sup>-2</sup>. The data on

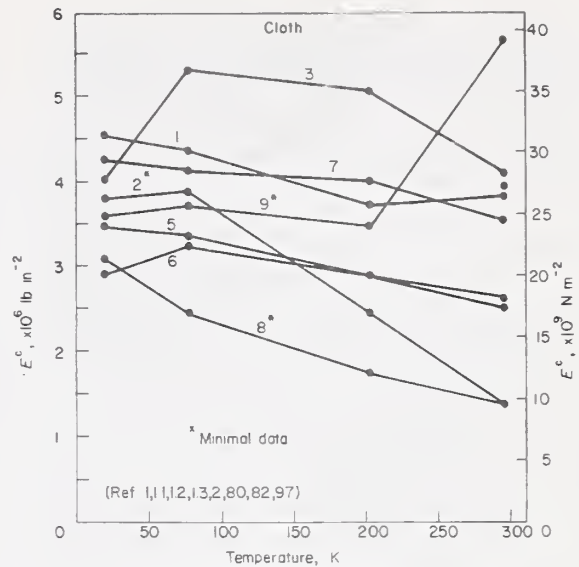


Fig. 7 Compressive modulus of glass-reinforced composites  
1 — epoxy; 2 — polyurethane; 3 — phenolic; 4 — polyimide;  
5 — polyester; 6 — silicone; 7 — phenyl silane; 8 — Teflon;  
9 — polybenzimidazole

glass-Teflon and glass-polybenzimidazole composites were provided by Chamberlain et al.<sup>2</sup> In contrast to its tensile modulus behaviour, the 181 glass/polybenzimidazole composite shows a sharp decline in both compressive strength and modulus on cooling from 295 K to 77 K. This is suggestive of experimental errors.

#### Composite interlaminar shear strength

Interlaminar shear strength is a property unique to composites; it is the resistance to shearing in the plane of the fibre reinforcement. It is believed to strongly affect structural integrity, particularly in compression loading. Like the flexural test, the results of interlaminar shear tests evaluate several composite parameters, including resin strength, resin-fibre bond strength, filament distribution, and matrix porosity. As such, interlaminar shear joins the flexure test in being a valuable indication of overall composite quality but providing little data directly useful in engineering calculations. Its most valuable application may well be in quality control during composite manufacture.

Nevertheless, it is of interest to consider the published values for interlaminar shear, if for no other reason than to compare the results obtained with the different methods. Interlaminar shear is usually measured either by the guillotine method in which interlaminar shear is forced by the imposition of opposing but offset cuts in a flat tensile specimen, or by a dimensional modification of the flat flexural specimen so as to force failure by shear on the central layers of the composite (short-beam shear). Of the two methods, the latter is most widely used. Unfortunately, the results obtained by the two methods are not comparable, the short-beam test usually yielding values higher than that of the guillotine. The overall situation is made still more complex by the understandable desire of some investigators to obtain interlaminar shear data from filament-wound composites prepared by the NOL ring method in which case the flexural method must be used with a short section of the ring. Because the specimen is not flat, the

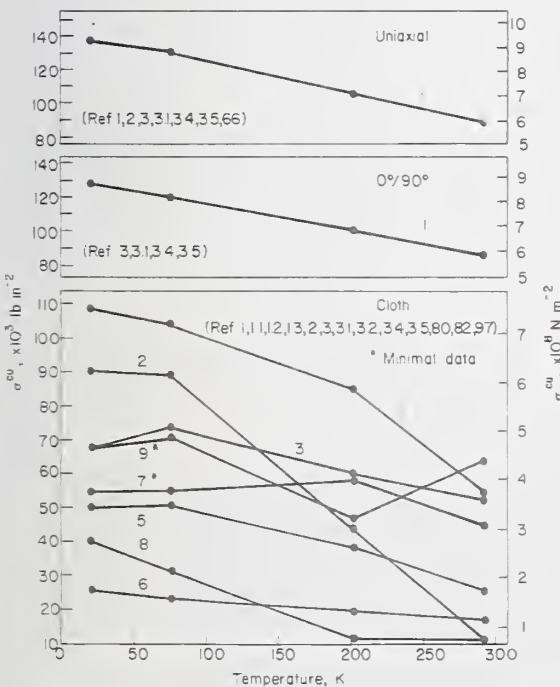


Fig. 6 Ultimate compressive strength of glass-reinforced composites  
1 — epoxy; 2 — polyurethane; 3 — phenolic; 4 — polyimide;  
5 — polyester; 6 — silicone; 7 — phenyl silane; 8 — Teflon;  
9 — polybenzimidazole

results are not comparable to either of the above methods. It is for this reason that the interlaminar data appearing on Fig.8 have been separated according to the various test methods.

The largest discrepancy is observed for the uniaxial composites, the values obtained by the NOL short-beam method being much higher than those in conventional short-beam or guillotine methods. It is obvious from Fig.8 that one must be very cautious in comparing interlaminar shear values published in the literature. In interpreting these kind of data, it is also necessary to take into consideration that the very high values developed in the NOL short-beam test may also reflect the generally lower void content in filament-wound composites as compared to vacuum-bagged or autoclave-cured flat lay-ups.

In the case of crossply or cloth laminates, only the conventional short-beam flexure test or the guillotine test may be used. Fig.8 shows that the results of these two test methods are in reasonably close agreement for the 0°/90° crossply lay-ups, while the cloth-reinforced composites show lower values for the guillotine as compared to the short-beam test mode. The same is true for the uniaxial lay-ups tested by these two methods.

The variety of test methods used and the variety of different epoxy matrices which have been evaluated make it almost an exercise in futility to attempt to identify those composite types which have the highest values of interlaminar shear. The S-901/E-787 composite reported by Toth et al<sup>3</sup> at 14.7 k lb in<sup>-2</sup> (77 K) in short-beam flexure has shear strength almost as high as those reported for the NOL short-beam test. The same composite also developed high values of interlaminar shear when tested by the same author in a 0°/90° biaxially-filament-wound lay-up. Other composites which appeared to have relatively high values of interlaminar shear among their group were S-901 glass in an experimental resin Epon 826/Empol 1040/Z-6077/DSA/BDMA<sup>5</sup> in NOL short-beam and a 0°/90° lay-up of Hi-Stren glass in Epon 828/LP-3/Cure agent D resin in conventional short-beam shear.<sup>4</sup> The data indicate that Resin 2 provides somewhat lower interlaminar shear strength than does E-787; for example, Soffer<sup>5</sup> reports a value of 9.3 k lb in<sup>-2</sup> for S-901/Resin 2 in short-beam shear of flat specimens at 77 K and 14.1 k lb in<sup>-2</sup> for the same composite in NOL short-beam shear.

Ignoring the NOL flexure data, one observes on Fig.8 that the interlaminar shear values are the highest for the cloth-reinforced composites and lowest for the 0°/90° crossplies with the uniaxial lay-ups in between. The relatively high values for the cloth composites probably reflect the added shear resistance provided by the convolutions in the woven glass cloth. By similar reasoning, the uniaxial composites may develop higher interlaminar strengths than the 0°/90° crossplies simply because the former provides no distinct lamella along which shear can propagate.

Again, in a repetition bordering on monotonous, the interlaminar shear strength is found to become erratic upon cooling from 77 K to 20 K, while the 200 K properties appear to be as expected.

#### Composite ultimate tensile strain

In view of the high strength of the glass-polymeric composites coupled with their relatively low modulus and absence of significant plastic flow at rupture, it might be expected

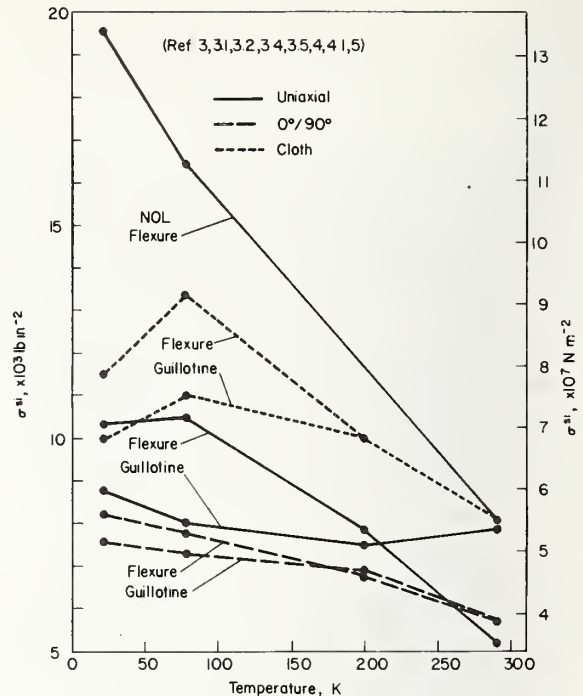


Fig.8 Interlaminar shear strength of glass-epoxy composites

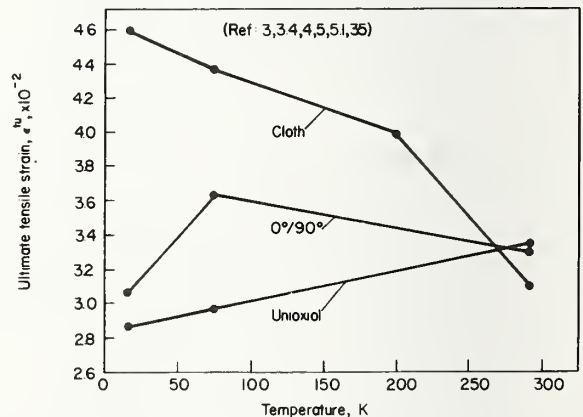


Fig.9 Ultimate tensile strain of glass-epoxy composites

that the strains accommodated at fracture would be somewhat larger than those of the higher-modulus advanced composites. This is substantiated by Fig.9 on which it is seen that ultimate tensile strains are in the 10<sup>-2</sup> range for glass reinforcement while, as we shall see in the second part of this review, similar data for the advanced composites are in the 10<sup>-6</sup> range.

This relatively high fracture strain is, of course, a direct reflection of the high fracture strain of the glass reinforcement. This has some interesting consequences because, while the fracture strain of some polymeric matrix materials may approach that of glass at 295 K, the ductility of almost

all polymers falls drastically upon cooling to cryogenic temperatures with the result that at low temperatures, fracturing the matrix occurs well before fracture of the glass fibres.<sup>6</sup> A dramatic example of this phenomenon is found during proof testing of filament-wound pressure vessels where the cracking of the polymeric matrix is very audible. It is surprising that, at least in the case of hydrostatically loaded pressure vessels, such rupturing of the matrix does not decrease the overall rupture strength of the tanks and may even produce an increase. One must emphasize, however that this does *not* imply that fracturing of the matrix is always acceptable or that it may be tolerated in other structures.

Fig.9 indicates that at 295 K, the average fracture strain will be similar for uniaxial, 0°/90° and woven-cloth glass-epoxy composites, the strains being on the order of  $3.2 \times 10^{-2}$ . On cooling, however, marked differences develop between the lay-up types. Ultimate tensile strains in the uniaxial composites (tested in the longitudinal direction) decreased upon cooling to 77 K while cooling the 0°/90° and cloth lay-ups resulted in increased fracture strain. Detailed examination of the data shows this to be a true behaviour, as five of the six composites forming the uniaxial data showed the decline (the exception being S-901/E-787<sup>3</sup>) while all eight of the 0°/90° and all three of the cloth composite types showed substantial increases upon cooling to 77 K.

Again, considering 77 K as a reference temperature, the uniaxial data were found to range from  $1.9-5.3 \times 10^{-2}$ , the highest being the previously noted work of Toth et al.<sup>3</sup> The data of Toth is somewhat suspect, as it is the only data reporting an increase in tensile strain upon cooling.

Among the 0°/90° crossply data, values showed a relatively narrow spread of  $3.2-4.5 \times 10^{-2}$ , the S-901/E-787 composite again showing the highest fracture strain.<sup>3</sup> A value of  $4.3 \times 10^{-2}$  was reported for Resin 2.<sup>5</sup> Cloth-reinforced data ranged from  $3.5-5 \times 10^{-2}$ , the highest ultimate tensile strain being reported for 1581/E-787.<sup>3</sup>

Data on strain to fracture at cryogenic temperatures are rare for other than the epoxy-matrix types. Kerlin et al<sup>64,65</sup> have reported a fracture strain of  $2.75 \times 10^{-2}$  for a Selection 5003 glass-cloth polyester composite at the same temperature. Also, Toth et al<sup>3</sup> have reported  $5.3 \times 10^{-2}$  for a crossply glass-polyester composite Selection 5003.

### Static fatigue of composites

Under sustained room temperature loading, glass filaments have been found to deteriorate and fracture when subjected to stresses substantially below that of their normal ultimate tensile strength. As such, the failure is analogous to stress corrosion in metals. Some published data indicate that glass-filament-wound pressure vessels may undergo similar deterioration,<sup>99</sup> although some indication has also been obtained that static fatigue of glass-reinforced composites may pose less of a problem at cryogenic temperature than at 295 K.<sup>66</sup> Static fatigue will be an important factor in any composite used in superconducting motors and generators and, in view of the minimal data presently available, further studies are needed to clarify the magnitude of the problem and to select formulations providing utmost resistance to such failure at cryogenic temperatures. T.T. Chiao of the Lawrence Livermore Laboratories is currently dir-

ecting an extensive static fatigue programme at room temperature on dead-weight loaded filaments coated with resin. As this latter method tests a basic structural element of the composite and permits many specimens to be run concomitantly, it should provide a useful and relatively inexpensive method of evaluating static fatigue at cryogenic temperatures.

### Composite bearing yield strength

Bearing yield strength is a test designed to determine bearing stress as a function of the deformation of a hole through the composite. The load is applied by a pin inserted into the hole. The intent of the test is to provide information on the stress that may be sustained across riveted or bolted joints without loosening the joint. Bearing yield strength is defined as that stress on the stress-strain curve which corresponds to a distance of 4% of the bearing hole diameter when measured from the intersection of a line tangent to the stress-strain curve at this point and the zero load axis (see insert, Fig.10).

Bearing yield strengths for a series of epoxy-matrix composites have been reported by Toth et al<sup>3</sup> while Chamberlain et al<sup>2</sup> have provided data on silicone, polyurethane, and phenyl silane-matrix composites. These data are summarized on Fig.10.

The glass-epoxy composites developed bearing yield strengths which increased from about 50 k lb in<sup>-2</sup> at 295 K to 70-75 k lb in<sup>-2</sup> at 77-20 K. The uniaxial and 0°/90° data were very similar, while the cloth-reinforced epoxies were lower at 295 K and at 200 K but increased their strength to equal that of the others at 77 K.

Data on the other matrix types were only available for cloth reinforcements. The phenyl silane composite developed a bearing strength equal to that of the epoxies, while the

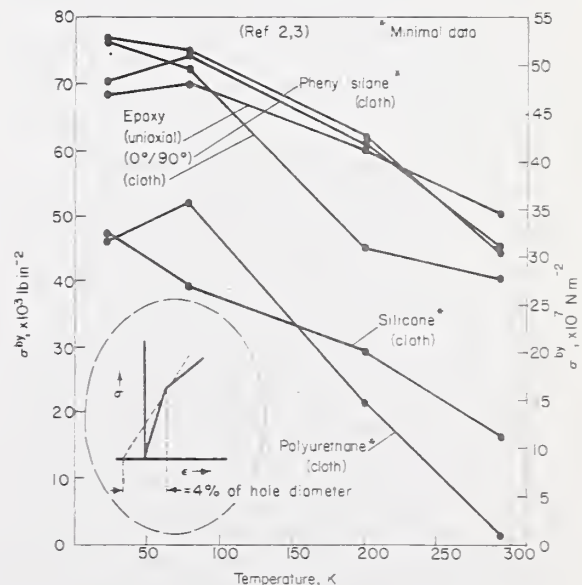


Fig.10 Bearing yield strength of glass-reinforced composites

silicone and polyurethane-matrix materials were distinctly inferior.

Again, there is indication of erratic behaviour on cooling from 77 K to 20 K.

### Cyclic fatigue of composites

Cyclic fatigue of glass-reinforced composites at cryogenic temperatures has been studied by Brink et al <sup>1</sup> and by Chamberlain et al <sup>2</sup> in tension and by Fontana et al <sup>34</sup> using a reciprocating beam. Lavengood and Anderson <sup>70</sup> have contributed data on torsional fatigue. The data are not extensive, reflecting the very high cost of generating complete *S-N* curves at cryogenic temperatures. Yet, such testing is mandatory to provide assurance that composite components will fulfill their life expectancy in such applications as rotating cryogenic machinery. Every effort must therefore be made to restrict such testing to composites which have the best chance of developing superior fatigue properties. The data reviewed herein provide some sense of direction; however, there remains an urgent need for some type of relatively inexpensive screening test which will permit relative ranking of composite cyclic fatigue performance at cryogenic temperatures.

In comparison to that of the advanced composites or to many conventional alloys, the dynamic fatigue properties of glass-reinforced composites are relatively poor. This is primarily due to the fatigue behaviour of glass-polymeric materials being controlled by the properties of the matrix. Even at room temperature, the strain accommodation of the most epoxy resins is less than that of the glass reinforcement, and as it is the latter which controls the ultimate strength of the composite, cracking of the matrix will occur at ultimate loads far below the composite ultimate strength, allowing corrodents to attack the glass. In crossply lay-ups, such cracking may occur at stress levels as low as 20% of the ultimate composite strength.

Lavengood has pointed out that since fatigue life of a glass-reinforced composite is related to the strain capability of the matrix, embrittlement of the matrix due to lowering of the temperature should lower the fatigue life. However, this is not always experimentally verified. Based on an analysis of experimental torsional fatigue data, Lavengood concluded that fatigue life at cryogenic temperatures is strongly affected by the composite interfacial stress which arises due to differential thermal contractions of the filament and the matrix. Cooling a composite increases the compressive forces at the interface and improves fatigue life. Where fatigue strains serve to increase the compressive interfacial stresses, the fatigue life may further increase, the reverse being true when strains decrease the interfacial stress.

The published tensile-fatigue data of Brink <sup>1</sup> and Chamberlain <sup>2</sup> and their co-workers were, with one exception, obtained on 181 cloth-reinforced composites. As an initial criteria, composites were screened by testing at 30% of their ultimate tensile strength developed at 295 K and 77 K. Those composites failing to achieve 10<sup>6</sup> cycles were dropped while those which were successful were further tested at 200 K and 20 K. The conventional polyester-matrix composites 181/Hetron 92, 181/Hetron H-31, 181/paraplex P-43, and 181/Narmco 527 were unsuccessful as was the silicone-matrix composite 181/Trevarno F-131.

It is beyond the scope of the present task to comprehensively review these data for which the reader may refer to the

original references. However, in order to provide the reader with a sense of the fatigue performance of glass-polymeric composites, we have prepared Fig.11 from the data of Brink <sup>1</sup> and Chamberlain.<sup>2</sup> This figure presents the fatigue strength of the various successful materials as a function of temperature after 10<sup>6</sup> fatigue cycles, the maximum studied in this work. It is also instructive to know the percent of the relevant ultimate strength retained by each composite type at each temperature after 10<sup>6</sup> cycles; consequently, these data also appear on Fig.11.

Fig.11 shows that the absolute magnitude of the stress required to induce fatigue failure at 10<sup>6</sup> cycles generally increases with decreasing temperature for all materials studied, only the high-temperature polyesters (Laminac 4232 and Vibrin 135) and perhaps the silicones (Narmco 513 and Trevarno F-130) not showing an appreciable increase below 200 K. At all temperatures, these data show that the polybenzimidazole composite demonstrated comparatively superior fatigue performance both in terms of absolute retained tensile strength after 10<sup>6</sup> cycles and in the percentage of the original strength retained. The epoxies also looked comparatively good, but primarily because of their somewhat higher initial strength – their percentage retention of strength was among the lowest of the group. The highest values were reported for Epon 828/DDS.<sup>2</sup> The polyurethane, phenyl silane, and phenolic-matrix composites appeared to group into an intermediate performance class while the polyester, silicone, and Teflon-matrix composites showed distinctly lower fatigue properties. Data at 77 K only were available for a Scotchply 1002 uniaxial glass-epoxy composite,<sup>2</sup> which Fig.11 shows to have a much higher strength after 10<sup>6</sup> fatigue cycles at 77 K than any of the cloth-reinforced types; nevertheless, even this composite showed retention of only about 52% of its original strength at that temperature.

Does the data indicate the existence of a stress limit below which fatigue life is essentially infinite? In most cases, testing was not carried out to a sufficiently large number of

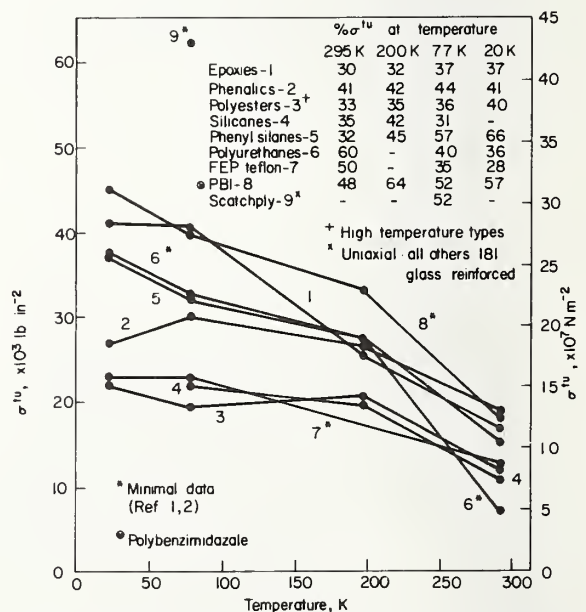


Fig.11 Cyclic tensile fatigue strength of glass-reinforced composites after 10<sup>6</sup> cycles

cycles to answer this question. However, judging from the shapes of the  $S-N$  curves developed with 181/Epon 1001 by Brink,<sup>1</sup> it appears that this glass-epoxy formulation may reach such a limit at about 30 k lb in<sup>-2</sup> for temperatures below 77 K (~30% UTS). Conversely, the  $S-N$  curve for the 181/Epon 828 composite showed no indication of flattening out at 10<sup>6</sup> cycles. With the possible exception of the silicone-resin composites, 181/Narmco 513 and 181/Trevarno F-130, there was no evidence that cooling the composites had any effect on establishment of a fatigue limit where none was evident in the room temperature data.

Again, one notices an apparent tendency for the data to become erratic when cooling from 77 K to 20 K.

#### Impact strength and fracture toughness of composites

Impact strength and its more sophisticated partner, fracture toughness, are measures of the amount of energy which can be stored in a structure before the energy is released by fracture. As it is only in recent years that fracture mechanics has been put on solid theoretical grounds and exploited in homogeneous metals, it is not strange to find that application of parallel concepts to composites is still in its infancy. Furthermore, there is a major problem in applying basic principles of fracture mechanics to composites where, in most cases, multiple cracking occurs so that a unique 'crack length' cannot be defined.

Measurement of the energy required to fracture specimens, the impact test, is the most simple method of obtaining data on relative material toughness. Such tests show the glass-reinforced composites to have much greater toughness than do the advanced composites, probably reflecting the much larger strain-accommodation of glass filaments in

comparison to the advanced fibre reinforcements. Unfortunately, the literature contains few low temperature data even on this simple parameter and those which are available are impossible to systematize due to differing test methods, specimen design, and filament orientation. Lewis and Bush<sup>4</sup> have evaluated a series of epoxies and modified epoxies reinforced with Hi-Stren glass using the Izod impact method. For unidirectional composites, they find the 295 K impact strength to vary from 82–128 ft lb in<sup>-1</sup> of notch. On cooling to 77 K, the measured values ranged from 67–162 ft lb in<sup>-1</sup>, some formulations showing 45% increase in impact strength, while others showed as much as a 26% decline. A 0°/90° crossply test with the same composite formulations yielded room temperature impact strengths from 49–96 ft lb in<sup>-1</sup> and 77 K values of 59–76 ft lb in<sup>-1</sup> with strength changes ranging from +36% to -26%, no consistent behaviour being shown by any specific composite formulation. Data published by other authors,<sup>71,80,103,109,110</sup> are equally confusing. Perhaps part of the answer is provided by Levin<sup>71</sup> who followed the change in impact strength of glass-phenolic and glass-epoxy specimens at closely spaced intervals from 295 K to 77 K and found that the impact properties peaked sharply at about -30°C followed by a rapid decline at lower temperatures. If the impact properties are indeed such a rapidly changing function of temperature, it might account for the lack of systematic change noted in data taken only at two or three temperatures. Clearly, this is an area which must be given more attention in the future if composite behaviour at cryogenic temperatures is to be understood well.

#### Thermal properties

##### Thermal contraction of composites

All of the glass-reinforced polymers contract when cooled. As we wish to review the behaviour of such composites on cooling from 295 K, the data have been plotted as thermal contraction, avoiding negative values of  $\Delta L/L$ .

Thermal contraction is very dependent on the type of composite lay-up as well as on the orientation of the composite. Figs 12 and 13, therefore, present data on values obtained normal and parallel to the fibre reinforcement for uniaxial, 0°/90° crossply and cloth lay-ups. Other factors affecting thermal contraction are the specific resin used and the composite fibre density.

The thermal contraction is always found to be higher in a direction normal to the fibres than in the fibre plane, the difference increasing as the temperature is lowered. This reflects the much higher thermal contraction of the polymer as compared to the glass reinforcement. This is very evident in the data for uniaxial epoxy-matrix composites, where at 20 K the thermal contraction normal to the fibres varies from about 2.5 to 5 times that in the fibre direction at 20 K. An apparent anomaly appears in the 0°/90° crossply data, which shows a remarkably small difference in contraction between these two directions. This occurs because, in a filament-wound crossply composite, each layer of glass is in close proximity to the orthogonal layer next to it and thus provides resistance to dimensional change in the thickness direction. This effect is much less evident in the cloth lay-ups because the latter are prepared by methods which produce a much lower filament density than is obtained in filament winding.

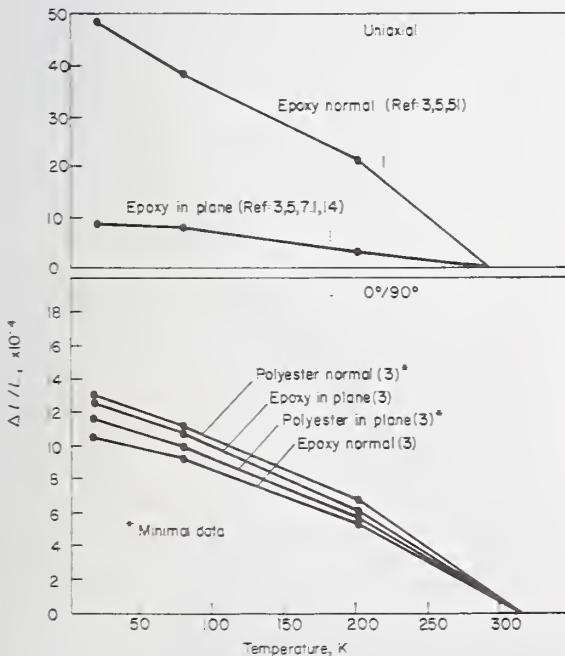


Fig. 12 Thermal contraction of glass-fibre reinforced composites

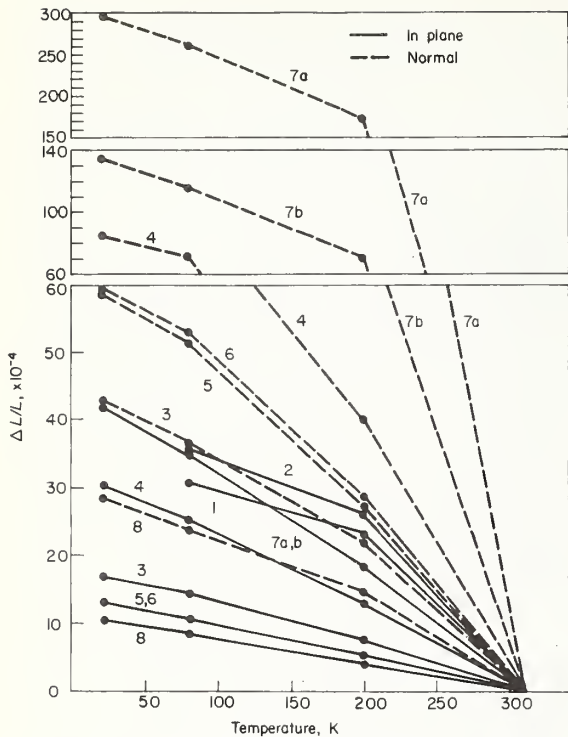


Fig. 13 Thermal contraction of glass-cloth reinforced composites 1 — epoxy<sup>85,101</sup>; 2 — polyurethane<sup>85</sup>; 3 — phenolic<sup>14</sup>; 6 — phenyl silane<sup>14</sup>; 7a — Teflon FFE<sup>14</sup>; 7b — Teflon FEP<sup>80</sup>; 8 — polybenzimidazole<sup>16</sup>

As the thermal contraction of the composite is dominated by the properties of the polymeric matrix on cooling, one might anticipate considerable variation in contraction even within a given matrix type, reflecting, for example, the effect of additives to epoxy resins. This is found to be true; for example, the  $\Delta L/L_0$  data for epoxy matrix composites varied from  $20\text{--}75 \times 10^{-4}$  in the thickness direction and from  $4.4\text{--}11.5 \times 10^{-4}$  in the fibre direction. In the  $0^\circ/90^\circ$  lay-ups, the epoxy composites showed variations of  $5.1\text{--}13.8 \times 10^{-4}$  in thickness and  $9.2\text{--}13 \times 10^{-4}$  in the fibre direction. The polyester resins gave similar data spread in the  $0^\circ/90^\circ$  lay-ups.

A much greater variation is observed in the thermal contraction among cloth-reinforced composites, reflecting both the larger variety of matrix materials for which data are available and the greater variation in fabrication method. The glass-Teflon composites have the highest thermal contractions of all the materials examined. Furthermore, the Teflon matrix may be either of the TFE or FEP type which have markedly differing thermal contraction characteristics. This difference does not appreciably affect contraction in the fibre plane due to the restraint provided by the fibres. However, the difference is marked in the direction normal to the fibres. As indicated by the dashed curves 7a and 7b on Fig. 13, the TFE-matrix composites have twice the transverse thermal contraction of the FEP-matrix types.

The epoxy and the polyurethane-matrix composites also have relatively high thermal contractions. Unfortunately, no data were available in the fibre normal directions for these composites. The data indicate that the polyester-matrix

composites are next in decreasing order of thermal contraction, with the fibre normal data being approximately 2.8 times greater than in the fibre plane. Showing the least thermal expansion in the fibre plane are the phenolic, silicone, phenyl silane, and polybenzimidazole-matrix composites. Of these, the phenolic composite data appear to be abnormally high for the fibre normal case, since, if all else were equal, the order in the fibre normal direction should follow that in the fibre plane.

All of the polymeric matrices create compressive stresses in the glass reinforcement upon cooling to cryogenic temperatures, such stresses being added to those already existing from cooling from the cure temperature to room temperature. This is primarily manifested as shear stress at the resin-fibre interface, so that it might be expected that an effect would be seen on those strength properties which are sensitive to debonding of the matrix-glass interface. One such property is fatigue, and from Fig. 11, it is noted that the fatigue properties of the Teflon-matrix composites are poor, while that for the polybenzimidazole is good, consistent with the respectively high and low thermal expansion of these two composite types. A similar relationship holds for the flexural strength, Fig. 3. Interfacial residual stress is but one of the factors influencing fibre debonding, others being the ability of the interface to sustain a shear load and the strength of the matrix itself.

#### Specific heat of composites

The specific heats of glass-reinforced composites show an almost linear dependence on temperature from 295 K to 77 K, and relatively small difference between matrix types. The specific heats are relatively high compared to most metals, being roughly comparable to that of aluminium but substantially above that of titanium, iron, or copper. Teflon and polyester-matrix composites have the highest specific heat. The epoxy, polybenzimidazole, silicone, and phenolic-matrix composites are bunched on the lower specific heat side of the group. The phenyl silane-matrix composite seems

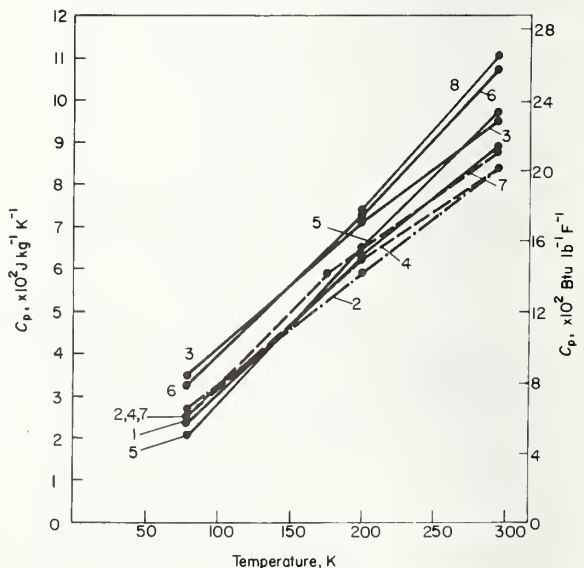


Fig. 14 Specific heat of glass-reinforced composites 1 — Epoxies<sup>15,16</sup>; 2 — phenolics<sup>15</sup>; 3 — polyester<sup>15</sup>; 4 — silicones<sup>15</sup>; 5 — phenyl silanes<sup>15</sup>; 6 — Teflon<sup>15</sup>; 7 — polybenzimidazole<sup>16</sup>; 8 — phenyl formaldehydes<sup>72</sup>

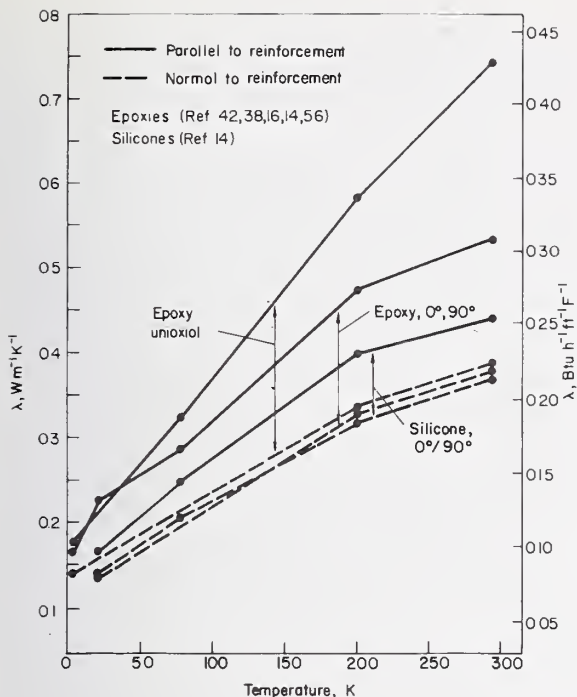


Fig. 15 Thermal conductivity of glass-fibre reinforced composites

to have a slightly larger temperature dependence, starting out in the middle of the group at 295 K, but showing the lowest specific heat at 77 K.

The data reflect the work of Campbell et al <sup>15,16</sup> with the sole exception of the phenyl formaldehyde contribution of Luikov.<sup>72</sup> Except for the epoxyes, the data reflect only one composite for each type of matrix. The epoxy data reflect the average of three compositions: a unidirectional and a crossply YM-31-A/DER-332 and a unidirectional S-994/E-787 composite. The spread in specific heat values for these three formulations at 295 K, 200 K, and 77 K was 8.16–9.21, 6.07–6.7, and 2.09–2.72 x 10<sup>-2</sup> J g<sup>-1</sup> K<sup>-1</sup>, respectively, with the highest value associated with the S-994/E-787 composite.

#### Thermal conductivity of composites

Thermal conductivity is also an important parameter in cryogenic design. Unfortunately, improper experimental technique invalidates some of the data in the literature; primarily, failure to properly compensate for radiation losses, which can introduce errors approaching 100–200% in the higher temperature ranges. Figs 15 and 16 presents what the author believes to be valid data.

As with thermal contraction, conductivity is dependent on the type of lay-up and on the orientation of the composite. Figs 15 and 16 therefore present data on values obtained normal to the fibre reinforcement (thickness direction) and in the plane of the reinforcement for uniaxial, 0°/90° crossply and for woven-glass cloth lay-ups. Also, as with contraction, the thermal conductivities are affected by the type of matrix resin, necessitating a differentiation on this basis in the figures.

Unlike the other thermal properties of composites, the thermal conductivity is affected by the ambient atmosphere in which the measurement is made, that is it differs in helium, nitrogen, or in vacuum. The literature indicates that, compared to values obtained in helium, data taken in nitrogen will average 7% lower, while in a vacuum the data will, on the average, be lowered 20%. Campbell et al <sup>16</sup> suggests that the lower value in vacuum primarily reflects the difficulty of obtaining good contact between the composite specimen and the mating parts of the thermal conductivity apparatus when operating in a vacuum. An ambient atmosphere of nitrogen or helium increases the measured conductivity by reducing the contact resistance; however, diffusion of the gas (particularly of helium) into pores within the composite also contributes to an increase as the gas provides an overall improvement in the thermal path within the composite. This explanation is consistent with the effect of different ambient atmospheres being observed over the entire 20–295 K temperature range. The present author believes, however, that consideration should also be given to the effect of matrix cracking at very low temperatures which should act to increase the difference between values measured in the various ambient media. The data appearing in Figs 15 and 16 are averages of data taken in all three media.

The difference between the fibre normal and the in-plane conductivities for a given composite and the absolute spread of conductivity values among the various composite classes is widest at room temperature, converging as the temperature is lowered, consistent with a theoretical zero value for conductivity at absolute zero temperature. The conductivity at 20 K varies from 30–50% of that at room temper-

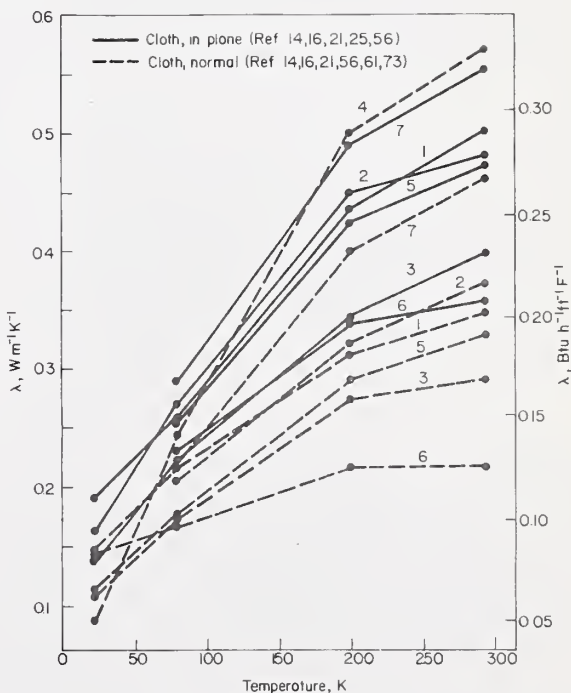


Fig. 16 Thermal conductivity of glass-cloth reinforced composites  
1 – epoxyes; 2 – phenolics; 3 – polyesters; 4 – silicones;  
5 – phenyl silanes; 6 – Teflons; 7 – polybenzimidazoles

ature for most of the composites. Exceptions are the cloth-reinforced silicones, curve 4, Fig.16, in which the 20 K value was only 15% of that at 295 K and the cloth-reinforced Teflon, curve 6, Fig.16, for which the 20 K value was reported to be 70% of the 295 K value, both of these exceptions being for the fibre normal direction.

Fig.15 contains data for uniaxial and  $0^\circ/90^\circ$  epoxy lay-ups and for a  $0^\circ/90^\circ$  silicone-matrix lay-up. The highest thermal conductivity was for the filament-wound uniaxial epoxy composite in the plane of the fibre. This is to be expected from the high density of continuous glass fibres in that direction. The conductivity in the fibre normal direction is 25–50% less, reflecting the lower thermal conductivity of the matrix. Thermal conductivity in the fibre plane of the  $0^\circ/90^\circ$  epoxy lay-up is only about 80% of that for the uniaxial composite, reflecting the lower effective fibre density in the direction of the heat flow.

Fig.15 shows the  $0^\circ/90^\circ$  silicone-matrix composite to have a substantially lower in-plane conductivity than the  $0^\circ/90^\circ$  epoxy lay-up. This does not imply that the conductivity of the silicone matrix is less than that of the epoxy; indeed, the marked similarity between the fibre normal data for both polymeric matrices indicates that the matrix conductivity is very similar in both materials. The difference reflects the relatively inferior heat transfer properties of glass roving (fibre bundles) which was used for the silicone-matrix composite as compared to the continuous filament used with the epoxy.

Among the cloth-reinforced composites, the highest thermal conductivity was found for the silicone-matrix composites. Only fibre normal data were available; however, even in this least conducting orientation, the conductivity exceeded that of all the other materials in their more favourable in-plane direction. The polybenzimidazole composite was next lowest, and in decreasing order were the epoxies, phenolics, and phenyl silanes, all with approximately equal conductivities, both in-plane and plane normal. The lowest conductivities were evidenced by the polyesters and the Teflons.

The only composites for which there was more than one literature reference were the epoxies. For the latter, the data spread was found to be much greater for the in-plane conductivity than for the plane normal, as would be expected in view of the relatively high conductivity of the fibres compared to the matrix. As an example, the data which averaged  $0.50 \text{ W m}^{-1} \text{ K}^{-1}$  for the 295 K cloth-reinforced epoxy ranged from  $0.30$  to  $0.65 \text{ W m}^{-1} \text{ K}^{-1}$ , while the plane normal data for the identical composites average  $0.35 \text{ W m}^{-1} \text{ K}^{-1}$  but ranged from  $0.30$  to  $0.40 \text{ W m}^{-1} \text{ K}^{-1}$ . The scatter decreased significantly at lower temperatures.

### Comments on glass-reinforced composites

We have reviewed the properties of filamentary-glass reinforced composites at cryogenic temperatures in order to provide the reader with an overall feel for their behaviour and the magnitude of the properties which may be expected. Having this information, for what applications should glass-reinforced composites be used? What composite formulation should be selected?

It would appear that glass-reinforced composites are most useful in applications requiring high tensile strength combined with high toughness and low thermal conductivity, but where stiffness is not required and where cyclic fatigue

is not a major problem. In such applications, glass-reinforced composites have given and will continue to give excellent performance at relatively low cost. Filament-winding techniques should be used whenever possible in order to obtain the highest quality composites; in particular, the lowest void content.

Resin 2 is unique in that it was developed specifically by NASA for use in glass-reinforced composites at cryogenic temperatures. This resin was found by Soffer and Molho<sup>5</sup> to be the overall choice among 41 candidate resins, using the criteria of composite and fibre tensile strength, composite tensile modulus, ultimate tensile strain, thermal shock resistance, coefficient of linear thermal contraction, and interlaminar shear strength as well as favourable processing characteristics. For this reason, as well as on the basis of the successful use of this resin in the cryogenic industry, the NASA 2 formulation must be considered as a prime candidate for general cryogenic use. The reader is cautioned, however, that the plasticizers used in this resin cause the resin to become weak at the elevated temperatures required for vacuum degassing of a composite assembly. Components made with this resin must be adequately supported during this operation.

Early in their investigation of cryogenic resins, Soffer and Molho<sup>5</sup> rejected the Polaris (E-787, 58–68R) formulation because its glass-transition temperature of over  $115^\circ\text{C}$  suggested brittleness at cryogenic temperatures. However, available data show that this resin formulation is capable of producing composite mechanical properties equal to those with Resin 2 at cryogenic temperatures, at least for certain filament orientations. This suggests that low temperature ductility and thermal shock resistance may not always be of primary significance in selecting a resin for cryogenic applications. Nevertheless, the reader is cautioned that inadequate data exist on degradation of composite properties during fatigue at cryogenic temperatures, and the effects of repeated thermal cycling are not well understood. Ductility may well play an important role under the latter circumstances. In the absence of further experimental data, critical composite components subjected to dynamic loads or to cyclic thermal stresses under service conditions should be tested under simulated operational conditions, regardless of the selected matrix resin.

The present review is restricted to those composites for which cryogenic property data are available in the literature. The contemporary purchaser of composite components may find other types of polymeric matrices recommended by various fabricators for use at cryogenic temperatures. The present review should not be construed as prejudicial to any such recommendation. The purchaser should, however, ascertain that any such recommendation is supported by adequate experimental or service data at the temperature of interest.

An unexpected result of the present review is the surprisingly good overall performance of the glass-polybenzimidazole types. Available data indicate that at 77 K, such a composite ranks second only to the epoxies in ultimate tensile strength and in flexural strength, while developing tensile and flexural moduli superior to that of the epoxies. Compressive properties appear only average; however, the data indicate that the polybenzimidazole-matrix composite withstands cyclic fatigue stresses with less strength loss than is the case for the other reported matrix materials, particularly in regard to the percent of original ultimate strength retained

after fatigue cycling. A key may be the comparatively low thermal contraction of the polybenzimidazole resin as compared to the other polymer types which should reduce residual interfacial stresses between the fibre and the matrix of the composite.

A pervasive characteristic of glass-polymeric composites is the erratic behaviour of the mechanical properties on cooling from 77–20 K. With few exceptions, the strength properties increase on cooling from 295–77 K; however, on further cooling to 20 K, the data indicate that such properties may either increase, decrease, or remain unchanged, the behaviour being quite unpredictable, even among composites of the same matrix type. It is difficult to attribute this simply to the matrix becoming suddenly much more brittle between 77 K and 20 K, as cooling to 77 K has already decreased the strain capability of the matrices to a level far below that of the glass reinforcement. The present task does not permit more than a cursory consideration of the possible factors involved in this phenomena; however, the author believes it relevant to call attention to recent studies on the low temperature properties of polymers which have provided convincing evidence that, in at least the linear polymers of the polycarbonate (PC) and polyethylene terephthalate (PET) types, the media in which the low temperature test is conducted can strongly affect the fracture mode and the resultant mechanical properties measured for the polymer.<sup>125,126</sup> The experimental evidence indicates that the failure in such polymers in the cryogenic range is controlled by a crazing phenomena which, in turn, is related to the activity of the gas or liquid in contact with the polymer surface. Such studies have not been extended to the strongly cross-linked polymers; however, until proved otherwise, it must be considered a possibility that the mechanical properties of glass-polymeric composites may be influenced by the ambient media such that data obtained at 20 K or 77 K in liquid hydrogen or nitrogen may not be the same as those which would be obtained in a helium atmosphere.

This review suggests that the following work would be of value in implementing expanded use of glass-reinforced composites for demanding cryogenic structural applications such as would be encountered in superconducting machinery:

1. The reason for the erratic mechanical property behaviour in polymeric-matrix composites below 77 K must be ascertained. In particular, it is imperative to determine whether or not the type of cryogen in which tests are conducted has a significant effect on the mechanical properties.

2. Material research and evaluation must be directed toward obtaining the type of basic composite cryogenic property data which will be of most value to the design engineer. Contemporary composite theory requires full mechanical characterization of a uniaxial lamella of the composite of interest, that is, an experimental determination of the strength and moduli values are required for the prediction of limiting property values in complex crossply lay-ups. Accurate tensile and compression data are required in the longitudinal and transverse modes plus accurate values for intralaminar shear. Even at room temperature, tensile and compression testing in the reinforcement direction has proved difficult to perform with acceptable accuracy. Testing problems will be further com-

pllicated at cryogenic temperatures; however, these problems must be solved.

3. Having come to terms with the problems posed in 1 and 2, the static mechanical property data and the thermal property data for the best of the glass-reinforced composites must be extended down to 4 K. Available data suggest that the major characterization effort should be made on S glass in a NASA Resin 2 matrix. S glass should be characterized in the Polaris formulation as well, but with emphasis on its potential special use as uniaxial filament-wound cryogenic support members. All test materials must be fully characterized for resin/fibre density, void content, and fibre alignment before mechanical or thermal investigation.

4. Data on the performance of composites under dynamic loading conditions at cryogenic temperatures are minimal to non-existent. Yet, these type of data are mandatory if composites are to be used in cryogenic machinery. The available data are encouraging in that they suggest that fatigue performance at cryogenic temperatures is generally superior to that at room temperature. However, this will have to be more fully documented. As high-cycle fatigue testing at 4 K is very expensive, the materials included in such a testing programme must be carefully selected. For this purpose, it would be very desirable to have an efficient screening type of test capable of correlating incipient damage with expected fatigue life. Data on thermal fatigue are also required, that is, the effect of repeated cool-downs on both the static and dynamic properties of composites must be determined.

The author wishes to thank Dr R. P. Reed for his consultation and for review of the completed manuscript. The author also wishes to express appreciation to the NBS-NOAA library staff of the Boulder Laboratories for their assistance in retrieving the many documents required for this work. This research was supported by the Advanced Research Projects Agency.

## Appendix

The following materials are referred to in this report. [The trade names used in this paper are those used by the cited authors. Generic names have been substituted whenever it was possible to do so without sacrificing clarity. The use of trade names in no way implies approval, endorsement or recommendation of specific commercial products by NBS.]

### *Glass fibres*

S-HTS, S-901, 1581, Owens-Corning Glass Company  
181, YM-31-A  
Hi-Stren Aerojet General Corporation

### *Epoxy resins*

Epon 822, 828, 1031, Shell Chemical Corp, Plastics  
58–68R & Resin Div  
E-787 US Polymeric Corporation  
ERL 2256 Union Carbide Plastics Company  
660 FW Stratoglas Div, Air Logistics Corp  
DER 332 Dow Chemical Corporation

### *Phenolic resins*

CTL-91-LD Cincinnati Testing Laboratories,  
Div of Studebaker-Packard  
Corp

Conolon 506, 507	Narmco Materials Div, Telecomputing Corp
<i>Phenyl silane resins</i>	
Narmco 534	Narmco Materials Div, Telecomputing Corp
<i>Polyester resins</i>	
Narmco 527	Narmco Materials Div, Telecomputing Corp
Hetron 31, 92	Durez Plastics Div Hooker Chemical Corp
Polyester C	US Polymeric Corp
Paraplex P-43	Rohm and Haas Corp
Laminac 4232	American Cyanamid Corp
Vibrin 135	Naugatuck Chemical Co, Div of US Rubber Corp
<i>Silicone resins</i>	
Trevarno F-130, F-131	Coast Manufacturing Company
Narmco 513	Narmco Materials Div, Telecomputing Corp

*Polyurethane resins*

Adiprene L-100 E. I. DuPont Corporation

*Polybenzimidazole resins*

Imidite Narmco Division, Whittaker Corp

*Flexibilizers, coupling agents, and hardners*

Empol 1040	Emery Industries, Inc
LP-3	Thiokol Chemical Corp
Z-6077	Dow Chemical Corporation
ZZL-0870	Union Carbide Plastics Company

*Miscellaneous materials*

Cure Agend D	polyamine salt
DDS	diaminodiphenyl sulphone
DSA	dodeceny succinic anhydride
BDMA	benzylidimethylamine
NMA	nadic methyl anhydride
TFE	polytetrafluoroethylene
FEP	polytetrafluoroethylene copolymer with hexafluoro propalene

**Bibliography**

**1. Mechanical properties**

*Contract AF-33 (616)-8289*

*Contractor:* Directorate of Materials and Processes, Aeronautical Systems Division, Air Force Systems Command, Weight-Patterson Air Force Base, Ohio

*Research Facility:* Narmco Research and Development, San Diego, California

- 1 **Brink, N. O.** 'Determination of the performance of plastic laminates under cryogenic temperatures', ASD-TDR-62-794 (AD 288 944)
- 1.1 **Brink, N. O.** 'Mechanical behaviour of reinforced plastics at cryogenic temperatures' Technical Papers: 20th Annual Technical Conference, Society of Plastics Engineers 10 Section 15-2 (1964)
- 1.2 **Brink, N. O.** 'Mechanical behaviour of reinforced plastics at cryogenic temperatures' *Society of Plastics Engineers Journal* 20 (1964) 1123
- 1.3 **Brink, N. O.** 'Mechanical behaviour of reinforced plastics at cryogenic temperatures', Narmco Research and Development Report, Code No 105-4 (1964)
- 2 **Chamberlain, D. W., Lloyd, B. R., Tennant, R. L.** 'Determination of the performance of plastics laminates at cryogenic temperatures', ASD-TDR-62-794, Part 2 (1964) (N64-24212)
- 2.1 **Chamberlain, D. W.** 'Tensile fatigue testing at temperatures down to 20 K' *Advances in Cryogenic Engineering* 9 (1964) 131
- 2.2 **Chamberlain, D. W.** 'Mechanical properties testing of plastic laminate materials down to 20 K', *Advances in Cryogenic Engineering*, 10 (1965) 117

*Contract NAS 8-11070*

*Contractor:* National Aeronautics and Space Administration, George C. Marshall Space Flight Center, Huntsville, Alabama

*Research Facility:* Goodyear Aerospace Corporation, Akron, Ohio

- 3 **Toth, L. W., Boller, T. J., Butcher, L. R., Kariotis, A. H., Yoder, F. D.** 'Programme for the evaluation of structural reinforced plastic materials at cryogenic temperatures', NASA CR-80061 (Final) (1966) (N67-12051)
- 3.1 **Toth, L. W.** 'Properties testing of reinforced plastic laminates through the 20 degree K range', Technical Papers, 20th Annual Technical Conference, Society of the Plastics Industry, Section 7-C (1965) 1
- 3.2 **Toth, L. W. and Kariotis, A. H.** 'An assessment of test specimens and test techniques useful to the evaluation of structural reinforced plastic materials at cryogenic temperatures', *Advances in Cryogenic Engineering* 10 (1965) 126
- 3.3 **Toth, L. W.** 'Properties of glass-reinforced epoxy through the 20 K range', *Modern Plastics*, 42 (1965) 123
- 3.4 **Toth, L. W., Burkley, R. A.** 'Mechanical response at cryogenic temperatures of selected reinforced plastic composite systems', Goodyear Aerospace Report GER-13169, Paper No 16, 70th Annual Meeting of the American Society for Testing and Materials (1967)
- 3.5 **Toth, L. W., Boller, T. J., Kariotis, A. H. and Yoder, F. D.** 'Programme for the evaluation of structural reinforced plastic materials at cryogenic temperatures', NASA CR-64005, (June 1963) through June 1964 (N65-29724)

*Contract NAS 3-6297*

*Contractor:* National Aeronautics and Space Administration, Lewis Research Center, Cleveland, Ohio

*Research Facility:* Aerojet General Corporation, Azusa, California

- 4 **Lewis, A., Bush, G. E.** 'Improved cryogenic resin-glass filament wound composites', NASA CR-72163 (Final) (1967) (N67-31856)
- 4.1 **Lewis, A., Bush, G. E. and Creedon, J.** 'Improved cryogenic resin glass filament-wound composites', NASA Interim Report CR-54867 (1966) (N66-28040)

### Contract NAS 6-6287

**Contractor:** National Aeronautics and Space Administration, Lewis Research Center, Cleveland, Ohio

**Research Facility:** Aerojet General Corporation, Azusa, California

- 5 Soffer, L. M., Molho, R. 'Cryogenic resins for glass filament-wound composites', NASA CR-72114 (Final) (1967) (N67-25076)
- 5.1 Soffer, L. N., Molho, R. 'Mechanical properties of epoxy resins and glass epoxy composites at cryogenic temperatures', *Cryogenic Properties of Polymers* [Koenig, J. L. (ed)] (Marcel Dekker, New York, 1968) 87 (Identical to NASA CR-84451 (1967) (N67-27217))

### Contract F04701-69-C-0059

**Contractor:** Space and Missiles Systems Organization, Air Force Systems Command, Los Angeles Air Force Station, Los Angeles, California

**Research Facility:** The Aerospace Corporation, El Segundo, California

- 6 Pepper, R. T., Rossi, R. E., Upp, U. W. and Riley, W. E. 'Development of an aluminum-graphite composite', SAMSO-TR-70-301 (1970) (AD 718 409)
- 6.1 Pepper, R. T., Upp, J. W., Rossi, R. C. and Kendall, E. G. 'Aluminum-graphite composites', SAMSO-TR-70-114, April 1970 (AD 706 883). (Identical to *Metallurgical Transactions*, 2 (1971) 117)
- 6.2 Rossi, R. C., Pepper, R. T., Upp, J. W., Riley, W. C. 'Development of aluminum-graphite composites', *Ceramic Bulletin* 50 (1971) 484

### Contract NAS 8-11508

**Contractor:** National Aeronautics and Space Administration, George C. Marshall Space Flight Center, Huntsville, Alabama

**Research Facility:** Harvey Engineering Laboratories, Torrance, California

- 7 Sumner, E. V., Davis, L. W. 'Development of ultrahigh strength, low density aluminum sheet and plate composites', NASA CR-85863 (Final) (1966) (N67-31181)
- 7.1 Davis, L. W. 'Composites at Low Temperature' 70th Annual Meeting of the American Society for Testing Materials (1967)

### Contract NASA DPR C 10360-E

**Contractor:** National Aeronautics and Space Administration, Lewis Research Center, Cleveland, Ohio

**Research Facility:** Naval Ordnance Laboratory, Silver Springs, Maryland

- 8 Simon, R. A., Alfring, R. 'Properties of graphite fiber composites at cryogenic temperatures', NASA CR-72652 (NOLTR 69-183) (1970) Tasks I and II (AD 746 885)
- 9 Larsen, J. V. 'Properties of graphite fiber composites at cryogenic temperatures - effect of elastomeric additions to resin systems', NASA CR-72804 (NOLTR 70-195) (1971) Task III (AD 882 972)
- 10 Larsen, J. V., Simon, R. A. 'Carbon fiber composites for

- 10.1 cryogenic filament-wound vessels', NASA CR-120899 (NOLTR 71-201) (1972) Tasks IV, V and VI, (N73-11553)
- 10.1 Simon, R. A. 'Graphite fiber composites at cryogenic temperatures', Technical Papers, 26th Annual Technical Conference, Society of the Plastics Industry, Section 10-D (1971) 1
- 10.2 Larsen, J. V. 'Fracture energy of CBTN/epoxy-carbon fiber composites', Technical Papers, 26th Annual Technical Conference, Society of the Plastics Industry Section 10-D (1971) 1

### Contract NAS 8-26198

**Contractor:** George C. Marshall Space Flight Center, Huntsville, Alabama

**Research Facility:** General Dynamics/Convair, San Diego, California

- 11 Scheck, W. G. 'Development of design data for graphite reinforced epoxy and polyimide composites', NASA TN-D2970, Report No GDC-DBG-70-005, final, National Aeronautics and Space Administration, Marshall Space Flight Center, Alabama (1974)
- 12 Scheck, W. G. 'Development of design data for graphite reinforced epoxy and polyimide composites', Report No GDC-DBG70-005, General Dynamics Quarterly Report No 1 (1970) [See also Maximovich, M., Scheck, W. G. *Quarterly Report No 2* (1970)]
- 12.1 Stuckey, J. M., Scheck, W. G. 'Development of graphite/polyimide composites', National-Technical Conference, Society of Aerospace Material and Process Engineers, Vol 3 (1971) 717

### Contract F33615-70-1442

**Contractor:** Air Force Materials Laboratory, Wright-Patterson Air Force Base, Ohio

**Research Facility:** General Dynamics/Convair, San Diego, California

- 13 Hertz, J., Christian, J. L., Varlas, M. 'Advanced composite applications for spacecraft and missiles, Phase I final report, volume II: Material development', AFML-TR 71-186, Vol 2 (1972) (AD 893 715L)
- 13.1 Forest, J. D., Fujimoto, A. F., Foelsh, G. F. 'Advanced composite applications for spacecraft and missiles, Phase I Final Report, Volume I: Structural development', AFML-TR-71-186, Vol 1 (1972)
- 13.2 Forest, J. D., Varlas, M. 'Advanced composite applications for spacecraft and missiles, Final Report', AFML-TR-72-278 (1973)
- 13.3 Christian, J. L., Campbell, M. D. 'Mechanical and physical properties of several advanced metal-matrix composite materials', *Advances in Cryogenic Engineering* 18 (1973) 175

## 2. Thermophysical properties

### Contract AF-33(657)-9160

**Contractor:** Air Force Materials Laboratory, Wright-Patterson Air Force Base, Ohio

**Research Facility:** General Dynamics/Astronautics, San Diego, California

The following reports are in a series entitled 'Thermophysical properties of plastic materials and composites to liquid hydrogen temperature (-423°F)'

- 14 Haskins, J. F., Campbell, M. C., Hertz, J., Percy, J. L., ML-TDR-64-33, Part I (1964) (AD 601 337)
- 15 Campbell, M. D., Hertz, J., O'Barr, H. L., Haskins, J. F., ML-TDR-64-33, Part II (1965) (X65--18921)

- 16 Campbell, M. D., O'Barr, G. L., Haskins, J. F., Hertz, J. ML-TDR-64-33, Part III (1965) (AD 468 155)
- 16.1 Hertz, J., Haskins, J. F. 'Thermal conductivity of reinforced plastics at cryogenic temperatures', *Advances in Cryogenic Engineering* 10 (1965) 163
- 16.2 Campbell, M. D. 'Thermal expansion characteristics of some plastic materials and composites from room temperature to  $-253^{\circ}\text{C}$ ', *Advances in Cryogenic Engineering* 10 (1965) 154
- 16.3 Campbell, M. D., Haskins, J. F., O'Barr, G. L., Hertz, J. 'Thermophysical properties of reinforced plastics at cryogenic temperatures', *Journal of Spacecraft* 3 (1966) 596
- (See also reference 13)
- Contract F33615-73-C1388 (Work currently in progress)**
- Contractor:** Air Force Materials Laboratory, Wright-Patterson Air Force Base, Ohio
- Research Facility:** General Dynamics/Convair, San Diego, California
- 17 Forest, J. D., Schaeffer, W. H. 'Advanced composite missile and space design data', General Dynamics Report GDCA-CHB72-001-2, Progress Report No 2 (1973)
- 18 Forest, J. D. 'Advanced composite missile and space design data', General Dynamics Report GDCA-CHB72-001-2, Progress Report No 2 (1973)
- ### 3. General bibliography
- 19 Aleck, B. 'Fiberglass-overwrapped 2219-T87 aluminum alloy low-pressure cryogenic tankage', Society of Aerospace Material and Process Engineers National Technical Conference, Space Shuttle Materials, Vol 3 (1971) 131
- 20 Alfring, R. J., Morris, E. E., Landes R. E. 'Cycle-testing of boron filament-wound tanks', NASA CR-72899, National Aeronautics and Space Administration, Lewis Research Center (1971) (N71-38023)
- 21 Barber, J. R. 'Design and fabrication of shadow shield systems for thermal protection of cryogenic propellants', NASA CR-72595, National Aeronautics and Space Administration, Lewis Research Centre, Cleveland, Ohio (1969) (N70-25098)
- 22 Baucom, R. M. 'Tensile behaviour of boron filament-reinforced epoxy rings and belts', NASA TN D-5053, Langley Research Center, Hampton, Virginia (1969) (N69-19918)
- 23 Benton, W., Carr, R., Cohen, A., Gustafson, G., Lankton, C., Zeldin, B. 'Propellant storability in space', RPL-TDR-64-75 (Final), Air Force Systems Command, Edwards Air Force Base, California (1964) (AD 603 215)
- 24 Brechna, H. 'Superconducting magnets for high energy physics applications' Proc ICECI (Heywood Temple Industrial Publishers Ltd, London, 1968) 119-(CESCI N67-36009)
- 25 Bullard, B. R. 'Cryogenic tank support evaluation', NASA CR-72546, NASA Lewis Research Center, Cleveland, Ohio (1969) (N70-13085)
- 26 Campbell, M. D. 'Development of thermal expansion capabilities and the investigation of expansion characteristics of space vehicle materials', General Dynamics/Astronautics Report ERR-AN-251 (December 1962)
- 27 Campbell, M. D. 'Development of the thermal expansion characteristics and the investigation of the thermal expansion characteristics of space vehicle materials (II)', General Dynamics/Astronautics Report ERR-AN-450 (1963)
- 28 Caren, R. P., Coston, R. M., Holmes, A. M. C., Dubus, F. 'Low-temperature tensile, thermal contraction and gaseous hydrogen permeability data on hydrogen-vapor barrier materials', *Advances in Cryogenic Engineering* 10 (1965) 171
- 29 Chiao, T. T., Moore R. L. 'Tensile properties of PRD-49 fiber in epoxy matrix', *Journal of Composite Materials* 6 (1972) 547
- 30 Cooper, G. A., Sillwood, J. M. 'Multiple fracture in a steel reinforced epoxy resin composite', *Journal of Materials Science* 7 (1972) 325
- 31 Darwish, F., Tetelman, A. S. 'Mechanical behaviour of SiO<sub>2</sub>-epoxy composite', Conference Proceedings No 63, Advisory Group for Aerospace Research and Development, Symposium on Composite Materials, Paper No 9, Paris (Hartford House, London, 1970)
- 32 Davis, J. G., Zender, G. W. 'Mechanical behaviour of carbon fiber reinforced-epoxy composites', 12th National Symposium, Society of Aerospace Material and Process Engineers, Vol 12 (1967) Section AC-10
- 33 Dervy, A. J. 'Reinforced plastics of high strength/weight ratio for space applications', Technical Papers, 17th Annual Technical Conference, Society of the Plastics Industry, Section 7-D (1962) 1
- 34 Fontana, M. G., Bishop, S. M., Spretnak, J. W. 'Investigation of mechanical properties and physical metallurgy of aircraft alloys at very low temperatures, Part 5 - Mechanical properties of metals and a plastic laminate at low temperatures', AF Technical Report 5662, Part 5, Materials Laboratory, Wright-Patterson Air Force Base, Ohio (1953) (AD 27726)
- 35 Freeman, S. M. 'Properties of vapor barriers, adhesives and foams at cryogenic and elevated temperatures', Lockheed Aircraft Corporation Report ER-5687 (1962)
- 36 Freeman, W. T., Campbell, M. D. 'Thermal expansion characteristics of graphite reinforced composite materials', Composite Materials: Testing and Design (Second Conference) ASTM STP 497, American Society for Testing and Materials (1972) 121
- 37 Funk, C. W., Dixon, C. E. 'Cryogenic radiation damage in structural polymers', *Transactions of the American Nuclear Society* 9 (1966) 406
- 38 Gille, J. P. 'Development of advanced materials for integrated tank insulation system for the long term storage of cryogenics in space', NASA CR-102570 (Final), National Aeronautics and Space Administration, Huntsville, Alabama (1969) (N70-23348)
- 39 Gleich, D. 'Development of a filament-overwrapped cryoformed metal pressure vessel', NASA CR-72753, National Aeronautics and Space Administration, Lewis Research Center, Cleveland, Ohio (1971) (N71-22401)
- 40 Gray, P. D., Cornelius, G. K., O'Donnell, J. D., Howards, W.W. 'Rockets in space environment, Volume 1: The experimental program', RTD-TDR-63-1050, Aerojet General Corporation (1963) (N63-20999)
- 41 Greer, F. 'Flexural properties of conolon 506 at room temperature,  $-320^{\circ}\text{F}$  and  $-423^{\circ}\text{F}$ ', Convair/Astronautics Report 55E 522 (1961) (AD 677 565)
- 42 Hale, D. V. 'Study of thermal conductivity requirements: MSFC 20-inch and 105-inch cryogenic tank analyses', NASA CR-61288, National Aeronautics and Space Administration, Marshall Space Flight Center, Alabama (1969) (N69-35811)
- 43 Hall, J. 'Cryogenics tensile tests - epoxy fiberglass', Douglas Aircraft Company Report MP 1348 (1961)
- 44 Hanson, M. P. 'Effects of temperature and creep characteristics of PRD-49 fiber-epoxy composites', NASA TN D-7120, National Aeronautics and Space Administration, Lewis Research Center, Cleveland, Ohio (1972) (N73-12607)
- 45 Hanson, M. P. 'Tensile and cyclic fatigue properties of graphite filament-wound pressure vessels at ambient and cryogenic temperatures', NASA TN D-5354, National Aeronautics and Space Administration, Lewis Research Center, Cleveland, Ohio (1969) (N69-31300) (Identical to SAMPE 15, 249)
- 46 Hanson, M. P., Richards, H. T., Hickel, R. O. 'Preliminary investigation of filament-wound glass-reinforced plastics and liners for cryogenic pressure vessels', NASA TN D-2741, National Aeronautics and Space Administration, Lewis Research Center, Cleveland, Ohio (1965)
- 47 Hanson, M. P. 'Glass-, boron-, and graphite-filament-wound resin composites and liners for cryogenic pressure vessels', NASA TN D-4412, National Aeronautics and Space Administration, Lewis Research Center, Cleveland, Ohio (1968) [Identical to NASA TM X-52350, (1967)]
- 48 Hanson, M. P. 'Static and dynamic fatigue behavior of glass filament-wound pressure vessels at ambient and cryogenic temperatures', NASA TN D-5807, National Aeronautics and Space Administration, Lewis Research Center, Cleveland, Ohio (1970) (CFSTI-CSC-120 K)
- 49 Haskins, J. F., Hertz, J. 'Thermal conductivity testing of coast F-224-6 phenolic-fiberglass laminate', General Dynamics Convair Report No AR-592-1-482 (1963)
- 50 Haskins, J. F., Hurlich, A. 'Measured values for the coefficients of linear expansion of Plycel 420 and Conolon 506 at low temperatures', Convair/Astronautics Report MRG-154 (1960)
- 51 Haylett, J. W., Rottmayer, E., Butcher, I. 'Advanced composite material study for millimeter wavelength antennas',

- Technical Report AFML-TR-71-205, Vol 1, Air Force Materials Laboratory, Wright-Patterson Air Force Base, Ohio (1971) (AD 893 368)
- 52 Haylett, C. E. 'Advanced composite material study for millimeter wavelength antennas, Volume II: Environmental tests', AFML-TR-71-205, Vol 2, Air Force Materials Laboratory, Wright-Patterson Air Force Base, Ohio (1971) (AD 893 358 L)
- 53 Herring, H. W., Baucom, R. M., Pride, R. A. 'Research on boron filaments and boron reinforced composites', 10th National Symposium, Society of Aerospace Material and Process Engineers 10 (1966) B-21
- 54 Hertz, J. 'Tensile testing of Conolon 506 at room and sub-zero temperatures', Convair/Astronautics Report MRG-120 (1959)
- 55 Hertz, J. 'Tensile testing of Adlock 851, Adlock PG-LA and Adlock EG-11A-81A from -423°F to 78°F' Convair/Astronautics Report MRG 237 (1961)
- 56 Hertz, J. 'Investigation of potential low temperature insulations', General Dynamics/Astronautics Report GS/A-ERR-AN-668 (1964)
- 57 Hertz, J. 'The effect of cryogenic temperatures on the mechanical properties of reinforced plastic laminates', General Dynamics Report AR-592-1-415 (1963) (AD 405 170)
- 58 Hertz, J. 'Investigation into the high-temperature strength degradation of fiber-reinforced resin composite during ambient aging', General Dynamics/Convair Report No GDCA-DBG73-005 (Final Contract NAS 8-27435) (1973)
- 59 Hoggatt, J. T. 'Development of cryogenic PRD-49-1 filament-wound tanks', NASA CR-120835, National Aeronautics and Space Administration, Lewis Research Center, Cleveland, Ohio (1971) (N72-24941)
- 60 Hoggatt, J. T. 'High performance filament wound composites for pressure vessel applications', Society of Aerospace Material and Process Engineers, National Technical Conference, Space Shuttle Materials, Vol 3 (1971) 157
- 61 Hust, J. G. 'Thermal conductivity of an epoxy-fiberglass laminate', NBS Cryogenic Division Unpublished Laboratory Note 73-1, (1973)
- 62 Johnston, H. L., Brooks, H. E. 'Impact strength of various metals at temperatures down to 20° Absolute', Ohio State University Cryogenic Laboratory Report TR 264-17 (1952)
- 63 Keller, C.W. 'Fiberglass supports for cryogenic tanks', NASA CR-120937 (Final), National Aeronautics and Space Administration, Lewis Research Center, Cleveland, Ohio (1972) (N72-33564)
- 64 Kerlin, E. E., Smith, E. T. 'Measured effects of the various combinations of nuclear radiation vacuum and cryotemperatures on engineering materials: Biennial Report', NASA CR-77772, National Aeronautics and Space Administration, George C. Marshall Space Flight Center, Huntsville, Alabama (1966) (N66-35963)
- 65 Kerlin, E. E., Smith, E. T. 'Measured effects of the various combinations of nuclear radiation, vacuum and cryotemperatures on engineering materials: Annual Report', NASA CR-58830, National Aeronautics and Space Administration, George C. Marshall Space Flight Center, Huntsville, Alabama (1964) (N64-33043)
- 66 Keys, R. D., Kiefer, T. F., Schwartzberg, F. R. 'Cryogenics properties of high-strength glass-reinforced plastics', *Advances in Cryogenic Engineering* 11 (1966) 470
- 67 Krause, D. R. 'Development of lightweight material composites to insulate cryogenic tanks for 30-day storage in outer space', NASA CR-123797, National Aeronautics and Space Administration, George C. Marshall Space Flight Center, Huntsville, Alabama (1972) (N72-30495)
- 68 Krause, D. R., Fredrickson, G. O., Klevatt, P. L. 'Effects of cyclical environments on high-performance multi-layer insulation materials', Society of Aerospace Material and Process Engineers National Technical Conference, Space Shuttle Materials, Vol 3 (1971) 639
- 69 Lantz, R. B. 'Materials for filament wound cryogenic pressure vessels', 6th National Symposium, Society of Aerospace Materials and Process Engineers, Vol 2, Engineering Paper No 1750
- 70 Lavengood, R. E., Anderson, R. M. 'Matrix properties controlling torsional fatigue life of fiber reinforced composites', Technical Papers, 24th Annual Technical Conference, Society of the Plastics Industry, Section 11-E (1969)
- 71 Levin, V. A., Naumenkov, P. G., Shchitov, M. V. 'Some properties of plastics at low temperatures', *Plasticheskaia Massy* 11 (1966) 64
- 72 Luikov, A. V., Vasiliev, L. L., Shashkov, A. G. 'A method for the simultaneous determination of all thermal properties of poor heat conductors over the temperature range 80 to 500 K', Proceedings 3rd American Society of Mechanical Engineers Symposium, Purdue University (1965) 314
- 73 Lyon, D. N., Parrish, W. R. 'Low temperature thermal conductivities of two high compressive strength materials', *Cryogenics* 7 (1967)
- 74 Maher, L. E. 'Some problems arising from the use of hydrogen-fuelled propulsion systems' *Journal of the Royal Aeronautical Society* 68 (1964) 765
- 75 McKannon, E. C., Gause, R. L. 'Effects of nuclear radiation and cryogenic temperatures on non-metallic engineering materials', *Journal of Spacecraft* 2 (1965) 558
- 76 Morris, E. E. 'Glass-fiber-reinforced metallic tanks for cryogenic service', 12th National Symposium, Society of Aerospace Materials and Process Engineers, Vol 12 (1967) Section AS-4 (also NASA CR-72224)
- 77 Morris, E. E. 'The performance of glass-filament-wound pressure vessels with metal liners at cryogenic temperatures', *Journal of Materials* 4 (1969) 970
- 78 Morris, E. E., Alfring, R. J. 'Cryogenic boron-filament-wound pressure vessels', Composite Materials: Testing and Design, ASTM STP 460 (American Society for Testing and Materials, 1969) 430
- 79 Morris, E. E., Landes, R. E. 'Cryogenics glass-filament-wound tank evaluation', NASA CR-72948 (Final), National Aeronautics and Space Administration, NASA Lewis Research Center, Cleveland, Ohio, (1971) (N72-14696)
- 80 Mowers, R. E., Leib, J. H., Sherman, S. 'Program of testing nonmetallic materials at cryogenic temperatures', Rocketdyne Corporation Report R-3498, Rocket Propulsion Laboratories, Edwards, California (1962) (AD 294 772)
- 81 Nadler, M. A., Yoshino, S. Y., Darms, F. J. Boron/epoxy support strut for non-integral cryogenic tankage', North American Rockwell Space Division Report SD 68-99501 (1969) [See also 15th National Symposium SAMPE (April 1969) and North American Rockwell Report SD 995 2 (1968)]
- 82 Nelson, L. F. 'Compressive strength of Conolon 506 at +75°F and -320°F', Convair/Astronautics Report No 27E 1336 (1962)
- 83 Nelson, L. R. 'Mechanical properties of Adlock 851 at room temperature, 1000°, -320° and -423°F', Convair/Astronautics Report No 55E 812 (1961)
- 84 Nelson, P. T., Archer, J. S. 'Graphite reinforced plastic EHF antenna', TRW Systems Group, Redondo Beach, California Report No 99900-7128-RO-11 (1969)
- 85 Patten, P. M. 'Internal insulation liner alteration', Douglas Aircraft Company Report No SM 45975 (1964)
- 86 Perkins-Elmer Optical Group, Norwalk, Connecticut: Work-in-Progress on Contract No F33615-72-C-2033, Air Force Systems Command, Wright-Patterson Air Force Base, Ohio
- 87 Pink, E., Campbell, J. D. 'The effect of strain rate and temperature on the deformation behavior of reinforced and unreinforced epoxy resin', Oxford University Department of Engineering Report No 1040/72, Oxford, England (1972) (N73-10568)
- 88 Pirgon, O., Wostenholm, G. H., Yates, B. 'Thermal expansion at elevated temperatures, IV. Carbon-fibre composites', *Journal of Physics D: Applied Physics* 6 (1973) 309
- 89 Pride, R. A., Stein, B. A., Schmidt, F. W. 'Mechanical properties of polyimide-resin glass-fiber laminates for various time, temperature and pressure exposures', Technical Papers, 23rd Annual Reinforced Plastics Technical and Management Conference, Washington, DC Section 17-c (1968) 1
- 90 Ratcliffe, E. H. 'Thermal conductivities of plastics with glass, asbestos and cellulosic fiber reinforcements', *Applied Material Research* 5 (1966) 200

- 91 Roseland, L. M. 'Materials for cryogenic usage', Technical Papers, 21st Annual Technical Conference, Society of the Plastics Industry Section 4-C (1966) 1
- 92 Roseland, L. M. 'Investigation of structural properties at cryogenic temperatures of filament-wound pressure vessels containing both organic and glass filaments', Douglas Aircraft Corporation Report No SM-48409, (1966)
- 93 Ross, J. E. 'Fiberglass laminate - ultimate tensile and flexural strength tests at room temperature,  $-100^{\circ}\text{F}$  and  $320^{\circ}\text{F}$ ', Convair Astronautics Report No 7E 1687 (1959) (AD 830 230)
- 94 Sanders, R. H., Weleff, W. 'Final report on GTR-17 effects of radiation on organic materials irradiated in liquid hydrogen', Aerojet-General Corporation Report No RN-S-0327 (1967)
- 95 Sanger, M. J., Molho, R., Howard, W. W. 'Exploratory evaluation of filament-wound composites for tankage of rocket oxidizers and fuels', AFML-TR-65-381, Air Force Materials Laboratory, Wright-Patterson Air Force Base, Ohio (1966) (AD 477 455)
- 96 Sanger, M. J., Reinhart, T. J. 'Development of filament-wound tankage for rocket oxidizers and fuels', Technical Papers 12th National Symposium, Society of Aerospace Material and Process Engineers Section AS-7 (1967)
- 97 Sewell, J. J., Kuno, J. K. 'Aerospace use of plastic hardware and thermal insulation', Technical Papers, 17th Annual Technical Papers, 17th Annual Technical Conference, Society of the Plastics Industry, Section 7-A (1962) 1
- 98 Shriver, C. B. 'Design and fabrication of an internally insulated filament wound liquid hydrogen propellant tank', NASA CR-127, National Aeronautics and Space Administration, Washington, DC (1964) (N65-10775)
- 99 Soltysiak, D. J., Toth, J. M. 'Static fatigue of fiber glass pressure vessels from ambient to cryogenic temperatures', Technical Papers, 22nd Annual Technical Conference, Society of the Plastics Industry, Section 14-E (1967)
- 100 Speare, J. C. 'Preliminary sizing of filament-wound RNS tanks', Report No TOR-0066 (5759-07)-13, Space and Missile Systems Organization, Air Force Systems Command, Los Angeles Air Force Station, Los Angeles, California (1970) (AD 872 626)
- 101 Steinhauer, R. A. 'Linear thermal expansion of 828CL 181 cloth laminate', Douglas Aircraft Company Report No MP 11, 979 (1961)
- 102 Stinnett, W. D. 'Cryogenic tensile properties of selected materials', NASA CR-71751, AEC-NASA Space Nuclear Propulsion Office, Report No 2712 (1964) (N66-22816)
- 103 Suezawa, Y., Hojo, H., Nakamura, K. 'Impact characteristics of fiberglass reinforced plastics at low temperatures', *Kagaku Kogaku (Chemical Engineering, Japan)* 33 (1969) 1051
- 104 Toth, J. M. 'Barrier films for filament-wound fiberglass cryogenic vessels', *Advances in Cryogenic Engineering I* (1964) 537
- 105 Toth, J. M., Soltysiak, D. J. 'Investigation of smooth-bonded metal liners for glass fiber filament-wound pressure vessels', NASA CR-72165 (Final), National Aeronautics and Space Administration, Lewis Research Center, Cleveland, Ohio (1967) (N67-25070)
- 106 Toth, J. M., Sherman, W. C., Soltysiak, D. J. 'Investigation of smooth-bonded metal liners for glass fiber filament-wound pressure vessels', Douglas Missile and Space Systems Division Report No SM-49384, Quarterly Report No 3, Contract No NAS 3 6293, NASA Lewis Research Center, Cleveland, Ohio (1966)
- 107 Toth, J. M., Sherman, W. C., Soltysiak, D. J. 'Investigation of structural properties of fiber-glass filament-wound pressure vessels at cryogenic temperatures', NASA CR-54393, National Aeronautics and Space Administration, Lewis Research Center, Cleveland, Ohio (1965) (N65-35392)
- 108 Toth, J. M., Barber, J. R. 'Structural properties of glass-fiber filament-wound cryogenic pressure vessels', *Advances in Cryogenic Engineering 10* (1965) 134
- 109 Voloshenko-Klimovitskii, Yu. Ya., Belyaev, Yu. A., Lvof, B. S., Sehpakovskaya, E. I. 'Strength of cold-hardening GRPs based on PN-1 resin under impact tension at normal ( $20^{\circ}\text{C}$ ) and low ( $-196^{\circ}\text{C}$ ) temperatures', *Plasticheski Massy* 6 (1964) 39
- 110 Voloshenko-Klimovitskii, Yu. Ya., Belyaev, Yu. A., Korenkov, Yu. A. 'Impact tensile tests on glass-fibre reinforced plastics at normal and low temperatures', *Plasticheski Massy* 5 (1963) 51
- 111 Watson, J. F., Christian, J. L., Hertz, J. 'Selection of materials for cryogenic applications in missiles and aerospace vehicles', Convair/Astronautics Report No MRG 132-1 (1960)
- 112 Weleff, W. 'Effect of nuclear radiation and liquid hydrogen on mechanical properties of three phenolic materials', *Advances in Cryogenic Engineering 11* (1966) 486
- 113 Weleff, W. 'Final Report, GTR-16 radiation effects test on structural materials at  $-423^{\circ}\text{F}$ ', Aerojet-General Corporation Report No RN-S-0290 (1966)

#### 4. Handbooks and reviews

- 114 Coston, R. M. 'Handbook of thermal design data for multi-layer insulation systems', LMSC-A847882, Vol II (Final), George C. Marshall Space Flight Center, Huntsville, Alabama (1967) (N67-34910)
- 115 Hertz, J. 'The effect of cryogenic temperatures on the mechanical properties of reinforced plastic laminates', *Society of Plastics Engineers Journal* 21 (1965) 181
- 116 Hertz, J., Knowles, D. 'Survey of thermal properties of selected materials', General Dynamics/Convair Report AAL-65-008 (AR-504-1-553) (1965) (N65-31775)
- 117 Jurevic, W. G., Rittenhouse, J. B. 'Structural applications handbook', AFML TR-67-332, Air Force Materials Laboratory, Wright-Patterson Air Force Base, Ohio (1968) (AD 804 585)
- 118 Lackman, L. M., Arvin, G. H. et al 'Advanced composite design guide, 3rd edn, Volume IV: Materials', Air Force Materials Laboratory, Wright-Patterson Air Force Base, Ohio (1973)
- 119 Landrock, A. H. 'Properties of plastics and related materials at cryogenic temperatures', Plastic Report No 20, Plastics Technical Evaluation Center, Picatinny Arsenal, Dover, New Jersey (1965) (AD 469 126)
- 120 Maximovich, M., Scheck, W. G. 'Data summary and reference file for graphite and boron reinforced composite materials', General Dynamics Convair Report No GDCA-DBG71-006 (1971) (Contract NAS 8-26198, George C. Marshall Space Flight Center, Huntsville, Alabama)
- 121 Nored, D. L., Hennings, G., Sinclair, D. H., Smith, G. T., Smolak, G. R., Stofan, A. J. 'Storage and handling of cryogenic fluids', NASA Special Publication SP-5053, Proceedings of Conference on Selected Technology for the Petroleum Industry, Lewis Research Center, Cleveland, Ohio, (1965) (N66-33674)
- 122 'Plastics for aerospace vehicles, Part I: Reinforced plastics', MIL-HDBK-17A, Department of Defense, Washington, DC (1971)
- 123 Rittenhouse, J. B., Singletary, J. B. 'Space materials handbook', 3rd edn, NASA Special Publication SP-3051, National Aeronautics and Space Administration, Washington, DC (1969) (limited publication as AFML-TR-68-205)
- 124 Schwartzberg, F. R., Hertzog, R. G., Osgood, S. H. et al 'Cryogenic materials data handbook (Revised), Volume II, AFML-TDR-64-280-Vol II (Revised), Air Force Materials Laboratory, Wright-Patterson Air Force Base, Ohio (1970) (AD 713 620)

#### Miscellaneous references

- 125 Kastelic, J. R., Hiltner, A., Baer, E. 'Crazing, yielding and fracture in polycarbonate and polyethylene terephthalate at low temperatures', *Journal of Macromolecular Science-Physics* B7(4) (1973) 679
- 126 Relationships Between Structure and Mechanical Behavior in Polymeric Solids, ASM Materials Science Seminar, Chicago, 111, 1973 (in preparation)

## Bibliography — Property Cross Reference

Property	Glass — Epoxy	Glass — Polyester	Glass — Phenolic	Glass — Teflon	Glass — Silicone	Glass — Polyurethane	Glass — Phenyl Silane	Glass — PBI**
$\sigma^{tu}$	1-1.3, 2-2.2, 3-3.5, 4, 5, 5.1, 22, 24, 28, 33, 35, 40, 43, 46, 47, 52, 54, 55, 57, 66, 71, 87	1-1.3, 2-2.2, 3-3.2, 3.4, 3.5, 34, 40, 55, 57, 63, 64, 66, 75, 109	1-1.3, 2-2.2, 40, 54, 55, 57, 64-66, 71, 75, 102, 113, 83, 93, 97, 111, 112	2-2.2, 37, 67, 68, 80, 94,	1-1.3, 2-2.2, 24, 40, 57, 64, 66, 68, 97	2-2.2, 85	2-2.2, 57, 67	2-2.2
$E_1^f$	1-1.3, 2-2.2, 3-3.5, 4.5, 5, 5.1, 24, 28, 35, 55, 56, 57, 66, 87	1-1.3, 2-2.2, 3, 34, 55, 57	1-1.3, 2-2.2, 54, 55, 57, 97, 111	2-2.2, 80	1-1.3, 2-2.2, 24, 57	2-2.2	2-2.2, 57, 66	2-2.2, 24
$E_2^f$	1-1.3, 2, 3-3.5, 28, 55, 56, 57	1-1.3, 2, 55, 57	1.1.3, 55, 57		1-1.3, 2, 57	2	2, 57	2
$\epsilon^f$	3-3.5, 4, 5, 5.1, 35, 64, 85	3-3.5, 64	64, 65, 112	80, 89, 102	64	85		
$\sigma^{fu}$	1-1.3, 2-2.2, 3-3.5, 4, 40, 57, 66, 71	1-1.3, 2-2.2, 3-3.3, 3.5, 40, 57, 66	1-1.3, 2-2.2, 40, 41, 57, 71, 83, 93, 97	2-2.2, 80	1-1.3, 2-2.2, 40, 57, 97	2-2.2	2.2.2	2-2.2
$E_1^f$	1-1.3, 2, 3-3.2, 3.4, 3.5, 57	1-1.3, 2, 2.2, 57	1-1.3, 2-2.2, 57, 83, 93, 97	2-2.2, 80	1-1.3, 2-2.2, 57	2-2.2	2-2.2	2-2.2
$E_2^f$	1-1.3, 2	1-1.3, 2	1-1.3, 2		1-1.3, 2	2	2	
$\sigma^{cu}$	1-1.3, 2, 2.2, 3-3.2, 3.4, 3.5, 24, 57, 66	1-1.3, 2, 2.2, 3-3.5, 34, 57	1-1.3, 2-2.2, 57, 82, 97	2-2.2, 80	1-1.3, 2-2.2, 24, 57	2-2.2	2-2.2, 57	2-2.2, 24
$E^c$	1, 1.2, 1.3, 2, 2.2, 57	1-1.3, 2, 2.2, 57, 66	1-1.3, 2-2.2, 57, 82, 97	2-2.2, 80	1-1.3, 2-2.2, 57	2-2.2	2-2.2	2-2.2
$\sigma^{si}$	3-3.2, 3.4, 3.5, 4.4.1, 5.5.1, 22, 47, 71	3-3.5						
$\eta^f$	1, 1.3, 2, 2.1, 2.2, 66, 70, 99	1-1.3, 2-2.2, 34, 70	1-1.3, 2-2.2		1-1.3, 2	2	2	2
$\sigma^{by}$	2-2.2, 3, 3.2, 3.4, 3.5				2	2	2	2
$\sigma^{I^*}$	4, 71, 103	62, 109	71, 97	80				
$\lambda$	3, 4.1, 14, 16-16.3, 21, 23-25, 38, 42, 56, 61, 63, 90, 114	3, 14, 16-16.3, 90	14, 16-16.3, 49	14, 16-16.3	14, 16-16.3, 24, 73, 90		14, 16-16.3	16, 24
$\Delta L/L$	3, 5, 14, 16, 16.2, 16.3, 28, 69, 85, 91, 100, 101, 104, 114	3, 14, 16-16.3	14, 16-16.3, 26, 27, 50, 111	14, 16-16.3	14, 16-16.3, 67	5, 85, 91	14, 16-16.3	16, 16.2
$C_p$	15, 16, 16.2, 16.3, 24, 114	15, 16-16.3	15, 16-16.3, 64	15, 16-16.3	15, 16-16.3, 24		15, 16-16.3	16-16.3, 24

\* includes fracture toughness  
 \*\* polybenzimidazole

**Bibliography – Property Cross Reference (Cont'd)**

Property	Graphite – Epoxy	Boron – Epoxy	Boron – Aluminum	PRD-49 Epoxy
$\sigma^{tu}$	8, 9, 10, 10.2, 13, 13.2, 32, 47, 51, 58	13, 20, 22, 47, 53, 58, 81	13, 13.3	29, 44, 59, 60
$E_1^t$	8, 9, 10, 10.1, 13, 51	13, 81	13, 13.3	44, 59, 60
$\epsilon^t$	13	20	13	
$\sigma^{fu}$	8, 10, 10.1, 11, 12, 13, 13.2, 58	58		
$E^f$	8, 10.1			
$\sigma^{cu}$	13		13, 13.3	
$E^c$	13	13, 81	13, 13.3	
$\sigma^{si}$	8, 9, 10, 10.1, 10.2, 12, 13, 13.2, 47, 58	13, 22, 47, 58, 81	13, 13.3	59, 60
$\eta^t$	45	20		
$\sigma^{ty}$			13, 13.3	
$\sigma^{I^*}$	9, 10.2	81		
$\lambda$	13, 17, 18, 38	13, 38, 63, 81		
$\Delta L/L$	10, 13, 13.2, 17, 18, 36, 51, 52, 84, 88	13	13, 13.3	59, 60
$C_p$	13	13	13, 13.3	

\* includes fracture toughness

*Miscellaneous Properties*

*Notch Tensile Strength* Glass-Epoxy (3–3.2, 3.4, 3.5, 43, 46)

*Vapor Permeability* Glass-Epoxy (28)

*Modulus of Rigidity* Glass-Epoxy (53), Glass-Teflon (80), Boron-Epoxy (53)

*Poissons Ratio* Glass-Epoxy (53), Boron-Epoxy (53)

*Proportional Limit in Tension* Glass-Epoxy (55, 56), Glass-Polyester (1–1.3, 55, 56)

*Static Fatigue* Glass-Epoxy (66, 99), PRD 49–Epoxy (44)

*Environmental Effects* Glass-Epoxy (4–4.1), Graphite-Epoxy (13, 13.2, 17, 58), Boron-Epoxy (13, 58), Boron-Aluminium (13, 36) PRD 49–Epoxy (44)

*Electrical Resistivity* Graphite-Epoxy (13), Boron-Epoxy (13)

*Thermo-Optical Effects* Graphite-Epoxy (13, 84), Boron-Epoxy (13)

*Density* Glass-Epoxy, Polyester, Phenolic, Silicone, Phenyl Silane (14, 57), Glass-Teflon (14), Glass-Polybenzimidazole (16), Graphite-Epoxy (9, 13), Graphite-Phenolic (14), Graphite-Polyimide (12.1)

*Radiation Effects* (13.2, 33, 37, 40, 51, 52, 64, 65, 75, 94, 112, 113)

*Cryogen Compatability* (33)

*Miscellaneous Composites*

*Glass-Polyimide*  $\sigma^{tu}$  (24, 67, 68),  $\sigma^{fu}$  (89),  $\sigma^{si}$  (12.1, 89),  $\Delta L/L$  (67)

*Glass-Melamine*  $\sigma^{tu}$  (65),  $\epsilon^t$  (65),  $\lambda$  (90)

*Glass-Viton*  $\sigma^{tu}$  (68)

*Glass-Phenyl Formaldehyde*  $\sigma^I$  (110),  $\lambda$  (72),  $C_p$  (72)

*SiO<sub>2</sub>-Epoxy*  $\sigma^{tu}$  (31),  $\Delta L/L$  (28)

*Graphite-Aluminium*  $\sigma^{tu}$  (thermal cycling effects 6–6.2)

*Graphite-Polyimide*  $\sigma^{tu}$  (13),  $\sigma^{fu}$  (11, 12.1, 13),  $\sigma^{si}$  (13),  $\Delta L/L$  (36)

*Graphite-Phenolic*  $\lambda$  (14, 16–16.3),  $\Delta L/L$  (14, 16–16.3)

*Steel-Aluminium*  $\sigma^{tu}$  (7, 7.1),  $\epsilon^t$  (7.1),  $\sigma^I$  (7, 7.1)

*Steel-Epoxy*  $\sigma^{tu}$  (2, 30),  $E^t$  (2, 30),  $\sigma^{fu}$  (2),  $E^f$  (2),  $\sigma^{cu}$  (2),  $E^c$  (2),  $n^t$  (2)

*Boron/Steel-Aluminium*  $\sigma^{tu}$ ,  $E^t$ ,  $\sigma^{cu}$ ,  $E^c$ ,

*Boron/Titanium-Aluminium*  $\sigma^{by}$ ,  $\Delta L/L$ ,  $C_p$ , (13, 13.3),  $\sigma^{si}$ ,  $\epsilon^t$ ,  $n^t$  (13)

*Potassium Titanate–Epoxy*  $\lambda$  (16),  $C_p$  (16)

*Pressure Vessel Applications*

*Glass-Filament*

(19, 20, 39, 42, 46–48, 53, 67, 69, 76, 77, 91, 92, 95, 96, 98–100, 104–108, 113)

*Graphite–Filament*

(8, 10, 10.1, 45, 47, 100)

*Boron-Filament*

(20, 47, 53, 78)

*PRD 49–Filament*

(59, 60)

from the desire to obtain improved mechanical properties at room and elevated temperatures, to save weight, and to reduce the cost for current and future aerospace hardware applications. Comparatively little effort has been expended on development of composites for use at cryogenic temperatures. A notable exception has been a fairly extensive body of work sponsored by the National Aeronautics and Space Administration (NASA) and the U.S. Air Force (USAF) wherein a series of glass-reinforced composites was evaluated down to 20 K. Such materials were subsequently successfully used as baffles and structural support components in various aerospace applications. The other major field of cryogenic composite development has been filament-winding for fabrication of cryogenic pressure vessels. In recent years, advanced fibers have also been investigated for the latter application. To a large extent, the remaining published data reflect work in which cryogenic properties were peripheral to the main work objective.

The relative lack of emphasis on cryogenic structural composites is understandable, as the majority of the applications are presently satisfied by well-characterized metals and alloys. Why then should one consider composites for such applications? The answer lies in the increasingly stringent demands being made on materials in advancing cryogenic technology, of which the development of superconducting machinery may serve as an example. While the first generation of such machines will be almost entirely dependent on metals technology, it is highly probable that succeeding generations will capitalize on composite technology for reasons of increased reliability, reduced weight, and increased overall efficiency, as composites offer higher specific strengths and moduli combined with a wider range of thermal and electrical properties than are available with any metal or alloy.

A major barrier to the wider use of structural composites for cryogenic applications is the lack of broad characterization and handbook-type data describing the properties and performance of such materials under cryogenic conditions. The Cryogenic Division of the National Bureau of Standards (NBS) has therefore undertaken a comprehensive survey of the literature on the mechanical and thermal properties of structural composites from about 1960 to the present time. In the course of the survey, it became apparent that there existed several bodies of work that were particularly outstanding and which deserved more detailed analysis than was possible in the more comprehensive review. It is the intent of the present paper to consider the results of these selected studies, reviewing their objectives, the scope of the work undertaken, and the general conclusions reached by the authors. Subsequently, selected composite types developed in each program are discussed in some detail. In the interest of brevity, discussions of the properties are restricted to ultimate tensile strength, tensile modulus, tensile fatigue, thermal contraction, and

M. B. Kasen<sup>1</sup>

## Properties of Filamentary-Reinforced Composites at Cryogenic Temperatures

**REFERENCE:** Kasen, M. B., "Properties of Filamentary-Reinforced Composites at Cryogenic Temperatures," *Composite Reliability*, ASTM STP 580, American Society for Testing and Materials, 1975, pp. 586-611.

**ABSTRACT:** This paper presents a review of a series of significant publications on the mechanical and thermal properties of filamentary-reinforced structural composites in the cryogenic temperature range. The objective, scope of work, and significant conclusions of the selected works are discussed. The temperature dependence of the ultimate tensile strength, tensile modulus, thermal conductivity, and thermal contraction (expansion) is presented for selected composites developed in each program. Problem areas are defined and suggestions are made for future work.

**KEY WORDS:** composite materials, reviews, structural composites, cryogenics, glass, boron, graphite, reinforced plastics, aluminum, tensile strength, modulus of elasticity, thermal conductivity, thermal expansion

### Nomenclature

NOL Naval Ordnance Laboratory  
UFW Uniaxial filament-wound  
BFW Biaxial filament-wound  
GFRP Glass fiber reinforced plastic  
CFRP Carbon fiber reinforced plastic  
BFRP Boron fiber reinforced plastic  
NMA Nadic methyl anhydride  
BDMA Benzyl dimethylamine  
L-100 Polyurethane resin (Adiprene)  
MOCA 4,4'-methylene dianiline  
DSA Dodecetyl succinic anhydride

The primary impetus for structural composite development has arisen

<sup>1</sup>Staff scientist, Cryogenic, NBS-Institute for Basic Standards, Boulder, Colo. 80302.

thermal conductivities, as these properties are of most interest to the potential users.

The discussion of properties given herein does not take into consideration the effect of variations in fiber/resin ratio of specific types of composites and test specimens, as this characteristic was not reported for all referenced works. Composite properties are strongly influenced by this ratio. The property data discussed in this paper reflect actual values and trends reported for specific composites. Controlled variations in many of the properties are obtainable in practice by specific variation of the fiber content of the composite.

As composites are frequently used where weight is critical, or where specific strengths are required, typical composite densities have been summarized in Table 1.

TABLE 1—Typical composite densities.

Composite System	Fiber/Resin Ratio	Density, lb·ft <sup>-3</sup> (kg·m <sup>-3</sup> )
S-glass-epoxy	60-67	0.068-0.074 (1.09-1.19)
Kevlar 49/epoxy	60-65	0.047-0.050 (0.753-0.801)
Boron-epoxy	55	0.070-0.074 (1.12-1.19)
Graphite-epoxy	55-60	0.050-0.055 (0.801-0.881)
Boron-aluminum (4 mil)	50	0.10

It must be emphasized that this survey is not exhaustive, that the results reported have not been experimentally confirmed by NBS, and that the conclusions and evaluations presented in this paper reflect those of the cited authors and do not imply approval, endorsement, or recommendation of any commercial product by NBS.

The presentation is in two parts—the first considering the work on glass-reinforced materials and the second considering a variety of advanced-fiber reinforced materials.

### Glass-Reinforced Composites

#### Overview

Brink, Chamberlain, and their associates made the initial significant contribution to understanding the cryogenic behavior of glass-fiber reinforced plastic (GFRP) materials in report ASD-TDR-62-794 to the USAF, Part I of which was published in 1962 [1]<sup>2</sup> and Part II in 1964 [2]. Part I of this work evaluated the mechanical properties of commercial composite products which conformed to existing military specifications.

<sup>2</sup> The italic numbers in brackets refer to the list of references appended to this paper.

Tensile, flexure, compressive, and fatigue properties were evaluated from 295 K to 20 K in epoxy, phenolic, polyester, and silicone matrices reinforced with 181 glass cloth. The results indicated a general increase in strength as the temperature was lowered, while the same relative fatigue resistance was observed at cryogenic temperatures as at room temperature, the cryogenic fatigue properties being equal to or above the room temperature values. Similar resin systems were found to produce similar trends on cooling, and toughness of the GFRP composites was maintained at cryogenic temperatures while the rate of cooling was not found to be important. Part II of this work investigated a series of additional resins, including Teflon,<sup>3</sup> polyurethane, phenyl silane and polybenzimidazole (PBI or Imidite), which were recommended by the manufacturers for use at low temperatures. Bearing yield strength, tensile fatigue, and impact properties were evaluated in addition to the properties investigated in Part I. In general, the properties of composites made with the modified resins were found to be inferior to those of the commercial materials studied in Part I. The authors concluded that epoxies were the most desirable matrix materials, with polyesters running a close second. Flexibilized matrix systems were judged useful only if flexibility was of paramount importance. The authors concluded that there existed a need for standardization of test procedures, a conclusion which is unfortunately still valid today.

Chronologically, the next major contribution was made by Toth et al in 1966 [3]. This report covered a three-year effort which had the following objectives: (a) to critically evaluate test methods for use at cryogenic temperatures, (b) to establish the relationship between test results and design performance, and (c) to apply the developed techniques to the evaluation of a variety of glass-polymeric composites. Unidirectional as well as woven cloth reinforcement of conventional and modified epoxy resins was studied. A limited test series was also run on silicon carbide whiskers combined with S-glass as reinforcement for an epoxy resin. Test temperatures ranged from 295 K to 20 K. The authors concluded that valid test procedures had been developed and proven by subsequent model testing. The test program included tensile, flexural, compressive, interlaminar, and bearing strength as well as thermal conductivity and thermal expansion. The S-glass in an epoxy of the Polaris formulation<sup>4</sup> was judged by Toth [3] to have the most optimum overall properties for cryogenic use. (Commercial designations for the Polaris resin are E-787 and 58-68R.)

<sup>3</sup> The use in this paper of trade names of specific products is essential to the proper understanding of the work presented. Their use in no way implies approval, endorsement, or recommendation by NBS.

<sup>4</sup> The Polaris resin consists of Epon 828/Epon 1031/NMA/BDMA in proportions 50/50/90/0.55 pbw. It is referred to as the Polaris resin because of its successful use in that missile.

Two major reports appeared in 1967. In January the publication of the work of Soffer and Molho [4] reported the results of an intensive effort to develop improved epoxy resins for use in filament-wound cryogenic pressure vessels. Forty-one candidate resins were evaluated for mechanical properties and for suitability in filament-winding operations. Composite specimens using S-901 glass were evaluated in tension, interlaminar shear, and thermal expansion. As a result of this work, Soffer and Molho selected a modified epoxy system designated Resin 2 as superior for cryogenic use.<sup>3</sup> As a final evaluation, Resin 2 was compared with 58-68R (E 787) in a series of burst tests on metal-lined, S-901 glass filament-wound pressure vessels, the results showing Resin 2 to be clearly superior in the longitudinal filament stress level developed in the vessels at 77 and 20 K.

The second significant publication in 1967 was that of Lewis and Bush [5]. Again oriented toward filament-wound cryogenic tankage, the objective was to determine the extent to which various fiber finishes and coupling agents could be used to improve the cryogenic properties of composites reinforced with Aerojet General Hi-Stren glass. Naval Ordnance Laboratory (NOL) rings and flat specimens were used to obtain tensile, interlaminar shear, and thermal expansion data. The study also evaluated various modified epoxy matrices in an attempt to improve impact strength, toughness, and extensibility at cryogenic temperatures. It was concluded that glass finishing treatments could be used to improve bonding of filaments to the resin, thereby improving the mechanical properties, but that coupling agents were effective only in improvement of wet strength. At 77 K and 20 K, the highest pressure vessel longitudinal and hoop-filmament tensile strengths were again developed with Resin 2.

The foregoing studies encompassed 45 separate types of glass-reinforced composites which varied not only in the glass/polymer combination, but in methods of fabrication and testing. The present paper makes no effort to discuss all of the results in detail; rather, we shall confine our attention to the tensile strength, tensile modulus, thermal contraction, and thermal conductivity properties reported for the best of the composites evaluated in these works. We shall consider only uniaxial filament-wound (UFW), biaxially filament wound (BFW) of 0/90 orientation, and woven-cloth layouts. Data for UFW composites are restricted to the longitudinal properties, while data for the BFW and cloth composites refer to properties parallel to one major fiber direction unless otherwise noted.

#### Mechanical Properties

Figure 1 shows the expected superiority of the UFW glass-epoxy

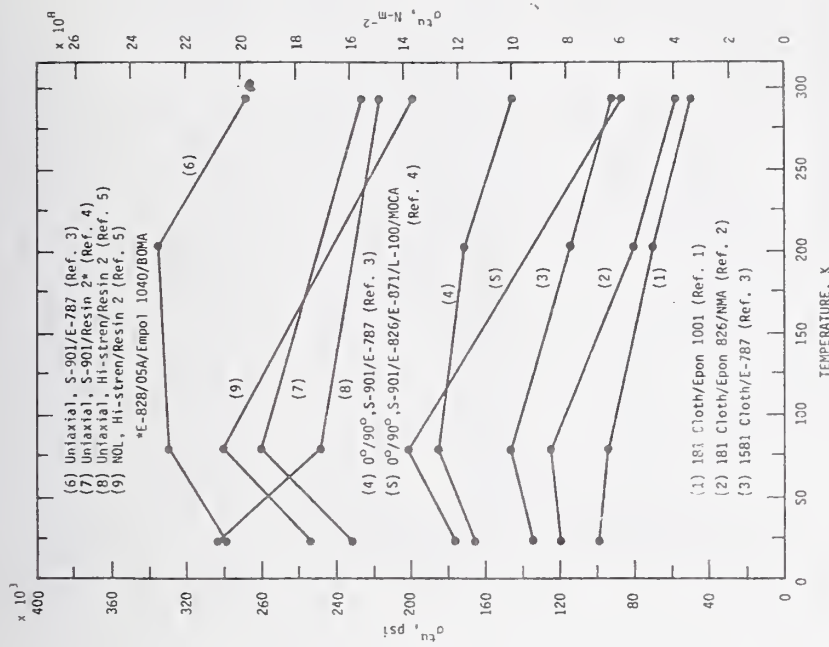


FIG. 1.—Ultimate tensile strength,  $\sigma_u$ , of glass-epoxy composites at cryogenic temperatures.

composites in ultimate tensile strength, with the BFW and cloth composites having sequentially lower strengths. The strength increased for all composite types upon cooling to 77 K; however, below 77 K the data appear erratic. The latter phenomenon is observed to some extent in all of the mechanical properties of filamentary-reinforced polymeric-matrix composites.

These data suggest that one can expect a maximum tensile strength on the order of 100 to 140 ksi at 77 K for cloth-reinforced epoxies, while BFW composites are capable of developing considerably higher strengths, on the order of 180 to 200 ksi at this temperature. More scatter is observed in the UFW data, which is somewhat surprising, as the tensile strength in this orientation should be essentially fiber controlled.

<sup>3</sup>Epon 828/DSA/EMIPOL 1040/BDMA in proportions 100/115.9/20/1 pbw. As this formulation was developed under NASA sponsorship, it will henceforth be referred to as NASA Resin 2.

It may be that, within the cryogenic temperature range, the temperature-sensitive properties of the matrix are affecting the overall strength even in the UFW composites, possibly by altering the neighbor fiber interactions at fracture sites. It may also be that the difficulty in obtaining valid test data from UFW composites at cryogenic temperatures accounts for some of this scatter. Nevertheless, it appears that about 280 ksi is not an unreasonable expectation for the tensile strength of UFW composites in the fiber direction at 77 K. It is this exceptional strength coupled with comparatively low cost that has maintained the popularity of glass-fiber reinforced composites.

Curve 5 has been included on Fig. 1 to illustrate the results obtained with an epoxy polyblend designed for greater flexibility at low temperatures. The strength of this polyblend<sup>6</sup> is low at 295 K, but increases rapidly on cooling. On the basis of the mechanical properties at cryogenic temperatures, this particular polyblend, designated Resin 4A by Soffer and Molho, was considered by them to be the best of the resins they studied, as it was the only resin tested that did not crack during thermal shock and impact testing at cryogenic temperatures, and its notch toughness was superior to all other resins tested in the program. The authors concluded, however, that the processing characteristics of this polyblend were unfavorable, and the NASA Resin 2 formulation was selected as their overall choice of matrix material for filament-wound composites.

The UFW composite data of Fig. 1 illustrate the results reported for the epoxy formulations E-787 (58-68R) and NASA Resin 2. On the basis of these data, E-787 (58-68R) produces the higher tensile values, at least to 77 K. However, these data may not be directly comparable because of possible differences in fiber/resin ratios. Composite tensile strengths of a specific specimen are dependent on this ratio (as well as on fiber orientation), higher fiber contents yielding higher composite strengths and moduli in the direction of the reinforcement. Also, the work of Soffer and Molho has shown that the specific application may affect the choice of matrix resin. At this point it must be concluded that both of these resins should receive equal consideration for cryogenic applications.

The initial tensile moduli for the same composites appear in Fig. 2. The moduli generally tend to increase upon cooling to 77 K; however, there does not appear to be consistent behavior, even among composites of the same type and layup, possibly due to resin content variations. As with the tensile strength, the tensile modulus appears to become erratic upon further cooling to 20 K.

The cloth-reinforced composites have the lowest modulus, ranging from  $4.5 \times 10^6$  psi at 77 K, the highest of these being reported for 1581/E-787. The S-901/E-787 BFW composite has a substantially higher modulus at

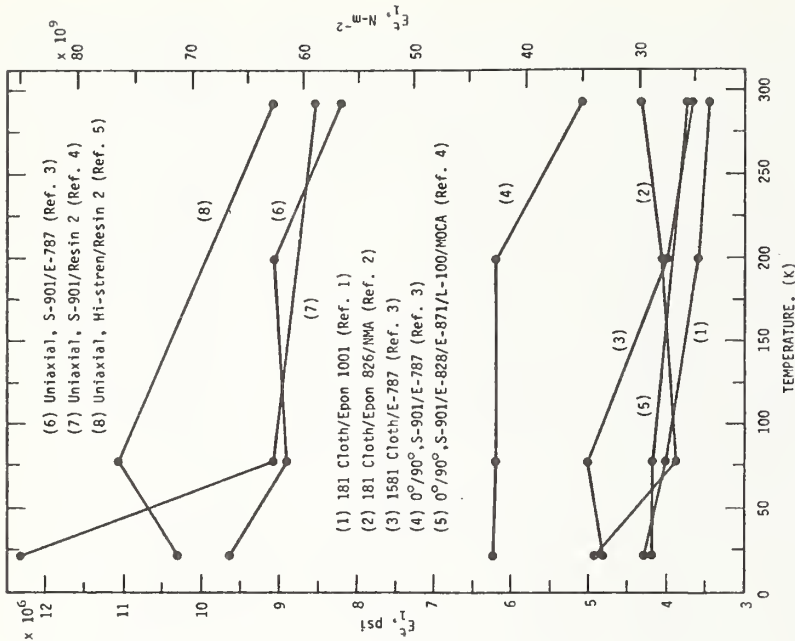


FIG. 2.—Initial tensile moduli,  $E_1$ , of glass-epoxy composites at cryogenic temperatures.

slightly over  $6 \times 10^6$  psi at this temperature. Note, however, that the polyblend BFW composite has a tensile modulus no better than that of the cloth-reinforced materials and shows very little temperature sensitivity. The UFW composites have the highest moduli, as is expected. The Hi-Stren/NASA Resin 2 composite appears to have the highest modulus; however, it should also be noted that Hi-Stren glass has a modulus 8 percent higher than S-901 glass. The latter data resulted from a series of tests investigating the effects of glass finishes on the mechanical properties, and the reported higher values of composite moduli may reflect superior bonding at the glass-matrix interface as well as higher fiber modulus. It would appear from these data that an initial tensile modulus of from  $9$  to  $10 \times 10^6$  psi might reasonably be expected from UFW glass-

epoxy composites at 77 K. It is these low moduli of glass-reinforced composites that have stimulated the development of advanced-fiber composites.

It is apparent from Figs. 1 and 2 that if one wishes to speak with any degree of specificity about the temperature dependence of the tensile properties of a glass-fiber reinforced composite in the cryogenic region, one is pretty well constrained to talk about a specific composite and fiber/resin ratio, particularly for temperatures below 77 K. This is further illustrated in Fig. 3, which is a frequency histogram compiled from all available literature data on the temperature dependence of the tensile properties of glass-epoxy composites of the three considered layup types. Figure 3a of this diagram shows that cooling from 295 K to 77 K produces an increase in tensile strength in all cases, the extent of the increase ranging from 10 ksi to as much as 130 ksi, with the highest probability of obtaining an increase on the order of 30 to 60 ksi. However, on cooling further to 20 K these data suggest a high probability of little or no change in tensile strength, but with the distinct possibility of a strength loss of as much as 70 ksi or a strength gain of as much as

40 ksi. The data also indicate that the probability of a strength change of a given magnitude is independent of the layup type, which, by inference, suggests that the erratic behavior below 77 K is a matrix-controlled phenomenon.

Comparable statistical data for the tensile modulus of glass-epoxy composites presented in Fig. 3b indicate the probability of a modest modulus increase on the order of from  $0.6$  to  $0.8 \times 10^6$  psi on cooling to 77 K, but with a finite chance that the modulus may decrease by as much as  $0.8 \times 10^6$  psi or that it may increase by as much as  $2 \times 10^6$  psi. The results of further cooling to 20 K are more difficult to interpret. In general, the data seem to cluster around a small increase of modulus up to about  $0.6 \times 10^6$  psi for cloth reinforcement and suggest that a somewhat larger increase on the order of from 0.6 to  $1.3 \times 10^6$  psi could be obtained with crossply or uniaxial composites. Nevertheless, the range of scatter from  $-0.8$  to  $3.2 \times 10^6$  psi is again indicative of very erratic behavior upon cooling below 77 K. Microbuckling of fibers due to resin shrinkage and minimal stress relaxation at cryogenic temperatures may lead to variations in initial tensile modulus and account for some of data scatter.

This erratic behavior in strength and modulus when testing at 20 K cannot be attributed to a sudden embrittling of the epoxy matrix, as 77 K is already far below the glass-transition temperature of the matrix. Nor can it be reasonably attributed to a sudden increase in the difficulty of obtaining reliable test data, as there is no *a priori* reason for a test method giving reliable data at 77 K to become entirely unsuitable at 20 K. The author does not know the answer to this problem. However, in searching for an explanation, consideration should be given to the results of some recent studies which have shown that, at least in the linear polymers of the polycarbonate and polyethylene terephthalate types, the medium in which a low-temperature test is conducted can strongly affect the resultant mechanical properties [6,7]. These studies indicate that yield and fracture of such polymers in the cryogenic temperature range are controlled by a crazing phenomenon which is strongly influenced by the activity of the gas or liquid in contact with the polymer surface. As all reported data on the mechanical properties of composites at cryogenic temperatures have been obtained at liquid nitrogen or liquid hydrogen temperatures, it must be considered at least a possibility that the observed anomalous behavior is a synergistic effect of a given type of polymer in contact with a given ambient medium.

#### Thermal Properties

Figure 4 presents the data reported by Toth et al. [3] for the temperature dependence of the thermal contraction of several of the E 787 matrix

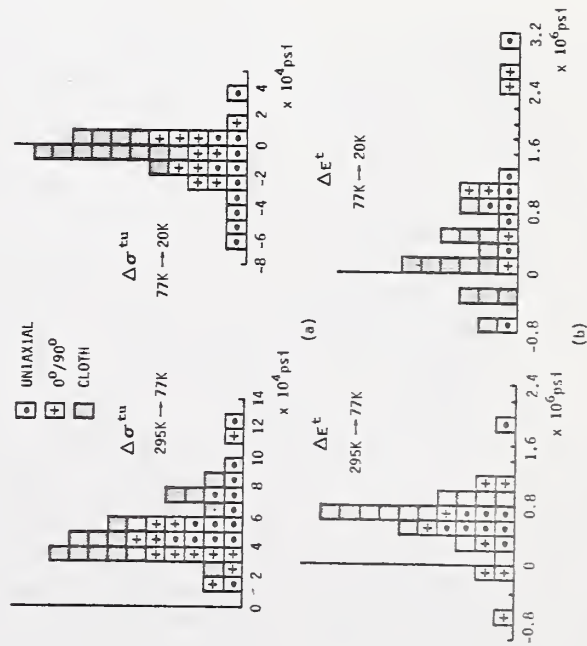


FIG. 3.—Histograms illustrating changes in tensile properties of glass-epoxy composites upon cooling into the cryogenic range. The ordinate represents the number of literature references reporting property changes of a given magnitude.

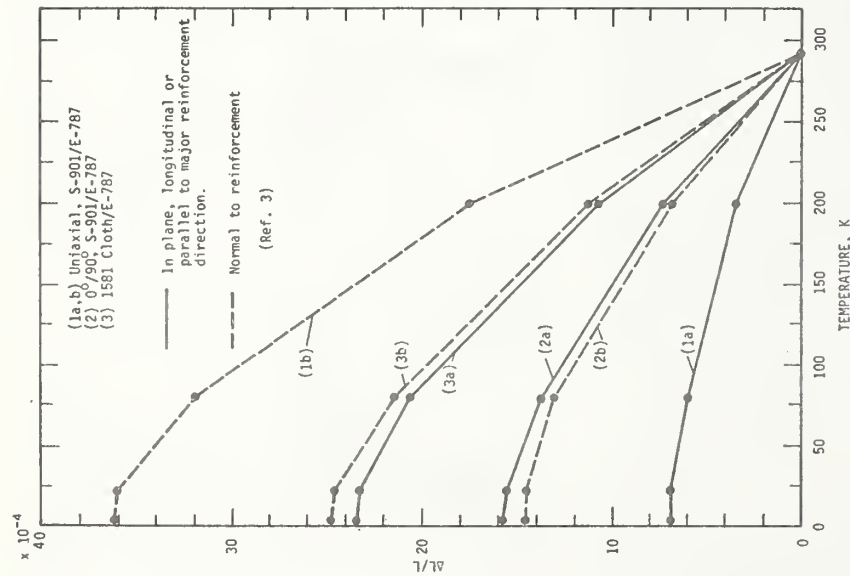


FIG. 4—Thermal contraction,  $\Delta L/L$ , of glass-epoxy composites at cryogenic temperatures.

composites that appear in Figs. 1 and 2. As the thermal contraction of the epoxy is significantly larger than that of the glass, there will generally be a difference between the thermal contraction in the plane of reinforcement and that normal to the plane (thickness direction). Contraction in the reinforcement direction in the case of a UFW composite is held to a minimum by restraint of the glass, as shown by curve 1a, while contraction in the reinforcement-normal direction in this type of composite is very large, the BFW case, the glass providing negligible restraint in the latter case. In the case of the UFW composite, about proportional to the decrease in

fiber density. However, contraction in the reinforcement-normal direction in this type of layup is also quite low, curve 2b, reflecting the effective restraint provided by the crossplied glass fibers, which are in close proximity. The in-plane contraction of the cloth composite is the highest of the group as shown by curve 3a, reflecting the lower glass content of such composites and the lesser restraint provided by the convoluted fibers, which, in general, do not lie parallel to the reinforcement plane. The reinforcement-normal contraction is also high for composites of this type, due both to the lesser total glass content and to the lesser restraint provided by the layered cloth.

It should be noted that, in general, the literature reports a reinforcement-normal contraction about twice that of the in-plane contraction for balanced-weave cloth-reinforced glass-polymeric composites in contrast to the similar values reported by Toth for 1581/E-787.

Thermal conductivity is also an important parameter in cryogenic design. Unfortunately, improper experimental technique invalidates some of the data in the literature—primarily, failure to properly compensate for radiation losses, which can introduce errors on the order of 100 to 200 percent in the higher temperature ranges. Figure 5 presents what the author believes to be the best available data for glass-epoxy composites, based on the work of Campbell et al [8] and of Hertz [10].

Thermal conductivity differs from the other thermal properties of composites in that it is significantly affected by the ambient atmosphere in which the test is conducted. The literature data suggest that, compared with the values obtained in helium, data taken in nitrogen will average about 7 percent lower, while data taken in vacuum will average about 20 percent lower. Campbell [8] suggests that the low value in vacuum primarily reflects the difficulty of obtaining good contact between the composite specimen and the mating parts of the thermal conductivity apparatus. An ambient atmosphere of nitrogen or helium increases the measured conductivity by reducing this contact resistance; however, diffusion of the gas (particularly of helium) into pores within the composite was also found to contribute to an increase in conductivity, as the gas provides an overall improvement in the thermal path within the composite. This explanation appears plausible, as it is consistent with the effect of the ambient atmosphere being observed over the entire 20 K to 295 K temperature range. The present author believes, however, that consideration should also be given to the effect on thermal conductivity of a matrix which has cracked due to thermal contraction at very low temperatures. The effect of the latter would be to increase the spread between conductivities measured in the various ambient media.

As the data taken in vacuum appear to be subject to the largest error, the data appearing on Fig. 5 are averages reported for tests in nitrogen and helium.

crossply; however, such a composite layup would be expected to develop intermediate conductivities in both directions, the in-plane conductivity being lower than the UFW due to lower fiber density in the direction of heat flow, while the plane-normal value should be higher than that for cloth due to the overall higher fiber density.

#### Other Matrices

For the sake of brevity, the author has had to confine the discussion thus far to epoxy matrix composites, although the referenced works contain data on many other matrix materials. Concentration on the epoxies is somewhat justified in that such materials are today the almost universal choice for demanding cryogenic service, based on their generally superior performance qualities. For example, if the tensile strength of cloth-epoxy specimens is taken at 100 ksi at 77 K, the next strongest composites consisting of the polyurethanes, polyesters, phenolics, Teflons, and polybenzimidazoles would form a group at about 70 to 80 ksi. The silicones, phenyl silanes, and polyimides form a third and lower strength group at about 40 to 50 ksi. The epoxies also excel in flexural and compressive strength. Only in modulus are the epoxies equaled (and often exceeded) by the phenolics, polybenzimidazoles, and phenyl silanes.

#### Fatigue

The author wishes to conclude this section on glass-reinforced composites with a brief discussion of the tensile fatigue studies of Brink [11] and of Chamberlain et al [2], as these data constitute almost the entire body of research on the dynamic properties of glass-reinforced composites at cryogenic temperatures. The only other work known to the author is the study by Fontana [11] using a reciprocating-beam method and by Laven-good and Anderson [12] in torsion.

The work of Brink and Chamberlain was, with one exception, conducted with 181-cloth reinforced composites and included the variety of matrix material listed in Fig. 6, which is a plot of the failure stress of each material after 10<sup>6</sup> cycles at the various temperatures. Figure 6 also records the percent of the original single-cycle ultimate tensile strength retained by each composite type after 10<sup>6</sup> cycles. Glass-reinforced polymers have reduced fatigue performance when compared with many alloys or with the advanced composites. However, these data show that the absolute magnitude of the stress required to induce failure after 10<sup>6</sup> cycles generally increases with decreasing temperature. At 200 K and 20 K, the polybenzimidazoles showed superior performance, while equalling the best at 77 K. Furthermore, the percentage of original strength retained by the polybenzimidazoles was consistently among the highest of the group. The better fatigue performance of this material may be accounted for by the

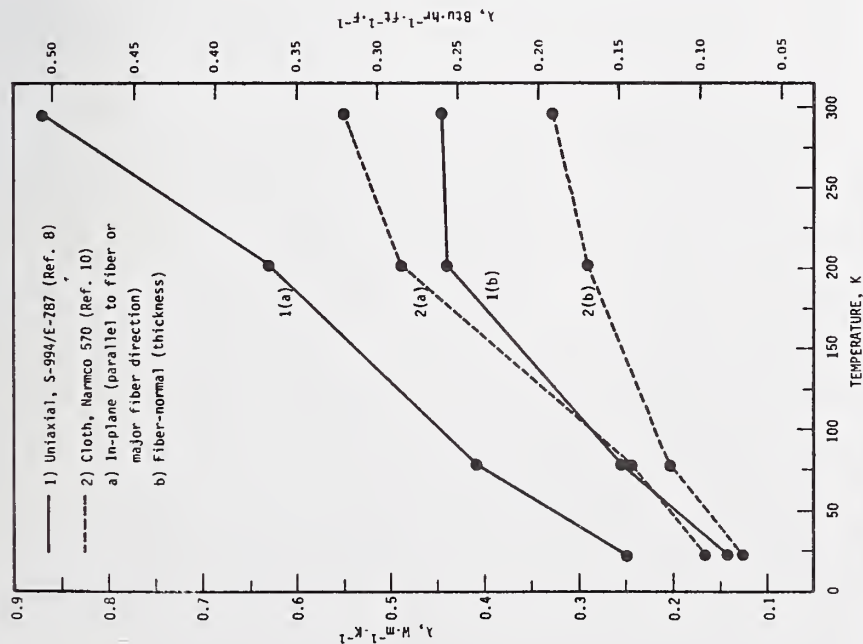


FIG. 5.—Thermal conductivities,  $\lambda$ , of glass-epoxy composites at cryogenic temperatures.

Thermal conductivity at 20 K is 30 to 40 percent of that at 295 K. The difference between both the fiber-normal and the in-plane conductivities and the absolute spread of values is widest at room temperature, converging as the temperature is lowered. Conductivity is the highest for the UFW composite in the fiber direction, reflecting both the high density of fibers and the higher conductivity of glass as compared with the epoxy matrix. Fiber normal conductivity in the UFW composite is much lower than the in-plane value. Lower conductivity in both directions is observed for the cloth-reinforced composite, reflecting the lower fiber density of such composites. No reliable data were available for a 0/90

The available data are insufficient to either prove or disprove the existence of a fatigue limit at cryogenic temperatures, although the S-N curve reported by Brink [1] for 181/Epon 1001 did appear to be reaching a limit at about 30 percent of the original strength at temperatures below 77 K.

### Advanced Composites

#### Overview

The application of carbon fiber reinforced epoxy composites to filament-wound cryogenic tankage was investigated by Simon, Larsen, and Alfring, their results appearing in a series of reports in 1970, 1971, and 1972 [13-15]. Their initial task was to evaluate the tensile, flexural, and laminar shear, bending fatigue, and thermal expansion properties of several fibers and resins in the form of strands, bars, and NOL rings from 295 K to 20 K. The tensile modulus of these CFRP composites was observed to increase up to 20 percent on cooling to 77 K, concomitant with a decrease in ultimate tensile strength by as much as 30 percent. Bending fatigue at 50 percent of the tensile ultimate was found to cause less deterioration after 1000 cycles at cryogenic temperatures than at room temperature. The thermal contraction tests revealed a slight negative coefficient, indicating that the resin matrix might see up to 1.5 percent strain when cooled. The second task was the design and testing of filament-wound tanks using Morganite (Modmor) II and Thornel 50 fibers in a NASA Resin 2 matrix. Results indicated that these CFRP wrapped tanks would be competitive with boron-reinforced tanks and possibly competitive with glass reinforcement in terms of strength/weight ratio.<sup>7</sup>

A third task undertook to study the effect of elastomeric additions on the strength and fracture toughness of epoxy resins and of CFRP composites. Results were generally unimpressive except for a CBTN-modified ERLB 4617 resin composite which demonstrated significantly improved tensile and short-beam shear strength at cryogenic temperatures at the expense of a decrease in room temperature shear strength. The remaining tasks in this program were directed at a continued study of the effect of elastomer additions to the epoxy matrix. Simon and Larsen concluded that, based on their data, Courtaulds HT-S fiber in a NASA Resin 2 matrix was a satisfactory combination for general cryogenic use for both UFW and BFW composites.

In 1972, Hertz, Christian, Varlas, et al published the results of a com-

<sup>7</sup>More recent work with improved graphite fibers indicates 295 K pressure vessel strength/weight ratios higher than for glass and slightly lower than for PRD 49-111 (Kevlar 49).

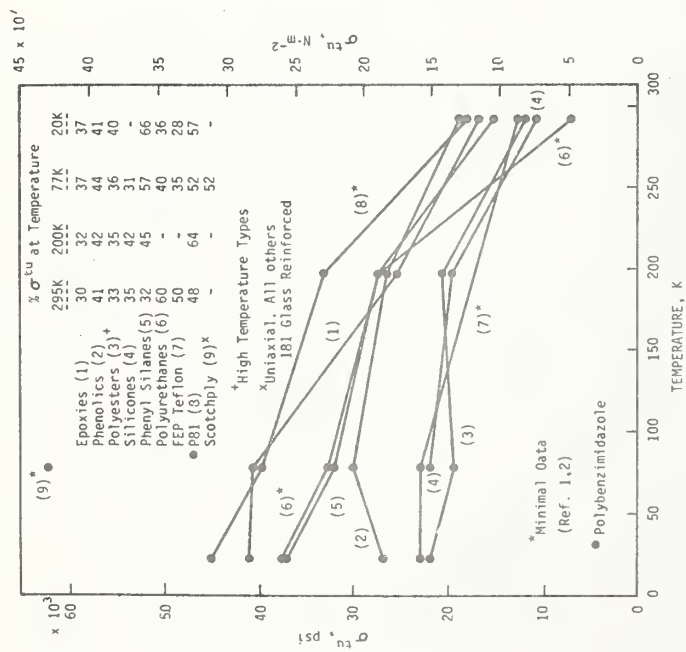


FIG. 6—Failure stress of glass-reinforced composites,  $\sigma_b$ , as a function of temperature after  $10^6$  fatigue cycles.

very low in-plane thermal contraction of polybenzimidazole composites—about one-third that of the epoxies—which decreases the residual stress at the glass-matrix interface at cryogenic temperatures. As the polybenzimidazole composites also compare well with the epoxies in static strength properties, another look at the polybenzimidazole types may be warranted for cryogenic applications requiring good dynamic performance.

The epoxies also look comparatively good, but primarily because of their high initial strength—their percentage of retained strength was among the lowest of the group. In general, the polyurethanes, phenyl silanes, and phenolics grouped into intermediate performance, while the polyesters, silicones, and Teflons had distinctly lower fatigue properties. Figure 6 contains only one data point for a UFW glass-epoxy composite at 77 K. This material had a much higher absolute strength after  $10^6$  cycles than any of the cloth-reinforced materials; however, it retained only about 52 percent of its original strength.

showed the presence of an initial accelerated stage, followed by a much lower secondary creep rate.

### Mechanical and Thermal Properties

Figures 7-12 illustrate the temperature dependence of the ultimate tensile strength, tensile modulus, thermal contraction (expansion), and thermal conductivities of a series of advanced composites selected by the authors of the aforementioned studies as being most useful in cryogenic applications. These data show the commercial BFRP and Borsic-aluminum composites to be almost in a class by themselves, having the highest

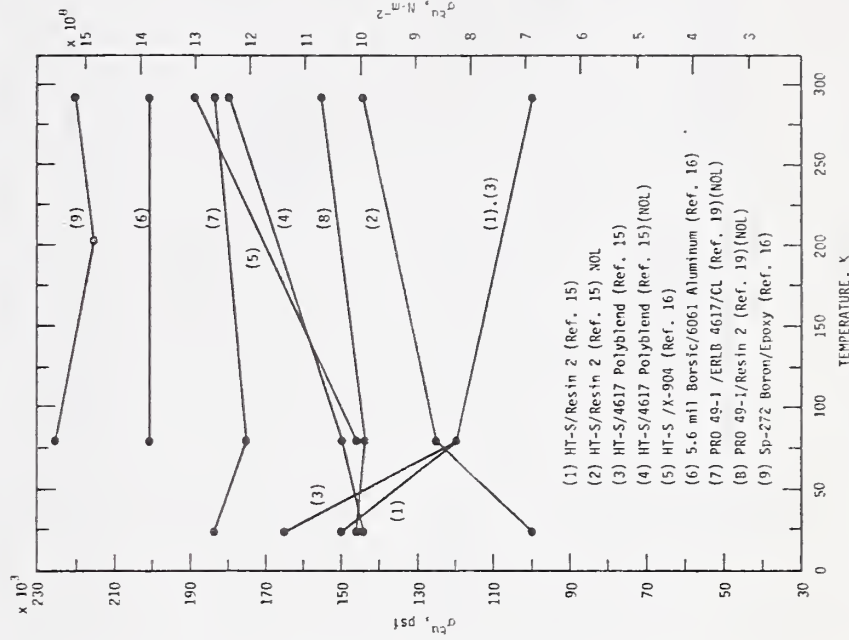


FIG. 7—Uniaxial longitudinal ultimate tensile strengths,  $\sigma_u$ , of advanced composites at cryogenic temperatures.

prehesive study on the materials development portion of a larger program investigating advanced composites for specific uses in spacecraft and missiles [16]. The associated studies on the structural development of part of this program may be found in Ref 17, while the development of hardware is reported in Ref 18. The objective of the study was to select advanced composites systems capable of operating for relatively short times over a 77 to 450 K temperature range. Work was directed toward the selection of two types of CRFP composites, one of high modulus and one of high strength. Boron-fiber reinforced aluminum (6061) was also studied to relate variations in mechanical properties to variables in production method or in fiber diameter. Boron-fiber reinforced plastic (BFRP) composites in the form of the commercial SP-272 material were also investigated. The mechanical and thermal properties of these materials were characterized from 77 to 450 K, including thermal expansion, thermal conductivity, specific heat, electrical resistivity, and thermo-optical properties. Three materials—5.7-mil Borsic/6061 aluminum, HT-S/X-904 epoxy, and a hybrid CFRP system utilizing both GY-70 and HM-S fibers in an X-904 epoxy matrix—were selected for determination of design allowable data. Some data on the effects of various environments on the mechanical and thermal properties of the selected composites were also reported.

Hoggatt in 1971 [19] and Hanson [20] in 1972 published the initial data on the cryogenic properties of PRD-49/epoxy composites. Hoggatt first investigated the suitability of PRD-49\* for filament-winding applications and subsequently determined the basic property data (tensile, interlaminar shear, and thermal expansion) down to 20 K. These data were then used in the design, fabrication, and testing of a series of cryogenic pressure vessels. Results indicated that the specific strength of vessels made with PRD-49-I fiber was about the same as that for S-glass; however, the specific modulus of the PRD-49 tanks was almost three times higher. These data were obtained with epoxy matrices of both the NASA Resin 2 and ERLA 4617/CL type. Hoggatt concluded that the results justified further investigation of PRD-49 for cryogenic applications. Some recent work by Chiao et al [20] supports this conclusion, showing that pressure vessels reinforced with PRD 49-III fiber may develop specific strengths 30 to 50 percent higher than that of comparable glass-reinforced vessels at both room and cryogenic temperatures.

The studies of Hanson [21] considered both the strength and creep behavior of PRD-49-I and PRD-49-III composites from 20 to 477 K, using an ERLA 4617 epoxy matrix. At 20 K, the ultimate tensile strength of the PRD-49-III composite was found to be about 90 percent of that at room temperature, while an increase in tensile modulus by about 40 percent was noted. The creep tests, all conducted at or above room temperature,

\* Product of the E. I. DuPont Company now called Kevlar 49.

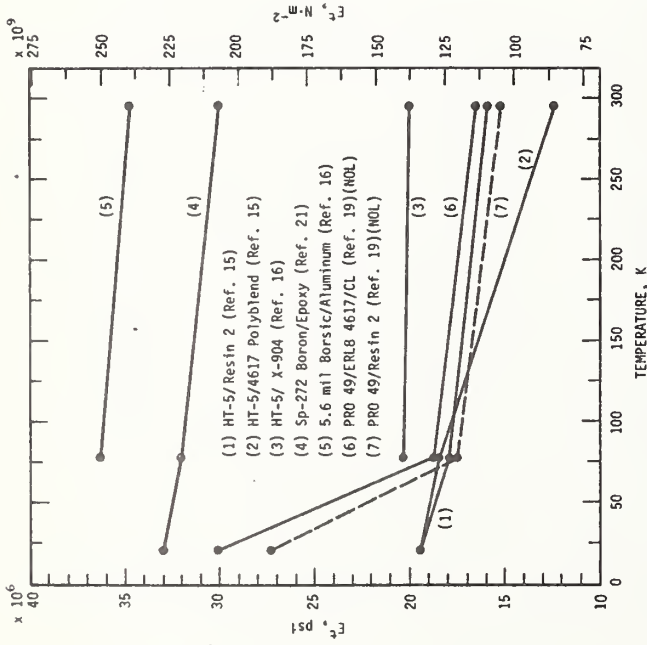


FIG. 8—Uniaxial longitudinal tensile moduli,  $E_L$ , of advanced composites at cryogenic temperatures.

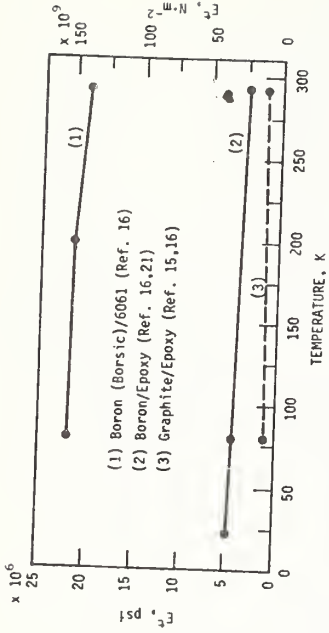


FIG. 10—Uniaxial transverse tensile moduli,  $E_T$ , of advanced composites at cryogenic temperatures.

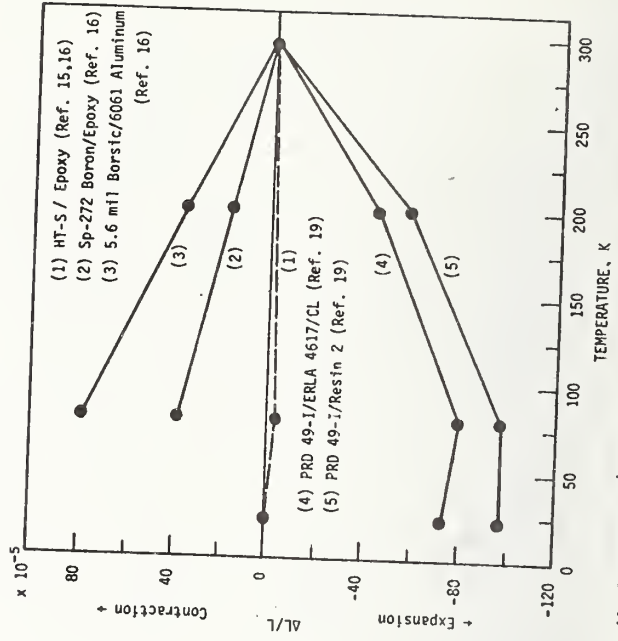


FIG. 11—Uniaxial longitudinal thermal expansion and contraction,  $\Delta L/L$ , of advanced composites at cryogenic temperatures.

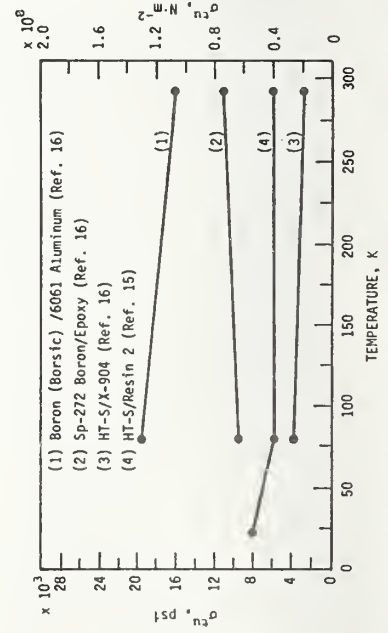


FIG. 9—Uniaxial transverse ultimate tensile strengths,  $\sigma^u$ , of advanced composites at cryogenic temperatures.

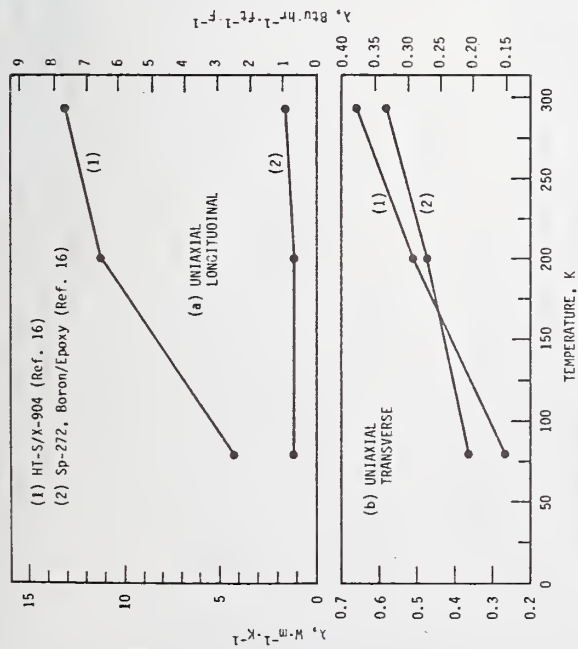


FIG. 12—Thermal conductivities,  $\lambda$ , of advanced composites at cryogenic temperatures.

strengths, highest moduli, and undergoing thermal contraction during cooling. Conversely, the CFRP and PRD-49 materials have somewhat lower strengths, considerably lower moduli, and undergo varying degrees of expansion upon cooling.

The strongest of these materials is the boron-epoxy, which develops about 225 ksi at 77 K and for which the tensile strength shows a relatively small temperature dependence. The modulus of this material is also very high, about  $32 \times 10^6$  psi at 77 K, with the modulus appearing to slightly increase on cooling. Boron-epoxy contracts a relatively modest amount in the fiber direction, with the transverse contraction being about half of that in the fiber direction. The data shown on Fig. 7 are for the commercial SP-272 product reinforced with 4.2-mil boron fiber. Nadler et al [22] have also evaluated this product as well as an equivalent material, Narmco 5505, reporting strength data very close to that of Hertz. The tensile modulus data plotted in Fig. 8 reflect the work of Nadler, as Hertz did not evaluate this parameter. The 4.2-mil fiber is currently being replaced by 5.6-mil fiber in many applications, as the latter produces a less costly composite with slightly higher tensile properties. The cryogenic properties of the 5.6-mil composites have not been reported.

The uniaxial transverse tensile strength of the BFRP material is lower than

that of boron-aluminum but is higher than that of the CFRP material. The uniaxial transverse modulus is about  $5 \times 10^6$  psi, distinctly lower than the boron-aluminum, but again higher than that of the CFRP material. The thermal conductivity is very low, particularly in the fiber-normal direction, which is an attribute in many cryogenic applications.

The plotted data illustrate the results reported by Hertz for the 5.6-mil boron fiber in its Borsic variant as a reinforcement for 6061 aluminum. Conventional 5.6-mil and 4.2-mil boron-reinforced 6061 alloys were also investigated; however, the ultimate tensile strengths of the latter were reported to be about 20 ksi lower than that for the Borsic reinforcement. Borsic (or boron) reinforced aluminum alloy appears to be an excellent choice for cryogenic applications wherever the high thermal contraction and high thermal conductivity can be tolerated. Hertz reports an ultimate tensile strength of 200 ksi at 77 K for uniaxial longitudinal Borsic/6061 combined with a very high tensile modulus of about  $35 \times 10^6$  psi. The 20-ksi transverse tensile strength and a transverse tensile modulus in excess of  $20 \times 10^6$  psi at 77 K are also impressive compared with the values for the other types of composites. These properties appear to have very little temperature sensitivity. No data were available on the thermal conductivity of boron-aluminum composites at cryogenic temperatures; however, it is certain to be matrix-dominated and very high.

Hoggatt's data for PRD 49 gives some evidence of why this new fiber is considered important. The present data suggest that the PRD 49/ERLB 4617/CL composite ranks next to the boron-aluminum in strength with a respectable 180 ksi, although the same fiber in a Resin 2 matrix comes in considerably lower at just over 140 ksi. Being NOL ring data, these values may be conservative, as the latter test is not strictly uniaxial. The moduli values of  $18$  to  $19 \times 10^6$  psi at 77 K do not appear at first to be outstanding; however, they are in the same range as the HT-S CFRP composites, and, furthermore, this value would be compared with the  $10 \times 10^6$  psi maximum modulus available for glass-reinforced composites for which PRD 49 is seen as a substitute. PRD 49 looks even better in modulus at 20 K, if the extremely large increase observed by Hoggatt in his NOL ring tests proves to be a real effect.

The data show PRD 49 composites to have a very high negative coefficient of thermal contraction—much higher than that of the CFRP composites. Normally, this would produce a sufficiently high interfacial strain at cryogenic temperatures to cause significant degrading of the mechanical properties. This does not appear to be the case with PRD 49 fiber.

Finally, a look at the CFRP data for the HT-S fiber in a series of epoxy matrices illustrates some of the problems encountered in attempting to characterize CFRP material for cryogenic use. While Simon and Larsen have shown that HT-S fiber can be put to good practical use in filament-

wound cryogenic vessels, the tensile strength data appearing in Fig. 7 would hardly justify optimism in this respect. As may be seen by comparing Curve 1 with Curve 2 and Curve 3 with Curve 4, the same composites show widely varying strengths and widely varying temperature sensitivities of strength depending on whether the test was conducted on flat uniaxial tension coupons or with NOL rings. This is, at the very least, good evidence of the need for more reliable test methods for use at cryogenic temperatures.

The moduli of the HT-S CFRP composites (all flat uniaxial coupons) show much less scatter and a tendency to converge to about  $19 \times 10^6$  psi at the lower temperatures. As regards the uniaxial transverse properties, the strength of the CFRP composites appears to be no more than half that of the BFRP composite at best, while the transverse moduli are extremely low, on the order of  $10^6$  psi. Curve 3 of Fig. 10 is dashed to indicate an approximate value, the actual data showing a spread from  $0.5$  to  $1.2 \times 10^6$  psi at 77 K.

The HT-S fiber composites have a very small negative coefficient of thermal contraction to 77 K. Curve 1 of Fig. 11 is also dashed to indicate approximate values. The slight reversal in contraction indicated below 77 K for this material (seen also in the PRD 49 composite in Curve 4) is apparently a real effect. Finally, from Fig. 12 we observe that the thermal conductivity of the CFRP composites is much higher in the fiber direction than is the case for the BFRP material, reflecting the relatively high thermal conductivity of the graphite itself. This difference largely disappears in the transverse direction.

### Summary

Glass-reinforced polymers will continue to be used in cryogenic applications requiring high tensile strength combined with high toughness but where stiffness is not required and where cyclic fatigue is not a major problem. The data reviewed in this paper suggest that, at this time, glass filament-wound with either Resin 2 or the Polaris formulation is satisfactory for cryogenic applications. When considering the use of NASA Resin 2, the reader should be aware that this resin formulation has been optimized for cryogenic service and therefore has relatively poor elevated temperature properties. Care must be taken to properly support components made with this resin whenever elevated temperature vacuum degassing of an assembly is required.

The commercial boron-epoxy and boron-aluminum materials appear to perform very well at cryogenic temperatures and should be among the first materials considered for applications requiring very good strength combined with exceptional stiffness.

The carbon fiber reinforced epoxies seem less advantageous, as their

mechanical properties appear to become substantially degraded upon cooling, however, some of this adverse behavior may reflect problems in obtaining valid test data on CFRP materials at cryogenic temperatures, as examples do exist of successful practical applications of CFRP structural materials in the cryogenic range.

The data on the cryogenic properties of composites made with PRD 49 fiber, although not very extensive, suggest that this relatively new material may be superior to carbon fibers for cryogenic use, although the large negative coefficient of thermal contraction may pose problems in some applications. In general, it appears that the epoxy resins most successful with glass-reinforcement are also very suitable for use with the advanced fibers.

This review suggests that the following work would be of value in implementing expanded use of structural composites for demanding cryogenic structural applications such as would be encountered in superconducting machinery:

1. The reason for the erratic mechanical property behavior in polymeric-matrix composites below 77 K must be ascertained. In particular, it is imperative to determine whether or not the type of cryogen in which tests are conducted has a significant effect on the mechanical properties.
2. Material research and evaluation must be directed toward obtaining the type of basic composite cryogenic property data which will be of most value to the design engineer. Contemporary composite theory requires full characterization of a uniaxial lamella of the composite of interest, that is, an experimental determination of the strength and moduli values is required for the prediction of limiting property values in complex crossply layups. Accurate tensile and compression data are required in the longitudinal and transverse modes plus accurate values for intralaminar (in-plane) shear. Even at room temperature, tension and compression testing in the reinforcement direction has proven difficult to perform with acceptable accuracy. Testing problems will be further complicated at cryogenic temperatures; however, these problems must be solved.
3. Having come to terms with the problems posed in (1) and (2), the static mechanical property data for the best of the glass-reinforced composites and of the state-of-the-art commercial boron-epoxy and boron (Borsic)-aluminum materials should be extended down to 4 K. Subsequently, PRD 49/epoxy composites should be evaluated over the entire cryogenic range and another look should be given to the CFRP materials, as the presently available data have an unacceptably large scatter which may well reflect difficulties in the testing procedures rather than inherent scatter in the material itself. All materials must be thoroughly characterized for resin/fiber density, void content, and fiber alignment.
4. Data on the performance of composites under dynamic loading conditions at cryogenic temperatures are minimal to nonexistent. Yet, these

types of data are mandatory if composites are to be used in cryogenic machinery. The available data are encouraging in that they suggest that fatigue performance at cryogenic temperatures is generally superior to that at room temperature. However, this will have to be more fully documented. As high-cycle fatigue testing at 4 K is very expensive, the materials included in such a testing program must be carefully selected. For this purpose, it would be very desirable to have an efficient screening type of test capable of correlating incipient damage with expected fatigue life. Data on thermal fatigue are also required, that is, the effect of repeated cool-downs on both the static and dynamic properties of composites must be determined.

#### Acknowledgments

The author wishes to thank Dr. R. P. Reed for his consultation and for review of the completed manuscript. This research was supported by the Advanced Research Projects Agency.

#### References

- [1] Brink, N. O., "Determination of the Performance of Plastic Laminates Under Cryogenic Temperatures," ASD-TDR-62-794, (AD 288 944), Air Force Systems Command, Wright-Patterson Air Force Base, Ohio, Aug. 1962.
- [2] Chamberlain, D. W., Lloyd, B. R., and Tennant, R. L., "Determination of the Performance of Plastic Laminates at Cryogenic Temperatures," ASD-TDR-62-794, Part II, (N64-24212), Air Force Systems Command, Wright-Patterson Air Force Base, Ohio, March 1964.
- [3] Toth, L. W., Boller, T. J., Butcher, I. R., Kariotis, A. H., and Yoder, F. D., "Program for the Evaluation of Structural Reinforced Plastic Materials at Cryogenic Temperatures," NASA CR-80061 (Final), (N67-12051), National Aeronautics and Space Administration, Marshall Space Flight Center, Ala., Aug. 1966.
- [4] Soffer, L. M., and Molloy, R., "Cryogenic Resins for Glass Filament-Wound Composites," NASA CR-72114 (Final), (N67-25076), National Aeronautics and Space Administration, Lewis Research Center, Cleveland, Ohio, Jan. 1967.
- [5] Lewis, A. and Bush, G. E., "Improved Cryogenic Resin-Glass Filament Wound Composites," NASA CR-72163 (Final), (N67-31856), National Aeronautics and Space Administration, Lewis Research Center, Cleveland, Ohio, March 1967.
- [6] Kastelic, J. R., Hillner, A., and Baer, E., *Journal of Macromolecular Science-Physics*, Vol. B7, No. 4, 1973, pp. 679-703.
- [7] *Relationships Between Structure and Mechanical Behavior in Polymeric Solids*, ASM Materials Science Seminar, Chicago, Ill., 1973 (to be published by American Society for Metals).
- [8] Campbell, M. D., O'Barr, G. L., Haskins, J. F., and Hertz, J., "Thermophysical Properties of Plastic Materials and Composites to Liquid Hydrogen Temperature (-423°F)," ML-TDR-64-33, Part III, (AD 468 155), Air Force Materials Laboratory, Wright-Patterson Air Force Base, Ohio, Aug. 1965.
- [9] Haskins, J. F., Campbell, M. C., Hertz, J., Percy, J. L., "Thermophysical Properties of Plastic Materials and Composites to Liquid Hydrogen Temperature (-423°F)," ML-TDR-64-33, Part I, (AD 601 337), Air Force Materials Laboratory, Wright-Patterson Air Force Base, Ohio, June 1964.
- [10] Hertz, J., "Investigation of Potential Low Temperature Insulations," General Dynamics/Astronautics Report GS/A-ERR-AN-688, Dec. 1964.

- [11] Fontana, M. B., Bishop, S. M., and Spretak, J. W., "Investigation of Mechanical Properties and Physical Metallurgy of Aircraft Alloys at Very Low Temperatures, Part 5—Mechanical Properties of Metals and a Plastic Laminate at Low Temperatures," AF Technical Report 5662, Part 5, (AD 27726), Air Force Materials Laboratory, Wright-Patterson Air Force Base, Ohio, Dec. 1953.
- [12] Lavengood, R. E. and Anderson, R. M., *Technical Papers*, 24th Annual Technical Conference, Society of the Plastics Industry, Section I1-E, 1969, pp. 107.
- [13] Simon, R. A. and Alfring, R., "Properties of Graphite Fiber Composites at Cryogenic Temperatures," NASA CR-72642, (AD 746 885), National Aeronautics and Space Administration, Lewis Research Center, Cleveland, Ohio, May 1970.
- [14] Larsen, J. V., "Properties of Graphite Fiber Composites at Cryogenic Temperatures—Effect of Elastomeric Additions to Resin Systems," NASA CR-72804, (AD 882 972), National Aeronautics and Space Administration, Lewis Research Center, Cleveland, Ohio, March 1971.
- [15] Larsen, J. V. and Simon, R. A., "Carbon Fiber Composites for Cryogenic Filament-Wound Vessels," NASA CR-120889, (N73-11553), National Aeronautics and Space Administration, Lewis Research Center, Cleveland, Ohio, May 1972.
- [16] Hertz, J., Christian, J. L., and Varias, M., "Advanced Composites Applications for Spacecraft and Missiles, Phase I Final Report, Volume II: Material Development," AFML-TR 71-186, Vol. 2, (AD 893 715L), Air Force Materials Laboratory, Wright-Patterson Air Force Base, Ohio, March 1972.
- [17] Forest, J. D., Fujimoto, A. F., and Foelsch, G. F., "Advanced Composite Applications for Spacecraft and Missiles, Phase I Final Report, Volume I: Structural Development," AFML-TR 71-186, Vol. 1, Air Force Materials Laboratory, Wright-Patterson Air Force Base, Ohio, March 1972.
- [18] Forest, J. D. and Varias, M., "Advanced Composites Applications for Spacecraft and Missiles, Final Report," AFML-TR 72-278, Air Force Materials Laboratory, Wright-Patterson Air Force Base, Ohio, March 1973.
- [19] Hoggatt, J. T., "Development of Cryogenic PRD 49-1 Filament-Wound Tanks," NASA CR-120835, (N72-24941), National Aeronautics and Space Administration, Lewis Research Center, Cleveland, Ohio, Dec. 1971 (also in *SAMPE*, Vol. 3, 1971, pp. 157-167).
- [20] Chiao, T. T., Hamstead, M. A., Marcon, M. A., and Hanasee, J. E., "Filament-Wound Kevlar 49/Epoxy Pressure Vessels," NASA CR-134506, National Aeronautics and Space Administration, Lewis Research Center, Cleveland, Ohio, Nov. 1973.
- [21] Hanson, M. P., "Effects of Temperature and Creep Characteristics of PRD-49 Fiber/Epoxy Composites," NASA TN D-7120, (N73-12697), National Aeronautics and Space Administration, Lewis Research Center, Cleveland, Ohio, Nov. 1972.
- [22] Nadler, M. A., Yoshino, S. Y., and Darms, F. J., "Boron/Epoxy Support Strut for Non-Integral Cryogenic Tankage," North American Rockwell Space Division Report SD-68-99501, Feb. 25, 1969 (see also 15th National Symposium, SAMPE, April 1969).

Appendix IV: R. E. Schramm and M. B. Kasen, "Static Tensile Properties of Boron-Aluminum and Boron-Epoxy Composites at Cryogenic Temperatures," Paper T3, Cryogenic Engineering Conference, Kingston, Ontario, July 22-25, 1975 (to be published).

STATIC TENSILE PROPERTIES OF BORON-ALUMINUM AND  
BORON-EPOXY COMPOSITES AT CRYOGENIC TEMPERATURES

R. E. Schramm and M. B. Kasen

Cryogenics Division  
Institute for Basic Standards  
National Bureau of Standards  
Boulder, Colorado

Paper T-3  
Preprinted for the  
Cryogenic Engineering Conference  
Kingston, Ontario, Canada  
July 22-25, 1975

STATIC TENSILE PROPERTIES OF BORON-ALUMINUM AND  
BORON-EPOXY COMPOSITES AT CRYOGENIC TEMPERATURES\*

R. E. Schramm and M. B. Kasen

Cryogenics Division  
Institute for Basic Standards  
National Bureau of Standards  
Boulder, Colorado 80302

ABSTRACT

State-of-the-art boron-aluminum and boron-epoxy composites have been mechanically characterized at 295, 76, and 4 K. Static tensile properties include elastic and shear moduli, Poisson's ratio, yield and ultimate strengths, and elongation. The data are in a form useful in strength or stiffness limiting predictions of complex crossply components using macromechanical composite theory. Both composite types performed well at cryogenic temperatures.

Key Words: Advanced fiber composites; boron-aluminum; boron-epoxy; cryogenics; static mechanical properties.

---

\* This research was supported by the Advanced Research Projects Agency of the Department of Defense under ARPA Order No. 2569; it is a contribution of the National Bureau of Standards, not subject to copyright.

# STATIC TENSILE PROPERTIES OF BORON-ALUMINUM AND BORON-EPOXY COMPOSITES AT CRYOGENIC TEMPERATURES

R. E. Schramm and M. B. Kasen

## INTRODUCTION

The Advanced Research Projects Agency is currently supporting research to characterize the properties of various structural materials at liquid helium temperature. The objective is to obtain design data for superconducting motors and generators. Fiber-reinforced polymer-matrix composites are included in this program because their low  $\lambda/E$  and  $\lambda/\sigma$  ratios suggest the possibility of substantial savings in refrigeration cost compared to metal construction. An aluminum-matrix composite is also included because the very high  $\sigma/\rho$  and  $E/\rho$  ratios of this electrically-conductive material suggests potential applications in components such as the eddy-current damper shield.

A comprehensive survey [1,2] suggested that the boron-reinforced composites require the least optimization for cryogenic service, as their room temperature mechanical properties are relatively unaffected by cooling to 76 K. We therefore selected boron-epoxy and boron-aluminum composites as the initial materials to be characterized. The static tensile mechanical properties at 295, 76 and 4 K of these materials are reported in this paper.

Macromechanical composite theories use key mechanical properties obtained from tensile, compressive, and shear tests on uniaxial laminates to predict strength and stiffness-limiting properties of complex crossply composites [3,4]. The key properties are the elastic constants,  $E_{11}$ ,  $E_{22}$ ,  $\nu_{12}$ ,  $G_{12}$ , and the associated strength parameters,  $\sigma_{11}$  and  $\sigma_{22}$ . Some analyses require additional parameters,  $\epsilon_{11}$ ,  $\epsilon_{22}$ , and  $\tau_{12}$ . This notation refers to the composite axes defined in Fig. 1. A complete characterization requires evaluation of compressive as well as tensile properties.

## MATERIALS AND TEST METHODS

Table 1 lists the materials studied in this program. All panels were obtained from commercial sources. Composite void content has not yet been determined; however, radiography failed to reveal any voids. The average ply

thickness was 0.017 cm (0.0067 in) for each material. The composite panels contained nominally 48% by volume 5.6 mil boron fiber. The 6061 aluminum alloy matrix was in the F temper (as diffusion bonded). The epoxy-matrix composite was fabricated from commercial prepreg tape. Uniaxial longitudinal ( $0^\circ$ ) tensile properties were determined from the 6-ply material, while the 15-ply material was used for evaluation of the uniaxial transverse ( $90^\circ$ ) tensile properties. The  $\pm 45^\circ$  panels were used to evaluate in-plane shear properties. Ideally, shear properties would also be determined directly from uniaxial laminates; however, the required specimens are expensive and require special test fixtures. The  $\pm 45^\circ$  tensile coupon method of calculating shear moduli is a simplified test procedure [5,6].

All testing was performed in air (295 K), liquid nitrogen (76 K), or liquid helium (4 K) on a universal testing machine at a strain rate of  $0.01 \text{ min}^{-1}$  using a tensile cryostat of conventional design [7]. Load cell calibration was confirmed by dead weights. Resistance strain gages, parallel and normal to the stress axis, were mounted on the uniaxial longitudinal and  $\pm 45^\circ$  specimens. The uniaxial transverse specimens were gaged only along the tensile axis. Strain values were calculated from manufacturer's gage factors and comparison with signal levels from precision shunt resistors in the commercial bridges. The strain gages failed at about 1% strain at cryogenic temperatures; however, larger strains were measured from crosshead displacement (corrected for load train strain) and from displacement of gage marks lightly scribed on the boron-aluminum specimens. Load and strain were recorded simultaneously with a two-pen recorder.

Test specimens were straight-sided coupons, 2.5 cm (1 in) wide for transverse and  $\pm 45^\circ$  orientations, and 1.3 cm (0.5 in) wide for the longitudinal fiber orientation. The boron-aluminum specimens were 15 cm (6 in) long with a 5 cm (2 in) gage length between grips; the boron-epoxy specimens were 28 cm (11 in) long with a 15 cm (6 in) gage length. Specimens were cut with a diamond saw. Before testing, the edges were lightly buffed with emery paper.

Grips were attached to the specimens in an alignment fixture. Specimen ends, wrapped with 100 mesh stainless steel screen, were sandwiched between serrated titanium plates attached to the load train by pins and clevises. Heavy

stainless steel pressure plates, each containing six pairs of screws, backed the titanium plates and provided compressive force on the grip. The torque on the screws was systematically increased toward the outer end of the grip to uniformly transfer the tensile load into the composite specimen. When finally assembled in the cryostat, the specimen alignment was within the limits prescribed in ASTM specification D 3039-71T [8].

The boron-epoxy specimens were conditioned for at least two days in 45 - 55% relative humidity at room temperature before testing. The boron-aluminum did not require preconditioning. At least three specimens were tested for each material, orientation, and temperature. The boron-epoxy was initially cycled three times within the elastic region (to about 25% of the tensile strength) to establish the repeatability of the modulus, before increasing the load to initiate fracture. The boron-aluminum was not cycled because of the low yield strength of the aluminum matrix.

Tensile fractures in composite materials commonly occur at the specimen grips, where a stress concentration inevitably exists. The gripping system described here reduced the frequency of grip failures to about 20%. Tensile strength data from specimens which failed close to the grips (within one specimen thickness) were rejected, even though there was no clear evidence that such failures affected the strength.

In-plane shear properties were calculated from analyses of the tensile stress-strain curves of the  $\pm 45^\circ$  specimens [5,6]. Poisson's ratio for the transverse specimens,  $\nu_{21}$ , was calculated from the reciprocity relation [5]:

$$\nu_{21} = \nu_{12} \frac{E_{22}}{E_{11}}$$

where  $E_{22}$  is from uniaxial transverse specimens and  $\nu_{12}$  and  $E_{11}$  is from uniaxial longitudinal tests.

#### RESULTS AND DISCUSSION

The static tensile properties and elastic constants for the boron-aluminum and boron-epoxy composites are presented in Table 2 and 3. In-plane shear moduli appear in Table 4. In accord with ASTM D 3039-71T, the number of specimens, standard deviation, and coefficient of variation (standard deviation

expressed as a percentage of the average value) are included. For only three or four tests, the calculated standard deviation is nearly equal to the data spread. Figures 2 and 3 illustrate the temperature dependence of the elastic moduli and tensile strengths of both composites.

Stress-strain curves for the uniaxial longitudinal test mode were essentially linear to fracture for both materials at all test temperatures. The uniaxial transverse boron-epoxy also failed with negligible yielding at 76 K and 4 K; however, some plastic deformation was observed at 295 K. All  $\pm 45^\circ$  and the boron-aluminum uniaxial transverse specimens yielded significantly prior to fracture at all test temperatures. The boron-aluminum uniaxial transverse and  $\pm 45^\circ$  specimens displayed discontinuous yielding at 295 and 4 K, but not at 76 K.

Cryogenic temperatures had relatively little effect on the measured mechanical properties. At 76 K, the averaged data indicate a minimum in the elastic modulus of boron-aluminum for the transverse and  $\pm 45^\circ$  orientations, as well as a decrease in the calculated in-plane shear modulus. However, the data scatter was such that this could be a statistical effect, rather than a true temperature effect. Significant temperature effects were noted in the orientations where the matrix contributes to the properties. Thus, the proportional limit of the  $\pm 45^\circ$  boron-aluminum slightly increased on cooling, while that of the boron-epoxy declined. Also, the elongation of the  $\pm 45^\circ$  boron-aluminum decreased sharply on cooling, while there was a relatively small change for boron-epoxy.

The aluminum-matrix composite exhibited less anisotropy than the epoxy-matrix composite, reflecting the higher strength and greater ductility of the aluminum. The boron-aluminum has a transverse modulus approximately 75% of that in the longitudinal direction, and about twice as high as that of the unreinforced 6061 aluminum alloy.

The in-plane shear modulus values calculated for the boron-epoxy appear to be in reasonable agreement with published room-temperature values [9]. However, the shear moduli calculated for the boron-aluminum are inordinately low. It has been shown that shear moduli calculated from analyses of  $\pm 45^\circ$  tensile stress-strain curves agree with moduli determined by more rigorous methods in

the case of graphite-epoxy and glass-epoxy composites [6]. However, Ramsey, Waszczak, and Klouman [10] report that the nonlinear stress-strain response of 5.6 mil boron-6061 aluminum in the F condition may invalidate the simplified  $\pm 45^\circ$  test method used here and lead to low shear moduli calculations for this material. The boron-aluminum values here serve only as lower boundaries and display the limits of this method.

#### ACKNOWLEDGMENT

The authors wish to thank Dr. Ralph Tobler of this laboratory for his careful reading of this manuscript.

#### NOTATION

E = Engineering Elastic Modulus

G = Engineering shear modulus

$\epsilon$  = Engineering strain

$\lambda$  = Thermal conductivity

$\nu$  = Poisson's ratio

$\rho$  = Mass density

$\sigma$  = Engineering stress

$\tau$  = In-plane shear stress

## REFERENCES

1. M. B. Kasen, "Properties of Filamentary-Reinforced Composites at Cryogenic Temperatures," to be published in ASTM STP 580, Composite Reliability.
2. M. B. Kasen, Cryogenics, 15(6): 327 (1975). (Also "Part II: Advanced Composites" to be published in Cryogenics).
3. Advanced Composites Design Guide, Third Edition, Volume II, Analysis, Air Force Materials Laboratory, Wright-Patterson Air Force Base, Ohio (1973).
4. M. E. Waddoups, in: Composite Materials Workshop, S. W. Tsai, J. C. Halpin, and N. J. Pagano, Eds., Technomic Publishing Co., Inc., Stanford, Ct. (1968), p. 254.
5. P. H. Pettit, in: ASTM STP 460, Composite Materials, Testing and Design, American Society for Testing and Materials, Philadelphia (1969), p. 83.
6. D. F. Sims and J. C. Halpin, in: ASTM STP 546, Composite Materials, Testing and Design, American Society for Testing and Materials, Philadelphia (1974), p. 46.
7. R. P. Reed and R. L. Durcholz, in: Advances in Cryogenic Engineering, Vol. 15, Plenum Press, New York (1970), p. 109.
8. 1973 Annual Book of ASTM Standards, Part 25, American Society for Testing and Materials, Philadelphia (1973), p. 608.
9. Advanced Composite Design Guide, Third Edition, Volume IV, Materials, Air Force Materials Laboratory, Wright-Patterson Air Force Base, Ohio (1973).
10. J. E. Ramsey, J. P. Waszczak, and F. L. Klouman, "An Investigation of the Non-Linear Response of Metal-Matrix Composite Laminates," AIAA/ASME/SAE 16th Structures, Structural Dynamics and Materials Conference, Denver, Colorado (May 27, 1974).

LIST OF TABLES

- Table 1. 5.6-mil Boron-Epoxy and Boron-Aluminum Composites.
- Table 2. Tensile Properties of Boron-Aluminum Composites (Averages of Specimens Tested).
- Table 3. Tensile Properties of Boron-Epoxy Composites (Averages of Specimens Tested).
- Table 4. In-Plane Shear Modulus (Averages of Specimens Tested).

LIST OF FIGURES

- Figure 1. Identification of composite Axes.
- Figure 2. Temperature dependence of the elastic modulus of boron-epoxy and boron-aluminum of various orientations. Error bars reflect  $\pm$  one standard deviation; in several instances, the error bars are smaller than the datum symbol.
- Figure 3. Temperature dependence of the ultimate tensile strength of boron-epoxy and boron-aluminum of various orientations. Error bars reflect  $\pm$  one standard deviation; in several instances, the error bars are smaller than the datum symbol.

Table 1. 5.6-mil Boron-Epoxy and Boron-Aluminum Composites.

Fiber Orientation	Number of Plies
Uniaxial	6
Uniaxial	15
$\pm 45^\circ$	10

Table 2

## Tensile Properties of Boron-Aluminum Composites

(Averages of Specimens Tested<sup>a</sup>)

Temperature (K)	Elastic Modulus, E (10 <sup>9</sup> N/m <sup>2</sup> ) (10 <sup>6</sup> psi) CV(%)	Poisson's Ratio, $\nu$		Proportional Limit, $\sigma^p$		0.2% Yield Strength, $\sigma_y$		Number of Specimens
		CV(%)	(10 <sup>-3</sup> psi)	CV(%)	(10 <sup>8</sup> N/m <sup>2</sup> ) (10 <sup>3</sup> psi)	(10 <sup>8</sup> N/m <sup>2</sup> ) (10 <sup>3</sup> psi)	CV(%)	
295	200(11)	29.0(1.6)	5.7	Longitudinal (0°)				4
	197(11)	28.5(1.6)	1.6					
	204(9)	29.6(1.3)	6.3					
295	161(18)	23.4(2.6)	11.0	Transverse (90°)				3
	128(24)	18.5(3.5)	18.7	0.241(0.027)	11.2 <sup>b</sup>	0.63(0.08)	9.1(1.1)	
	150(31)	21.8(4.6)	20.8	0.221(0.041)	18.6 <sup>b</sup>	0.76(0.11)	11.0(1.6)	
295	111(10)	16.0(1.4)	9.0	Crossply (± 45°)				3
	78(19)	11.3(2.8)	24.8	0.253(0.053)	20.8 <sup>b</sup>	0.72(0.19)	10.5(2.8)	
	101(15)	14.7(2.2)	14.9	0.396(0.021)	5.3	0.37(0.27)	5.4(4.0)	
76	197(11)	28.5(1.6)	1.6					3
	204(9)	29.6(1.3)	6.3					
	150(31)	21.8(4.6)	20.8	0.333(0.025)	7.5	0.15(0.06)	2.1(0.8)	
76	197(11)	28.5(1.6)	1.6					3
	204(9)	29.6(1.3)	6.3					
	150(31)	21.8(4.6)	20.8	0.373(0.034)	9.2	0.31(0.16)	4.4(2.2)	
76	197(11)	28.5(1.6)	1.6					3
	204(9)	29.6(1.3)	6.3					
	150(31)	21.8(4.6)	20.8	0.94(0.05)	19.4(0.7)	3.6	1.34(0.05)	
76	197(11)	28.5(1.6)	1.6					4
	204(9)	29.6(1.3)	6.3					
	150(31)	21.8(4.6)	20.8	1.78(0.14)	25.9(2.0)	7.8	1.96(0.09)	
76	197(11)	28.5(1.6)	1.6					3
	204(9)	29.6(1.3)	6.3					
	150(31)	21.8(4.6)	20.8	0.94(0.05)	19.4(0.7)	3.6	1.34(0.05)	
76	197(11)	28.5(1.6)	1.6					3
	204(9)	29.6(1.3)	6.3					
	150(31)	21.8(4.6)	20.8	0.94(0.05)	19.4(0.7)	3.6	1.34(0.05)	

Temperature (K)	Ultimate Strength, $\sigma_u$		Ultimate Elongation, $\epsilon_u$		Number of Specimens
	(10 <sup>8</sup> N/m <sup>2</sup> ) (10 <sup>3</sup> psi)	CV(%)	(%)	CV(%)	
295	12.7	184	Longitudinal (0°)		1
	16.4(0.6)	238(8)	-	0.6	
	16.1(0.9)	233(12)	3.4	0.8(0.0)	
295	1.67(0.18)	24.2(2.7)	Transverse (90°)		3
	2.49(0.08)	36.1(1.1)	5.3	0.8(0.1)	
	2.76(0.03)	40.0(0.5)	1.1	0.9(0.1)	
295	3.62(0.30)	52.5(4.4)	Crossply (± 45°)		3
	4.14(0.49)	60.0(7.1)	8.3	12.1(1.5)	
	4.11(0.12)	59.7(1.8)	3.0	4.2(1.0)	
76	4.14(0.49)	60.0(7.1)	11.8	6.7(2.1)	3
	4.11(0.12)	59.7(1.8)	3.0	4.2(1.0)	
	4.11(0.12)	59.7(1.8)	3.0	4.2(1.0)	

<sup>a</sup>Standard deviations are in parentheses. CV is coefficient of variation. Data from the specimens that broke at or in the grips are not included in the calculations of ultimate strength or elongation.

<sup>b</sup>Computed from  $\nu_{12}$ ,  $E_{11}$ , and  $E_{22}$ .

Table 3

Tensile Properties of Boron-Epoxy Composites  
(Averages of Specimens Tested<sup>a</sup>)

Temperature (K)	Elastic Modulus, E ( $10^9$ N/m <sup>2</sup> ) ( $10^6$ psi)		Poisson's Ratio, $\nu$		Proportional Limit, $\sigma^p$		0.2% Yield Strength, $\sigma^y$		Number of Specimens		
	( $10^9$ N/m <sup>2</sup> )	CV(%)	CV(%)	( $10^8$ N/m <sup>2</sup> ) ( $10^3$ psi)	CV(%)	( $10^8$ N/m <sup>2</sup> ) ( $10^3$ psi)	CV(%)				
295	231(4)	33.5(0.6)	1.6	0.228(0.019)	8.3				5		
76	233(5)	33.9(0.7)	2.1	0.241(0.012)	4.8				5		
4	238(6)	34.5(0.6)	2.3	0.239(0.014)	5.9				5		
				Longitudinal (0°)							
295	17.5(0.9)	2.54(0.12)	5.0	0.017(0.001)	6.1 <sup>b</sup>	0.344(0.071)	4.99(1.02)	20.7	6		
76	31.2(2.4)	4.53(0.34)	7.5	0.033(0.002)	7.3 <sup>b</sup>				4		
4	35.8(2.3)	5.19(0.32)	6.3	0.034(0.003)	7.8 <sup>b</sup>				3		
				Crossply ( $\pm 45^\circ$ )							
295	18.1(1.1)	2.62(0.17)	6.3	0.017(0.0034)	4.1	0.406(0.013)	5.89(0.19)	3.3	0.956(0.016)	13.9(0.3)	1.8
76	32.7(0.7)	4.72(0.13)	2.8	0.071(0.0050)	7.4	0.411(0.020)	5.96(0.29)	4.9	0.951(0.038)	13.8(0.5)	3.9
4	33.3(1.9)	4.83(0.28)	5.8	0.700(0.051)	7.2	0.296(0.028)	4.29(0.40)	9.3	0.830(0.016)	12.0(0.2)	1.9

Temperature (K)	Ultimate Strength, $\sigma^u$		Ultimate Elongation, $\epsilon$		Number of Specimens	
	( $10^8$ N/m <sup>2</sup> ) ( $10^3$ psi)	CV(%)	(%)	CV(%)		
295	16.3(0.6)	237(8)	3.3	0.73(0.04)	5.1	3
76	16.8(0.9)	243(13)	5.4	0.77(0.07)	9.3	3
4	18.2(0.4)	263(6)	2.2	0.76(0.01)	1.5	3
				Transverse (90°)		
295	0.470(0.035)	6.81(0.51)	7.4	0.27(0.06)	21.7	3
76	0.490(0.033)	7.09(0.47)	6.7	0.15(0.03)	17.6	3
4	0.414(0.096)	6.01(1.39)	23.1	0.12(0.04)	33.6	3
				Crossply ( $\pm 45^\circ$ )		
295	1.30(0.02)	18.8(0.3)	1.4	1.88(0.14)	7.5	3
76	1.11(0.02)	16.1(0.3)	1.7	0.85(0.05)	5.3	3
4	1.01(0.03)	14.7(0.4)	2.8	0.83(0.05)	6.3	3

<sup>a</sup> Standard deviations are in parentheses. CV is coefficient of variation. Data from the specimens that broke at or in the grips are not included in the calculations of ultimate strength or elongation.

<sup>b</sup> Computed from  $\nu_{12}$ ,  $E_{11}$ , and  $E_{22}$ .

Table 4. In-Plane Shear Modulus<sup>a</sup>  
(Averages of Specimens Tested)

Temperature	Shear Modulus, $G_{12}$		
	$10^9 \text{ N/m}^2$	$10^6 \text{ psi}$	CV(%)
Boron-Aluminum <sup>b</sup>			
295	39.7(4.0)	5.75(0.58)	10.0
76	27.0(5.5)	3.92(0.80)	20.4
4	32.6(5.5)	4.73(0.80)	16.9
Boron-Epoxy			
295	4.72(0.44)	0.684(0.064)	9.3
76	9.19(0.38)	1.33(0.06)	4.1
4	9.28(0.19)	1.35(0.03)	2.0

<sup>a</sup>These values are calculated from cross-ply ( $\pm 45^\circ$ ) data using the method of Sims and Halpin [6]. Standard deviations are in parenthesis; CV is the coefficient of variation.

<sup>b</sup>The boron-aluminum moduli are only lower limits to the true values.

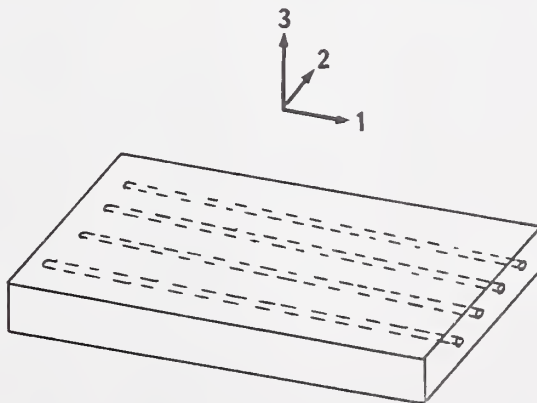


Fig. 1. Identification of composite axes.

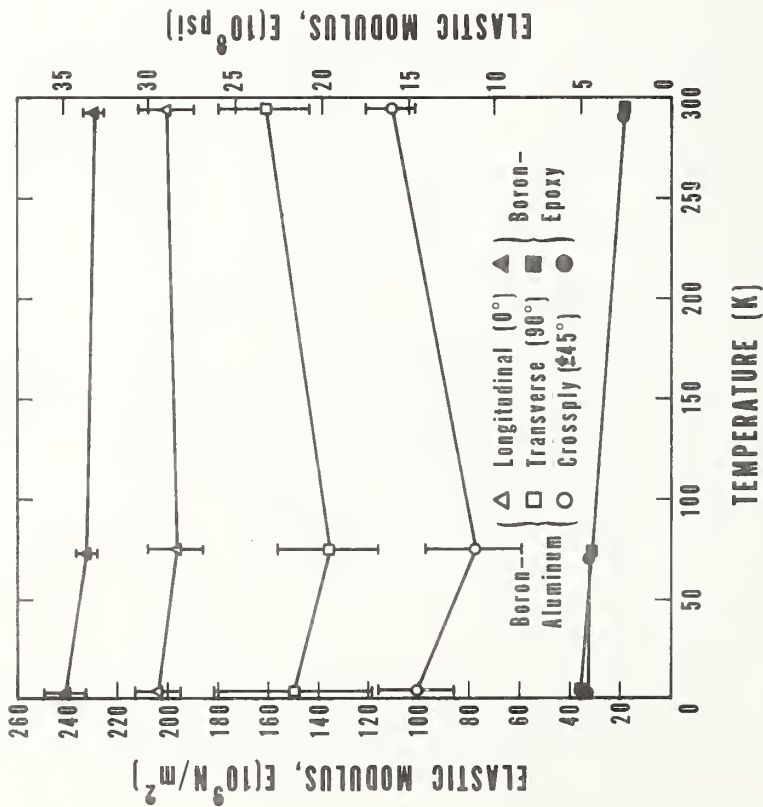


Figure 2. Temperature dependence of the elastic modulus of boron-epoxy and boron-aluminum of various orientations. Error bars reflect  $\pm$  one standard deviation; in several instances, the error bars are smaller than the datum symbol.

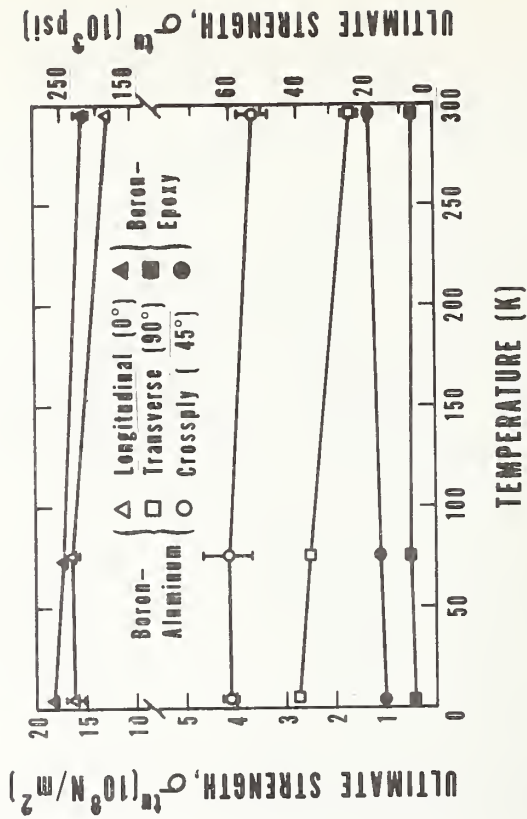


Figure 3. Temperature dependence of the ultimate tensile strength of boron-epoxy and boron-aluminum of various orientations. Error bars reflect  $\pm$  one standard deviation; in several instances, the error bars are smaller than the datum symbol.

SEMI-ANNUAL REPORT ON MATERIALS RESEARCH  
IN SUPPORT OF SUPERCONDUCTING MACHINERY

ELASTIC PROPERTIES OF ENGINEERING MATERIALS  
AT CRYOGENIC TEMPERATURES

H. M. Ledbetter, E. R. Naimon, and W. F. Weston

Cryogenics Division  
Institute for Basic Standards  
National Bureau of Standards  
Boulder, Colorado 80302

October 1975

## Summary: Elastic Properties

During the six months preceding October, 1975, the following studies were completed:

- (1) Oxygen-free copper. Room-temperature elastic constants of this material were determined by a pulse-echo method. Low-temperature Young's and shear moduli were determined by a resonance method. Results of this study are included in the accompanying manuscript describing copper-nickel alloys (See p. 73).
- (2) Copper-nickel alloys. Two alloys, Cu-10 Ni and Cu-30 Ni, were studied as described above for copper. Also, the longitudinal modulus of Cu-30 Ni was determined by a pulse-echo method at low temperatures. Advantages of combining resonance and pulse-echo data for these materials are described along with results in the accompanying manuscript "Low-temperature elastic properties of some copper-nickel alloys" by H. M. Ledbetter and W. F. Weston. This study was presented at the 1975 IEEE Ultrasonics Symposium in Los Angeles, and it will be published in the proceedings of that symposium (see p. 73).
- (3) Copper alloy PD135. This material, supplied and characterized by J. M. Wells of Westinghouse, was studied at room temperature by a pulse-echo method to determine its elastic constants. They are surprisingly different from those of unalloyed copper, and they are described in an accompanying manuscript "Elastic properties of a copper-cadmium-chromium precipitation-hardened alloy" by H. M. Ledbetter (See p. 77).
- (4) Invar. Low-temperature elastic properties of an iron-36 nickel invar-type alloy were determined by both resonance and pulse-echo methods. This study is described in an accompanying manuscript "Low-temperature elastic properties of invar" by H. M. Ledbetter, E. R. Naimon, and W. F. Weston. This study was presented at the 1975 ICMC-CEC in Kingston, Ontario, and it will be published in the proceedings of that conference (See p. 81).
- (5) Nickel-chromium-iron-alloys (Inconels). There is an accompanying reprint "Dynamic low-temperature elastic properties of two austenitic nickel-chromium-iron alloys," Mater. Sci. Engg. 20 (1975) 185-94 (See p. 95).
- (6) Austenitic stainless steels. There is an accompanying reprint "Low-temperature elastic properties of four austenitic stainless steels," J. Appl. Phys. 46 (1975) 3855-60 (See p. 105).

H. M. Ledbetter and W. F. Weston†  
 Cryogenics Division, National Bureau of Standards  
 Boulder, Colorado 80302

**ABSTRACT.** The polycrystalline elastic properties of Cu, Cu-10 Ni, and Cu-30 Ni were determined between room temperature and liquid-helium temperature using both pulse-echo (10 MHz) and resonance (60 kHz) methods. The temperature dependence of all three materials is regular. The composition dependence of the elastic constants is reviewed and new composition dependences are proposed.

INTRODUCTION

The study reported here was undertaken to elucidate the composition dependence and, especially, the temperature dependence of the elastic properties of copper-nickel alloys. Despite many previous studies, these properties are not known satisfactorily.

Copper-nickel alloys are well known for their resistances to corrosion and to stress-corrosion cracking. They are used in condensers and in heat exchangers. Recently, these alloys have become candidates for applications in superconducting machinery. The elastic properties (Young's modulus, shear modulus, etc.) of these alloys have been studied extensively at room temperature, and one high-temperature elastic-property study has been reported. At cryogenic temperatures only the Young's modulus has been studied, and only at liquid-nitrogen and liquid-helium temperatures. The complete set of polycrystalline elastic properties is reported here for Cu, Cu-10 Ni, and Cu-30 Ni semi-continuously between room temperature and liquid-helium temperature. The elastic constants are essential engineering design parameters, and they are related simply to interatomic forces. Copper-nickel alloys are especially interesting elastically because nickel increases copper's elastic stiffness, contrary to usual alloying effects.

Materials

Materials were obtained from commercial sources in the form of 1.9-cm (3/4-in) rods. Their chemical analyses by weight are: 9.98 Ni, 1.16 Fe, 0.07 Zn, 0.02 Pb for the Cu-10 alloy; 30.05 Ni, 0.72 Mn, 0.59 Fe, 0.04 Zn, <0.01 Pb, <0.01 Sn, <0.01 Al, <0.01 As. The copper was an oxygen-free high-conductivity grade. Their physical and metallurgical characterizations are given in Table I.

Table I. Physical and metallurgical characterization of the materials studied

	Cu	Cu-10 Ni	Cu-30 Ni
Mass density (g/cm <sup>3</sup> )	8.952	8.903	8.914
Hardness (DPH No., 1 kg load)	45	87	124
Average grain size (mm) by linear intercept method	1.0	0.05	0.03
Condition	Cold drawn 60%, annealed.	Annealed 677°C, 40 min	Commercially annealed

Experimental

Two methods, resonance (60 kHz) and pulse-echo (10 MHz), were used to determine sound velocities in the alloys. Both methods were described previously.<sup>2,3</sup> Low-temperature pulse-echo data were determined by a superposition method. The resonance specimens were right

circular cylinders 0.48 cm (3/16 in) in diameter and about 3 cm and 2 cm long for the longitudinal and transverse cases, respectively. The pulse-echo specimens were 1 cm cubes. Temperatures were monitored with chromel-constantan thermocouples.

The problem of the effect of texture on the elastic constants was studied by measuring the sound velocities both parallel and perpendicular to the rolling axis and also measuring the shear-wave birefringence for the latter case. The shear and longitudinal wave velocities were found to vary with direction by an average of 0.6 and 0.3 percent, respectively. The birefringence in the shear velocity was found to have a maximum value of 1.5 percent. Thus, the specimens had negligible texture, and the velocities were simply averaged over direction.

Results

Some of the low-temperature elastic constants are shown in Figs. 1-3, and room-temperature values are given in Table II. Young's modulus E was determined by a resonance method, the shear modulus G by resonance (shown in Fig. 2) and by pulse method, and C<sub>ℓ</sub> by pulse method.

Table II. Elastic constants of Cu-Ni alloys at room temperature, units of 10<sup>11</sup> N/m<sup>2</sup> except ν (dimensionless)

	C <sub>ℓ</sub>	B	E	G	ν
Cu	2.013	1.376	1.286	0.478	0.345
Cu-10Ni	2.092	1.424	1.345	0.501	0.343
Cu-30Ni	2.250	1.517	1.472	0.550	0.339

While there are only two independent elastic constants for an isotropic material, several are useful for various applications. Besides E, G, and C<sub>ℓ</sub> already mentioned, the bulk modulus B (reciprocal compressibility) and Poisson's ratio ν are often required. Relationships among these elastic constants and their relationship to the sound velocities are well known:

$$G = \rho v_t^2, \tag{1}$$

$$C_\ell = \rho v_\ell^2, \tag{2}$$

$$B = C_\ell - \frac{4}{3} G, \tag{3}$$

$$E = \frac{9BG}{3B + G}, \tag{4}$$

and 
$$\nu = \frac{E}{2G} - 1. \tag{5}$$

Since three elastic constants were measured -- E, G, and C<sub>ℓ</sub> -- the problem is, in principle, overdetermined. However, as can be inferred from Table III, this is effectively not the case. It is to be recalled that in a pulse-echo experiment v<sub>ℓ</sub> and v<sub>t</sub> are measured with typical errors of ± 1/2 percent. In a resonance experiment, E and G are measured with typical errors of + 1 percent.

\* Contribution of NBS, not subject to copyright.

† Present address: Rocky Flats Plant, Rockwell International, Golden, Colorado, 80401.

Table III. Maximum percent propagation errors involved in elastic-constant determinations, assuming  $\nu = 1/3$ . Boxed parameters are those measured, others are calculated.

	$\nu_\ell$	$\nu_t$	$C_\ell$	E	G	$\nu$	B
Pulse-echo	1/2	1/2	1	1	1	2/3	1
Resonance	5-1/2	1/2	11	1	1	8	17

Thus, when E and G are determined (as in a resonance experiment), derived values of  $C_\ell$ ,  $\nu$ , and B are quite inaccurate compared to pulse-echo results. Usual resonance methods are useful for determining E and G, but much less useful for determining the other elastic constants. The superiority of the pulse-echo method is apparent. However, in many cases, including copper-nickel alloys longitudinal ultrasonic velocities can be determined accurately while transverse ultrasonic velocities cannot, because of higher attenuation. Thus, it becomes advantageous to combine pulse-echo data ( $C_\ell$ ) with resonance data (E or G). In the present work, it was found that the resonance value of E was slightly more accurate than the resonance value of G. Thus, the  $C_\ell$  (pulse-echo) - E (resonance) pair is the best choice. Then it is necessary to solve a quadratic equation for G:

$$G = \frac{(E + 3C_\ell) \pm [(E + 3C_\ell)^2 - 16EC_\ell]^{1/2}}{8}, \quad (6)$$

discarding the non-physical root.

The data in Figs 1-3 were fitted to a theoretical relationship suggested by Varshni<sup>4</sup>:

$$C = C^0 - \frac{s}{e^{t/T} - 1} \quad (7)$$

where  $C^0$ ,  $s$ , and  $t$  are adjustable parameters, and  $T$  is the temperature.

The composition dependence of the elastic constants is shown in Figs 4-9, where the present results are compared with results of sixteen previous studies.<sup>5-20</sup> Two of these previous studies were made on single crystals rather than on polycrystalline aggregates. These single-crystal results were averaged by a Voigt-Reuss-Hill method.<sup>21</sup> The lines in Figs 4-8 are linear least-squares fits to the averaged single-crystal results and to the present results.

Temperature coefficients of the elastic constants are given in Table IV.

Table IV. Temperature derivatives of elastic constants at room temperature ( $10^{-4}K^{-1}$ )

Alloy	$\frac{1}{B} \frac{dB}{dT}$	$\frac{1}{E} \frac{dE}{dT}$	$\frac{1}{G} \frac{dG}{dT}$	$\frac{1}{\nu} \frac{d\nu}{dT}$
Cu	-1.64	-3.64	-4.01	4.65
Cu-10Ni	--	-3.78	-3.61	--
Cu-30Ni	-1.29	-2.30	-3.20	8.22

## Discussion and Conclusions

1. The low-temperature elastic properties of Cu-Ni alloys resemble those of copper, except for scaling factors. Like Cu, their behavior is quite regular--monotonically decreasing, linear at high temperature, lower slope at lower temperatures, and zero slope at zero temperature.

2. The composition dependence of the elastic constants is approximately linear over the composition range studied. The Young's-modulus/composition curve goes through the value for copper ( $1.27 \times 10^{11} N/m^2$ ) and not through the fictitious value of E for Cu ( $1.30 \times 10^{11} N/m^2$ ), as suggested by Köster.<sup>22</sup> The parameters proposed here for the change of E and G with composition ( $\Delta C/\Delta x = 0.690$  and  $0.259$ , respectively, where C denotes elastic constant and x denotes atomic fraction) differ from those proposed by Subrahmanyam<sup>20</sup> (0.798 and 0.319, respectively).

3. In some cases, there is considerable advantage in studying elastic properties of solids by both pulse and resonance methods. In the present case, the specimens transmitted longitudinal waves thus permitting the determination of  $C_\ell$ . But they damped shear waves, precluding determination of G by a pulse method. G, or alternatively E, could be determined by a resonance method. The  $C_\ell$ -E data gave better values of B and  $\nu$  than could be obtained from resonance experiments alone.

## Acknowledgment

This work was supported by the Advanced Research Projects Agency of the U.S. Department of Defense.

## References

1. Handbook on Materials for Superconducting Machinery, Battelle Metals and Ceramics Information Center, Columbus, Ohio, 1974.
2. E. R. Naimon, W. F. Weston and H. M. Ledbetter, Cryogenics 14 (1974) 246-9.
3. W. F. Weston, J. Appl. Phys., forthcoming.
4. Y. P. Varshni, Phys. Rev. B 2 (1970) 3952-8.
5. E. Grüneisen, Ann. Phys. Leipz. [IV] 22 (1907) 801.
6. Z. Nishiyama, Sci. Rep. Tohoku Univ. Sendai 18 (1929) 359-400.
7. S. Aoyama and T. Fukuroi, Bull. Sci. Res. Inst. Tokyo 20 (1941) 809-11. In Japanese.
8. H. Masumoto and H. Saito, Nippon Kingoku Gakkai-Shi 8 (1944) 49-55. In Japanese.
9. T. Fukuroi and Y. Shibuya, Sci. Rep. Tohoku Univ. A 2 (1950) 748.
10. W. F. Simmons, B. J. Sirois, D. N. Williams and R. J. Jaffee, ASTM Proc. 59 (1959) 1035-45.
11. R. E. Schmunk and C. S. Smith, Acta Metall. 8 (1960) 396-401.
12. B. Subrahmanyam and Bh. Krishnamurty, Indian J. Pure Appl. Phys. 1 (1963) 185-7.
13. J. B. Greer and E. H. Bucknall, Trans. ASM 57 (1964) 555-60.
14. A. F. Orlov and S. G. Fedotov, Fiz. Metal. Metalloved. 22 (1966) 137-8.

15. R. P. Reed and R. P. Mikesell, J. Mater. ASTM 2 (1967) 370-92.
16. G. Faninger, Z. Metallk. 60 (1969) 601-5.
17. K. Salama and G. A. Alers, IEEE Trans. Sonics Ultrasonics (Jan. 1969) 28. Abstract.
18. L. M. T. Hopkin, H. Pursey and M. F. Markham, Z. Metallk. 61 (1970) 535-40.
19. H. Masumoto, H. Saito and S. Sawaya, Trans. Japan Inst. Met. 11 (1970) 88-90.
20. B. Subrahmanyam, Mater. Sci. Eng. 15 (1974) 177-9.
21. R. Hill, Proc. Phys. Soc. Lond. A65 (1952) 349-54.
22. W. Köster, Mater. Sci. Eng. 18 (1975) 289.

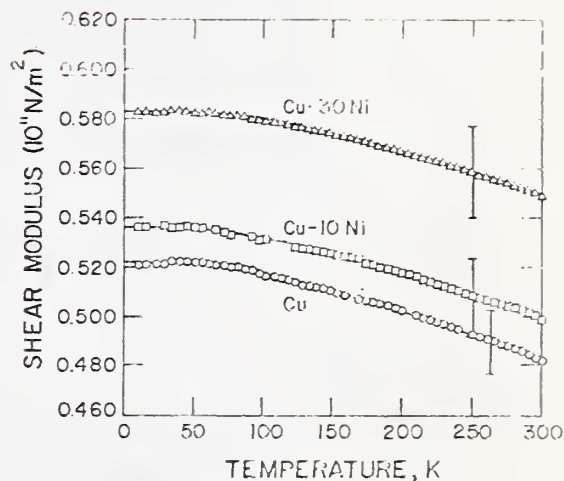


Fig. 2. Shear modulus of some Cu-Ni alloys versus temperature. Resonance results.

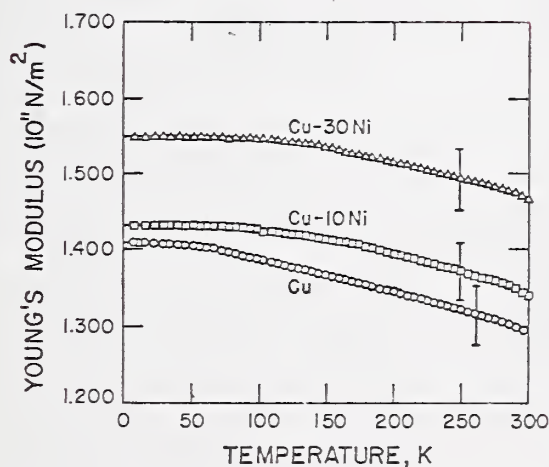


Fig. 1. Young's modulus of some Cu-Ni alloys versus temperature. Error bars are  $\pm 2\sigma$  where  $\sigma$  is the standard deviation of nine measurements, and they reflect both experimental errors and material variability;  $2\sigma$  represents, approximately, the 95% confidence interval. Resonance results.

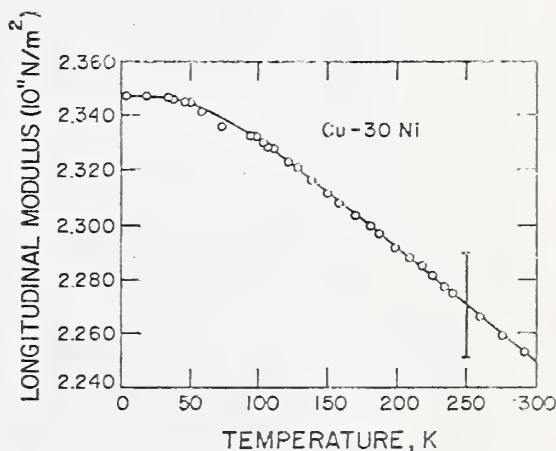


Fig. 3. Longitudinal modulus versus temperature for a Cu-30 Ni alloy. Pulse-echo results.

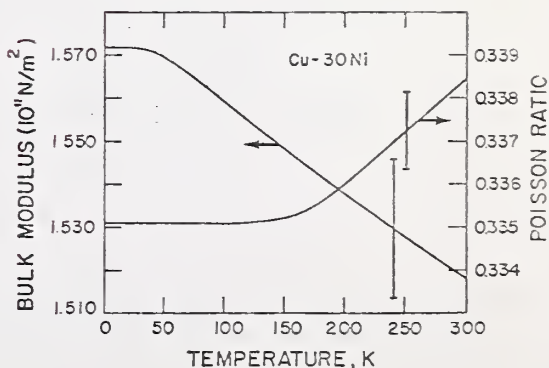


Fig. 4. Bulk modulus and Poisson ratio of Cu-30 Ni, calculated from  $C_L$  (pulse-echo) and  $G$  (resonance).

- LEGEND
- Grüneisen (1907)
  - Nishiyama (1929)
  - ▲ Aoyama & Fukuroi (1941)
  - Masumoto & Saito (1944)
  - Fukurai & Shibuya (1950)
  - Simmons et al (1959)
  - Schmunk & Smith (1960)
  - Subrahmanyam & Krishnamurly (1963)
  - ▷ Greer & Bucknall (1964)
  - ◇ Urtov & Fedotov (1966)
  - ▽ Pao & Mackay (1967)
  - △ Faninger (1969)
  - ◇ Salama & Aiers (1969, unpublished)
  - Hopkin et al (1970)
  - ◇ Masumoto et al (1970)
  - Subrahmanyam (1974)
  - Present Study

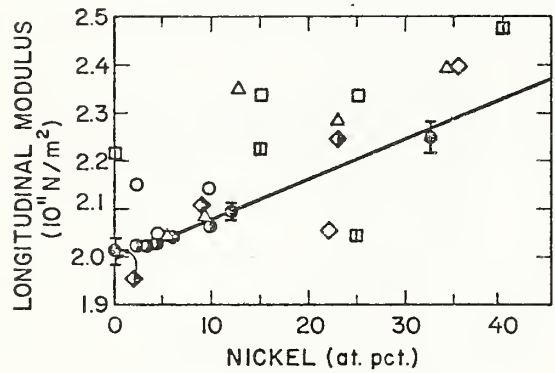


Fig. 5. Compositional variation of  $C_L$  for Cu-Ni alloys. Half-filled diamonds and circles represent single-crystal results averaged by the Voigt-Reuss-Hill arithmetic method. Line is a least-squares fit of present results and averaged single-crystal results. See first figure caption for meaning of error bars.

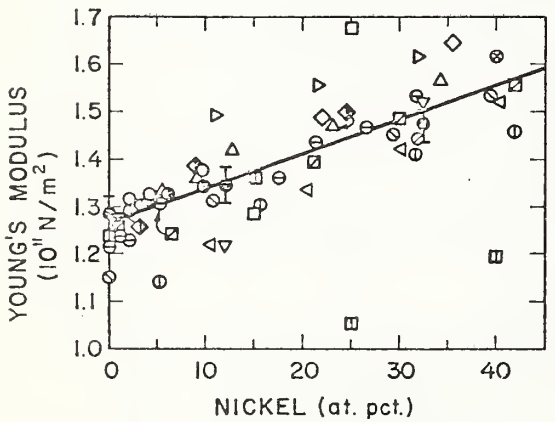


Fig. 6. Compositional variation of  $E$  for Cu-Ni alloys.

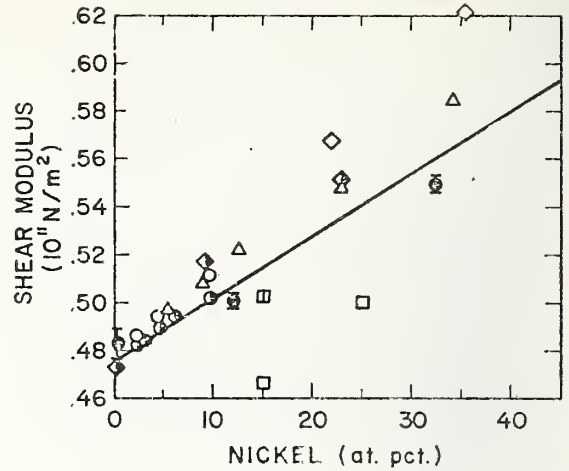


Fig. 7. Compositional variation of  $G$  for Cu-Ni alloys.

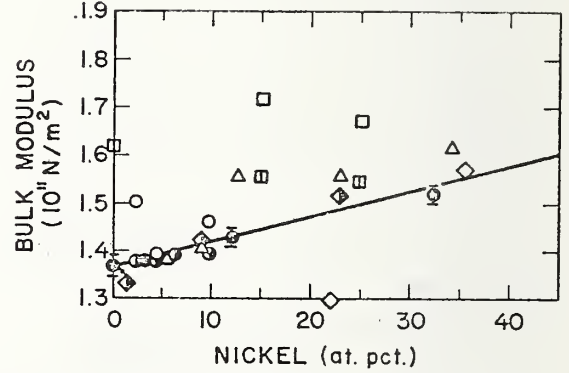


Fig. 8. Compositional variation of  $B$  for Cu-Ni alloys.

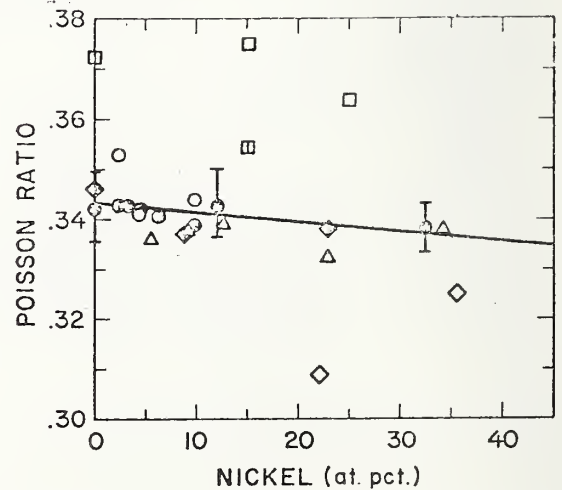


Fig. 9. Compositional variation of  $\nu$  for Cu-Ni alloys.

H. M. Ledbetter

Cryogenics Division  
National Bureau of Standards  
Boulder, Colorado 80302Abstract

The room-temperature elastic constants of a polycrystalline precipitation-hardened copper-cadmium-chromium alloy were determined by a 10 MHz pulse-echo method. With respect to copper the alloy has a fifteen-percent-lower bulk modulus, a fifteen-percent-higher shear modulus, and a fourteen-percent-lower Poisson ratio. These changes, especially in the Poisson ratio, are much larger than those observed in the more familiar copper-beryllium precipitation-hardened alloy and compare to those usually obtained only by mechanical deformation or by phase transformation.

Key words: Bulk modulus; compressibility; copper alloy; elastic constant; Poisson ratio; precipitation hardening; shear modulus; sound velocity; Young's modulus.

The elastic constants of a material are essential in engineering design for predicting load-deflection behavior. They are also essential for understanding material behavior related to interatomic bonding forces. Effects of many metallurgical variables on elastic constants have been studied extensively;<sup>1-3</sup> these variables include alloying, annealing, magnetic field, mechanical deformation, phase transformation, pressure, stress, and temperature. This subject was reviewed recently for copper by Ledbetter and Naimon.<sup>4</sup>

Some experimental results on the elastic constants of a precipitation-hardened copper alloy are described here. Compared to previous studies, the observed elastic-constant changes are large.

The studied material<sup>†</sup> is characterized as follows: Chemical composition by weight is 0.31 Cd, 0.33 Cr, < 0.01 Pb, < 0.01 Fe, < 0.01 Ni, < 0.01 Mn, balance Cu. Mass density determined by hydrostatic weighing is 8.94 g/cm<sup>3</sup>. Hardness is 57.5 on a Rockwell 30-T scale. ASTM grain size number is five. The material was produced by extruding a 20.3-cm diameter, 40.6-cm long billet at 1227 K and following with an 866-K, 1-hour precipitation heat treatment.

The elastic constants were determined by measuring the ultrasonic longitudinal-wave and shear-wave velocities,  $v_\ell$  and  $v_t$ , using a McSkimin<sup>5</sup> pulse-echo method near 10 MHz.

The usual engineering elastic constants are related to these velocities by:<sup>6</sup>

$$\text{Shear modulus} = G = \rho v_t^2, \quad (1)$$

$$\text{Longitudinal modulus} = C_\ell = \rho v_\ell^2, \quad (2)$$

$$\text{Bulk modulus} = B = C_\ell - \frac{4}{3} G, \quad (3)$$

$$\text{Young's modulus} = E = 3GB / (C_\ell - G), \quad (4)$$

$$\text{and Poisson ratio} = \nu = (E/2G) - 1 = \frac{1}{2} (C_\ell - 2G) / (C_\ell - G), \quad (5)$$

where  $\rho$  is the mass density.

\* Contribution of NBS, not subject to copyright.

† This material was obtained from the Phelps-Dodge Corporation, denoted as their alloy PD135. This trade name is used here to characterize the material; it is not an NBS endorsement of this material.

The specimen consisted of a 0.95 x 1.35 x 1.35 cm "cube" whose opposite sides were flat and parallel within 2.5  $\mu\text{m}$ . For each of the three cube directions, longitudinal-wave and shear-wave sound velocities were measured. Shear-wave birefringence was found to be negligible. Both longitudinal and shear velocities varied less than one percent with direction. Thus, velocities were simply averaged over the three directions.

Results of the present study are given in Table I. For comparison, similar data are shown for unalloyed copper and for a copper -1.85 beryllium precipitation-hardening alloy. Copper data are from the single-crystal results of Overton and Gaffney<sup>7</sup> averaged by a Voigt-Reuss-Hill-arithmetic method.<sup>8</sup> Such data agree with data obtained by measuring polycrystalline specimens, and they are believed to be more reliable.<sup>4</sup> Cu-Be data are due to Frederick and were reported by Richards.<sup>9</sup> They were obtained from sound-velocity measurements on a 1.4-cm diameter specimen obtained from material that was cold drawn and then precipitation hardened.

Table I. Room-temperature elastic constants of copper, precipitation-hardened Cu-1.85 Be, and precipitation-hardened Cu-0.3 Cd-0.3 Cr. Velocities have units of  $10^6$  cm/sec; elastic constants have units of  $10^{11}$  N/m<sup>2</sup>;  $\nu$  is dimensionless. Quantities in parentheses were calculated from reported results. Error limits represent one standard deviation; they reflect both experimental errors and elastic anisotropies.

	Cu	Cu-Be	Cu-Cd-Cr
$\rho$	8.93	8.332	8.936
$v_l$	0.4733	(0.4848)	0.4582 $\pm$ 0.0053
$v_t$	0.2295	(0.2414)	0.2459 $\pm$ 0.0021
$C_l$	2.000	(1.958)	1.876 $\pm$ 0.043
G	0.473	0.485	0.540 $\pm$ 0.009
B	1.371	(1.311)	1.156 $\pm$ 0.016
E	1.271	1.296	1.402 $\pm$ 0.012
$\nu$	0.346	0.335	0.298 $\pm$ 0.003

Results in Table I show for the copper alloys considered that the effect of precipitation hardening is to decrease  $C_l$ , B, and  $\nu$  and to increase G and E. Since there are only two independent elastic constants for a polycrystalline (isotropic) aggregate, these changes in the elastic constants are not independent; and it is useful to consider their interrelationships. The most fundamental choice of an elastic-constant pair is the pair B and G because these constants characterize the two extreme types of mechanical deformation -- volume change without shape change and shape change without volume change, respectively. From Eqs. (1)-(4) it follows that:

$$\frac{dC_l}{C_l} = \frac{B}{B + \frac{4}{3}G} \frac{dB}{B} + \frac{4G}{3(B + \frac{4}{3}G)} \frac{dG}{G}, \quad (6)$$

$$\frac{dE}{E} = \frac{G}{G + 3B} \frac{dB}{B} + \frac{3B}{G + 3B} \frac{dG}{G}, \quad (7)$$

and

$$\frac{d\nu}{\nu} = \frac{9GB}{(G + 3B)(3B - 2G)} \left( \frac{dB}{B} - \frac{dG}{G} \right). \quad (8)$$

For a typical value of  $\nu$ , near 1/3, these relationships become:

$$\frac{dC_l}{C_l} \approx \frac{2}{3} \frac{dB}{B} + \frac{1}{3} \frac{dG}{G}, \quad (6a)$$

$$\frac{dE}{E} \approx \frac{1}{9} \frac{dB}{B} + \frac{8}{9} \frac{dG}{G}, \quad (7a)$$

and

$$\frac{dv}{v} \approx \frac{4}{9} \left( \frac{dB}{B} - \frac{dG}{G} \right) - \frac{4}{9} \left( \frac{dE}{E} - \frac{dG}{G} \right). \quad (8a)$$

Thus, it is clear that E and G will change similarly with respect to most metallurgical variables, that  $C_{\rho}$  depends more on B than on G, and that  $v$  is expected to be relatively invariant.

There are three principal unexpected results of the present study. First, the elastic constants are changed significantly -- G is increased fourteen percent and B is decreased fifteen percent with respect to unalloyed copper. Second, Poisson's ratio is changed significantly. Köster and Franz<sup>3</sup> showed that  $v$  is relatively insensitive to most metallurgical variables except mechanical deformation and phase transformation. Both these variables introduce strong elastic anisotropies, and it is not clear that these anisotropies have been carefully considered with respect to changes in  $v$ . In the present case, however, no elastic anisotropy due to precipitation is expected and none was detected experimentally. Thus, present results demonstrate a large change in the elastic constants of copper due to precipitation. As shown by Eq. (8a), the unusually large change in  $v$  is due to B and G being oppositely affected by precipitation. Third, the opposite behavior of B and G is unexpected; usually G and B are roughly proportional, typically  $G \approx 3/8 B$ .<sup>10</sup> As shown by the data in table I, G/B is 0.35, 0.37, and 0.47 for copper, copper-beryllium, and copper-cadmium-chromium, respectively.

Understanding the non-parallel behavior of B and G due to precipitation hardening emerges as the principal problem of the present study. Very few experimental studies on the elastic properties of precipitation-hardening alloys have been reported. The usual elastic theories of precipitation<sup>11</sup> cannot explain the anomaly, either by precipitate-matrix, precipitate-precipitate, or combined elastic-interaction energies. Also, the problem remains to assure that this anomaly is not an artifact, an effective slowing of the longitudinal ultrasonic wave due to its interactions with the precipitates. If the apparent longitudinal velocity is real, then it may be necessary to invoke two mechanisms to explain the elastic-constant changes due to precipitation hardening. One mechanism would increase (decrease) both B and G while the other would decrease B (increase G), leaving G(B) unaffected.

#### Acknowledgment

This work was supported by the Advanced Research Projects Agency of the U.S. Department of Defense. Dr. J. M. Wells of Westinghouse supplied the material and its characterization.

#### References

1. R. F. S. Hearmon, Rev. Mod. Phys. 18 (1946) 409, Adv. Phys. 5 (1956) 323.
2. H. B. Huntington, in Solid State Physics, vol. 7 (F. Seitz and D. Turnbull, Eds.), Academic, New York, 1958.
3. W. Köster and H. Franz, Metall. Rev. 6 (1961) 1.
4. H. M. Ledbetter and E. R. Naimon, J. Phys. Chem. Ref. Data 3 (1974) 897.
5. H. J. McSkimin, J. Acoust. Soc. Amer. 33 (1961) 12.
6. G. Bradfield, in Physical Examination of Metals (B. Chalmers and A. G. Quarrell, Eds.), Arnold, London, 1960, p. 565.
7. W. C. Overton, Jr. and J. Gaffney, Phys. Rev. 98 (1955) 969.
8. R. Hill, Proc. Phys. Soc. Lond. A65 (1952) 349.

9. J. T. Richards, in Symposium on Determination of Elastic Constants, Spec. Tech. Publ. No. 129, ASTM, Philadelphia, 1952, p. 71.
10. C. Zwikker, Physical Properties of Solid Materials, Pergamon, London, 1954, p. 90.
11. G. Sauthoff, Z. Metallkde. 66 (1975) 106.

## LOW-TEMPERATURE ELASTIC PROPERTIES OF INVAR<sup>††</sup>

H. M. Ledbetter, E. R. Naimon,<sup>\*†</sup> and W. F. Weston<sup>\*</sup>

Cryogenics Division  
Institute for Basic Standards  
National Bureau of Standards  
Boulder, Colorado 80302

### ABSTRACT

The elastic properties of a polycrystalline invar alloy were determined between room temperature and liquid-helium temperature by two methods: measurement of ultrasonic (10 MHz) wave velocities with a pulse-echo technique, and measurement of resonance frequencies (60 kHz) of cylindrical specimens with a composite piezoelectric-oscillator technique. The shear moduli obtained by the two methods are essentially the same. However, the other elastic constants (all of which have a dilatational component) differ both in magnitude and in temperature dependence. Present pulse-echo results agree closely with previous results obtained for both polycrystals and single crystals in a saturating magnetic field. The following elastic constants are reported: longitudinal modulus, Young's modulus, the shear modulus, the bulk modulus (reciprocal compressibility), and Poisson's ratio. The role of magnetic effects on invar's elastic properties is discussed briefly.

Key words: Bulk modulus; compressibility; Debye temperature; elastic constant; invar; iron alloy; nickel alloy; Poisson's ratio; shear modulus; sound velocity; Young's modulus.

---

<sup>††</sup> Contribution of NBS, not subject to copyright.

<sup>\*</sup> NRC-NBS Postdoctoral Research Associate, 1973-4.

<sup>†</sup> Present address: Dow Chemical, Rocky Flats Division, Golden, Colorado 80401.

# LOW-TEMPERATURE ELASTIC PROPERTIES OF INVART††

H. M. Ledbetter, E. R. Naimon,\*† and W. F. Weston\*

Cryogenics Division  
Institute for Basic Standards  
National Bureau of Standards  
Boulder, Colorado 80302

## INTRODUCTION

Because invar has nearly temperature-invariant dimensions, it is studied scientifically and used technologically [1-5]. It is a face-centered-cubic iron-base alloy containing about thirty-six percent nickel. Invar's unusually low thermal expansivity is related to its magnetic properties [3]. The usual thermal expansion is canceled approximately by magnetostriction, the coupling between magnetization and strain.

Other physical properties of invar are also anomalous. It has *positive* thermoelastic coefficients over a large temperature range. This anomaly is useful in developing alloys with nearly temperature-invariant elastic constants.

Knowledge of invar's elastic constants is important. First, elastic constants are related simply to interatomic potentials, and they reflect the nature of the interatomic bonding. Second, they are essential design parameters for predicting deflections in stressed components; they become particularly important in cases of large stresses, large deflections, or acute tolerances. The elastic constants of invar are of interest at low temperatures because invar is a candidate low-temperature material [6], and (as discussed below) its elastic behavior is especially anomalous below about 50 K.

The elastic properties of invar between room temperature and liquid-helium temperature are reported in the present paper. Elastic constants were determined by two dynamic methods. Longitudinal and transverse ultrasonic wave velocities were measured at 10 MHz using a pulse-echo technique. And the resonance frequencies of both longitudinal and transverse 60 kHz

---

†† Contribution of NBS, not subject to copyright.

\* NRC-NBS Postdoctoral Research Associate, 1973-4.

† Present address: Dow Chemical, Rocky Flats Division, Golden, Colorado 80401.

standing waves were determined by a three-component piezoelectric composite-oscillator technique. The following elastic constants are reported: Young's modulus  $E$ , the shear modulus  $G$ , the bulk modulus  $B$  (which is the reciprocal compressibility), Poisson's ratio  $\nu$ , and the longitudinal modulus  $C_{\ell}$ .

#### PREVIOUS STUDIES

Five experimental studies on the low-temperature elastic properties of invar have been reported [7-11], and these studies are summarized in Table I. Despite considerable experimental study on them, the low-temperature elastic properties of invar are not well characterized. The curves of Durham et al. [7] are based on a few fixed-temperature measurements, the lowest of these being at 20 K. The extrapolation of these data to lower temperatures is questionable. The Meincke and Litva [8] data are limited to temperatures below 160 K. Fletcher [9] reported only relative values and limited his measurements to temperatures below 77 K. Maeda's [10] values are about twenty percent lower than other reported results for  $E$  and  $G$ . Hausch and Warlimont [11,12] measured single-crystal elastic constants; the averaging process for obtaining polycrystalline elastic constants from single-crystal elastic constants is uncertain; in particular, averaging has not been discussed for magnetic materials that may have a magnetostrictive strain component. Also, the Hausch and Warlimont data do not extend below 77 K. Thus, further experimental studies are required to better characterize the low-temperature elastic properties of invar.

High-temperature elastic-property studies were reported by: Chevenard [13]; Köster [14]; Fine and Ellis [15]; Hill, Shimmin, and Wilcox [16]; and Tino and Maeda [17].

Besides dependence on variables such as temperature, mechanical deformation, and magnetic field, the elastic properties of invar are sensitive to nickel content. This variable must be considered carefully in comparing results from specimens of different materials, particularly near thirty-six percent nickel where properties such as  $E$  and  $G$  have sharp minima [18].

## EXPERIMENTAL

For brevity, most experimental details are omitted here. Both the pulse-echo technique [19] and the resonance technique [20] are described elsewhere.

Samples of invar were obtained from a commercial source in the form of 3/4-in (1.9-cm) diameter rods. The room-temperature mass density of the sample was found to be  $8.084 \text{ g/cm}^3$  by an Archimedean method. The diamond-pyramid hardness number was 226 for a 1 kg load. Grain size was found by a linear intercept method to be approximately 0.02 mm. The composition of the sample, obtained from a mill analysis, was: 0.08 C, 0.01 P, 0.01 S, 35.99 Ni, 0.81 Mn, 0.35 Si, 0.17 Se, and the balance Fe. Materials were tested in the as-received condition, about fifteen-percent cold drawn. Annealing the specimens increased their attenuations, reducing considerably the quality of their pulse-echo patterns. (Magnetic domain walls attenuate more in the annealed state than in the mechanically deformed state.)

The possible existence of preferred orientations (textures) in the specimen was investigated by measuring the longitudinal sound-wave velocity  $v_\ell$  in three orthogonal directions at room temperature. The longitudinal modulus is given by:

$$C_\ell = \rho v_\ell^2 = B + \frac{4}{3} G, \quad (1)$$

where  $\rho$  is the mass density. Thus, both dilatational and shear deformation modes are sampled simultaneously. The results for the three directions are: 0.4821, 0.4825, and  $0.4929 \times 10^6$  cm/sec for the two transverse and for the longitudinal axes, respectively (longitudinal axis = rolling direction). These results were interpreted to indicate that the specimen had a slight preferred orientation, but that practically it could be ignored. The rolling direction of the bar was chosen as the wave-propagation direction for the pulse-echo experiments, and it was the specimen axis for the resonance experiments.

## RESULTS

Results of the present study are shown in Figs. 1-5, together with the low-temperature elastic constants of invar reported by others. Values of the elastic constants at selected temperatures are given in Table II. Based on previous measurements on standard materials, errors in  $E$ ,  $G$ ,  $B$ , and  $C_\rho$  determined by a pulse-echo method are estimated to be  $\pm 1\%$ . Errors in  $E$  and  $G$  by a resonance method are also estimated to be  $\pm 1\%$ . Errors in the pulse-echo value of  $\nu$  are larger. In particular, values of  $B$ ,  $C_\rho$ , and  $\nu$  obtained from resonance data tend to be inaccurate because of the propagation of measurement errors; these derived resonance values are not reported here. For the pulse-echo case, the elastic constants were obtained from the following formulas:

$$G = \rho v_t^2, \quad (2)$$

$$B = C_\rho - \frac{4}{3} G, \quad (3)$$

$$E = \frac{9GB}{G + 3B}, \quad (4)$$

and

$$\nu = \frac{E}{2G} - 1, \quad (5)$$

where  $v_t$  is the transverse wave velocity.

## DISCUSSION

### Pulse-echo Results

The present pulse-echo results agree within a few percent with results reported by Meincke and Litva [8] for polycrystalline specimens, and also with the results obtained by averaging the single-crystal results of Hausch and Warlimont [11] by a Voigt-Reuss-Hill method. Both these experiments were done in a saturating magnetic field; the present experiments were done in zero applied magnetic field.

The agreement between the zero-field and the saturated-field results can be understood as follows. At a high frequency (10 MHz in this case),

domain-wall motion is suppressed since the domain walls cannot follow the high-frequency applied stress. In nickel, it was reported that the decrement is a maximum at 150 kHz [21]; thus, domain-wall motion can contribute significantly to the strain at this frequency. At higher frequencies the domain-wall motion contributes a smaller strain. Therefore, the elastic stiffnesses determined at high frequencies for unmagnetized materials are nearly as large as the elastic stiffnesses determined for magnetically saturated materials. Thus, present pulse-echo results are consistent with the previous three pulse-echo experiments [8,9,11], independent of magnetic field.

The present pulse-echo experiments were precluded below 40 K because of the high attenuation of elastic waves in invar at these temperatures. This attenuation phenomenon was detected first by Meincke and Litva [8], and it was studied in detail by Fletcher [9] who described it by a general relaxation-mechanism.

### Resonance Results

The present resonance results disagree with the results reported by Maeda [10], both in magnitude and in temperature dependence. Present results are about twenty percent larger for both E and G, and the present temperature coefficients are higher. It is difficult to understand this discrepancy. It may be a frequency-dependent effect. If so, it is a large effect and deserves further study.

### Pulse-echo and Resonance Results Compared

For the shear modulus, present resonance and pulse-echo results are identical within experimental error. The unusual behavior of the shear modulus of invar is shown in Fig. 1. A regularly behaved material has a shear modulus that *decreases* monotonically with increasing temperature. The two temperature coefficients are approximately the same, although the slope in the resonance case is slightly higher than in the pulse-echo case. The resonance data for G also show a minimum near 50 K and a slight upturn at lower temperatures, similar to the previously reported pulse-echo data [8-9].

For Young's modulus, the resonance and pulse-echo values differ by a few percent in magnitude, but considerably in their temperature dependence. These differences are shown in Fig. 2. The resonance value of  $E$  reaches a minimum near 150 K and then increases steadily with lower temperatures. If this is related to the minimum of  $E$  near 50 K shown by the pulse-echo data, then a frequency-dependent attenuation mechanism is indicated. Fletcher [9] found no appreciable frequency dependence of the damping in his experiments between 10 and 35 MHz, but these frequencies may be so high that the attenuation mechanism associated with the minimum is immeasurably small. It is interesting that the resonance values of  $E$  are higher at all temperatures than the pulse-echo values. From the usual  $\Delta E_\lambda$  effect, an elastic softening would be expected in going from pulse-echo to resonance values [5]. Maeda [10] did find an elastic stiffening due to the  $\Delta E_\lambda$  effect, as evidenced by increased values of  $E$  in a saturating magnetic field.

From the results shown for  $G$  and  $E$ , the disparity between resonance values and pulse-echo values of the elastic constants would be expected for any elastic constant that contained a dilatational component. Besides Young's modulus, these include: the longitudinal modulus, the bulk modulus (reciprocal compressibility), and Poisson's ratio. While the results of the present study confirm this disparity, resonance-derived values of  $C_\lambda$ ,  $B$  and  $\nu$  are not reported here because of the large errors propagated in computing them from  $E$  and  $G$  data. The basic reason for this disparity between dilatational-type and shear-type elastic constants is unclear.

However, a more fundamental problem is also unresolved -- how can the anomalous elastic behavior of invar be understood, independent of the resonance/pulse-echo disparity? Despite many attempts, no consensus of thinking on the theory of invar exists. The  $\Delta E_\lambda$  effect due to linear magnetostriction due to domain walls accounts only for anomalies in shear-type elastic constants. The  $\Delta E_\omega$  effect due to volume magnetostriction accounts only for anomalies in dilatation-type elastic constants. As described above, both types of elastic constants are anomalous in invar. Thus, a combined  $\Delta E_\lambda - \Delta E_\omega$  effect would have to be invoked. Hausch [5] disputed this approach and proposed that the Heisenberg magnetic exchange energy must be considered for invar. Before these questions can be resolved, additional low-temperature elastic measurements must be made on invar-type materials to permit quantitative checks on proposed theories.

## REFERENCES

1. W. S. McCain and R. E. Maringer, DMIC Memorandum 207 (1965).
2. S. J. Rosenberg, NBS Monograph 106, U.S. Govt. Print. Off. (1968).
3. G. Hausch and H. Warlimont, Z. Metallk. 64:152 (1973).
4. W. F. Schlosser, J. Phys. Chem. Solids 32:939 (1971).
5. G. Hausch, Phys. Status Solidi (a) 15:501 (1973).
6. Handbook on Materials for Superconducting Machinery, Metals and Ceramics Information Center, Battelle Columbus Laboratories, Columbus, Ohio (1974).
7. T. F. Durham, R. M. McClintock, R. P. Reed, C. J. Guntner, and K. A. Warren, Cryogenic Materials Data Handbook, U.S. Dept. of Commerce (1961).
8. P. P. M. Meincke and J. Litva, Phys. Lett. 29A:390 (1969).
9. R. Fletcher, J. Phys. C 2:2107 (1969).
10. T. Maeda, J. Phys. Soc. Japan 30:375 (1971).
11. G. Hausch and H. Warlimont, Acta Met. 21:401 (1973).
12. G. Hausch and H. Warlimont, Z. Metallk. 63:547 (1972).
13. P. Chevenard, Trav. Mem. Bur. Int. Poids Mes. 27:142 (1927).
14. W. Köster, Z. Metallk. 35:194 (1943).
15. M. E. Fine and W. C. Ellis, Trans. AIME 188:1120 (1950).
16. W. H. Hill, K. D. Shimmin, and B. A. Wilcox, Amer. Soc. Test. Mater. Proc. 61:890 (1961).
17. Y. Tino and T. Maeda, J. Phys. Soc. Japan 18:955 (1963).
18. H. M. Ledbetter and R. P. Reed, J. Phys. Chem. Ref. Data 2:531 (1973).
19. E. R. Naimon, W. F. Weston, and H. M. Ledbetter, Cryogenics 14:246 (1974).
20. W. F. Weston, J. Appl. Phys., forthcoming.
21. R. M. Bozorth, W. P. Mason, and H. J. McSkimin, Bell System Tech. J. 30:970 (1951).

## LIST OF TABLES

- I. Summary of low-temperature elastic studies on invar.
- II. Elastic constants of invar at selected temperatures.

## LIST OF FIGURES

1. Temperature variation of the shear modulus of invar.
2. Temperature variation of the Young's modulus of invar.
3. Temperature variation of the longitudinal modulus of invar.
4. Temperature variation of the bulk modulus of invar.
5. Temperature variation of Poisson's ratio of invar.

Table I. Summary of low-temperature elastic studies on invar

Reference	Alloy (wt. pct. Ni)	Temperature Range (K)	Magnetic Field (kG)	Frequency of Measurement	Elastic Constants Measured	Comments
Durham et al. [7]	36.0	19-300	0	Static	E, G	
Meincke and Litva [8]	35.0	2-160	15	10 MHz	$v_{\ell}, v_t$	Annealing effect
Fletcher [9]	35.0	2-77	0	10-30 MHz	$v_{\ell}, v_t$	Relative values only; four alloys, 36-48 nickel; attenuation measure- ments
Maeda [10]	35.0	100-800	0-1.9	kHz region	E, G	Magnetic-field dependence
Hausch and Warlimont [11]	35.3	77-700	6	10 MHz	$v_{\ell}, v_t$	Single crystals; nine alloys, 32-53 nickel
Present	36.0	4-300	0	10 MHz 60 kHz	$v_{\ell}, v_t$ E, G	

Table II. Elastic constants of invar at selected temperatures, all units  $10^{11}$  N/m<sup>2</sup> except  $\nu$  (which is dimensionless)

T(K)	Pulse-echo Results						Resonance Results		
	E	G	B	C <sub>ℓ</sub>	$\nu$	E	E	G	
300	1.433	0.558	1.109	1.853	0.285	1.523	1.523	0.565	
250	1.408	0.547	1.107	1.835	0.288	1.475	1.475	0.551	
200	1.379	0.533	1.112	1.823	0.293	1.427	1.427	0.535	
150	1.353	0.521	1.125	1.819	0.300	1.399	1.399	0.522	
100	1.334	0.511	1.139	1.821	0.305	1.398	1.398	0.509	
77	1.328	0.508	1.146	1.823	0.307	1.403	1.403	0.506	
4	-	-	-	-	-	1.417	1.417	0.505	

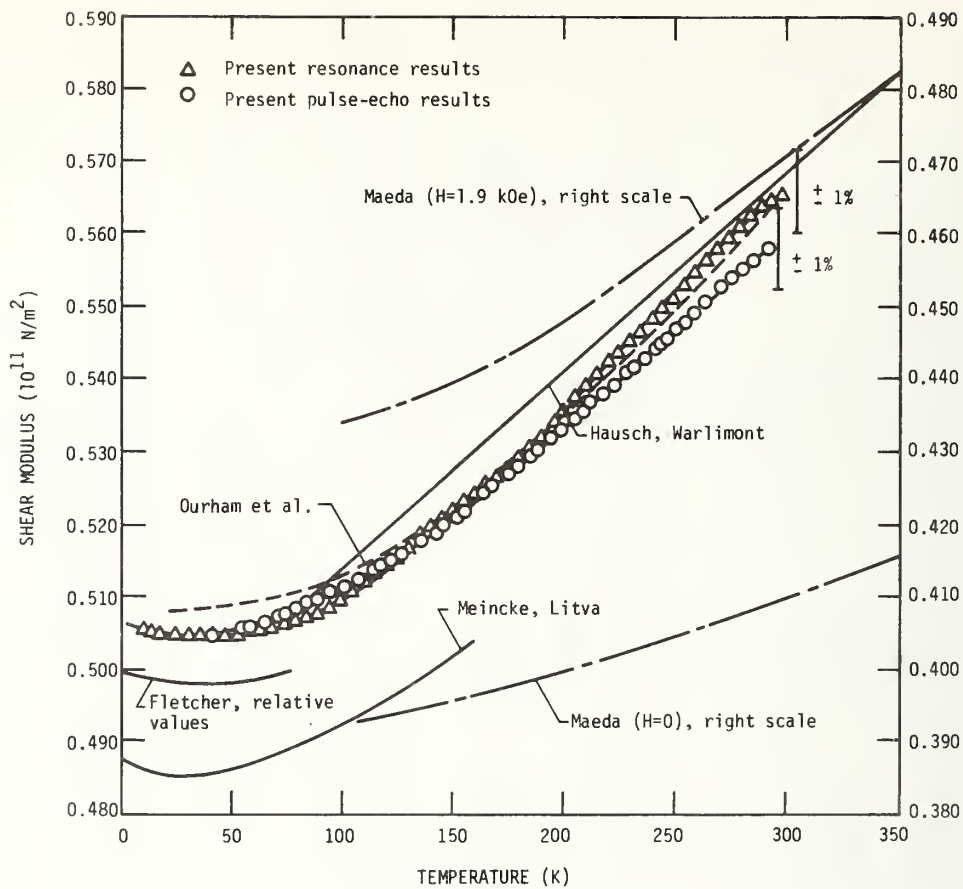


Figure 1. Temperature variation of the shear modulus of invar.

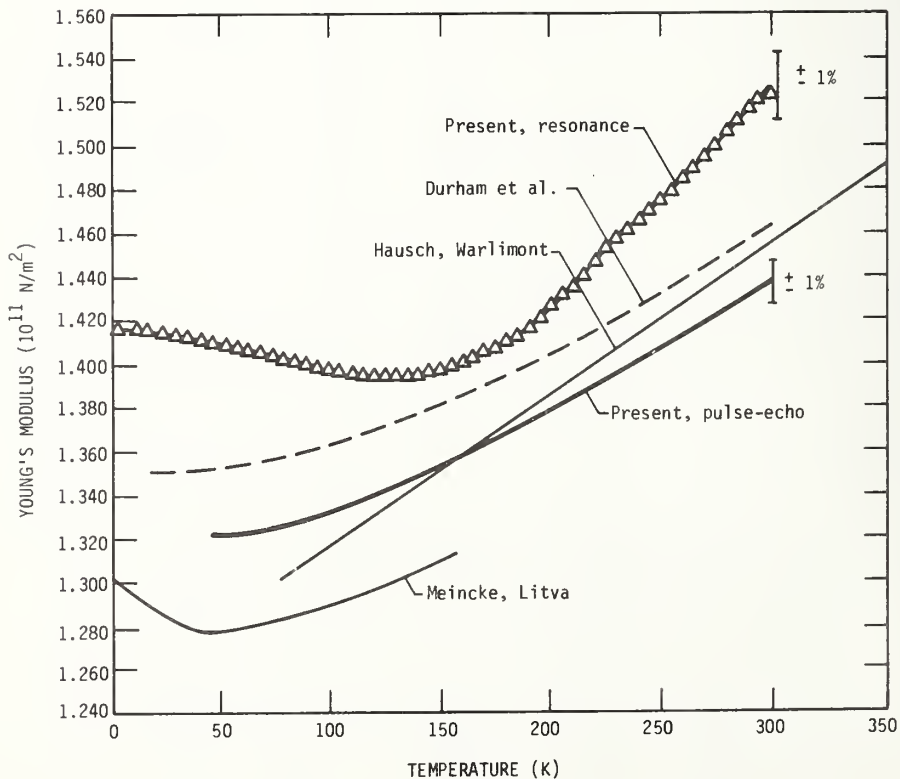


Figure 2. Temperature variation of the Young's modulus of invar.

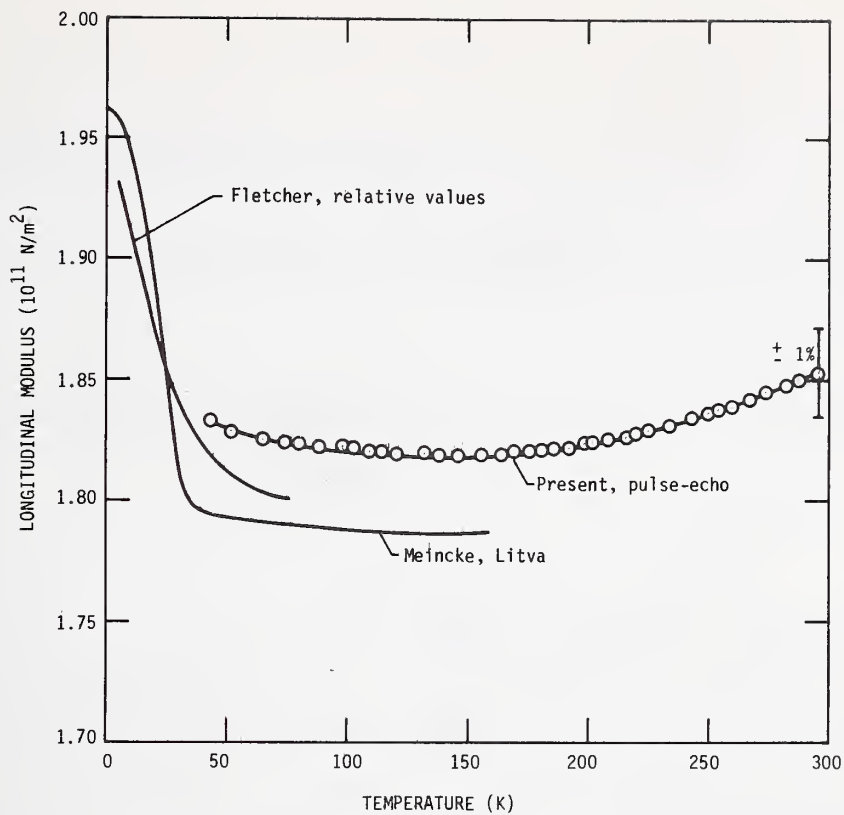


Figure 3. Temperature variation of the longitudinal modulus of invar.

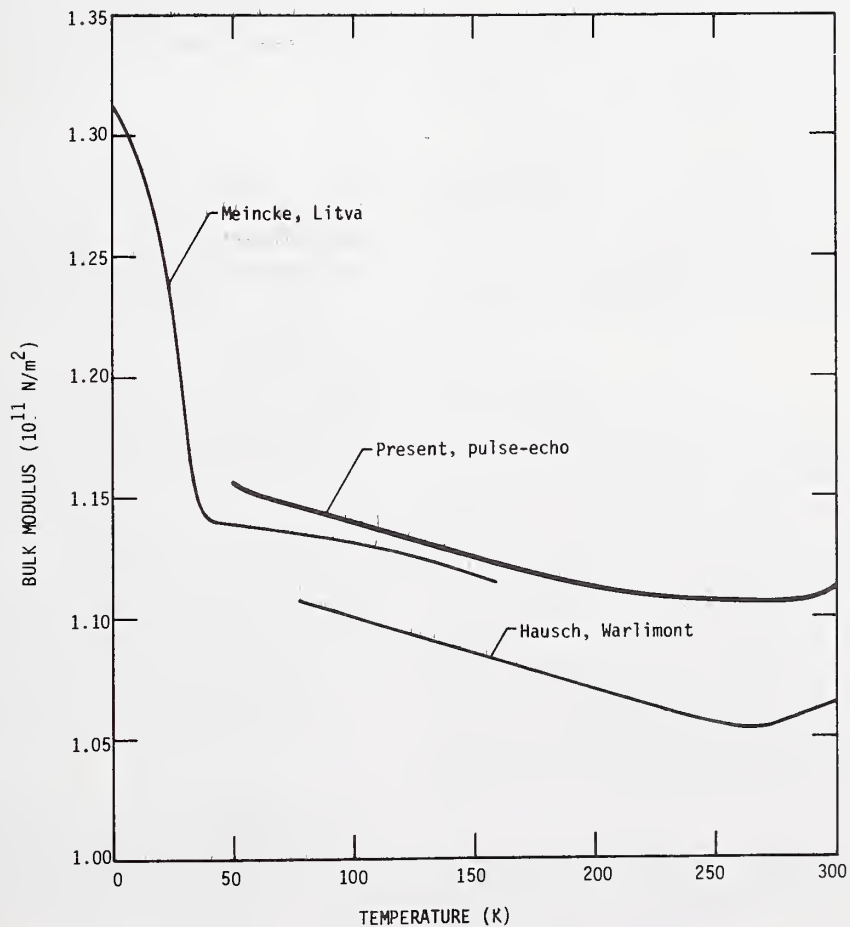


Figure 4. Temperature variation of the bulk modulus of invar.

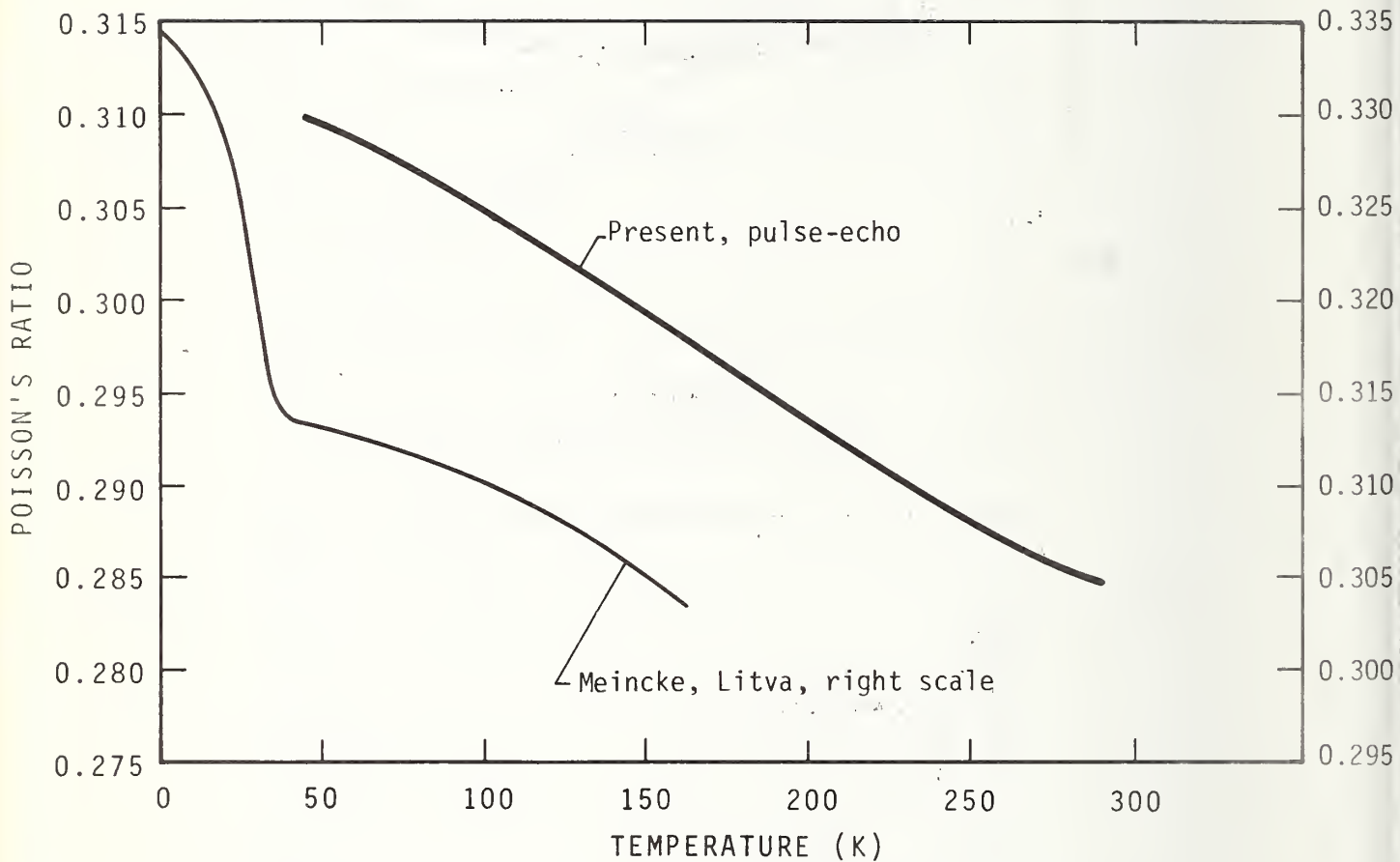


Figure 5. Temperature variation of Poisson's ratio of invar.

## Dynamic Low-Temperature Elastic Properties of Two Austenitic Nickel—Chromium—Iron Alloys\*

W.F. WESTON<sup>†</sup>, H.M. LEDBETTER and E.R. NAIMON<sup>††</sup>

*Cryogenics Division, Institute for Basic Standards, National Bureau of Standards, Boulder, Colorado 80302 (U.S.A.)*

(Received in revised form March 3, 1975)

### SUMMARY

The zero-magnetic-field low-temperature elastic properties of two polycrystalline nickel-chromium-iron alloys were determined ultrasonically between 4 and 300 K. Results are given for: longitudinal and transverse sound velocities, Young's modulus, shear modulus, bulk modulus, Poisson's ratio and elastic Debye temperature. Effects of alloying are discussed. The elastic property changes due to additions of chromium and iron to nickel are reviewed comprehensively.

### INTRODUCTION

Elastic properties of metals at low temperatures have twofold interest. First, such information is essential for understanding the basic aspects of mechanical deformation, which are often described by dislocation models that contain the elastic constants explicitly. Second, low-temperature elastic properties are essential design parameters for cryogenic structures, for predicting deflections due to any combination of stress and temperature.

Austenitic nickel-base alloys containing chromium and iron are standard engineering materials. They have high heat resistance, high corrosion resistance, good high-temperature strength, and can be readily fabricated into structures. Many of these materials also have low-temperature applications. In particular,

because of its mechanical properties, Inconel\* 600 is used extensively at cryogenic temperatures. Its strength increases with decreasing temperature, while its ductility and toughness are preserved. Inconel X-750 (formerly Inconel X) is similar to Inconel 600, but it contains small amounts of aluminum, titanium and niobium. Aluminum and titanium make precipitation hardening possible by forming  $Ni_3(Al, Ti)$  by suitable thermal treatment. (Inconel 600 is usually hardened by low-temperature mechanical deformation.) Niobium further stiffens the matrix through solid-solution hardening and stabilizes the carbides.

The zero-magnetic-field dynamic low-temperature elastic properties of Inconel 600 and Inconel X-750 are reported here. A pulse-superposition method was used to determine ultrasonic wave velocities in specimens prepared from as-received commercial bar stock.

### EXPERIMENTAL

Inconel 600 and X-750 alloys were obtained from commercial sources in the form of about 3-in. (7.6-cm) and 4-in. (10.2-cm) diameter rods, respectively. Cylindrical specimens  $\frac{3}{8}$ -in. (1-cm) long and  $\frac{5}{8}$ -in. (1.6-cm) diam. were prepared by grinding. Opposite faces were flat and parallel within  $100 \times 10^{-6}$  in. ( $2.5 \mu m$ ). Chemical compositions (obtained from mill analyses), hardness numbers and mass densities are given in Table 1. Hardnesses were determined by a standard method, and mass densities were determined by hydrostatic

\* Contribution of NBS, not subject to copyright.

<sup>†</sup> NRC-NBS Postdoctoral Research Associate, 1973-4.

<sup>††</sup> Present address: Dow Chemical USA, Golden, Colorado 80401.

\* Tradenames are used to characterize materials; they are not NBS endorsements of particular products.

TABLE 1

Compositions and properties of alloys

Alloy	Chemical composition, mill analyses (wt.%)										
	Ni	Cr	Mn	Fe	S	Si	Cu	C	Al	Ti	Nb + Ta
Inconel 600	Bal	15.8	0.20	7.20	0.007	0.20	0.10	0.04	—	—	
Inconel X-750	73.52	15.2	0.20	6.58	0.007	0.25	0.04	0.04	0.78	2.51	0.89

Alloy	Hardness (DPH No., 1 kg load)	Mass density at 294 K (g/cm <sup>3</sup> )	Condition
Inconel 600	179	8.415	As received; hot rolled annealed
Inconel X-750	330	8.238	As received; hot rolled 1625°F (1158 K) and aged

weighing using distilled water as a standard.

A pulse-superposition method [1] was used to determine all ultrasonic velocities except the shear mode in Inconel X-750. This particular mode was highly attenuated, and for its measurement a standard pulse - echo technique was used. All velocities were measured along the rolling direction of the rod.

Quartz transducers (10 MHz) were bonded to the specimens with phenyl salicylate for room-temperature measurements and with a stopcock grease for lower temperatures. When these bonds failed occasionally at very low temperatures, a silicone fluid (viscosity = 200,000 cP at 25°C) was used for bonding.

The specimen holder is shown schematically in Fig. 1. The holder was placed in the ullage of a helium dewar and lowered stepwise to achieve cooling. Temperatures were monitored with a chromel - constantan thermocouple contacting the specimen.

Velocity measurements were made over the range of 4 - 300 K for Inconel 600. For Inconel X-750, however, measurements were made over the range of 40 - 300 K. Below 40 K, the ultrasonic attenuation for both longitudinal and transverse waves was too high to permit accurate velocity determinations to be made. However, if a material is well behaved, little change is expected in its sound velocities from 40 to 0 K, and semi-theoretical curves fitted to the data points (as explained in the next section) should give accurate low-temperature values.

The experimental quantity of interest is the transit time  $t$  for an ultrasonic wave to propa-

gate from one end of the specimen to the other and back. The ultrasonic wave velocity  $v$  is then given by

$$v = 2l/t, \quad (1)$$

where  $l$  is the specimen length. Elastic moduli  $C$  are related to ultrasonic velocities by

$$C = \rho v^2, \quad (2)$$

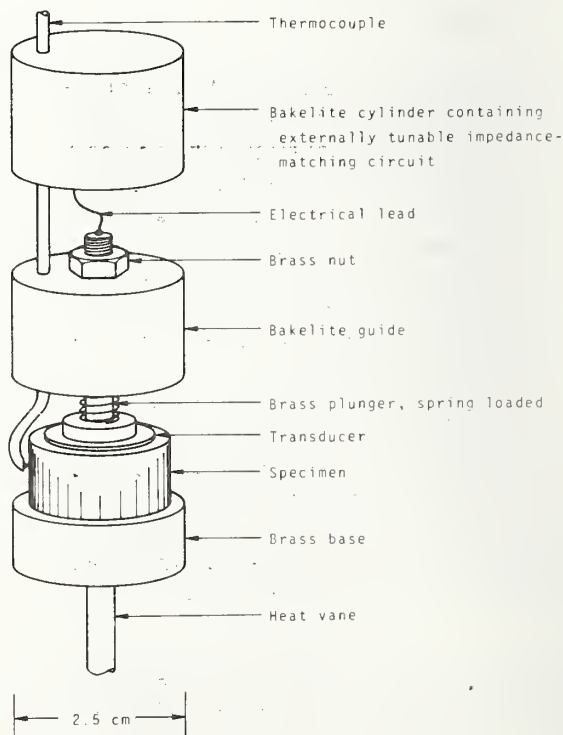


Fig. 1. Specimen holder.

where  $\rho$  is the mass density.

Denoting room-temperature values by the subscript r, it follows that

$$\rho/\rho_r = (l_r/l)^3. \quad (3)$$

Then eqn. (2) can be rewritten as

$$C = C_r(l_r/l)(t_r/t)^2. \quad (4)$$

Thus, the temperature dependence of an elastic modulus is determined from the change in transit time and from the length change due to thermal expansion or contraction. However, the relative length change for Inconel over the temperature range from 300 K to 4 K is only about 0.23% [2]. These small thermal-contraction corrections are neglected here; their omission introduces a maximum error also of 0.23% in the low-temperature values of velocity and modulus. Such small errors are insignificant for the purposes of the present study. Based on previous work in our laboratory, maximum uncertainties in the velocity measurements are estimated to be about 1%.

A quantity of some interest is the temperature coefficient  $(1/C)(dC/dT)$ , which is a measure of the relative modulus change due to temperature changes. From eqn. (4), it follows that

$$(1/C)(dC/dT) = -2(1/t)(dt/dT) - \alpha \quad (5)$$

where  $\alpha = (1/l)(dl/dT)$  is the coefficient of linear thermal expansion. For Inconel,  $\alpha$  is  $0.13 \times 10^{-4} \text{ K}^{-1}$  at room temperature [2].

## RESULTS

Temperature dependences of the longitudinal and transverse moduli are shown in Figs. 2 and 3. These moduli are given by

$$C_l = \rho v_l^2 = B + \frac{4}{3}G, \quad (6)$$

and

$$C_t = \rho v_t^2 = G. \quad (7)$$

Here  $v_l$  and  $v_t$  are the longitudinal and transverse sound-wave velocities,  $\rho$  is the mass density,  $B$  is the bulk modulus, and  $G$  is the shear modulus.

Temperature dependences of both  $C_l$  and  $C_t$  were least-squares fitted to a theoretical relationship suggested by Varshni [3]:

$$C = C^0 - s/(e^{t/T} - 1), \quad (8)$$

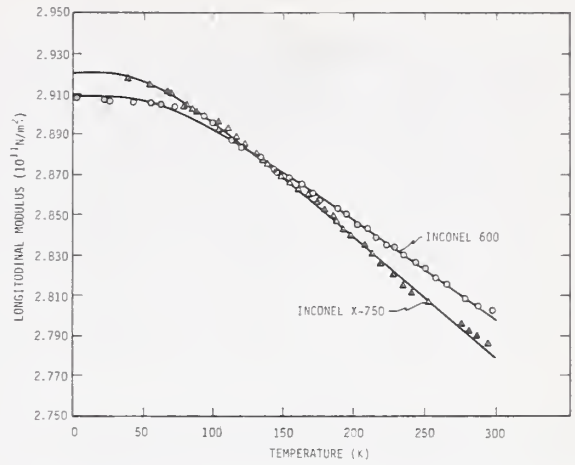


Fig. 2. Temperature dependence of longitudinal modulus  $C_l = \rho v_l^2$  of two nickel - chromium - iron alloys.

where  $C^0$ ,  $s$ , and  $t$  are adjustable parameters and  $T$  is temperature. The value of  $C$  at  $T = 0 \text{ K}$  is  $C^0$ , and  $-s/t$  is the high-temperature limit of  $dC/dT$ . By invoking an Einstein oscillator model of solids, it can be shown (in the absence of electronic effects) that  $t$  is the Einstein characteristic temperature. Parameters  $C^0$ ,  $s$  and  $t$  for Inconels 600 and X-750 are given in Table 2. Room-temperature values of the temperature coefficients of the elastic moduli are given in Table 3.

Curves in Figs. 2 and 3 are plots of eqn. (8) determined by an unweighted least-squares fit of the data. For Inconel 600, average percentage differences between measured and curve values

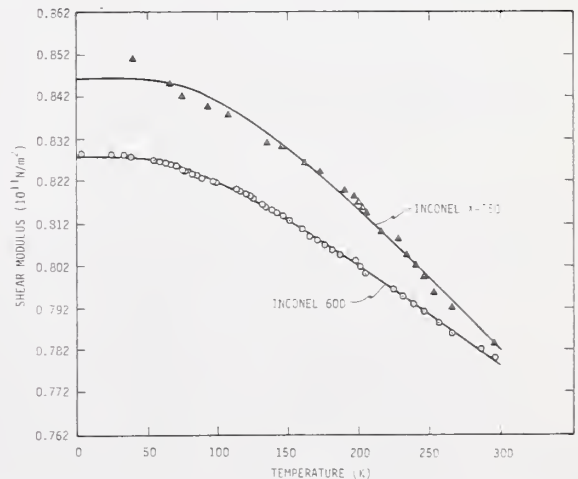


Fig. 3. Temperature dependence of transverse or shear modulus  $C_t = \rho v_t^2 = G$  of two nickel - chromium - iron alloys.

TABLE 2  
Parameters in the temperature-dependence eqn. (8)

Alloy	Mode	$C^0$ ( $10^{11}\text{N/m}^2$ )	$s$ ( $10^{11}\text{N/m}^2$ )	$t$ (K)
Inconel 600	$\rho v_{\ell}^2$	2.909	0.107	203.1
	$\rho v_t^2$	0.828	0.063	246.0
Inconel X-750	$\rho v_{\ell}^2$	2.920	0.105	165.9
	$\rho v_t^2$	0.846	0.120	315.8

are 0.05% for both the longitudinal and transverse moduli. For Inconel X-750, the average percentage differences between measured and curve values are 0.04% and 0.18% for the longitudinal and transverse moduli, respectively. The comparatively large error for the transverse modulus of Inconel X-750 was due to a relatively poor echo pattern resulting from ultrasonic-wave scattering. There are many possible sources of this scattering — for example lattice inhomogeneities and crystalline anisotropy.

While polycrystalline aggregates (quasi-isotropic solids) have only two independent elastic constants, several constants are commonly used for various applications. The four most common are the bulk modulus  $B$ , Young's modulus  $E$ , the shear modulus  $G$  and Poisson's ratio  $\nu$ . The relationships among these are:

$$\frac{1}{E} = \frac{1}{3G} + \frac{1}{9B} \quad (9)$$

and

$$\nu = \frac{E}{2G} - 1. \quad (10)$$

These elastic constants were calculated from the moduli shown in Figs. 2 and 3 by the

TABLE 3  
Temperature derivatives of elastic constants at room temperature ( $10^{-4} \text{K}^{-1}$ )

Source	Material	$\frac{1}{B} \frac{dB}{dT}$	$\frac{1}{E} \frac{dE}{dT}$	$\frac{1}{G} \frac{dG}{dT}$	$\frac{1}{\nu} \frac{d\nu}{dT}$
Present	Inconel 600	-1.20	-2.95	-3.21	1.10
Present	Inconel X-750	-1.02	-4.07	-4.53	1.97
Ref. 4	Nickel*	-1.56	-4.16	-4.53	1.72
Ref. 5	Inconel X			-3.09	
Ref. 6	Inconel X		-2.67		
Ref. 12	Inconel X			-3.16	

\* Based on single-crystal data averaged by the Voigt - Reuss - Hill method.

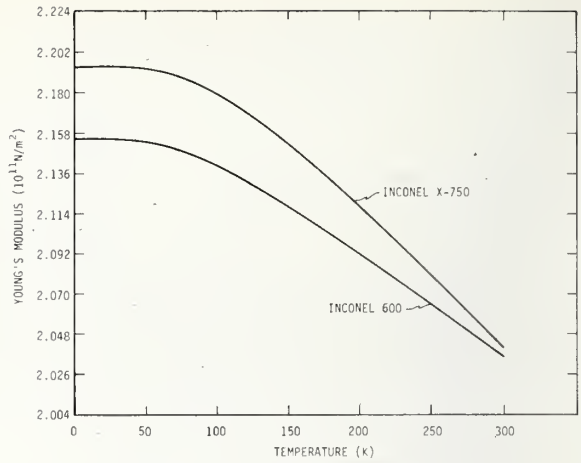


Fig. 4. Temperature dependence of Young's modulus of two nickel - chromium - iron alloys.

relationships:

$$E = 3C_t(C_{\ell} - \frac{4}{3}C_t)/(C_{\ell} - C_t), \quad (11)$$

$$B = C_{\ell} - \frac{4}{3}C_t, \quad (12)$$

and

$$\nu = \frac{1}{2}(C_{\ell} - 2C_t)/(C_{\ell} - C_t) \quad (13)$$

where  $C_{\ell}$  and  $C_t$  are the least-squares values obtained from fitting the experimental data with eqn. (8). The constants  $E$ ,  $B$  and  $\nu$  are shown in Figs. 4 - 6.

It is of interest to calculate the elastic Debye temperature  $\theta$  for the two alloys. This fundamental parameter is important in the lattice properties of solids and is related to the average elastic wave velocity by [7]

$$\theta = K(\nu), \quad (14)$$

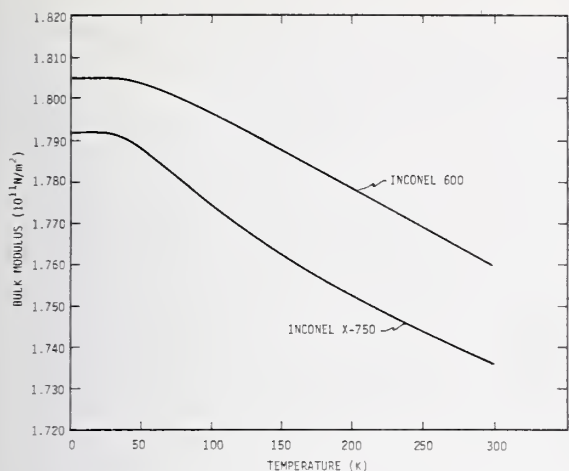


Fig. 5. Temperature dependence of bulk modulus (reciprocal compressibility) of two nickel - chromium - iron alloys.

where

$$K = \frac{h}{k} \left( \frac{3N\rho}{4\pi A} \right)^{1/3} \quad (15)$$

Here  $h$  is Planck's constant,  $k$  is Boltzmann's constant,  $N$  is Avogadro's constant,  $\rho$  is the mass density, and  $A$  is the effective atomic weight. The average velocity is given by

$$\langle v \rangle = \left( \frac{v_l^{-3} + 2v_t^{-3}}{3} \right)^{-1/3} \quad (16)$$

The Debye temperature of each alloy at  $T = 0$  K, and also of nickel, is given in Table 4.

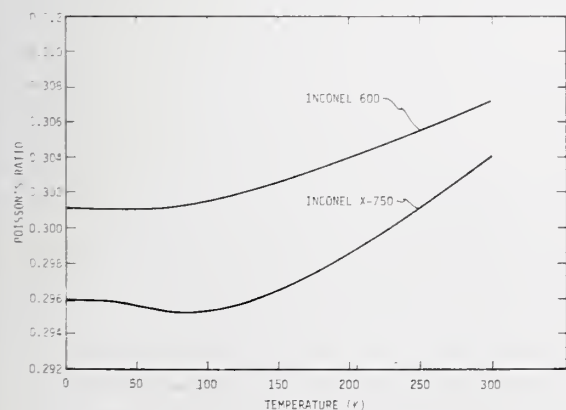


Fig. 6. Temperature dependence of Poisson's ratio of two nickel - chromium - iron alloys.

TABLE 4

Elastic Debye temperatures at  $T = 0$  K

Source	Material	$\theta$ (K)
Present	Inconel 600	464.9
Present	Inconel X-750	473.5
Ref. 8	Nickel	476.0

## DISCUSSION

The elastic properties of both Inconel 600 and Inconel X-750 behave regularly with respect to temperature. The elastic moduli ( $C_L$ ,  $C_t = G$ ,  $B$ ,  $E$ ) decrease with increasing temperature, show a relative flatness at low temperatures, achieve zero slope at  $T = 0$  K, and approach linear behavior at high temperatures. Poisson's ratio also behaves regularly, having a positive temperature coefficient. For both the bulk modulus and Poisson's ratio, Inconel X-750 shows unusual curvatures in the modulus - temperature curves. The reason for this is not understood; atomic ordering based on the  $Ni_3(Cr, Fe)$  composition is a possible explanation. Ordering often occurs on cooling and usually causes an increase in the elastic stiffnesses. Magnetic ordering might also affect the elastic stiffnesses.

Assuming that the specimens studied are representative of the two alloys, then conclusions concerning their relative elastic behavior can be drawn. Not surprisingly, as shown in Figs. 2 - 6 and in Tables 2 and 3, for most practical purposes the two alloys are elastically identical. Thus, additions of small amounts of aluminum, titanium and niobium have little effect on the elastic properties of nickel alloys containing about 15% chromium and about 7% iron.

Very few elastic data exist for these alloys [5,6,9 - 13], especially Inconel 600. Most information has appeared in engineering reports and is summarized in refs. 9 - 13. For comparison the room-temperature values of  $E$ ,  $G$ ,  $B$  and  $\nu$  are given in Table 5. Good agreement is observed between previous and present results. The polycrystalline elastic constants of nickel are also given in Table 5, both those determined from experiments on polycrystalline aggregates [4] and those obtained from single-crystal data [15,16] using a Voigt - Reuss - Hill average. The elastic Debye temperatures of

TABLE 5

Room-temperature elastic constants of Inconel 600 and Inconel X-750; units of  $10^{11}\text{N/m}^2$  except  $\nu$  (dimensionless)

Source	Inconel 600				Inconel X-750			
	$E$	$G$	$B$	$\nu$	$E$	$G$	$B$	$\nu$
Present	2.036	0.780	1.760	0.307	2.040	0.784	1.736	0.304
Ref. 5	—	—	—	—	—	0.789	—	—
Ref. 6	—	—	—	—	2.144	—	—	—
Refs. 9,10	2.11	0.75	—	—	2.11	0.75	—	0.29
Ref. 11	—	—	—	—	2.075	0.714	—	0.29
Ref. 12	—	—	—	—	2.041	0.824	—	—
Ref. 13	2.109	—	—	—	2.109	0.749	—	—
	Nickel - 26 iron							
Ref. 14	2.059	0.792	1.731	0.302				
	Nickel (polycrystal, zero magnetic field)							
Ref. 4	1.97	0.785	1.903	0.296				
	Nickel (VRH-averaged single crystal, zero magnetic field)							
Ref. 4	2.10	0.799	1.863	0.312				

the alloys are also within 2% of the value calculated from the single-crystal elastic data of nickel.

Low-temperature elastic data have been reported only once previously for either of these alloys; based on static measurements, Young's modulus and the shear modulus of Inconel X-750 were reported between room temperature and liquid-hydrogen temperature (20 K) [12]. The reported Young's modulus agrees closely with present results while the reported shear modulus is about 4% higher than the present results and has a lower room-temperature temperature derivative.

It is emphasized that the data reported here are dynamic (adiabatic) rather than static (isothermal) and apply to rapid, rather than slow, loading. In most cases the differences between adiabatic and isothermal elastic constants are small. The conversion formulas can be written as [17]

$$E_s = E_T(1 + E_T T \alpha^2 / C_p \rho), \quad (17)$$

$$B_s = B_T(1 + 9B_T T \alpha^2 / C_p \rho), \quad (18)$$

$$\nu_s = \nu_T + (1 + \nu_T) E_T T \alpha^2 / C_p \rho, \quad (19)$$

and

$$G_s = G_T, \quad (20)$$

where subscripts  $S$  and  $T$  denote adiabatic and isothermal, respectively. In the above equations

$T$  is the absolute temperature,  $\alpha$  is the linear thermal expansion coefficient,  $C_p$  is the heat capacity per unit mass at constant pressure, and  $\rho$  is the mass density. For the Inconel alloys at room temperature it is found that

$$(E_s - E_T) / E_s = 0.003, \quad (B_s - B_T) / B_s = 0.022,$$

$$(\nu_s - \nu_T) / \nu_s = 0.012 \text{ and } (G_s - G_T) \equiv 0. \quad (21)$$

At lower temperatures the differences are smaller; they vanish at  $T = 0$  K.

Alloying effects on material properties can be analyzed many ways. The simplest approach is a linear mixture model:

$$C = \sum_{i=1, N} x_i C_i, \quad (22)$$

where, in present context,  $C$  represents a general elastic constant of the alloy, which has  $N$  components of species  $i$ ;  $x_i$  are the weight fractions, and  $C_i$  are the elastic constants of the unalloyed species. This model works best for mixtures of similar metals where effects of atomic ordering, phase transformations, etc. are absent. It can be shown simply that this model fails for transition-metal alloys, even for simpler, binary systems such as iron - nickel.

A better model proceeds on the basis of

alloy data rather than component data:

$$\frac{C}{C_0} = 1 + \frac{1}{C_0} \sum_{i=1, N} \left( \frac{\partial C}{\partial x_i} \right) \Delta x_i, \quad (23)$$

where  $C_0$  is the elastic constant of the reference material, usually (but not necessarily) a pure component,  $(\partial C/\partial x_i)$  are slopes of the  $C - x_i$  curves, and  $x_i$  are the weight fractions. Expressions like eqn. (23) have been used previously to describe the elastic properties of ternary alloys [18]; it assumes that alloying effects  $(\Delta C/\Delta x)$  are composition independent in the range of interest and are linearly additive. Considering Inconel alloys to be, in a first approximation, alloys of iron and chromium in nickel, then three data are required (besides composition) to solve eqn. (23) — the elastic constants of nickel and the changes of these constants with iron and with chromium additions. Nickel's elastic constants are well known [4].

Effects of iron additions on the elastic properties of nickel have been studied extensively [19 - 32], although the subject has apparently not been reviewed. A summary of the results is given in Table 6, which gives the logarithmic composition derivatives  $(1/C)(\Delta C/\Delta x)$ , where  $C$  represents an elastic constant such as  $E$ ,  $G$ ,  $B$  or  $\nu$ , and  $x$  denotes weight per-

cent iron alloyed into nickel. The effects of alloying iron into nickel are best defined for the Young's modulus and the bulk modulus; the change of the bulk modulus is quite large.

Effects of chromium additions on the elastic properties of nickel have been reported only by Chevenard [21] and are shown in Table 7. If the value of  $(1/G)(\Delta G/\Delta x)_{Fe}$  from Table 6 is substituted into eqn. (23) along with the other input data, a value of  $(1/G)(\Delta G/\Delta x)_{Cr} = -6.6$  is calculated. Since this disagrees with Chevenard's value of 2.9, the model represented by eqn. (23) also fails for the alloys of interest here.

The necessity of invoking higher-order terms in the Taylor expansion is indicated:

$$\begin{aligned} \frac{C}{C_0} = 1 + \frac{1}{C_0} \sum_{i=1, N} \left( \frac{\partial C}{\partial x_i} \right) \Delta x_i \\ + \frac{1}{6C_0} \left( \frac{\partial^2 C}{\partial x_i \partial x_j} \right) \Delta x_i \Delta x_j + \dots \end{aligned} \quad (24)$$

In particular, the interaction term in this case:

$$\frac{1}{C_0} \left( \frac{\partial^2 C}{\partial x_{Cr} \partial x_{Fe}} \right) x_{Cr} x_{Fe} \quad (25)$$

may be quite important since alloying alters 3d-shell electronic structure, which in turn affects cohesion and elastic properties. At

TABLE 6

Effects of iron on the elastic properties of nickel at room temperature (evaluated from 0 - 7% iron)

Source	$\frac{1}{C} \left( \frac{\Delta C}{\Delta x} \right) \times 10^3$			
	$E$	$G$	$B$	$\nu$
Honda (1919)	2.4	1.4		
Honda, Tanaka (1926)	0.3	0.7		1.7
Chevenard (1927)		0.0		
Nishiyama (1929)	4.1			
Ebert, Kussmann (1937)			-15.0	
Förster, Köster (1937)	1.7			
Engler (1938)	1.0			
Köster (1940)	1.9			
Chevenard, Crussard (1943)	0.0			
Köster (1943)	1.7			
Yamamoto (1959)	7.8			
Sakurai <i>et al.</i> (1964)*		-0.4		
Shirakawa <i>et al.</i> (1969)*	5.3	9.8	-17.5	-17.3
Tanji <i>et al.</i> (1970)	0.8	2.3	-16.8	-10.7
Average observed values	2.4	2.3	-16.4	-8.8
Linear mixture model	-0.6	-0.5	-1.1	-0.3

\* Single-crystal data were averaged by the method of Voigt.

TABLE 7

Effects of chromium on the elastic properties of nickel

Source	$\frac{1}{E} \left( \frac{\Delta E}{\Delta x} \right) \times 10^3$	$\frac{1}{G} \left( \frac{\Delta G}{\Delta x} \right) \times 10^3$	$\frac{1}{B} \left( \frac{\Delta B}{\Delta x} \right) \times 10^3$	$\frac{1}{\nu} \left( \frac{\Delta \nu}{\Delta x} \right) \times 10^3$
Linear mixture model	2.2	3.1	-1.1	-3.2
Chevenard (1927)		2.9		

present, data are insufficient for evaluating this interaction term. Chevenard's [21] data on Ni - Cr - Fe alloys indicate that for the shear modulus the interaction term might be as large as  $40 \times 10^{-3} x_{Fe} x_{Cr}$ , which is large relative to the first-order coefficients in Tables 6 and 7. It is difficult to make any quantitative estimate of the second-order mutual interaction terms (Fe - Fe, Cr - Cr). But from the existing data they seem to be smaller than the cross-term (Fe - Cr). Additional evidence for a large interaction term results from the following reasoning. Since the elastic properties of the two Inconel alloys are so similar, additional alloying elements beyond chromium and iron seem to have negligible effects or to cancel. In either case, considering Inconels to be ternary alloys of nickel, chromium and iron seems justified from the viewpoint of their elastic properties. However, both alloys behave elastically very much like a nickel - iron alloy with the same nickel content; chromium behaves as if it were iron. This is shown in Table 5, which includes the elastic properties of a nickel-26 iron alloy, which were obtained from single-crystal data by using a Voigt - Reuss - Hill-arithmetic average. Why chromium should behave like iron is not understood.

Another anomaly of the Ni - Cr - Fe system is that the elastic stiffnesses of nickel are increased by either chromium or iron additions. Usually the elastic stiffness of a host metal is reduced by alloying. The reverse effect in this case could be magnetic in origin, as discussed below.

Magnetic interactions contribute to the energy of a material and therefore also to its elastic constants, which are related to the second spatial derivative of the total energy. However, extra energies due to magnetism take many forms, and several models have been suggested to account for the anomalous elastic

behaviour of magnetic materials. At least two of these models are relevant here.

Khomenko and Tseytlin [33] showed for alloys in the invar region (Fe ~ 35 Ni) that chromium additions increased Young's modulus with  $(1/E)(\Delta E/\Delta x)$  having a value near  $30 \times 10^{-3}$ , a very large effect compared with the coefficients in Tables 6 and 7. These authors showed that chromium increases  $E$  because it suppresses the usual  $\Delta E$  effect  $\Delta E_\lambda$ , owing to linear magnetostriction, which reduces  $E$ . Since  $\Delta E_\lambda$  is proportional to a magnetostriction constant  $\lambda$  that is quite large for nickel, this is a possible model for the anomalous elastic behaviour of nickel - chromium - iron alloys.

Hausch [34] used a molecular-field approximation to evaluate the Heisenberg exchange-energy  $J(r)$  contribution to the elastic constants of magnetic materials. For nickel it was shown that  $\partial^2 J(r)/\partial r^2$  is negative (therefore the elastic constant contribution is negative), while for face-centered cubic iron the derivative is positive. The derivative has not been evaluated for chromium; it is probably positive as deduced from its approximate position on a Bethe - Slater curve. Thus, it is clear qualitatively that Hausch's model might also be able to explain the anomalous elastic behaviour of these alloys.

The two models could be tested by low-frequency elastic measurements on appropriate alloys, with and without a saturating magnetic field. The  $\Delta E_\lambda$  variation with alloying disappears in a saturating magnetic field since the magnetic domain walls are immobilized.

Finally, a speculative suggestion is made concerning the source of the very high acoustic attenuation in Inconel X-750 below 40 K. Iron and nickel have Curie temperatures of 1040 K and 630 K, respectively. Alloying with chromium reduces both of these drastically; about 50% chromium in iron suppresses completely the paramagnetic - ferromagnetic

transition; for nickel, fewer data exist, but only about 12% chromium may be required to suppress the Curie transition in nickel. No studies seem to have been reported on the Curie temperatures of Ni - Cr - Fe alloys [35]. Thus, a paramagnetic - ferromagnetic transition in Inconel X-750 at low temperatures is possible. If it occurs, the exact transition temperature should depend strongly on chromium content. Such a transition would explain the attenuation increase as due to acoustic-wave scattering from ferromagnetic domain walls. The attenuation would not be associated with the Curie transition itself, but with a change in the magnetic state, a state produced by the Curie transition. Simple dip tests using a small permanent magnet indicated that both Inconels 600 and X-750 are ferromagnetic at liquid-nitrogen temperatures. Tests for ferromagnetism between room and nitrogen temperatures were not made. Further studies on this problem are planned. Studies that would be valuable include low-temperature acoustic wave-velocity and attenuation measurements in a saturating magnetic field. If a ferromagnetic transition occurs, then lower-frequency elastic measurements would be useful for determining the so-called  $\Delta E$  effect. No  $\Delta E$  effect is seen in the MHz region because ferromagnetic domain walls cannot respond to a high-frequency mechanical stress [36]. Measurements of Curie temperatures and saturation magnetic moments would also be useful.

#### CONCLUSIONS

From the results of this study the following conclusions are drawn:

1. The elastic properties of Inconel 600 and Inconel X-750 are quite similar.
2. At lower temperatures, Inconel X-750 has a slightly higher shear modulus and Young's modulus than has Inconel 600, but a slightly lower bulk modulus.
3. At low temperatures, Poisson's ratio is slightly lower for Inconel X-750 than for Inconel 600.
4. Inconel 600 shows a regular temperature dependence in all its elastic properties.
5. The temperature dependence of the elastic properties of Inconel X-750 is regular except for the bulk modulus, which has a region of positive curvature, and Poisson's ratio, which has a minimum near 80 K.

6. Inconel X-750 highly attenuates 10 MHz sound waves, both longitudinal and transverse, below about 40 K. This is speculated to result from a change in the magnetic state, which results from a paramagnetic-to-ferromagnetic transition that occurs above 77 K. Why Inconel 600, which also undergoes a magnetic transition, has lower attenuation is not understood.

7. The composition dependence of the elastic properties of these alloys cannot be described by a simple model, probably because of d-shell and magnetic interactions.

#### ACKNOWLEDGEMENTS

This work was supported in part by the Advanced Research Projects Agency of the U.S. Department of Defense. Dr. R.L. Moment of Dow Chemical contributed a critical reading of the manuscript.

#### REFERENCES

- 1 H.J. McSkimin, *J. Acoust. Soc. Am.*, 33 (1961) 12.
- 2 R.J. Corruccini and J.J. Gniewek, *Thermal Expansion of Technical Solids at Low Temperatures*, NBS Monograph 29, 1961, p. 10.
- 3 Y.P. Varshni, *Phys. Rev.*, B2 (1970) 3952.
- 4 H.M. Ledbetter and R.P. Reed, *J. Phys. Chem. Ref. Data*, 2 (1973) 531.
- 5 H.C. Burnett, unpublished results, 1956.
- 6 W.H. Hill, K.O. Shimmin and B.A. Wilcox, *Am. Soc. Testing Mater. Proc.*, 61 (1961) 890.
- 7 P. Debye, *Ann. Phys. (Leipzig)*, 39 (1912) 789.
- 8 R. Wanner, *Can. J. Phys.*, 48 (1970) 1270.
- 9 Intern. Nickel Co., Rept. on Inconel Alloy 600, 1973.
- 10 Intern. Nickel Co., Rept. on Inconel Alloy X-750, 1970.
- 11 NERVA Program Materials Properties Data Book, Vol. 1A, Nickel Base Alloys, Aerojet Nuclear Systems, Sacramento, Calif., 1970.
- 12 Cryogenic Materials Data Handbook, AFML Rept. No. ML-TDR-64-280, PB 171809, revised, Aug. 1964.
- 13 Aerospace Structural Metals Handbook, Vol. II, AFML Rept. No. ASD-TDR-63-741, Mar. 1966.
- 14 N.G. Einspruch and L.T. Claiborne, *J. Appl. Phys.*, 35 (1964) 175.
- 15 S.G. Epstein and O.N. Carlson, *Acta Met.*, 13 (1965) 487.
- 16 G. Simmons and H. Wang, *Single Crystal Elastic Constants and Calculated Aggregate Properties: A Handbook*, M.I.T. Press, Cambridge, 1971, p. 223.
- 17 L.D. Landau and E.M. Lifshitz, *Theory of Elasticity*, Pergamon Press, London, 1959, p. 17.
- 18 J.B. Greer and E.H. Bucknall, *Trans. Am. Soc. Metals*, 57 (1964) 554.

- 19 K. Honda, Sci. Rept. Tohoku Univ., 8 (1919) 59.
- 20 K. Honda and T. Tanaka, Sci. Rept. Tohoku Univ., 15 (1926) 1.
- 21 P. Chevenard, Trav. Mem. Bur. Int. Poids Meas., 27 (1927) 116.
- 22 Z. Nishiyama, Sci. Rept. Tohoku Univ., 18 (1929) 539.
- 23 H. Ebert and A. Kussmann, Physik. Z., 38 (1937) 437.
- 24 F. Förster and W. Köster, Naturwiss., 25 (1937) 436.
- 25 O. Engler, Ann. Physik, 31 (1938) 145.
- 26 W. Köster, Arch. Eisenhuettenw., 6 (1949) 271.
- 27 P. Chevenard and Ch. Crussard, Compt. Rend., 216 (1943) 685.
- 28 W. Köster, Z. Metallk., 10 (1943) 194.
- 29 M. Yamamoto, Sci. Rept. Tohoku Univ., 11 (1959) 102.
- 30 J. Sakurai, M. Fujii, Y. Nakamura and H. Takaki, J. Phys. Soc. Japan, 19 (1964) 308.
- 31 Y. Shirakawa, Y. Tanji, H. Moriya and I. Oguma, J. Japan Inst. Metals (Sendai), 33 (1969) 1196.
- 32 Y. Tanji, Y. Shirakawa and H. Moriya, Rept. No. 1462, Res. Inst. for Iron, Steel and Other Metals (1970), p. 84; also in J. Japan Inst. Metals (Sendai), 34 (1970) 417.
- 33 O.A. Khomenko and A.M. Tseytlin, Fiz. Metal. i Metalloved., 28 (1969) 246.
- 34 G. Hausch, Phys. Status Solidi, 15 (1973) 501.
- 35 T.F. Connolly (ed.), Bibliography of Magnetic Materials and Tabulation of Magnetic Transition Temperatures, Vol. 5, Solid State Physics Literature Guides, Plenum Press, New York, 1972.
- 36 W.P. Mason, Phys. Rev., 83 (1951) 683.

# Low-temperature elastic properties of four austenitic stainless steels

H. M. Ledbetter, W. F. Weston,<sup>\*†</sup> and E. R. Naimon<sup>\*†</sup>

Cryogenics Division, Institute for Basic Standards, National Bureau of Standards, Boulder, Colorado 80302  
(Received 11 February 1975)

The elastic properties of four austenitic stainless steels—AISI 304, AISI 310, AISI 316, and A286—are reported over the temperature range 300–4 K. These properties include longitudinal modulus, shear modulus, Young's modulus, bulk modulus (reciprocal compressibility), Poisson's ratio, and elastic Debye temperature. Elastic constants were determined from measurements of longitudinal and transverse sound-wave velocities using an ultrasonic (10 MHz) pulse-superposition method. Measurements were made in the absence of a magnetic field; these alloys undergo paramagnetic-to-antiferromagnetic transitions at low temperatures. For all four alloys, the shear modulus behaves regularly with respect to temperature. The other elastic constants, all of which have a dilatational component, decrease anomalously at temperatures below 80 K. The largest anomaly, about 3%, is in the bulk modulus of the 304 alloy; this modulus is lower at 0 K than at 300 K. Results are interpreted on the basis of the Döring effect, which results from a large volume magnetostriction in the magnetic phase. This may be the first report of a Döring effect in antiferromagnetic materials.

PACS numbers: 62.20.D, 65.70., 75.80.

## I. INTRODUCTION

Austenitic stainless steels are attractive materials for mechanical applications at low temperatures. Primarily, this is due to their having, at room temperature, a face-centered cubic (fcc) crystal structure. Metals having this crystal structure usually do not become brittle at lower temperatures. In general, steels that remain austenitic at cryogenic temperatures show increased tensile strength, a smaller increase in yield strength, and little change in ductility. However, it is not axiomatic that fcc materials will always perform well at low temperatures. For example, lower temperatures may promote a change of the crystal structure from fcc to body-centered cubic (bcc) or to close-packed hexagonal (cph), thus probably embrittling the material. Other changes such as atomic ordering or magnetic ordering may also occur at low temperatures; these also effect mechanical behavior. Thus, the nature and the magnitude of a material's low-temperature properties cannot be predicted *a priori* from room-temperature observations, and there is no substitute for careful low-temperature experimental determinations of the important properties of each material of interest. Gilman<sup>1</sup> concluded that "the most important mechanical characteristic of a crystal is its elastic modulus".

The same elastic constants that are related to fundamental interatomic forces in solids are also used in engineering design. For example, Poisson's ratio is an essential design parameter in problems of plate buckling or of pressure-vessel design. Young's modulus and Poisson's ratio are required if plane-stress

data and plane-strain data are to be interconverted, a technique used often in the elastic stress-strain analysis of solids.

In this paper, the dynamic zero-magnetic-field elastic properties of four austenitic stainless steels—commonly designated AISI 304, AISI 310, AISI 316, and A286<sup>2</sup>—are reported between 300 and 4 K. These properties include longitudinal modulus, shear modulus, Young's modulus, bulk modulus (reciprocal compressibility), and Poisson's ratio. These elastic constants were determined dynamically, by measuring the velocity of longitudinally polarized and transversely polarized ultrasonic (10 MHz) pulses propagating through polycrystalline specimens of commercial as-received alloys. At low temperatures, elastic anomalies were observed in all four materials. These are believed to be associated with transitions to antiferromagnetic states. A magneto-elastic interpretation of the anomalies is given.

## II. EXPERIMENTAL

### A. Specimens

Materials were obtained from commercial sources in the form of  $\frac{3}{8}$ -in. (1.9-cm)-diam rods. Their chemical compositions are given in Table I. Hardness and mass-density data on the alloys are given in Table II. Hardnesses were measured by standard metallurgical methods, and mass densities were measured by Archimedes's method using distilled water as a standard. Materials were tested in their as-received conditions. Samples were prepared by grinding cylinders

TABLE I. Chemical analyses of the alloys, wt%, obtained from mill analyses.

Alloy	Al	C	Cr	Cu	Mo	Mn	Ni	P	S	Si	Ti	V	Fe
304		0.02	18.4			1.4	9.7	0.02	0.01	0.6			balance
310		0.08	24.8	0.1	0.1	1.7	20.8	0.02	0.02	0.7			balance
316		0.05	16.8	0.2	2.1	1.9	11.7	0.03	0.02	0.4			balance
A286	0.2	0.04	14.8		1.2	1.4	25.4	0.01	0.01	-0.6	2.1	0.3	balance

TABLE II. Densities and hardnesses of the alloys.

Alloy	Mass density (g/cm <sup>3</sup> )	Hardness (DPHN, 1 kg load)
304	7.86	225
310	7.85	220
316	7.97	210
A286	7.95	275

$\frac{1}{2}$  in. (1.2 cm) thick with faces flat and parallel within  $10^{-4}$  in. ( $2.5 \mu\text{m}$ ).

**B. Procedures**

A pulse-superposition<sup>3</sup> method was used to measure the longitudinal and transverse sound-wave velocities between room temperature and liquid-helium temperature. The specimen holder, which was described previously<sup>4</sup>, was placed in the ullage of a helium Dewar and lowered (raised) stepwise to achieve cooling (heating). Measurements were made semicontinuously on cooling, and a few points were checked on heating to verify reversibility. Temperatures were measured by a chromel-constantan thermocouple contacting the specimen. Quartz transducers (10 MHz) were bonded to the specimens with phenyl salicylate for room-temperature measurements and with stopcock grease for lower temperatures. No bond corrections were made since these are insignificant for present purposes. No thermal-contraction corrections were made; for the alloys of interest this introduces a maximum error of 0.3% over the 300 K temperature range. Maximum uncertainties in the absolute velocity measurements are estimated to be about 1%. The imprecision in the relative velocities is a few parts in  $10^5$ .

**III. RESULTS**

Longitudinal and transverse moduli are shown in

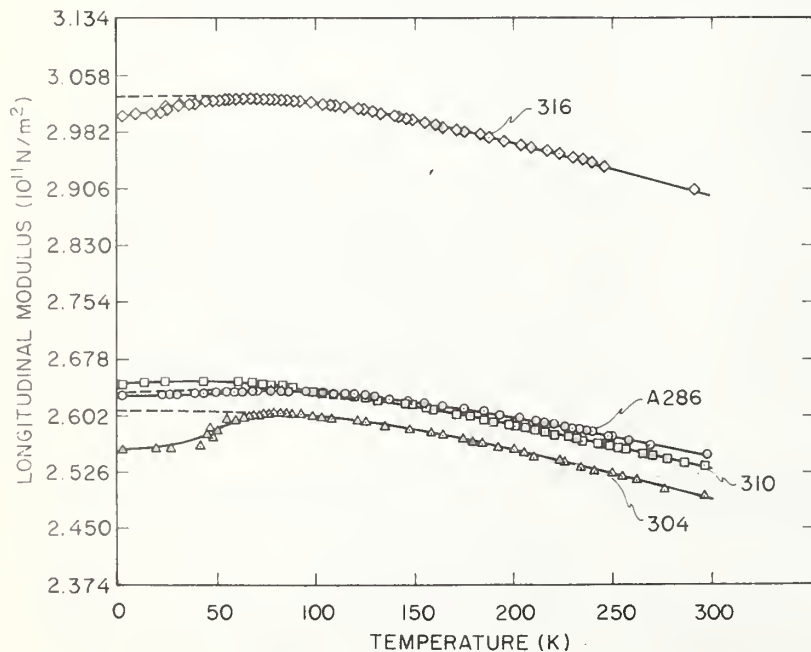


FIG. 1. Temperature dependence of the longitudinal moduli of four stainless-steel alloys.

Figs. 1 and 2 as a function of temperature. The longitudinal modulus  $C_l$  is given by

$$C_l = \rho v_l^2, \tag{1}$$

where  $\rho$  is the mass density and  $v_l$  is the longitudinal wave velocity. The transverse modulus  $C_t$  is identically equal to the shear modulus  $G$  and is given by

$$C_t = G = \rho v_t^2, \tag{2}$$

where  $v_t$  is the transverse wave velocity. Young's modulus  $E$  is given by

$$E = 3C_l(C_l - \frac{4}{3}C_t)/(C_l - C_t) \tag{3}$$

and is shown in Fig. 3. The bulk modulus  $B$ , or reciprocal compressibility, is given by

$$B = C_l - \frac{4}{3}C_t, \tag{4}$$

and is shown in Fig. 4. Poisson's ratio  $\nu$  is given by

$$\nu = \frac{1}{2}(C_l - 2C_t)/(C_l - C_t) \tag{5}$$

and is shown in Fig. 5.

Temperature dependences of both  $C_l$  and  $C_t$  were fitted by a least-squares method to a theoretical relationship suggested by Varshni<sup>5</sup>:

$$C = C^0 - s/(e^{t/T} - 1), \tag{6}$$

where  $C^0$ ,  $s$ , and  $t$  are adjustable parameters and  $T$  is temperature. The value of  $C$  at  $T=0$  K is  $C^0$ , and  $-s/t$  is the high-temperature limit of the temperature derivative  $dC/dT$ . By invoking an Einstein oscillator model of solids, it can be shown (in the absence of electronic effects) that  $t$  is the Einstein characteristic temperature. Parameters  $C^0$ ,  $s$ , and  $t$  are given in Table III. The average differences between the Varshni-curve values and measured values were 0.04 and 0.05% for  $C_l$  and  $C_t$  respectively. Of course, the low-temperature elastic anomalies are not described by Eq. (6),

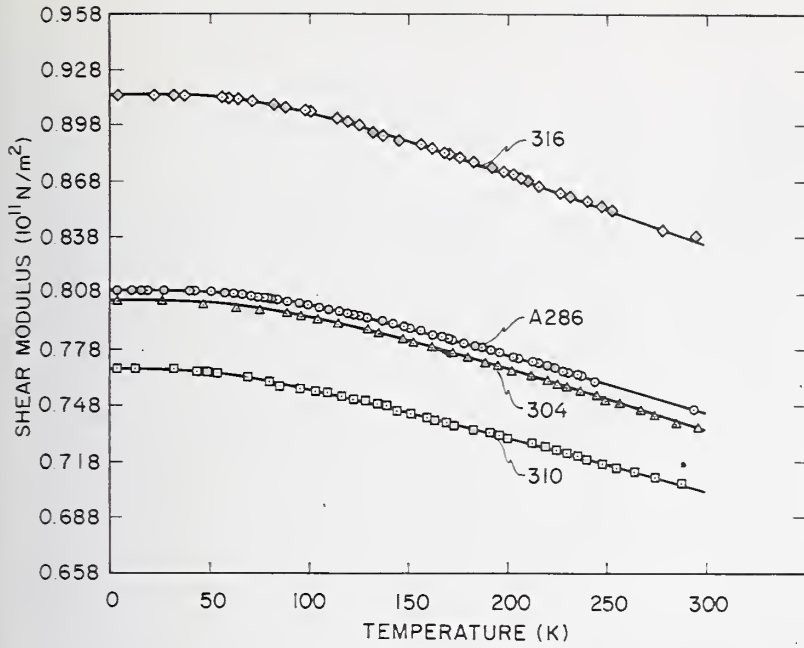


FIG. 2. Temperature dependence of the transverse (shear) moduli of four stainless-steel alloys.

which describes the extrapolated higher-temperature behavior shown as dashed lines in the figures. Temperature coefficients of the elastic constants at room temperature are given in Table IV.

Elastic Debye temperatures at  $T=0$  K were calculated for both the antiferromagnetic and the extrapolated paramagnetic states, and these are given in Table V. The elastic Debye temperature  $\Theta$  is related to the average sound-wave velocity according to

$$\Theta = K\langle v \rangle, \quad (7)$$

where

$$K = (\hbar/k)(3N_D/4\pi A)^{1/3}. \quad (8)$$

Here  $\hbar$  is Planck's constant,  $k$  is Boltzmann's constant,  $N$  is Avogadro's number,  $\rho$  is the mass density, and  $A$

is the effective atomic weight. The average velocity is given by

$$\langle v \rangle = [\frac{1}{3}(v_l^{-3} + 2v_t^{-3})]^{-1/3}. \quad (9)$$

For comparison, the elastic Debye temperatures at  $T=0$  K of iron, chromium, and nickel are also included in Table V.

#### IV. DISCUSSION

The elastic constants of all four materials exhibit regular behavior from room temperature to about 80 K or lower. Below about 80 K, anomalous changes in the elastic constants occur for all four materials. These anomalies occur only in the elastic constants that have a dilatational component—the longitudinal modulus, the

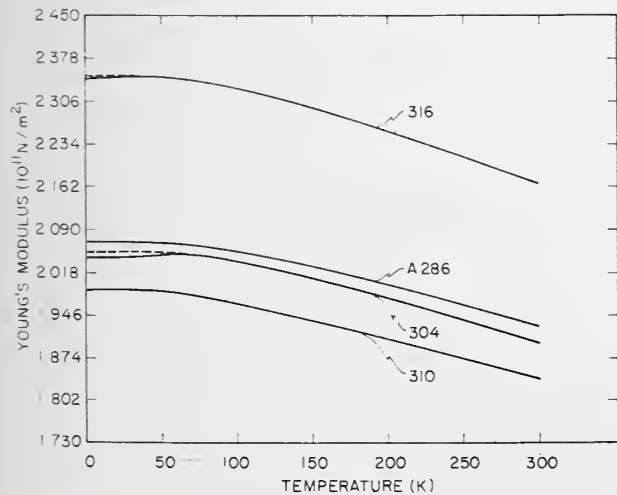


FIG. 3. Temperature dependence of the Young's moduli of four stainless-steel alloys.

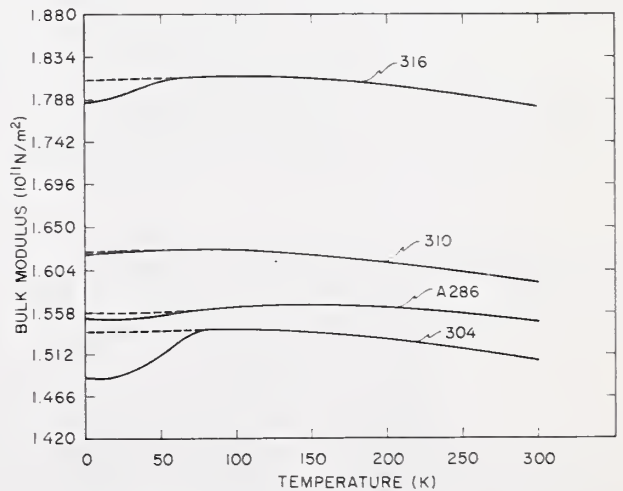


FIG. 4. Temperature dependence of the bulk moduli (reciprocal compressibilities) of four stainless-steel alloys.

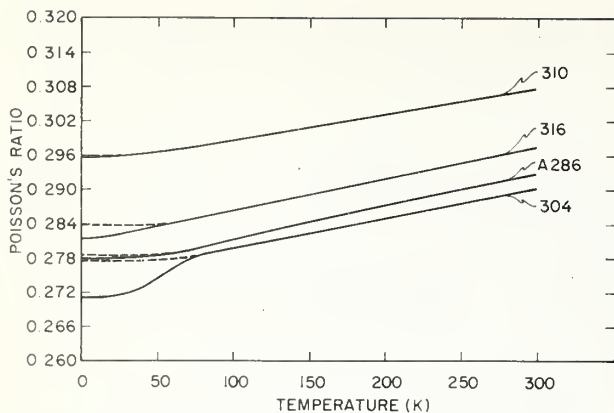


FIG. 5. Temperature dependence of Poisson's ratios of four stainless-steel alloys.

bulk modulus, Young's modulus, and Poisson's ratio. No anomalies occur for the shear modulus.

The elastic properties of some of these alloys have been studied previously at low temperatures. For example, stress-strain tests for  $E$  and  $G$  at 295, 77, and 4 K indicated anomalies somewhere below 77 K for both AISI 302 and AISI 303, but not for AISI 310.<sup>6</sup> Resonance tests on AISI 303 for  $E$  and  $G$  simultaneously at temperatures between 320 and 4 K showed anomalies below 80 K.<sup>7</sup> All these anomalous results can be interpreted in terms of the usual  $\Delta E = \Delta E_\lambda$  effect (discussed below) and are not directly related to the low-temperature elastic anomalies reported in the present work.

The most likely causes of the anomalies are magnetic transitions. Stainless-steel-type alloys have been shown to be antiferromagnetic at lower temperatures; Néel temperatures near 40 K have been reported<sup>6,8</sup> for 304-type alloys. However, no Néel transition was detected for a 310-type alloy cooled to liquid-helium temperature.<sup>9</sup> This suggests that effects due to local, rather than long-range, magnetic ordering may be occurring in these alloys. This would also account for the difference in the 304 alloy between the Néel temperature (40 K) and the temperature below which anomalous elastic behavior is observed (80 K). Short-range magnetic-order effects have been discussed by Schlosser<sup>9</sup> for fcc iron-nickel alloys. Changes of crystal structure are probably not the cause of the anomalies since the changes were observed to be reversible within experimental error; changes of elastic constants due to crystal-structure changes are generally irreversible, show-

TABLE III. Parameters in the temperature-dependence equation, Eq. (6).

Alloy	Mode	$C^0$ ( $10^{11}$ N/m <sup>2</sup> )	$s$ ( $10^{11}$ N/m <sup>2</sup> )	$t$ (K)
304	$l$	2.608	0.297	371.8
	$t$	0.803	0.089	251.8
310	$l$	2.647	0.175	271.8
	$t$	0.767	0.051	173.7
316	$l$	3.028	0.332	369.7
	$t$	0.914	0.099	243.5
A286	$l$	2.636	0.334	454.4
	$t$	0.809	0.080	243.1

TABLE IV. Temperature-coefficients of the elastic constants at room temperature ( $10^{-4}$  K<sup>-1</sup>).

Alloy	$\frac{1}{B} \frac{dB}{dT}$	$\frac{1}{E} \frac{dE}{dT}$	$\frac{1}{G} \frac{dG}{dT}$	$\frac{1}{\nu} \frac{d\nu}{dT}$
304	-1.69	-4.15	-4.54	1.78
310	-1.39	-3.71	-4.05	1.45
316	-1.41	-4.17	-4.61	1.89
A286	-1.22	-3.77	-4.18	1.81

ing a particularly large hysteresis in iron-base alloys. The elastic constants reported here showed a reversible behavior and indicate that the magnetic transition occurs smoothly over a range of temperatures rather than at a unique transition temperature. Thus, the transition seems to be of the second-order type.<sup>10</sup>

The usual so-called  $\Delta E$  effect, better designated  $\Delta E_\lambda$ , due to linear magnetostriction strains induced by an applied stress, and usually interpreted by invoking a Weiss domain model (with domain rotations and domain-wall motions), can also be excluded as a possible source of the anomalous elastic behavior. Linear magnetostriction affects Young's modulus, the shear modulus, and Poisson's ratio, but it does not affect the bulk modulus because no magnetomechanical process will respond to the application of a hydrostatic stress.<sup>11</sup> Also, effects due to  $\Delta E_\lambda$  are not observed at high frequencies<sup>12</sup> because the domain-wall displacements cannot follow the applied stress, and therefore cannot contribute an additional strain that lowers the observed elastic stiffness. Thus, for present purposes, a high-frequency applied stress is essentially equivalent to applying a saturating magnetic field; both nullify domain-wall contributions to the strain.

In the presence of a saturating magnetic field (or its effective equivalent), the only magnetic effect that alters  $E$ ,  $B$ , and  $\nu$  without affecting  $G$  is the effect due to spontaneous volume magnetostriction. This effect is designated  $\Delta E_\omega$ , where  $\omega = (V - V_p)/V_p$  is the spontaneous volume magnetostriction,  $V$  is the total volume, and  $V_p$  is the volume in the paramagnetic state. The effect was first reported by Engler<sup>13</sup> for an Fe-42 Ni alloy. It was explained first by Döring<sup>14</sup> using a thermodynamic analysis. Herein, this phenomenon will be called the Döring effect. Döring reasoned that in the paramagnetic region the elastic constant is measured at constant magnetization  $M$ , while in the ferromagnetic or antiferromagnetic

TABLE V. Elastic Debye temperature at  $T = 0$  K.

Alloy	$\theta$ (K) magnetic	$\theta$ (K) extrapolated paramagnetic
304	467.8	468.1
310	459.0	459.0
316	496.7	496.8
A286	467.6	467.7
Iron (bcc) <sup>a</sup>	472.4	
Chromium <sup>b</sup>	453.0	
Nickel <sup>a</sup>	476.0	

<sup>a</sup>R. Wanner, Can. J. Phys. 48, 1270 (1970).

<sup>b</sup>F. H. Herbstein, Adv. Phys. 10, 313 (1961).

region the elastic constant is measured at constant magnetic field  $H$ . Döring showed that the magnitude of the anomaly in the Young's modulus is given by

$$\frac{\Delta E_{\omega}}{E^2} = \left(\frac{1}{E}\right)_M - \left(\frac{1}{E}\right)_H = -\frac{1}{9} \left(\frac{\partial \omega}{\partial H}\right)_{\sigma, T}^2 \left(\frac{\partial M}{\partial H}\right)_{\sigma, T}^{-1}, \quad (10)$$

where  $\partial \omega / \partial H$  is the forced volume magnetostriction due to the magnetization,  $\partial M / \partial H$  is the high-field susceptibility  $\chi$ ,  $E^2$  is  $E_M E_H$  and  $\sigma$  is the tensile stress. An alternative derivation of Eq. (10) was given by Hausch.<sup>15</sup> [Wohlfarth<sup>16</sup> stated, without proof, that the factor of  $\frac{1}{9}$  in Eq. (10) should be replaced by  $(1 - 2\nu)^2$  where  $\nu$  is Poisson's ratio. For the present materials this introduces a factor of approximately 2, which is insignificant for present purposes.] It should be noted that the Döring effect always lowers the moduli ( $E_M > E_H$ ), whether the volume magnetostriction is positive or negative. This is related to the fact that a relaxation mechanism is involved in going to an antiferromagnetic state, and such mechanisms always soften the elastic stiffness. The Döring effect in iron-nickel alloys was discussed by Köster,<sup>17</sup> who denoted it as  $\Delta E_{\lambda}$  rather than as  $\Delta E_{\omega}$ . The effect has been invoked by several authors to explain elastic anomalies in magnetic materials, usually of the Invar type. Hausch<sup>15</sup> criticized the relevance of the Döring effect in most of these cases. Schlosser<sup>18</sup> discussed the magnetovolume contribution to the compressibility of Invar, but Hausch<sup>15</sup> showed that an exchange-energy contribution is also required in this case. The present data for iron-chromium-nickel (stainless steel) alloys seem to constitute a clear case of the Döring effect.

If the Döring effect is responsible for the elastic anomalies observed in stainless-steel-type alloys, then  $\Delta E_{\omega}$  calculated from Eq. (10) should agree roughly with the magnitude of the observed anomalies. Apparently, the volume magnetostriction of these alloys has not yet been determined. Using data for Invar,<sup>15</sup> an iron alloy containing about 35% Ni and having the same crystal structure as the alloys considered here, it is calculated from Eq. (10) that  $\Delta E_{\omega} / E^2 = -1.4 \times 10^{-14}$  cm<sup>2</sup>/dyn. For the 304 stainless steel alloy, the present results give for the bulk modulus  $\Delta E / E^2 = -0.2 \times 10^{-14}$  cm<sup>2</sup>/dyn. Thus, the observed anomalies show a reasonable correspondence to the magnitude of the predicted Döring effect. A more exact correspondence could be established if the volume magnetostrictions of these alloys were known. If the Döring effect is the correct interpretation of the data, then the volume magnetostriction of these alloys must be quite large since it is large in Invar-type alloys. Besides Invar and other iron-nickel alloys, large magnetovolume effects have also been observed in iron-manganese, iron-palladium, iron-platinum, and iron-cobalt alloys.<sup>19</sup> A quantitative correspondence is also precluded because the alloys reported on here were studied in mechanically deformed states. Köster<sup>17</sup> showed that the  $\Delta E$  effect depends sensitively on metallurgical variables. The usual  $\Delta E = \Delta E_{\lambda}$  effect is generally suppressed by mechanical deformation. No studies seem to have been made on the effect of mechanical deformation on  $\Delta E_{\omega}$ . It would be expected that the  $\Delta E_{\omega}$  effect will be enhanced in annealed materials since the

residual stresses due to mechanical deformation would not interfere with domain-wall motions.

Of the four alloys, the smallest elastic anomalies were observed in the 310 alloy and in the A286 alloy. These materials have a much higher nickel content. Thus, it is suggested that in stainless-steel-type alloys the effect of nickel is to reduce the volume magnetostriction but not to suppress the occurrence of the antiferromagnetic phase.

The desirability of further studies on these alloys, especially with respect to the Döring effect, is indicated. Ideally, carefully prepared alloy single crystals would be tested in magnetic fields.

Since changes in elastic constants are usually accompanied by significant changes in internal friction, it would also be interesting to study the low-temperature anelastic properties of these alloys. The magnitude of the mechanical damping determines the magnitude of stresses established in vibrating parts. And all of these alloys are candidate materials for low-temperature uses where vibrations may occur. Magnetomechanical hysteresis has already been established as an important damping mechanism in ferromagnetic materials.<sup>20</sup>

## V. CONCLUSIONS

From the results of the present study the following conclusions are drawn:

- (i) Stainless-steel alloys AISI 304, AISI 310, AISI 316, and A286 have qualitatively similar elastic-property variations with temperature.
- (ii) The shear modulus behaves regularly over the entire temperature range studied.
- (iii) The elastic constants with dilatational components—Young's modulus, the longitudinal modulus, the bulk modulus, and Poisson's ratio—behave regularly above about 75 K but anomalously at lower temperatures. The anomalies are largest for the bulk modulus and smallest for Young's modulus.
- (iv) The anomalies are largest in the AISI 304 and AISI 316 alloys and smallest in the AISI 310 and A286 alloys. A relationship between the magnitude of the anomaly and nickel content is suggested.
- (v) As suggested first by Döring, the anomalies can be interpreted thermodynamically as the difference between constant-magnetization and constant-field bulk moduli.

*Noted added in proof.* Subsequent studies on other samples of these materials showed that the values of  $E$ ,  $G$ , and  $B$  reported here for AISI 316 are all higher than the average values by about 6%. All data reported for other materials are believed to be typical.

## ACKNOWLEDGMENT

This work was supported in part by the Advanced Research Projects Agency of the Department of Defense.

\*NRC-NBS Postdoctoral Research Associate, 1973-4.  
<sup>†</sup>Present address: Rockwell International, Rocky Flats Plant, Golden, Colo. 80401.  
<sup>1</sup>J. J. Gilman, *Aust. J. Phys.* **13**, 327 (1960).  
<sup>2</sup>This trade name is used to describe the material; its use does not imply an endorsement by NBS of a particular product.  
<sup>3</sup>H. J. McSkimin, *J. Acoust. Soc. Am.* **33**, 12 (1961).  
<sup>4</sup>E. R. Naimon, W. F. Weston, and H. M. Ledbetter, *Cryogenics* **14**, 246 (1974).  
<sup>5</sup>Y. P. Varshni, *Phys. Rev. B* **2**, 3952 (1970).  
<sup>6</sup>R. P. Mikesell and R. P. Reed, *J. Res. Natl. Bur. Std. (U.S.)* **70C**, 207 (1966).  
<sup>7</sup>P. E. Armstrong and D. T. Eash, in *Advances in Cryogenic Engineering*, Vol. 14, edited by K. D. Timmerhaus (Plenum, New York, 1959), p. 64.

<sup>8</sup>E. I. Kondorsky and V. L. Sedov, *Sov. Phys.-JETP* **35**, 1104 (1959).  
<sup>9</sup>W. F. Schlosser, *J. Phys. Chem. Solids* **32**, 939 (1971).  
<sup>10</sup>J. W. Christian, *The Theory of Transformations in Metals in Metals and Alloys* (Pergamon, Oxford, 1965), p. 214.  
<sup>11</sup>W. F. Brown, Jr., *Phys. Rev.* **50**, 1165 (1936).  
<sup>12</sup>R. M. Bozorth, W. P. Mason, and H. J. McSkimin, *Bell Syst. Tech. J.* **30**, 970 (1951).  
<sup>13</sup>O. Engler, *Ann. Phys. (Leipz.)* **31**, 145 (1938).  
<sup>14</sup>W. Döring, *Ann. Phys. (Leipz.)* **32**, 465 (1938).  
<sup>15</sup>G. Hausch, *Phys. Status Solidi A* **15**, 501 (1973).  
<sup>16</sup>E. P. Wohlfarth, *Phys. Status Solidi A* **10**, K39 (1972).  
<sup>17</sup>W. Köster, *Z. Metallkde.* **35**, 194 (1943).  
<sup>18</sup>W. F. Schlosser, *Phys. Status Solidi A* **18**, 235 (1973).  
<sup>19</sup>W. F. Schlosser, *Int. J. Magn.* **2**, 167 (1972).  
<sup>20</sup>A. Cochardt, *Trans. Am. Soc. Mech. Eng.* **75**, A196 (1953).

NBSIR

SEMI-ANNUAL REPORT ON MATERIALS RESEARCH  
IN SUPPORT OF SUPERCONDUCTING MACHINERY

FATIGUE RESISTANCE AND FRACTURE TOUGHNESS OF  
ENGINEERING MATERIALS AT CRYOGENIC TEMPERATURES

R. L. Tobler, D. T. Read, and R. P. Reed

Cryogenics Division  
Institute for Basic Standards  
National Bureau of Standards  
Boulder, Colorado 80302

October 1975

## Summary: Fatigue and Fracture Toughness

This section of the report contains two manuscripts, the results of which are summarized as follows:

- 1) The fatigue life of a uniaxial glass-filament reinforced epoxy composite at liquid helium temperature can be an order of magnitude greater than at room temperature. Tensile and fatigue results for this material indicate that such composites can be attractive structural materials for cryogenic applications.
- 2) The yield strength of an Fe-21Cr-6Ni-9Mn stainless steel tripled between 295 and 4 K, reaching a value of  $1.24\text{GNm}^{-2}$  (180ksi) at 4 K. Over this temperature interval the fracture toughness was considerable, and inversely related to yield strength. This alloy should be useful at temperatures as low as 4 K, for applications requiring a balance of high strength and fracture toughness.

FATIGUE RESISTANCE OF A UNIAXIAL S-GLASS/EPOXY  
COMPOSITE AT ROOM AND LIQUID  
HELIUM TEMPERATURES

Ralph L. Tobler and David T. Read\*

Cryogenics Division  
Institute for Basic Standards  
National Bureau of Standards  
Boulder, Colorado 80302

Abstract

Tension-tension axial fatigue tests of a uniaxial glass filament-reinforced epoxy were conducted at 295 K and 4 K. The fatigue life was found to be an order of magnitude greater at 4 K than at 295 K. These results are believed to be the first 4 K fatigue data reported for a composite material.

Key words: Cryogenics; fatigue; fiber composites; liquid helium;  
low temperature tests; mechanical properties.

---

\* NRC-NBS Postdoctoral Research Associate, 1974-75.

FATIGUE RESISTANCE OF A UNIAXIAL S-GLASS/EPOXY  
COMPOSITE AT ROOM AND LIQUID  
HELIUM TEMPERATURES

Ralph L. Tobler and David T. Read

INTRODUCTION

Glass-reinforced epoxy composites are prospective structural materials at cryogenic temperatures where high strength-to-density and strength-to-thermal-conductivity ratios are required and where relatively low elastic moduli can be tolerated. At temperatures from 295 to 4 K, these composites offer a combination of physical and mechanical properties unmatched by structural metals. Unfortunately, structural design data for composites at low temperatures are scarce, a fact which hinders the utility of these materials.

The advent of superconducting machinery prompted the need for mechanical property data for materials in a liquid helium environment at 4 K. Accordingly, programs were instituted to establish a data base [1]. Kasen's review [1,2] of the mechanical behavior of glass-reinforced composites concludes that tensile and fatigue strengths generally increase between 295 and 76 K; but, on further cooling to 20 K, there is a high probability that strengths will decrease. According to Kasen [1,2], below 20 K, tensile behavior has rarely been investigated, and fatigue data are non-existent.

In this study, fatigue tests of a filamentary-reinforced composite at room temperature and 4 K are described. Cycle life as a function of applied stress is evaluated to provide baseline fatigue data for a specific primary load carrying component of a superconducting motor. Some experimental aspects of fatigue testing at 4 K are discussed.

## EXPERIMENTAL PROCEDURE

The material tested was a unidirectional composite of Owens-Corning S-901\* glass roving and an epoxy resin, SCI REZ 80\*. Specimens were fabricated in the form of 12.38 cm long bands, as shown in Figure 1, using a single material lot and constant fabrication procedure. The specimen is a scaled down version of 68.5 cm long support bands designed for suspension of superconducting motor components in liquid helium. All specimen dimensions, except length, are equal to those of the service component. As specified by the manufacturer, the specimen fiber content is 82% by weight, 69% by volume; the void content is less than 1% by volume, and the density is  $2.1 \text{ g} \cdot \text{cm}^{-3}$  at room temperature.

Using flanged bushings, the specimens were pinned to the grips of a cryostat enabling fatigue tests in a liquid helium environment, as shown in Figure 2. The cryostat frame has a load carrying capability of 100 kN; it consists of two tubular compression members which are bridged at the bottom. The lower halves of these members are AISI 304 stainless steel having a wall thickness of 3.18 mm. The upper sections, which experience a thermal gradient during testing, were fabricated from fiberglass-reinforced plastic tubes, 6.35 mm thick. This lightweight construction provides high specific strength and low thermal conductivity, with some sacrifice of rigidity; the stiffness of the frame and load train at 4 K is approximately 23 kN/mm. Details of this cryostat design were described by Fowlkes and Tobler [3].

---

\* Tradenames are used in this report for clarity; in no way does this imply recommendation or endorsement by the National Bureau of Standards, nor does it imply that the material is the best available for the purpose.

Room temperature tests were performed with the apparatus in ambient air at  $295 \pm 2$  K, and at a relative humidity of  $30 \pm 5\%$ . The tests at 4 K were accomplished using the double-dewar arrangement illustrated in Figure 2. The specimen was enclosed in a fiberglass-reinforced plastic dewar, having a volumetric capacity of 9 liters. This dewar is vacuum insulated, and is surrounded by a fiberglass-epoxy dewar containing liquid nitrogen. Tests began by cooling the specimen and apparatus to 4 K, according to the two and one-half hour cool-down procedure previously described [3]. The liquid level was maintained several inches above the specimen, and was constantly monitored with a carbon-resistor level indicator. Liquid helium was continuously transferred into the cryostat to replenish the amounts evaporated during fatigue tests.

All tests were conducted using a 100 kN closed-loop servo-hydraulic test machine. Replicate tensile tests were conducted at a loading rate of  $5.7 \text{ N} \cdot \text{s}^{-1}$  to determine the nominal fracture strength and load-deflection ( $P$ - $\delta$ ) characteristics of virgin specimens. Load cell and LVDT outputs were used in recording load-versus-actuator displacement curves. The nominal fracture strength,  $\sigma_f$ , was calculated from the maximum load,  $P_{\text{max}}$ , and the mean cross-section area,  $2A$ , of the unloaded specimen at room temperature:

$$\sigma_f = P_{\text{max}}/2A \quad (1)$$

The specimen stiffness,  $P/\delta_S$ , was obtained by deducting the load frame deflection,  $\delta_F$ , from the total actuator displacement,  $\delta_T$ :

$$\frac{P}{\delta_S} = \frac{P}{(\delta_T - \delta_F)} \quad (2)$$

where the load frame stiffness was measured separately by replacing the specimen with a rigid steel block. The nominal or effective value of specimen modulus was also calculated:

$$M_S = \frac{PL}{A\delta_S} \quad (3)$$

where L is the initial specimen length at room temperature, and  $\delta_S$  is the specimen deflection at a 10 kN load.

The axial fatigue tests were conducted under controlled load, using a sinusoidal load cycle, at frequencies from 25 to 27 Hz. The ratio, R, of minimum/maximum load was 0.1, except as noted in the text. A digital indicator was used to measure the peak loads, which were controlled to within 2% of the specified values.

## RESULTS

A representative load-displacement record obtained at 4 K is shown in Figure 3a, and static tensile results are listed in Table 1. There was no measureable change in stiffness or modulus between 295 and 4 K, but tensile strength increased by 28% above the room temperature value of  $133.4 \text{ kN} \cdot \text{cm}^{-2}$ . The scatter in tensile strength at 4 K was higher than at room temperature, with one specimen at 4 K failing at a stress lower than any of the room temperature values. This anomalous result was not included in the average value of fracture strength listed in Table 1: the load-displacement record of the test of this specimen shows a noticeable increment in the displacement without a corresponding increase in the load at a low value of the load, as can be seen in Figure 3b.

The room temperature fatigue results are shown in Figure 4, where the maximum fatigue stress is plotted as a fraction of the static strength. The

data trend and scatter are similar to other results, particularly those reported by Hofer and Olsen [5] for a unidirectional S-994 glass filament-reinforced epoxy. Hofer and Olsen's data pertain to conventional hour-glass specimens having a tensile strength of about  $162 \text{ kN} \cdot \text{cm}^{-2}$ . Although their material exhibited a higher cycle life capability at a given absolute stress value, the results for both composites can be normalized on the basis of differences in static strength as shown in Figure 4. It is also significant to note that these materials at room temperature do not exhibit a fatigue limit at cyclic stress levels as low as 20% of the static strength.

The effect of varying the load ratio was investigated briefly at room temperature where two specimens were fatigued to fracture at  $R = 0.5$ . As shown in Figure 4, the cycle life appeared to improve at the higher load ratio; further conclusions are not justified in view of the limited data.

The fatigue data obtained at liquid helium and room temperatures are summarized in Table 2 and Figure 5. These results clearly demonstrate a superior fatigue resistance at 4 K. Two specimens survived  $10^6$  stress cycles of maximum levels  $29.0$  and  $30.0 \times 10^7 \text{ N} \cdot \text{m}^{-2}$  (17.6% of tensile strength) at 4 K without failure; their tensile strength and effective modulus after cycling were only slightly less than the average values for virgin specimens, as shown in Table 2b. These high values of residual strength and residual modulus indicate that cyclic loading at these levels at 4 K does not significantly degrade the load-bearing capability of these composite specimens. A third specimen failed after  $1.49 \times 10^4$  cycles at a stress level of  $71.0 \times 10^7 \text{ N} \cdot \text{m}^{-2}$ , exceeding the room temperature endurance by a factor of 30. A final specimen was cycled for specified intervals at the increasing stress levels listed in Table 2. The results show that the

cycle life at 4 K is at least ten times greater than at room temperature for maximum cyclic stresses from 38 to  $82 \times 10^7 \text{ N} \cdot \text{m}^{-2}$ .

Although a reliable S-N curve at 4 K could not be constructed without more extensive data, it appears that the stress level required for failure at a specified number of cycles may approach twice the value required at room temperature. The improvement in fatigue resistance at 4 K exceeds that which might be predicted based on scaling the fatigue stress levels to account for the increase in static strength alone.

Fatigue and tensile specimens fractured at 4 K are shown in Figure 6. Failure invariably occurred at points of tangency where the specimen contacted the bushings. Fatigue cracks initiated concurrently at all four of the points of tangency; the cracks penetrated the specimen ligaments along planes normal to the tensile axis, and delaminations subsequently emanated from the gripped regions. The delaminations propagated gradually in a direction parallel to the loading axis, along the entire length of the specimen. When fatigue damage reached critical proportions the weakest ligament splintered into filaments, which was the failure mode of tensile specimens, as shown in Figure 6. The epoxy at the four points of tangency in specimens fractured in fatigue at both 4 K and 300 K was quite dark, possibly indicating charring. Temperature had no obvious influence on the appearance of these failures.

Specimen deflection at a constant fatigue load increased progressively, as shown in Figure 7 for room temperature specimens fatigued at  $25.5 \times 10^7 \text{ N} \cdot \text{m}^{-2}$ . The rate of increase of deflection differed by an order of magnitude for these specimens, as did their fatigue lifetimes,  $N_f$ . This suggests that scatter in cycle life is due to specimen-to-specimen variability in resistance to

fatigue damage propagation, as well as initiation. The loss of stiffness was always most pronounced during the last few cycles to failure, and extreme adiabatic heating was also noted in the terminal stages of fatigue.

## DISCUSSION

Relating laboratory results to service behavior is a practical problem which was minimized in this study by performing a limited number of tests under conditions nearly equivalent to those of the service application. The results must be regarded as lower bounds on the uniaxial tensile properties of the material itself, since the gripping fixture influenced the results. However, the gripping fixture is a practical one for service applications, and the data reported here are directly applicable in design.

It can be concluded from the 4 K results and known trends between 295 and 20 K [2] that the fatigue and tensile strengths of this material are lower at room temperature than at any cryogenic temperature. In the application under consideration, the component will experience temperatures ranging from 295 to 4 K. The room temperature properties are therefore limiting, and should form the basis for design. In certain applications where a component operates exclusively at cryogenic temperatures, it would also be possible to design conservatively on the basis of room temperature properties. However, a maximum level of design efficiency at cryogenic temperatures requires more extensive low temperature mechanical property data.

In many structural applications, it is essential to monitor fatigue damage and to replace critical components before catastrophic failure becomes probable. The occurrence of delaminations in this composite after

25% of total cycle life provides obvious evidence of degradation. Damage could be detected earlier by dismounting the specimen to examine the surfaces in contact with the bushing. Surface deterioration and discoloration were noted at these locations. The loss of stiffness also provides a means of detecting fatigue damage. Thus, a simple inspection of service components should provide ample evidence of degradation prior to failure.

Cyclic stressing produces specimen heating and agitation of the cryogen. This agitation increases the heat leak into the cryogen due to convection, because the cryogen is splashed into the warmer regions of the cryostat. The heat input to the cryogen from both of these sources increases strongly with displacement. In these tests the helium loss under static load was only  $0.15 \text{ l} \cdot \text{h}^{-1}$ . This increased during fatigue tests, varying from 7 to  $15 \text{ l} \cdot \text{h}^{-1}$ , over the range of stress levels investigated.

Adiabatic heating in glass-reinforced plastics results from their high internal friction and low thermal conductivities [6]. Internal temperature rises as high as  $70^\circ\text{F}$  were noted in room temperature fatigue tests of such materials [7]. At 4 K, adiabatic heating should be more significant since the thermal conductivity of glass reinforced epoxies is lowered by a factor of three [4]. Furthermore, the temperature in the interior of the specimen depends on the specimen thickness and cycling rate. Since the present data pertain to a specimen thickness and frequency equivalent to service conditions, the effects of adiabatic heating on fatigue resistance here are academic from an applications viewpoint. However, this effect must be accounted for in future tests if fatigue results are to be independent of specimen geometry and test variables.

## CONCLUSIONS

From these tests, the following conclusions can be drawn:

1. The tensile strength and fatigue resistance exhibited by a glass roving reinforced epoxy plastic (GFRP) composite material indicate that such composites can be attractive structural materials for cryogenic applications.
2. The fatigue life of a GFRP composite material can be an order of magnitude greater at liquid helium temperature than at room temperature.
3. A measurable decrease in the stiffness of GFRP specimens may precede high cycle fatigue fracture at 300 K.

## ACKNOWLEDGMENT

The cooperation of M. Calderon of Airesearch, Torrance, California in providing the specimens and reviewing the manuscript is gratefully acknowledged.

## REFERENCES

1. R. P. Reed and A. F. Clark, Eds., "Materials Research for Superconducting Machinery," National Bureau of Standards, Boulder, Colorado, AD 780596 and AD/A 004 586, Nat. Tech. Inf. Serv., Springfield, Virginia (1974).
2. M. B. Kasen, "Mechanical and Thermal Properties of Filamentary-Reinforced Structural Composites at Cryogenic Temperatures-I: Glass-Reinforced Composites", Cryogenics, Vol. 15, No. 4, 230-240 (1975).
3. C. W. Fowlkes and R. L. Tobler, "Fracture Testing and Results for a Ti-6Al-4V alloy at Liquid Helium Temperature," to be published.
4. M. Segimoto, "Qualification Test Results for Glass Filament-Wound Support Bands," Report No. 7581, Structural Composites Industries, Inc., California (Jan. 1975).
5. K. E. Hofer, Jr., and E. M. Olsen, "An Investigation of Fatigue and Creep Properties of Glass Reinforced Plastics for Primary Aircraft Structures," Report M6104, Ill. Inst. Tech. Res. Inst. (Apr. 1967).
6. L. J. Broutman, "Fibre-reinforced Plastics," Chap. 13 in Modern Composite Materials, L. J. Broutman and R. H. Krock, Eds., Addison-Wesley, Massachusetts (1967).
7. R. B. Heywood, Present and Potential Fatigue and Creep Strengths of Reinforced Plastics, Tech. Note. No: Chem. 1337, Royal Aircraft Establishment, Ministry of Supply, London, W. C. 2 (Oct. 1958).

## LIST OF TABLES

- Table 1. Static tensile properties of S-901 glass/epoxy specimens.
- Table 2a. Fatigue results for S-901 glass/epoxy at 295 K.
- Table 2b. Fatigue results for S-901 glass/epoxy at 4 K.

Table 1. Static tensile properties of S-901 glass/epoxy specimens.

Temperature (K)	Specimen (No.)	Mean X-sect. Area, 2A (cm <sup>2</sup> )	Stiffness P/δ <sub>S</sub> (10 <sup>5</sup> N·m <sup>-1</sup> )	Effective Modulus, M <sub>S</sub> (10 <sup>9</sup> N·m <sup>-2</sup> )	Nominal Failure Strength, σ <sub>f</sub> (10 <sup>7</sup> N·m <sup>-2</sup> )
295	1 <sup>a</sup>	.3612	N/A	N/A	134.6
	2 <sup>a</sup>	.3604	"	"	133.8
	3 <sup>a</sup>	.3648	"	"	131.6
	Avg.				<u>133.4</u>
	13	.3677	159	62.8	N/A
	14	.3652	148	61.8	"
Avg.	19	.3613	<u>151</u>	<u>60.5</u>	"
			153	61.7	
4	4	.3664	160	66.7	158.8
	5	.3664	147	61.1	182.1
	21	.3652	<u>145</u>	<u>60.6</u>	<u>126.7<sup>b</sup></u>
	Avg.		151	62.8	170.4

Tests performed by the manufacturer [4].

Not included in the average (see text).

Table 2a. Fatigue results for S-901 glass/epoxy at 295 K.

Specimen (No.)	Maximum Cyclic Stress, $\sigma_M$ ( $10^7 \text{ N}\cdot\text{m}^{-2}$ )	Fatigue Cycles to failure (No.)
13	25.5	$7.246 \times 10^6$
19	25.5	$5.76 \times 10^5$
9	29.3	$6.75 \times 10^4$
16	29.3	$8.36 \times 10^4$
18	29.3	$7.38 \times 10^4$
7	31.0	$1.96 \times 10^5$
12	31.0	$1.42 \times 10^5$
20	31.0	$7.46 \times 10^5$
6	37.9	$8.85 \times 10^3$
10	37.9	$2.22 \times 10^4$
11	37.9	$2.09 \times 10^4$
24	71.0	$3.93 \times 10^2$
22 <sup>a</sup>	41.4	$2.00 \times 10^4$
23 <sup>a</sup>	55.2	$5.40 \times 10^3$

<sup>a</sup>R = 0.50

Table 2b. Fatigue results for S-901 glass/epoxy at 4 K.

Specimen (No.)	Maximum Cyclic Stress, $\sigma_M$ ( $10^7 \text{ N}\cdot\text{m}^{-2}$ )	Fatigue Cycles (No.)	Residual Strength ( $10^7 \text{ N}\cdot\text{m}^{-2}$ )	Residual Modulus ( $10^9 \text{ N}\cdot\text{m}^{-2}$ )
8	29.0	$1 \times 10^6$ (run-out)	139	58.2
17	31.0	$1 \times 10^6$ "	156	65.8
14	71.0	$1.49 \times 10^4$ (failure)	N/A	N/A
15 <sup>b</sup> - 1	37.9	$2.36 \times 10^5$ (run-out)	"	"
2	44.8	$6.92 \times 10^4$ "	"	"
3	55.2	$1 \times 10^4$ "	"	"
4	62.1	$1 \times 10^4$ "	"	"
5	69.0	$1 \times 10^4$ "	"	"
6	82.7	$2.52 \times 10^4$ (failure)	"	"

<sup>b</sup>Cycled at increasing stress levels.

#### LIST OF FIGURES

- Figure 1. S-901 glass/epoxy test specimen.
- Figure 2. Liquid helium fatigue cryostat.
- Figure 3. Static test records; (a) ordinary failure, (b) premature failure.
- Figure 4. Room temperature fatigue data.
- Figure 5. 4 K fatigue results.
- Figure 6. Tensile and fatigue failures of specimens tested at 4 K.
- Figure 7. Deflection-versus-cycles for specimens tested at 295 K.

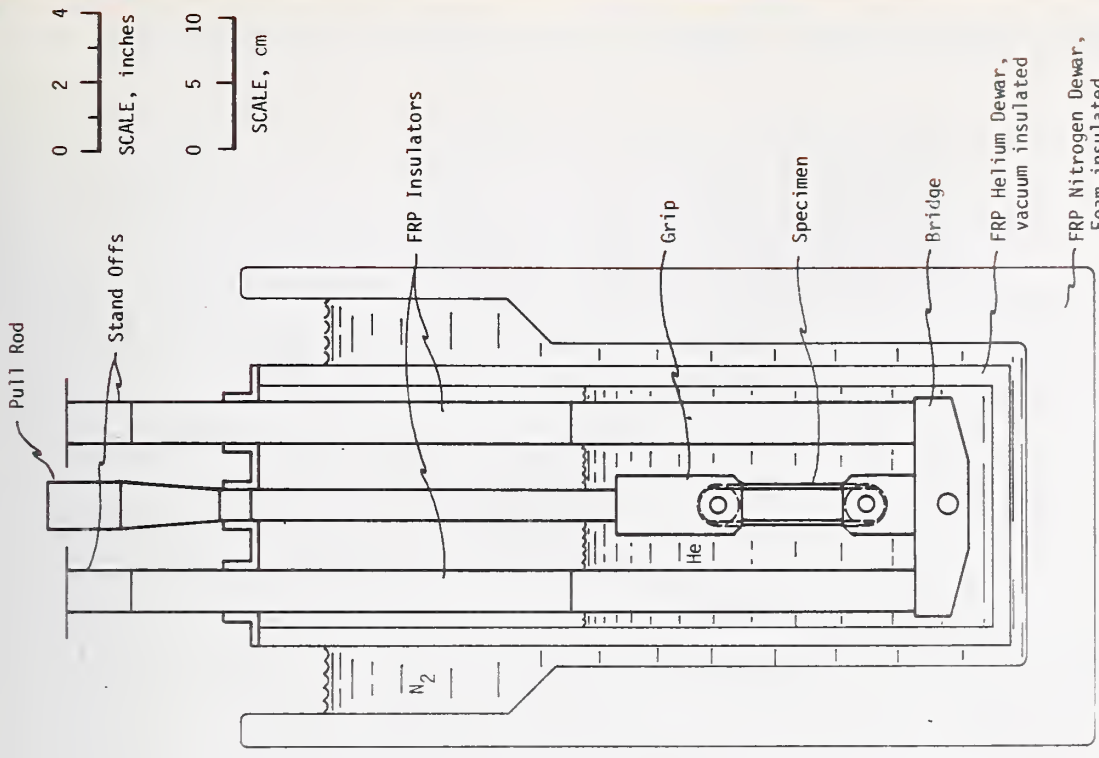


FIGURE 2 - Liquid Helium Fatigue Cryostat.

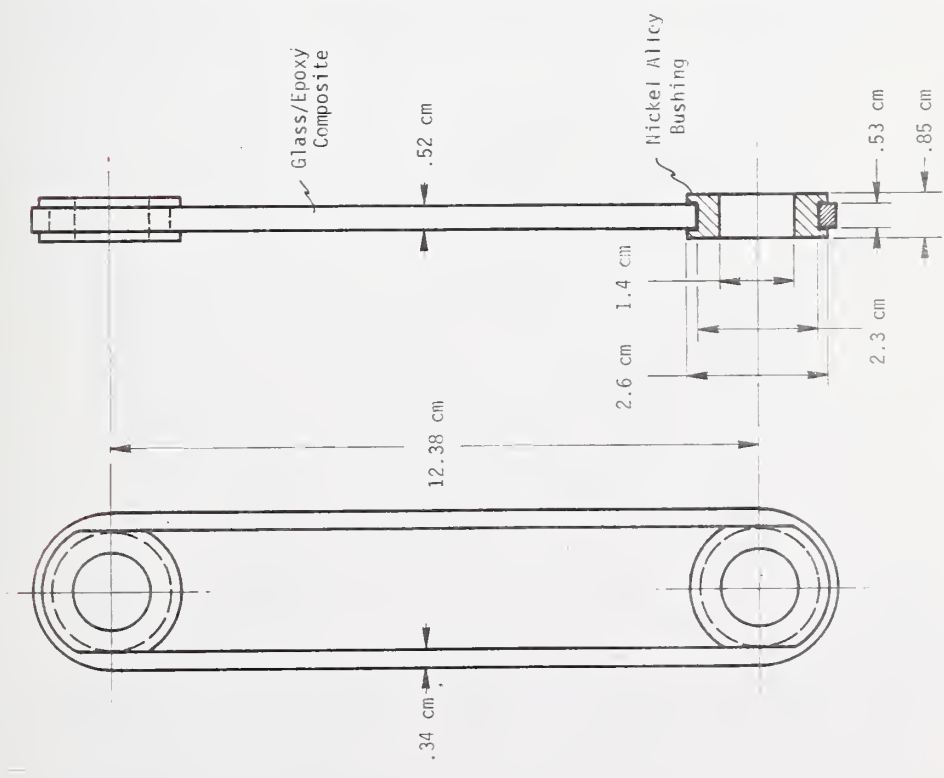


FIGURE 1 - Test specimen geometry.

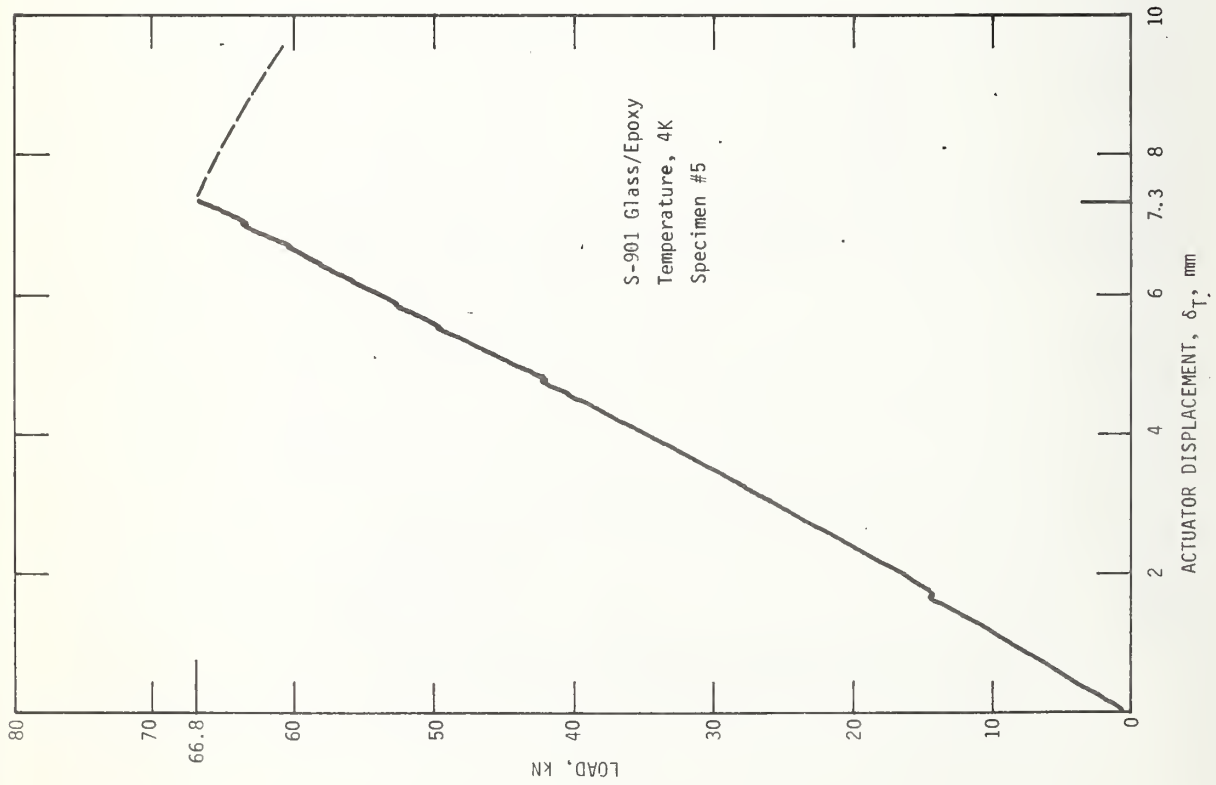


FIGURE 3a-Static test record.

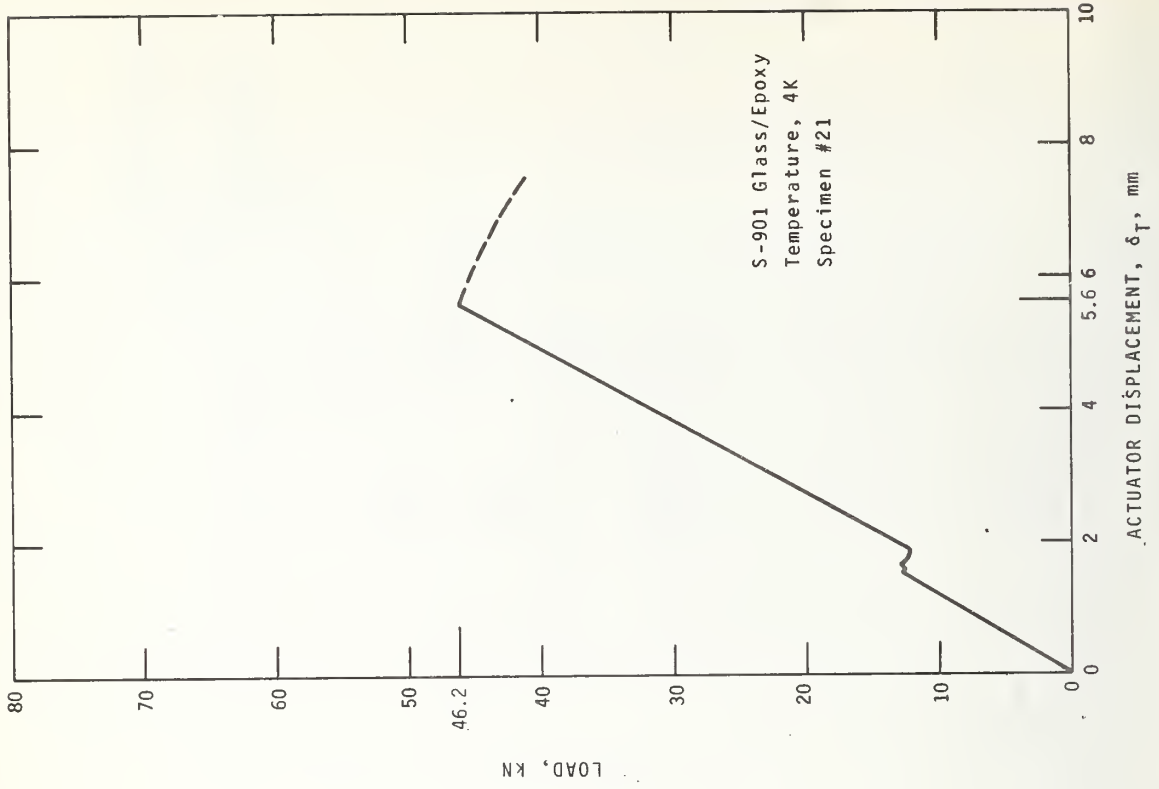


FIGURE 3b-Static test record

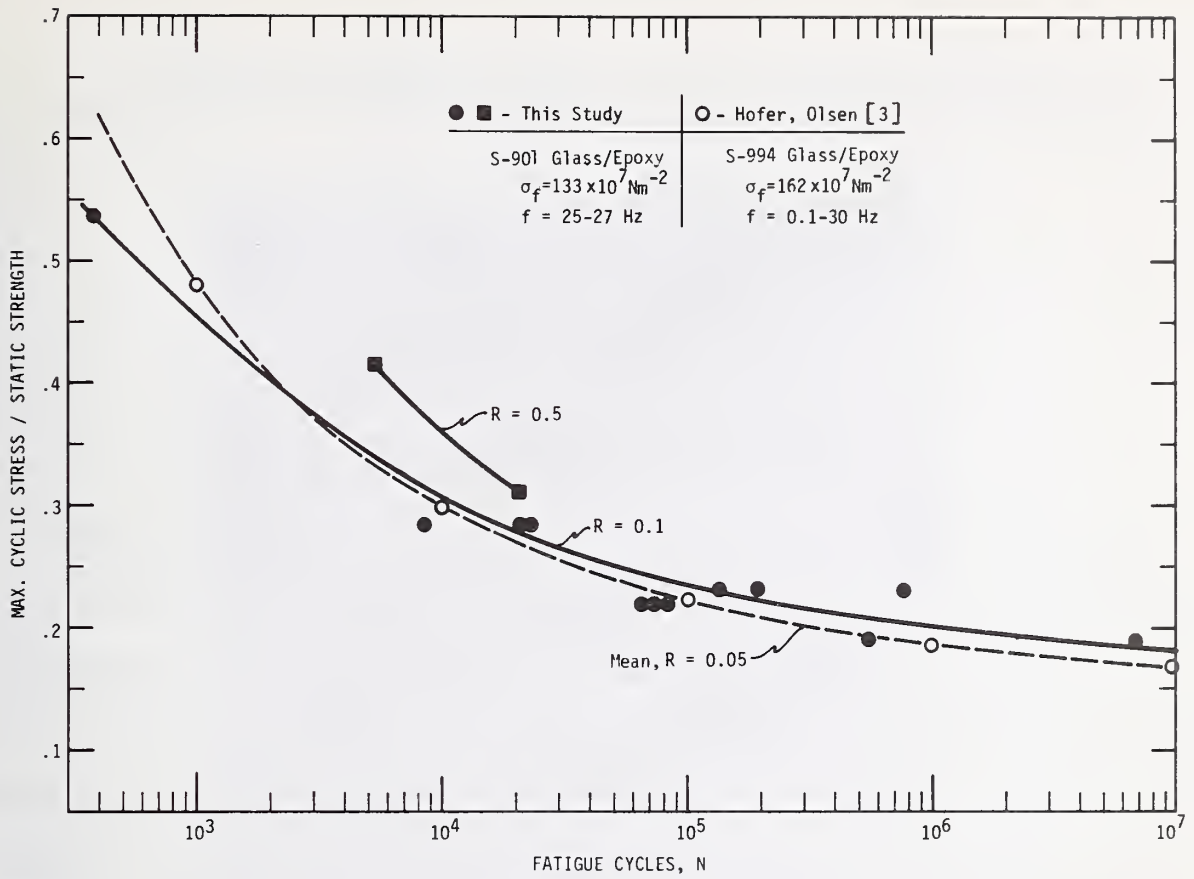


FIGURE 4 - Room temperature fatigue data.

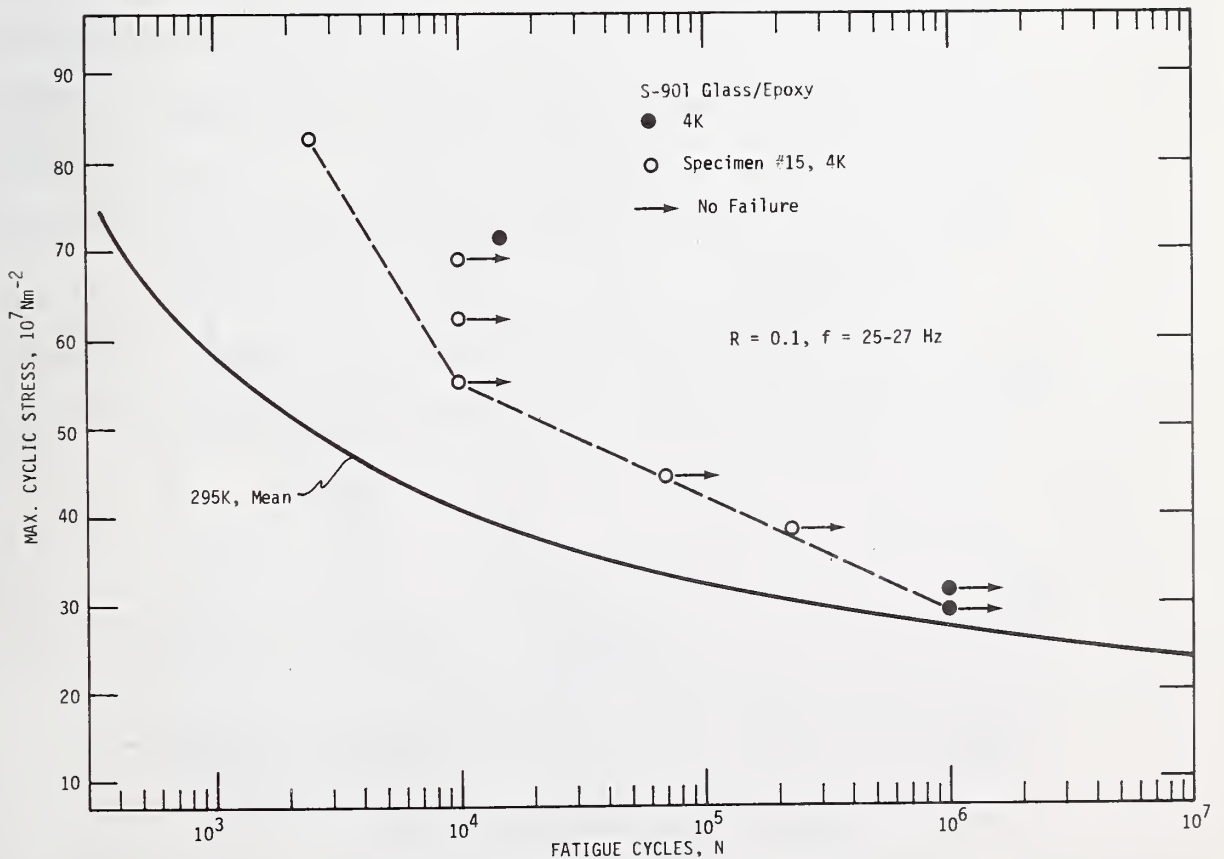


FIGURE 5 - 4K Fatigue results.



Figure 6. Tensile (lower) and fatigue (upper) failure of specimens tested at 4 K.

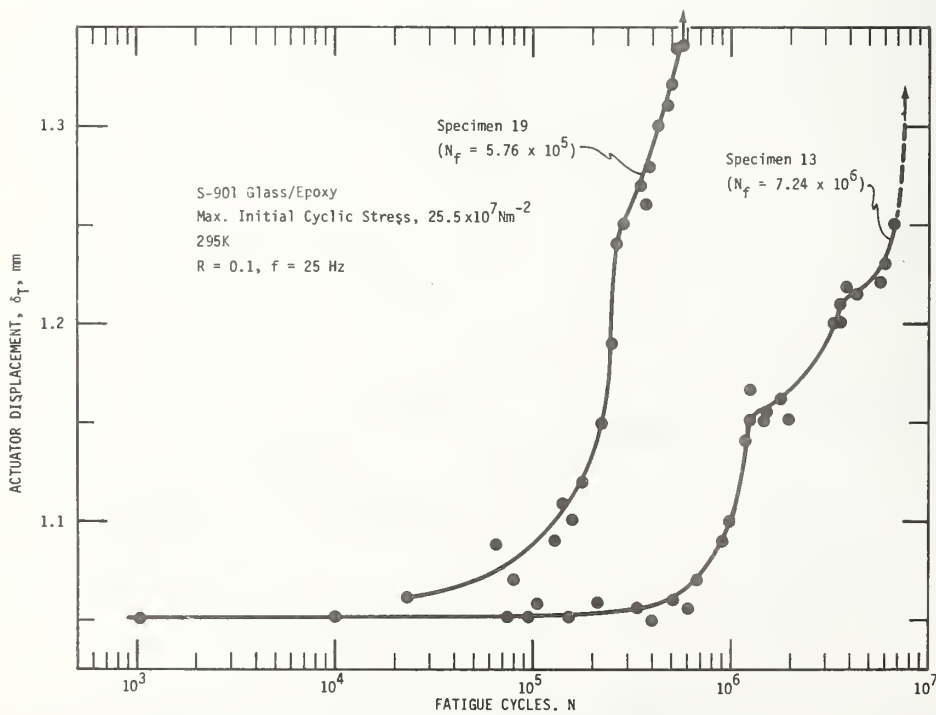


FIGURE 7 - Deflection-versus-cycles for specimens at 295K.

TENSILE AND FRACTURE BEHAVIOR OF A NITROGEN-STRENGTHENED,  
CHROMIUM-NICKEL-MANGANESE STAINLESS STEEL AT CRYOGENIC TEMPERATURES\*

R. L. Tobler and R. P. Reed

Cryogenics Division  
Institute for Basic Standards  
National Bureau of Standards  
Boulder, Colorado 80302

ABSTRACT

J-integral fracture and conventional tensile properties are reported for an Fe-21Cr-6Ni-9Mn austenitic stainless steel which contains 0.28 N as an interstitial strengthening element. Results at room (295 K), liquid nitrogen (76 K), and liquid helium (4 K) temperatures demonstrated that the yield strength and fracture toughness of this alloy were inversely related, exhibiting opposite temperature dependences. Over the temperature range investigated, the yield strength tripled, reaching a value of  $12.4 \times 10^8 \text{ N}\cdot\text{m}^{-2}$  (180 ksi) at 4 K. The fracture toughness, as measured using 3.8 cm thick compact specimens, decreased considerably from 295 to 4 K. During plastic deformation at 295 K the alloy undergoes little martensitic phase transformation, but at 76 and 4 K it transforms extensively to hcp and bcc martensitic products. The amount of bcc transformation product was measured as a function of elongation.

Key words: Cryogenics; fracture; low temperature tests; martensitic transformations; mechanical properties; stainless steel alloys.

\*NBS contribution, not subject to copyright.

## Introduction

Recently, austenitic stainless steel strengths have been increased considerably by the substitution of nitrogen and manganese for nickel. In addition to the interstitial and solid solution strengthening, these elements serve to retain, and in some cases, increase the austenite stability with respect to martensitic transformations. Compared to nickel, these elements are more abundant and less expensive. The alloy studied in this report, Fe-21Cr-6Ni-9Mn-0.3N (21-6-9), has a room temperature yield strength nearly twice that of AISI 304. Available tensile and impact data<sup>(1-4)</sup> suggest that the alloy retains good toughness at low temperatures, leading to consideration of its use for applications benefiting from high strength and toughness.

Accordingly, 21-6-9 is currently being considered for such critical components as the coil for the prototype controlled thermonuclear reaction superconducting magnets and the torque tube for rotating superconducting machinery. To insure satisfactory service life and to compare with other material contenders it is necessary to evaluate the fracture resistance of the alloy. This study presents the first fracture toughness data for this alloy.

## Material

The 21-6-9 austenitic stainless steel was provided by Lawrence Livermore Laboratories, Livermore, California. The chemical composition (in weight percent) of this heat is 19.75 Cr, 7.16 Ni, 9.46 Mn, 0.019 C, 0.15 Si, 0.004 P, 0.003 S, and 0.28 N.

The steel was subsequently hot rolled from 30.5 x 30.5 x 10 cm slabs to 50 x 50 x 3.6 cm plate using the following schedule:

soak for 4 hours at 1366 K;  
roll from 10 cm to 9.4 cm, screw down (compress) to 9.3 cm;  
roll from 9.3 cm to 8.7 cm, screw down to 8.6 cm, rotate 90°;  
roll from 8.6 cm to 8.0 cm, screw down to 7.9 cm;  
roll from 7.9 cm to 7.4 cm, screw down to 7.3 cm, rotate 90°;  
roll from 7.3 cm to 6.9 cm, screw down to 6.7 cm;  
roll from 6.7 cm to 6.3 cm, screw down to 6.2 cm, rotate 90°;  
roll from 6.2 cm to 5.9 cm, screw down to 5.7 cm;  
roll from 5.7 cm to 5.4 cm, screw down to 5.3 cm, rotate 90°;  
roll from 5.3 cm to 5.0 cm, screw down to 4.8 cm;  
roll from 4.8 cm to 4.5 cm, screw down to 4.3 cm, rotate 90°;  
roll from 4.3 cm to 4.2 cm, screw down to 4.0 cm;  
roll from 4.0 cm to 3.8 cm, screw down to 3.6 cm.

The final plate temperature after this hot rolling was 1089 K. Each plate was then annealed at 1283 K for 1-1/2 hours and air cooled, followed by an anneal at 1366 K for 1-1/2 hours and a water quench. The resultant hardness was Rockwell B92 and the average grain diameter was 0.16 mm.

#### Procedure

##### Tensile:

Tensile specimens were machined following ASTM specification E8-72<sup>(5)</sup>; the reduced section diameter was 0.635 cm and length was 3.8 cm.

The tensile axis was oriented transverse to the final rolling direction of the plate. Tests were performed using a 44.5 kN screw-driven machine at a cross-head rate of 0.05 cm per minute. The cryostat assembly was designed by Reed.<sup>(6)</sup>

Measurements at 76 K used liquid nitrogen and at 4 K used liquid helium. Load was monitored with a 44.5 KN commercial load cell while specimen strain was measured with a clip-on, double beam, strain gage extensometer. Yield strength was determined as the flow stress at 0.2% offset plastic strain.

#### Magnetic:

To detect the amount of ferromagnetic, body-centered cubic (bcc) martensitic phase in the paramagnetic, fcc austenitic matrix a simple bar-magnet, torsion balance was used.<sup>(7)</sup> Previous measurements on Fe-Cr-Ni austenitic steels established a correlation between the force required to detach the magnet from the specimen and the percent bcc martensite.<sup>(7)</sup> This same correlation was used for this study to estimate the amount of bcc martensite in the Fe-Cr-Ni-Mn alloy.

#### Fracture:

The J-integral specimens were 3.78 cm thick compact specimens of a geometry described in ASTM E-399-74.<sup>(8)</sup> The specimen width,  $W$ , and width-to-thickness ratio,  $W/B$ , were 7.6 cm and 2.0, respectively. Other dimensions are shown in Figure 1. The notch, machined parallel to the final rolling direction of the plate, was modified to enable clip gage attachment in the loadline.

The J-integral test specimens were precracked using a 100 kN fatigue testing machine and attached cryostat.<sup>(9)</sup> Specimens were precracked at their test temperature. All precracking operations were conducted using load control and a sinusoidal load cycle at the rate of 20 Hz. Maximum fatigue precracking loads ( $P_f$ ) were, except for room temperature, well below the maximum load to fracture after precracking ( $P_{max}$ ) as indicated in Table 1. The maximum stress intensity during precracking ( $K_f$ ) and the approximate final average relative crack length (the ratio of the crack length,  $a$ , to the specimen width,  $W$ ) are also listed in Table 1.

Subsequent to precracking, the specimens were transferred to a 267 kN (60,000 lb) hydraulic tensile machine for fracture testing. Thus, the 76 and 4 K fracture specimens were warmed to room temperature prior to testing at 76 and 4 K. This was necessary since the load limitations of the fatigue machine precluded loading this alloy to fracture at the low temperatures.

The J-integral tests followed a resistance curve technique similar to that described originally by Begley and Landes.<sup>(10,11)</sup> A series of nearly identical specimens was tested at each temperature. Each specimen was loaded to produce given amounts of crack extension. The specimens were then unloaded and heat tinted to mark the amount of crack extension associated with a particular value of J. The amount of crack extension could be identified after fracturing the specimen into halves.

Using the approximate solution for deeply cracked compact specimens,<sup>(12)</sup>

$$J = 2A/B(W-a), \quad (1)$$

the value of J for each test was calculated from the total area, A, under the load-versus-loadline deflection record. The five values of J obtained at each temperature were plotted versus the average crack extension,  $\Delta a$ , which was measured at five locations equidistant across the specimen thickness, and averaged.

The critical value of the J integral,  $J_{IC}$ , identified as the J value at the initiation of crack extension, is obtained by extrapolation of the best fit J- $\Delta a$  curve to the point of actual material separation. Conversion to the plane-strain fracture toughness parameter,  $K_{IC}$ , is made using<sup>(10-12)</sup>

$$K_{IC}^2 = \frac{E}{1-\nu} (J_{IC}) \quad (2)$$

where E is Young's modulus and  $\nu$  is Poisson ratio. Here E is taken as

the range of the ratio of the length of the crack near the specimen edges ( $a_e$ ) to the length of the cracks near the specimen centers ( $a_c$ ) is included in Table I. To satisfy the fracture criteria of ASTM E-399-74<sup>(8)</sup> a value of  $a_e/a_c = 0.90$  or greater is necessary.

Table 1. Precracking Parameters for Fracture Test Specimens

Test Temperature (K)	$P_f/P_{max} \times 100$ (percent)	$K_f$ ( $10^6 \text{ N}\cdot\text{m}^{2}\cdot\text{m}^{1/2}$ )	Final Average Relative Crack Length, $a/W$	$a_e/a_c$
295	40-45	48-54	0.638	0.90-0.91
76	22-27	52-63	0.640	0.87-0.90
4	30-35	52-63	0.647	0.88-0.89

### Results and Discussion

#### Tensile:

The yield and tensile strengths, elongation, and reduction of area were obtained for the 21-6-9 alloy at 295, 76, and 4 K. These data are summarized in Table 2. The data from this study are combined in Figures 2-4 with the unpublished results of Landon<sup>(1)</sup> for the same heat, also hot rolled and annealed, and with the results of Scardigno,<sup>(2)</sup> Malin,<sup>(3)</sup> and Masteller<sup>(4)</sup> on annealed bar stock. The correlations are very good except for the ultimate strength data of Masteller. Although his alloy was described as annealed, perhaps it was tested in a worked condition. The spread of the Malin data represent specimens machined from both longitudinal and transverse directions to the rolling direction.

Typical stress-strain curves at each temperature are presented in Figure 6. The large discontinuous yield behavior at 4 K probably is associated with adiabatic specimen heating. Significant local heating is indicated, as the flow stress

drops to stress levels less than that which is sustained at 76 K. An indication of significant local heating is the rise of the reduction of area to values higher than that obtained during 76 K tests. Specimens tested at 4 K developed very local areas of increased plastic deformation, which resulted in sizable specimen necking prior to fracture. These load drops should not be attributed to martensitic phase transformations for three reasons: (1) more extensive transformation was detected in this alloy at 76 K, compared to 4 K (see later discussion) and no discontinuities in the stress-strain mode at 76 K were observed, (2) load drops have been observed in both metastable (e.g., AISI/304) and stable (e.g., AISI 310) austenitic stainless steels at 4 K and no distinction is apparent between the two alloy groups,<sup>(13)</sup> and (3) in austenitic steels the amplitude and frequency of the load drops at 4K is a function of the strain rate<sup>(13)</sup> which would be expected if local heating were responsible.

From these data it is clear that the alloy 21-6-9 has a significant decrease of ductility in the temperature range below 195 K, and that tensile elongation continues to decrease to 4 K.

A primary advantage offered by this alloy is its higher yield strength with respect to other austenitic alloys. At room temperature the yield strength of the 21-6-9 alloy is about  $3.8 \times 10^8 \text{ N}\cdot\text{m}^{-2}$  (55 ksi), compared to AISI 300 series steel values of  $2.1$  to  $2.5 \times 10^8 \text{ N}\cdot\text{m}^{-2}$  (30-35 ksi). The yield strength of the 21-6-9 steel approximately triples to a value of  $12.4 \times 10^8 \text{ N}\cdot\text{m}^{-2}$  (180 ksi) as the temperature is decreased to 4 K. The Fe-Cr-Ni austenitic alloys achieve values about double or triple their room temperature value (60-110 ksi) at 4 K. The strength advantage offered by 21-6-9 is greatest at lower temperatures.

## Fracture

The load-versus-loadline deflection curves at 295, 76 and 4 K are shown in Figure 6. The curves at 295 K extended to larger deflections than indicated on the axis of the diagram. The crack remained stable and did not propagate quickly in the J- $\Delta a$  tests of room temperature tests. The fracture test data are tabulated in Table 3. There are no ASTM E-399-74 valid  $K_{IC}$  data; the 5% secant offset data are denoted  $K_Q$ . Both the ASTM E-399-74 thickness and crack front curvature criteria are not satisfied at the temperatures 4, 76 and 295 K. Using  $B \geq 2.5 (K_Q/\sigma_y)^2$ , a specimen thickness of 4.2 cm at 4 K is required, slightly larger than the 3.8 cm thickness. As shown in Figure 7, the crack front curvature is slightly excessive as the crack lengths of the surface are between 88 and 89% of the average of the internal crack length; 90% is suggested in E-399 as the minimum deviation.

The J versus  $\Delta a$  results at room temperature are plotted in Figure 8. Large extensions were observed due to plastic deformation at the crack tip; only in two specimens at the highest values of  $\Delta a$  was actual material separation noted. These two values fall on the same linear curve as the specimen data that did not exhibit material separation and, furthermore, the entire J versus  $\Delta a$  linear curve has approximately the same slope as that suggested ( $J/2\sigma_f$ ) by Landes and Begley.<sup>10,11</sup> It seems that the response of this extremely ductile material to J integral tests at room temperature is inconclusive, with no well-defined break from the linear portion of the plastic deformation curve observable.

According to the tentative size criterion suggested by Landes and Begley<sup>(11)</sup>, the specimen thickness for valid  $J_{IC}$  measurements should satisfy the relationship:

$$B \geq \alpha (J/\sigma_f)$$

where  $\alpha$  is a factor greater than 25 and  $\sigma_f$  represents the average of the yield and tensile strengths. In the tests at 295 K, the conditional

critical J values were in the range  $1350$  to  $1450 \times 10^2 \text{ N} \cdot \text{m}/\text{m}^2$ . Using the flow stress value of  $5.3 \times 10^8 \text{ N} \cdot \text{m}^{-2}$  (76.5 ksi), the J-integral results at room temperature are invalid for the specimen thickness tested here. Apparently, a specimen thickness of at least 6.3 cm (2.5 inches) is needed to insure valid data.

The J-resistance curve at 76 K is also shown in Figure 8. The data fit a regular trend, with the exception of the datum point representing the largest observed crack extension. The curve drawn for the remaining specimens indicates that crack extension initiates at J values in the range  $310 < J_{IC} < 350 \times 10^2 \text{ N} \cdot \text{m}/\text{m}^2$ . The corresponding value of  $K_{IC}(J)$ , estimated using Equation 2, is  $318 \text{ N} \cdot \text{m}^{1/2}/\text{m}^2 \pm 5\%$  (292 ksi in<sup>1/2</sup>).

At 4 K, the alloy approached linear-elastic behavior, but the results of the first three tests failed to satisfy the ASTM validity criteria<sup>(8)</sup> for direct  $K_{IC}$  measurements. These data are listed in Table 3. Three J- $\Delta a$  tests were conducted and these are included in Figure 8. Although more thorough testing is needed to confirm these, it appears that the J- $\Delta a$  curve is horizontal. The resulting  $J_{IC}$  is about  $150 \times 10^3 \text{ N} \cdot \text{m}/\text{m}^2$ .

#### Phase Transformations

Subsequent to tensile tests at 76 and 4 K, it was noticed that the deformed specimens were magnetic. Therefore, these specimens were measured, using bar-magnet, torsion balance equipment, to correlate magnetic attraction with specimen reduction of area. The magnetic readings were converted to percent bcc martensite and the reduction of area converted to elongation, assuming constant volume. These data are plotted in Figure 9 and typical microstructures are shown in Figure 10. Several aspects deserve discussion.

Although not positively identified, it is extremely probable that hcp martensite has formed in the 21-6-9 alloy during low temperature deformation.

The microphotographs after deformation at 4 K (Figure 10) identify transformed regions which are parallel to the  $\{111\}$  slip band traces. These appear identical to the hcp areas identified in earlier research on AISI 304, an Fe-Cr-Ni alloy.<sup>(7,13)</sup>

The amount of bcc martensite formed is large and only slightly less than that which is formed in AISI 304 at the same temperatures<sup>(7,13)</sup>. Permeability values of the order of 10 were measured in heavily deformed specimen portions at 76 K. It is difficult to identify bcc martensite in the Figure 10 photomicrographs. Normally, in austenitic stainless steels the bcc martensitic product has an acicular, plate-like morphology with the habit plane of the plate not  $\{111\}$ . Examination of specimen microstructures, typified by Figure 10 indicate that only at  $\{111\}$  band intersections are plate-like and distinctive microstructures observed.

There is clear evidence that the amount of the transformation is suppressed, as a function of either stress or strain, at 4 K when compared to 76 K measurements. This is similar to the Fe-Cr-Ni (AISI 304) alloy martensitic transformation behavior<sup>(7,13)</sup>. Our earlier work<sup>(7,13)</sup> also indicated that the hcp martensitic phase was suppressed at 20 and 4 K. Apparently, in the complicated energy balance affecting martensitic transformation for these alloy systems at low temperatures the increase of flow stress and the decrease of dislocation mobility more than offset the gradually increasing free energy difference between the structures.

Finally, it is not clear that the observance of martensitic transformations is deleterious to material application. Normally, the material is used in service at stress levels less than the yield strength; under these conditions no martensitic transformations occur. The complexities and concern usually are discussed when one considers welds and weld techniques. Chemical

segregation and stress concentrations are both more likely, permitting particular sections to be less stable and, locally, stressed above the yield strength. In these situations martensitic products will form.

AISI 304 behaves in a similar manner; it is stable on cooling to low temperatures but transforms to hcp and bcc martensitic products during plastic deformation. But, unlike 21-6-9, the fracture toughness of AISI 304 remains extremely high at 4 K<sup>(14)</sup>. This implies that martensitic transformations are not harmful to the fracture toughness of the Fe-Cr-Ni stainless steel. This is not clear in the case of the Fe-Cr-Ni-Mn-N alloy, however, as the toughness is rapidly decreasing at 4 K. For appropriate safety of operation at 4 K, additional research is necessary to understand the effect of martensitic transformations on fracture toughness.

#### Acknowledgements

The authors would like to thank Dr. P. R. Landon, Lawrence Livermore Laboratories, for kindly supplying the rolled material. Dr. R. P. Mikesell conducted the tensile tests, R. L. Durcholz contributed technical assistance to tensile, fracture, and metallographic preparation, and Dr. M. B. Kasen was responsible for the photomicrographs.

## References

1. P. R. Landon, Unpublished data, Lawrence Livermore Laboratories, Livermore, CA (1975).
2. P. F. Scardigno, Masters Thesis, Naval Postgraduate School, Monterey, CA, AD/A-004555 (1974).
3. C. O. Malin, NASA SP-5921(01), Technology Utilization Office, NASA, Washington, D.C. (1970).
4. R. D. Masteller, NASA CR-72638(N70-27114), Martin Marietta Corp., Denver, CO (1970).
5. "Tension Testing of Metallic Materials", E8-72, Annual Book of ASTM Standards, Part 31 (ASTM, Philadelphia, PA, 1973).
6. R. P. Reed, Advances in Cryogenic Engineering, Vol. 7 (Plenum Press, New York, 1962) p. 448.
7. R. P. Reed and C. J. Guntner, Trans. AIME, 230, 1713 (1964).
8. ASTM Standards, E399-74, part 10 (ASTM, Philadelphia, PA 1974).
9. R. P. Reed, R. L. Tobler, and R. P. Mikesell, "Advances in Cryogenic Engineering - ICMC", Vol. 22 (Plenum Press, New York, 1976), to be published.
10. J. D. Landes and J. A. Begley, Westinghouse Research Laboratory Scientific Paper 73-1E7-FMPWR-P3, Pittsburgh, PA (1973).
11. J. D. Landes and J. A. Begley, "Fracture Analyses", ASTM STP 560, (American Society for Testing and Materials, Philadelphia, PA 1974) p. 170-186.
12. J. R. Rice, P. C. Paris, and J. G. Merkle, ASTM STP 536 (ASTM, Philadelphia, PA 1973) p. 231.
13. C. J. Guntner and R. P. Reed, ASM Trans. 55, 399 (1962).
14. R. P. Reed, A. F. Clark and E. C. van Reuth, Eds. "Materials Research for Superconducting Machinery III", AD-A012365/3WM, National Technical Information Service, Springfield, VA (1975).
15. R. R. Vandervoort, Metals Engr. Quart. 12, No. 1, 10 (1972).

### List of Figures

- Figure 1. Compact specimen for fracture testing of Fe-19Cr-6Ni-9Mn alloy.
- Figure 2. Summary of tensile and yield strength data as a function of temperature for the Fe-21Cr-6Ni-9Mn alloy.
- Figure 3. Summary of tensile elongation as a function of temperature for the Fe-21Cr-6Ni-9Mn alloy.
- Figure 4. Summary of tensile reduction of area as a function of temperature for the Fe-21Cr-6Ni-9Mn alloy.
- Figure 5. Stress-strain curves for the Fe-21Cr-6Ni-9Mn alloy at 295, 76 and 4 K.
- Figure 6. Typical load-deflection curves at 295, 76 and 4 K for annealed Fe-21Cr-6Ni-9Mn alloy.
- Figure 7. Fracture characteristics of Fe-21Cr-6Ni-9Mn alloy at 295, 76 and 4 K.
- Figure 8. The J-integral as a function of crack extension at 295, 76 and 4 K for annealed alloy Fe-21Cr-6Ni-9Mn.
- Figure 9. Estimated percent bcc martensite that forms during tensile tests as a function of tensile elongation.
- Figure 10. Microstructures of alloy 21-6-9 after deformation at 4 K. Bands lie on {111} austenite planes and probably represent hcp and bcc martensite, (a) 800X, (b) 1200X.

### List of Tables

- Table 1. Precracking Parameters for Fracture Test Specimens.
- Table 2. Tensile Properties of Fe-21Cr-6Ni-9Mn alloy.
- Table 3. Fracture Results for 377 cm Thick Compact Tensile Specimens of Alloy Fe-21Cr-6Ni-9Mn.

Table 2. Tensile Properties of Fe-21Cr-6Ni-9Mn Alloy

Temperature (K)	Yield Strength 0.2% offset ( $10^8 \text{ N}\cdot\text{m}^{-2}$ )	Tensile Strength ( $10^8 \text{ N}\cdot\text{m}^{-2}$ )	Elongation 2.5 cm gage length (percent)	Reduction of Area (percent)
295 K	3.50	6.96	61	79
	<u>3.57</u>	<u>7.05</u>	<u>61</u>	<u>78</u>
Average	3.53 (51 ksi)	7.01 (102 ksi)	61	78
76 K	9.13	14.62	42	32
	<u>8.86</u>	<u>14.85</u>	<u>43</u>	<u>41</u>
Average	8.99 (130 ksi)	14.74 (214 ksi)	43	37
4 K	12.58	16.33	16	40
	<u>12.24</u>	<u>16.34</u>	<u>16</u>	<u>40</u>
Average	12.41 (180 ksi)	16.34 (237 ksi)	16	40

Table 3.

Temperature (K)	a/W	J ( $10^3 \text{ N}\cdot\text{m}/\text{m}^2$ )	$\Delta a$ (cm)	$K_Q^{(a)}$ ( $\text{MN}/\text{m}^{3/2}$ )
295	0.638	177	0.013*	58
	0.636	744	0.051*	61
	0.640	905	0.069*	55
	0.635	1355	0.097*	63
	0.642	1423	0.112*	50
76	0.612	261	0	134
	0.634	413	0.028	153
	0.640	499	0.053	131
	0.637	674	0.079	137
	0.645	788	0.091	130
	0.643	698	0.198	130
4	0.670	100	0	---
	0.655	147	0.020	167
	0.670	158 <sup>(b)</sup>	0.080	158
	0.645	152 <sup>(b)</sup>	N/A	164
	0.648	163 <sup>(b)</sup>	N/A	162
	0.643	173 <sup>(c)</sup>	N/A	159
	0.656	162	.076	

$$1 \frac{\text{in}\cdot\text{lb}}{\text{in}} = 1.75 \times 10^2 \frac{\text{N}\cdot\text{m}}{\text{m}^2}, \quad 1 \frac{\text{ksi}}{\text{in}} = 1.099 \times 10^6 \frac{\text{N}}{\text{m}^2} \cdot \text{m}^{-1/2}.$$

(a) from E-399-74 method; invalid due to insufficient thickness.

(b) calculated at the first load discontinuity (pop-in)

(c) calculated at the maximum load.

\* refer not to crack opening distances, but to stretch zone distances.

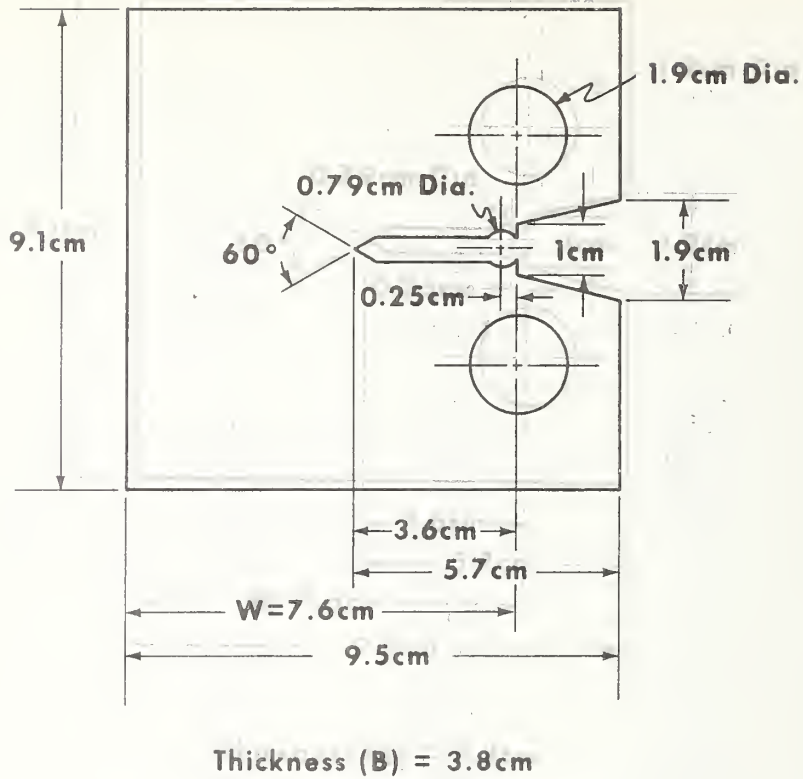


Figure 1. Compact specimen for fracture testing of Fe-19Cr-6Ni-9Mn alloy.

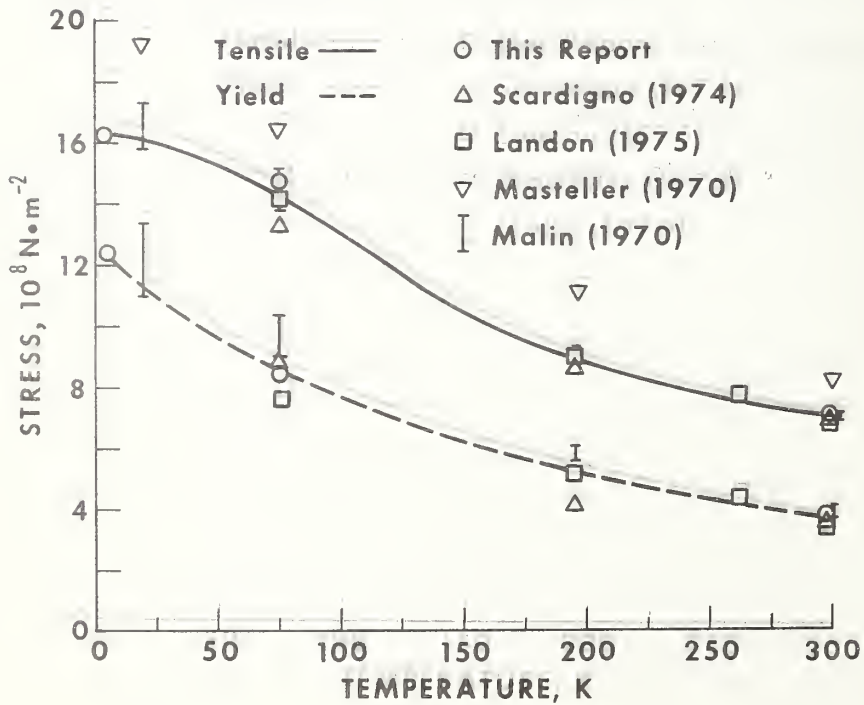


Figure 2. Summary of tensile and yield strength data as a function of temperature for the Fe-21Cr-6Ni-9Mn alloy.

Figure 4. Summary of tensile reduction of area as a function of temperature for the Fe-21Cr-6Ni-9Mn alloy.

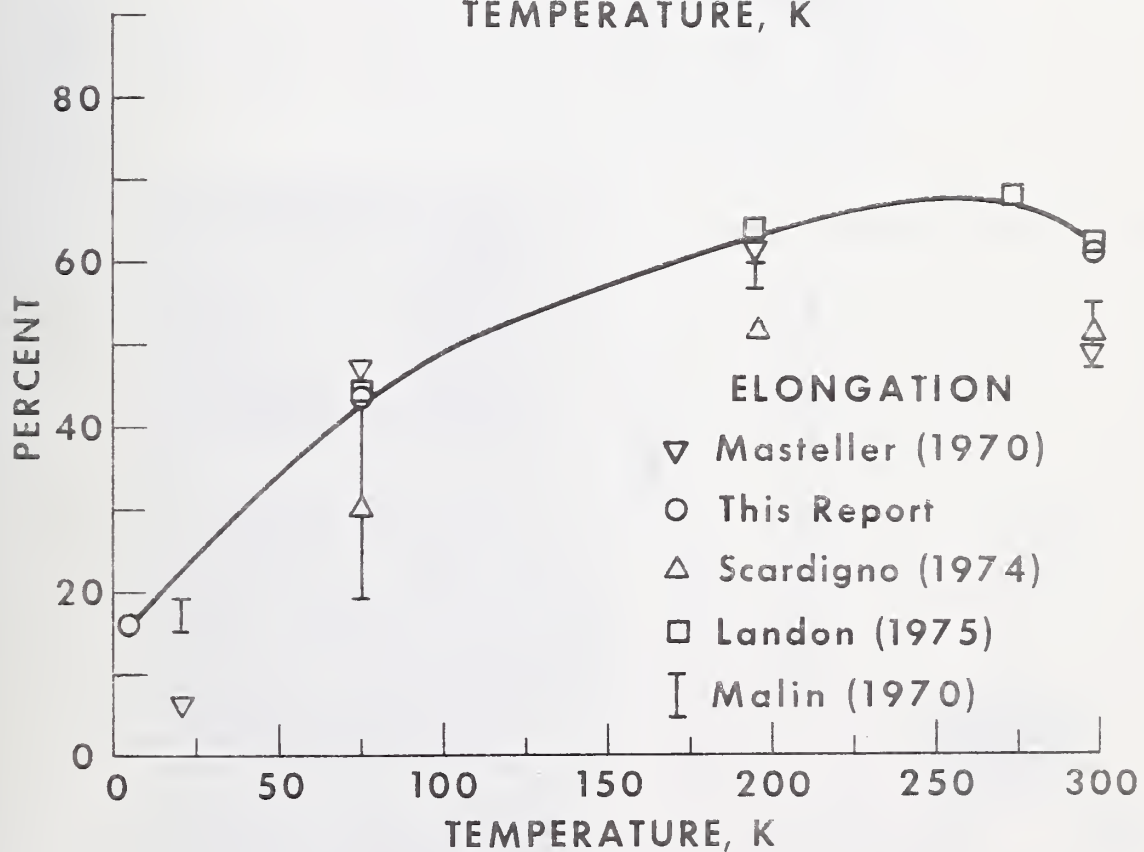
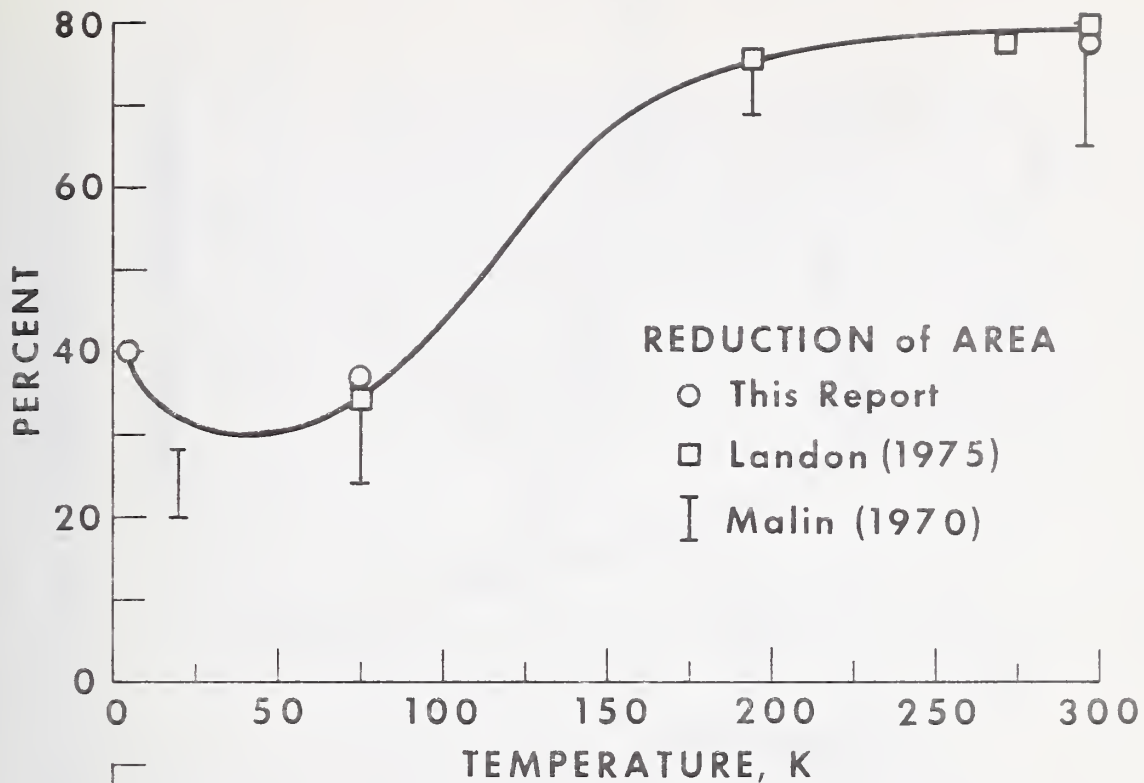


Figure 5. Summary of tensile elongation as a function of temperature for the Fe-21Cr-6Ni-9Mn alloy.

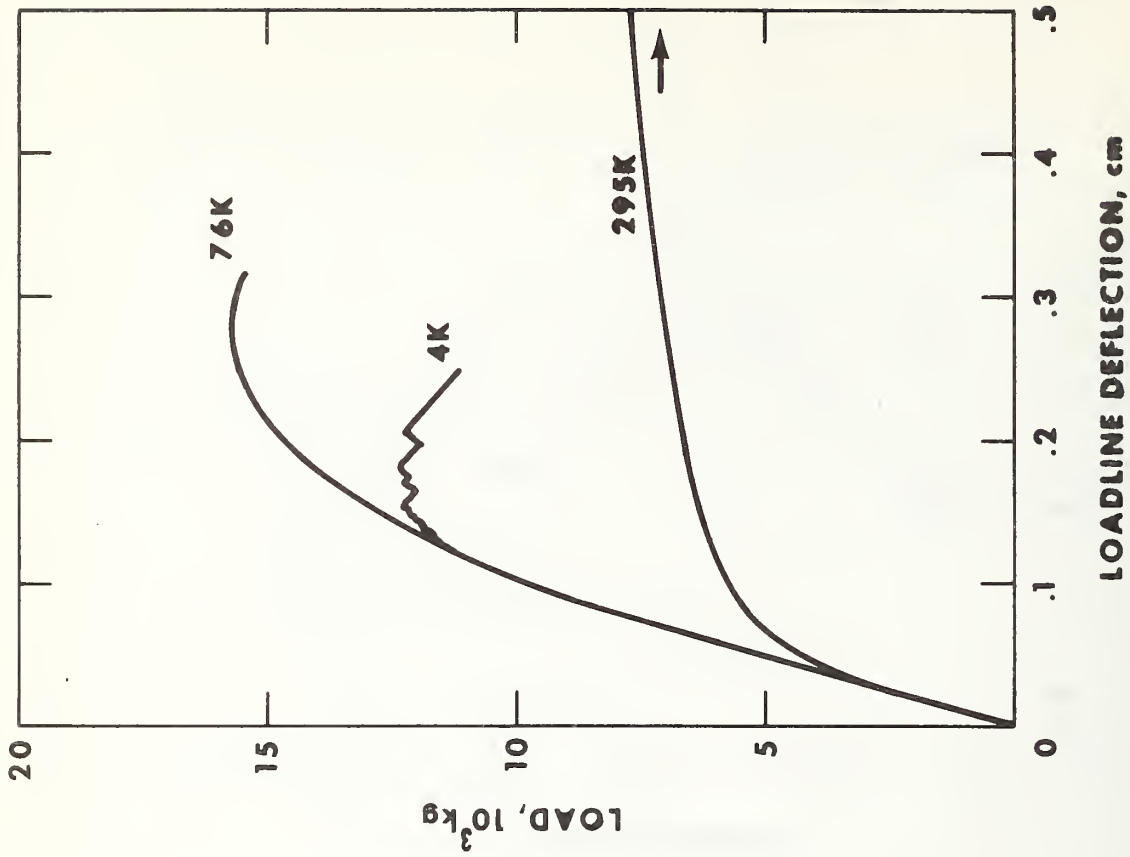


Figure 6. Typical load-deflection curves at 295, 76, and 4 K for annealed Fe-21Cr-6Ni-9Mn alloy.

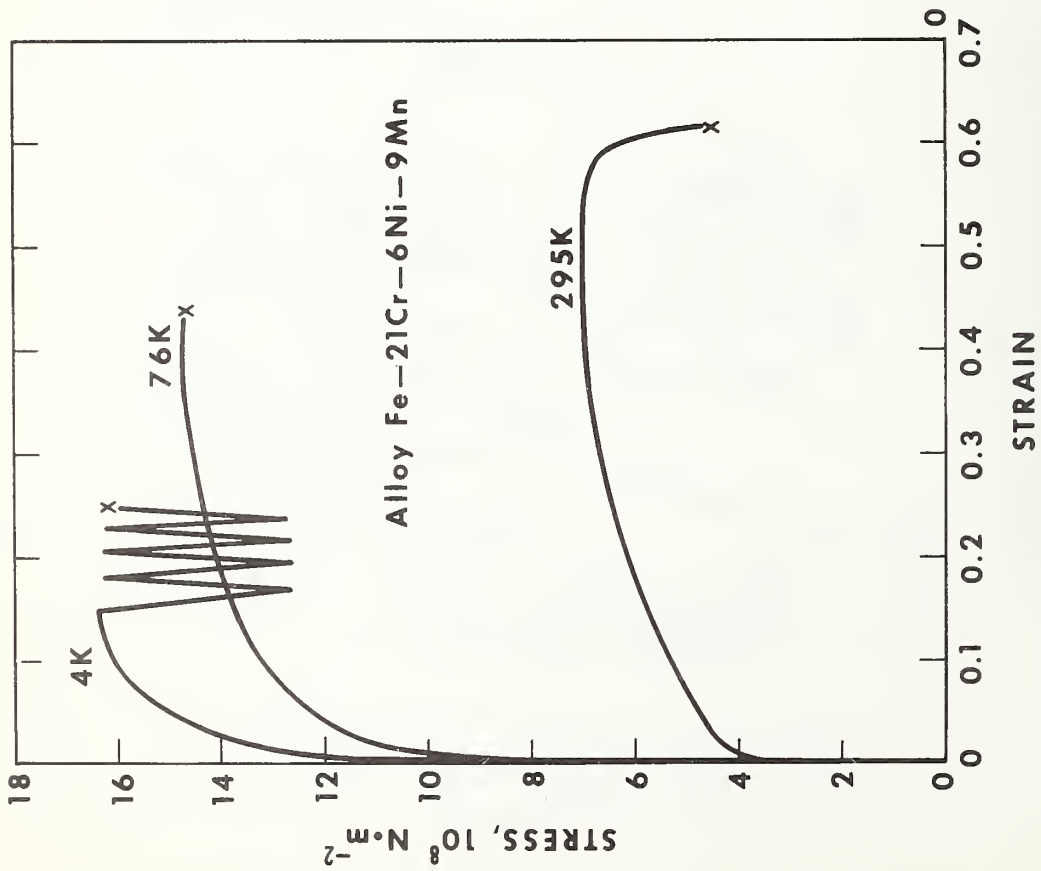


Figure 5. Stress-strain curves for the Fe-21Cr-6Ni-9Mn alloy at 295, 76, and 4 K.

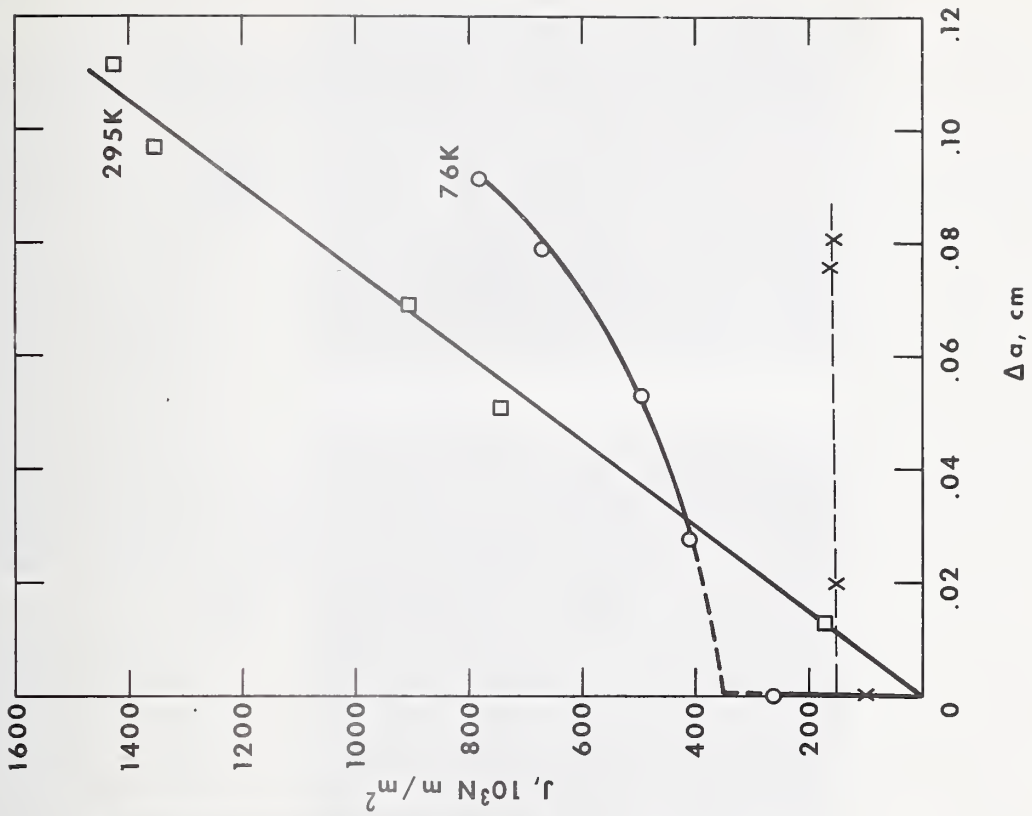


Figure 8. The J-integral as a function of crack extension at 295, 76, and 4 K for annealed alloy Fe-21Cr-6Ni-9Mn.



Figure 7. Fracture characteristics of Fe-21Cr-6Ni-9Mn alloy at 295, 76, and 4 K.

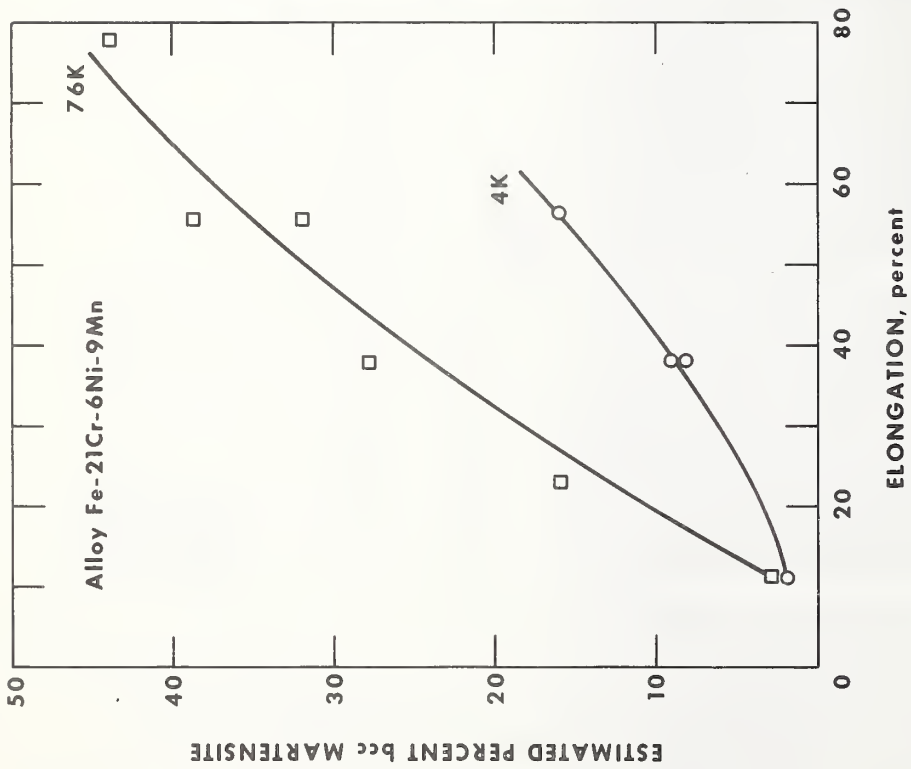
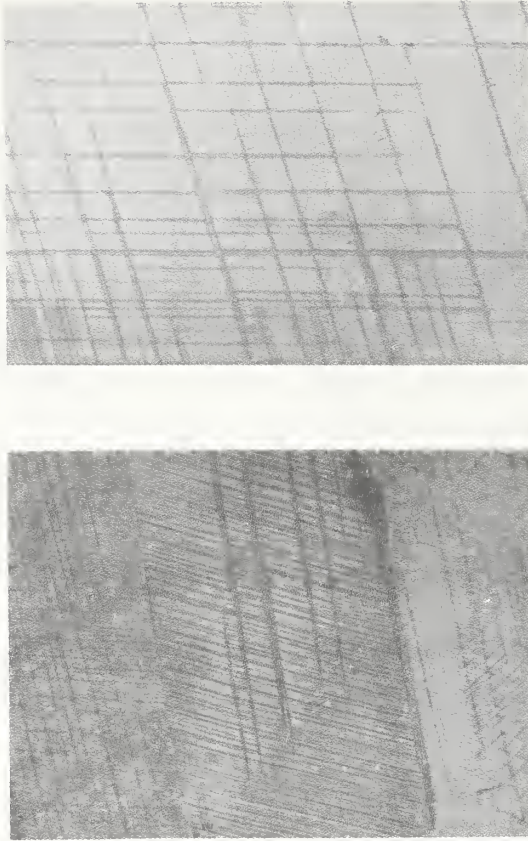


Figure 9. Estimated percent bcc martensite that forms during tensile tests as a function of tensile elongation.



(a) (b)

Figure 10. Microstructures of alloy 21-6-9 after deformation at 4 K. Bands lie on {111} austenite planes and probably represent hcp and bcc martensite, (a) 800X, (b) 1200X.

NBSIR

SEMI-ANNUAL REPORT ON MATERIALS RESEARCH  
IN SUPPORT OF SUPERCONDUCTING MACHINERY

MAGNETOTHERMAL CONDUCTIVITY

L. L. Sparks

Cryogenics Division  
Institute for Basic Standards  
National Bureau of Standards  
Boulder, Colorado 80302

October 1975

Summary: Magnetothermal Conductivity

The thermal conductivity and effect of a magnetic field on the thermal conductivity of S30400 have been determined in the temperature range from 5 to 20 K. The results indicate that a 6366 kA/m (80 kOe) magnetic field reduces the thermal conductivity of this material by 9.2% at 5.5 K and by 6.7% at 19.75 K. The present data at  $H = 0$  compares very well with literature data on similar materials. Several minor modifications have been incorporated primarily to provide better thermal contact between the specimen and the thermometers. Based on the S30400 tests, the precision of the measurements has been improved. The reproducibility of the results now appears to be about 5% in thermal conductivity except at the temperature extremes where it is near 8%.

Contents: Magnetothermal Conductivity

	Page
1. Introduction . . . . .	153
2. Procedures . . . . .	153
2.1 Apparatus . . . . .	153
2.2 Materials . . . . .	154
3. Results and Discussion . . . . .	154
4. Conclusions. . . . .	155
5. References . . . . .	156
List of figures . . . . .	156
Preprint: Magnetothermal Conductivity of Selected Pure Metals and Alloys . . .	160

L. L. Sparks

Cryogenics Division  
Institute for Basic Standards  
National Bureau of Standards  
Boulder, Colorado 80302

## 1. Introduction

The objective is to determine the effect of magnetic fields on the thermal conductivity of technically important metals. The need for this information arises from the development of rotating machinery operating at cryogenic temperatures. The existing world's literature on magnetothermal conductivity,  $\lambda(H)$ , is concerned almost exclusively with scientific materials, e.g., very pure materials and single crystals. A complete bibliography of the subject was given by Sparks and Fickett [1].

The materials studied in this program are being used or are candidates for use in superconducting motors and generators. Optimum design of these machines, which must operate at low temperatures while in magnetic fields, requires a detailed knowledge of how the thermal properties of the constituent materials are affected by a magnetic field. The broad material categories of interest include superconductor stabilizing materials such as copper and aluminum, and structural materials such as nickel alloys, stainless steels, and metallic composites.

Results of the  $\lambda(H)$  work were presented at three conferences since the last semi-annual ARPA report: American Physical Society (Denver, March), 14th International Conference on Thermal Conductivity (University of Connecticut, June), and the joint meeting of the Cryogenic Engineering Conference and the International Cryogenics Materials Conference (Kingston, Canada, July). A preprint of the paper presented at the ICMC Conference is included at the end of this report. The work was well received in each case and led to several worthwhile discussions on the effect of a magnetic field on metals.

Several changes have been made in the apparatus and instrumentation in an attempt to improve the precision of the results. The details of these changes are discussed in the procedures section of this report. Tests on S30400 (AISI 304 stainless steel) have been used to evaluate the system with the changes incorporated.

## 2. Procedures

### 2.1 Apparatus

The principle components of the  $\lambda(H)$  system are shown schematically in figure 1. The basic operation of the system has been described in previous reports [1,2] and will not be repeated here except in relation to the changes.

Thermal conductivity is calculated using the equation

$$\lambda = \frac{\dot{Q}}{A/l \Delta T} .$$

Errors made in the measurement of the temperature difference along the specimen,  $\Delta T$ , are reflected directly in  $\lambda$ . Perhaps the most difficult problem encountered in measuring small temperature differences is that of making good thermal contact with the temperatures of interest. Before the current changes were instituted, the carbon resistance thermometers, (CRT's), were press fit into wells in the THERMOMETER BLOCK and packed with a thermally conducting grease. The THERMOMETER BLOCKS were machined so that knife edge contacts were made when they were clamped to the specimen. This system had the following shortcomings which are eliminated or minimized by the changes made in the method of sensing the specimen temperatures: (1) It was impossible to be sure that the thermal contacts between the specimen and the THERMOMETER BLOCK and between the THERMOMETER BLOCK and the CRT's were the same

for the upper and lower THERMOMETER BLOCKS; (2) the THERMOMETER BLOCKS were comparable to the specimen in mass and heat capacity. This was the case even though the dimensions of the BLOCKS were as small as possible consistent with the CRT wells and the clamping screw; (3) it was difficult to attach the clamps to the small specimens without introducing some strain in the specimen. The new "thermometer holder", designed to alleviate the problems discussed above, is shown schematically in figure 2. Thermal contact to the specimen is achieved by soldering the 20 AWG copper wire directly to the specimen; this method assures good thermal contact and should be identical for both the upper and lower thermometer stations. Thermal contact and electrical isolation between the copper wire and the CRT is provided by the sapphire chip as shown in the figure. The thermal conductivity of sapphire is similar to that of copper at low temperatures and it is also an electrical insulator. The mass (and heat capacity) of the thermometer attachment system has been significantly reduced which allows a faster time response than was possible before.

Another change in the  $\lambda(H)$  system was made to allow better null temperature control between the TEMPERING POST and the specimen. The condition  $T(\text{specimen}) - T(\text{tempering post}) = 0$  must be maintained in order to eliminate heat flow between the specimen and the tempering post. A differential thermocouple is used as a sensor in the automatic control circuit used to maintain this zero temperature difference. It is essential that the thermocouple be electrically isolated from the system ground and yet be in very good thermal contact with both the POST and the specimen. The thermal and electrical properties of sapphire are again used to advantage as shown in figure 3. The previous method of electrically isolating the junctions was to place cigarette paper between the wires and the surfaces where the temperature was to be sensed.

The resistance of the CRT's had been measured using an a.c. lock-in amplifier as both the bridge power supply and null detector. This system has been replaced, at least for the present time, by a d.c. Wheatstone bridge. Resistance measurements made with the d.c. system are more precise; however, current reversing procedures must be followed which amounts to doubling the number of readings compared to the a.c. system.

## 2.2 Materials

One alloy, S30400 (AISI 304), was tested during this reporting period. The composition in weight percent of a specimen of this material taken from the same stock as the  $\lambda(H)$  specimen is as follows: C = 0.07, Cr = 17.82, Mn = 1.05, Ni = 8.94, P = 0.022, Si = 0.37, S = 0.012, and the balance is Fe. The test specimen was annealed at 1000°C for 1.5 hours in a vacuum of 0.133 Pa. The residual resistance ratio (RRR) for the specimen is 1.43. The Rockwell hardness of material adjacent to the  $\lambda(H)$  specimen is B93 in the unannealed condition and B71 in the annealed condition.

## 3. Results and Discussion

The changes in the method of mounting the thermometers and in reading the thermometer resistances appear to have increased the precision of the temperature measurements. Previously, the calibration of the CRT's by comparison to the calibrated germanium resistance thermometer yielded an analytical representation with an imprecision of 5 mK for the CRT nearest the TEMPERATURE CONTROLLED HEAT SINK and 9 mK for the CRT nearest the SPECIMEN HEATER. The initial tests on S30400 indicate that these imprecisions have been reduced to about 2 mK and 4 mK respectively.

The present data for the thermal conductivity of S30400 at  $H = 0$  and  $H = 6366$  kA/m (80 kOe) are shown in figure 4. Data were also taken at 796 kA/m (10 kOe), but are indistinguishable from the  $H = 0$  data. A comparison of the present zero field thermal conductivity data with data for a similar material indicates that there are no significant systematic errors present in the  $H = 0$  determination. Table 1 shows the compositions of the present specimen and a similar material for which there are low temperature thermal conductivity data [3].

ELEMENT	COMPOSITION (wt. %)	
	S30400	S34700
Cr	17.82	17.17
Ni	8.94	11.52
Si	0.37	0.59
C	0.07	0.057
Mn	1.05	1.34
P	0.022	0.14
S	0.012	0.007
Ni + Ta	--	1.10
Fe	bal.	bal.

Table 1. Comparative compositions of two stainless steels.

A comparison of the thermal conductivities at  $H = 0$  for these materials is given in table 2.

TEMPERATURE	$\lambda_{S34700} / \lambda_{S30400}$
6	0.92
8	0.97
10	1.00
14	1.01
16	1.01
18	1.01

Table 2. Ratio of thermal conductivities of two stainless steels at  $H = 0$ .

Clark, et al. [4] found the RRR for their S30400 specimen to be 1.42. The RRR for the present specimen was determined to be 1.43. This excellent agreement indicates that the specimen used by Clark and the present specimen are electrically similar.

The general effect of a magnetic field is to reduce the thermal conductivity as shown in figure 4. The reduction from zero field values caused by a 6366 kA/m (80 kOe) field is 9.2% at 5.5 K and 6.7% at 19.75 K for S30400. Similar data reported earlier [5] show the corresponding reduction in conductivity for N07718 to be 8% at 5.5 K and 3% at 19.5 K; for S31000 the reduction is 20% at 5.25 K and 11% at 19.5 K. The field effect is seen to be slightly greater in the S30400 than in the N07718, as would be expected. The Lorenz numbers for the Ni-Cr alloys are typically higher than those for stainless steels. This indicates a stronger lattice component of thermal conductivity and therefore a smaller magnetic field effect. The present data exhibit a considerably smaller field dependence of thermal conductivity than was observed for the S31000 specimen. The variation in the field effect on the two stainless specimens is not understood at the present time.

#### 4. Conclusions

The zero field thermal conductivity data for S30400 is very close to that taken for a similar steel in a high precision, zero field thermal conductivity system. The reduction in  $\lambda$  of S30400 caused by a 6366 kA/m magnetic field is 9.2% at 5.5 K and 6.7% at 19.75 K.

## 5. References

1. Sparks, L. L. and Fickett, F. R., Materials research in support of superconducting machinery, National Bureau of Standards, Boulder, Colorado, Cryogenics Division, March, 1974 NBSIR-74-359, AD-780 596/3WM.
2. Sparks, L. L. and Fickett, F. R., Materials research in support of superconducting machinery, National Bureau of Standards, Boulder, Colorado, Cryogenics Division, October, 1974 NBSIR-74-393, AD-A0004586.
3. Hust, J. G., Thermal Conductivity, Electrical Resistivity, and Thermopower of Aerospace Alloys from 4 to 300 K: II AISI 347 Stainless Steel, unpublished NBS Report.
4. Clark, A. F., Childs, G. E. and Wallace, G. H., Electrical resistivity of some engineering alloys at low temperatures, Cryogenics 10, No. 4, 295 (August, 1970).
5. Sparks, L. L., Materials research in support of superconducting machinery, National Bureau of Standards, Boulder, Colorado, Cryogenics Division, April, 1975 NBSIR-75-810, AD-A012365.

## List of Figures

- Figure 1. Magnetothermal conductivity probe and magnet.
- Figure 2. Modified method of attaching the carbon resistance thermometers to the specimen.
- Figure 3. Modified method of making thermal contact with the differential thermocouple junctions.
- Figure 4. Thermal conductivity of S30400 stainless steel as a function of temperature for  $H = 0$  and 6366 kA/m (0 and 80 kOe respectively).

## List of Figures

- Figure 1. Magnetothermal conductivity probe and magnet.
- Figure 2. Modified method of attaching the carbon resistance thermometers to the specimen.
- Figure 3. Modified method of making thermal contact with the differential thermocouple junctions.
- Figure 4. Thermal conductivity of S30400 stainless steel as a function of temperature for  $H = 0$  and  $6366 \text{ kA/m}$  ( $0$  and  $80 \text{ kOe}$  respectively).

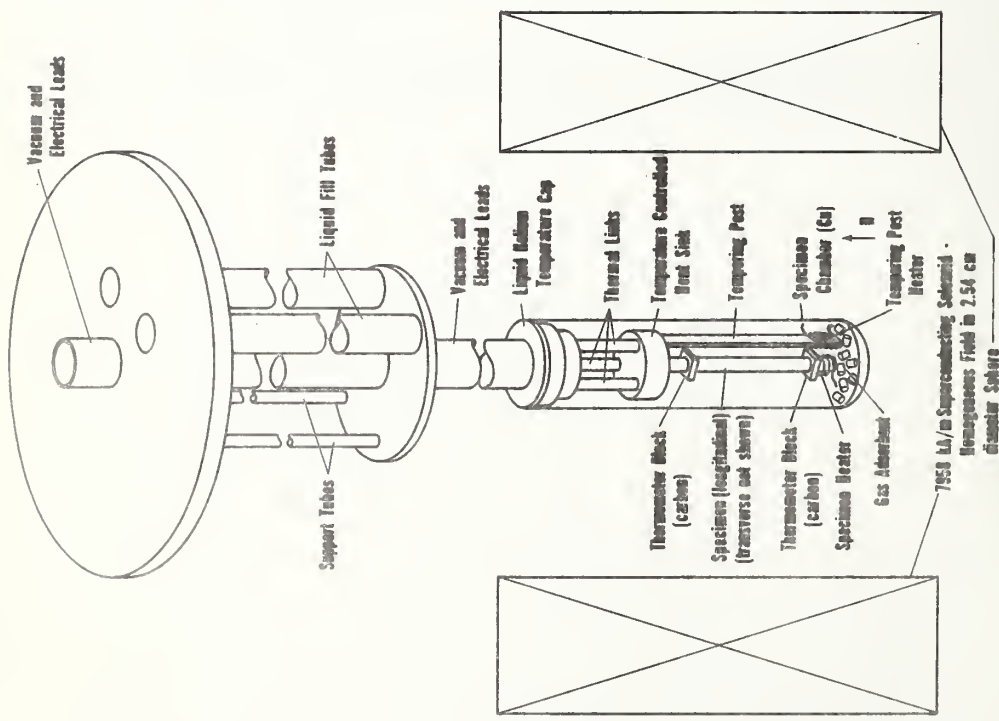


Figure 1. Magneto-thermal conductivity probe and magnet.

795-1992

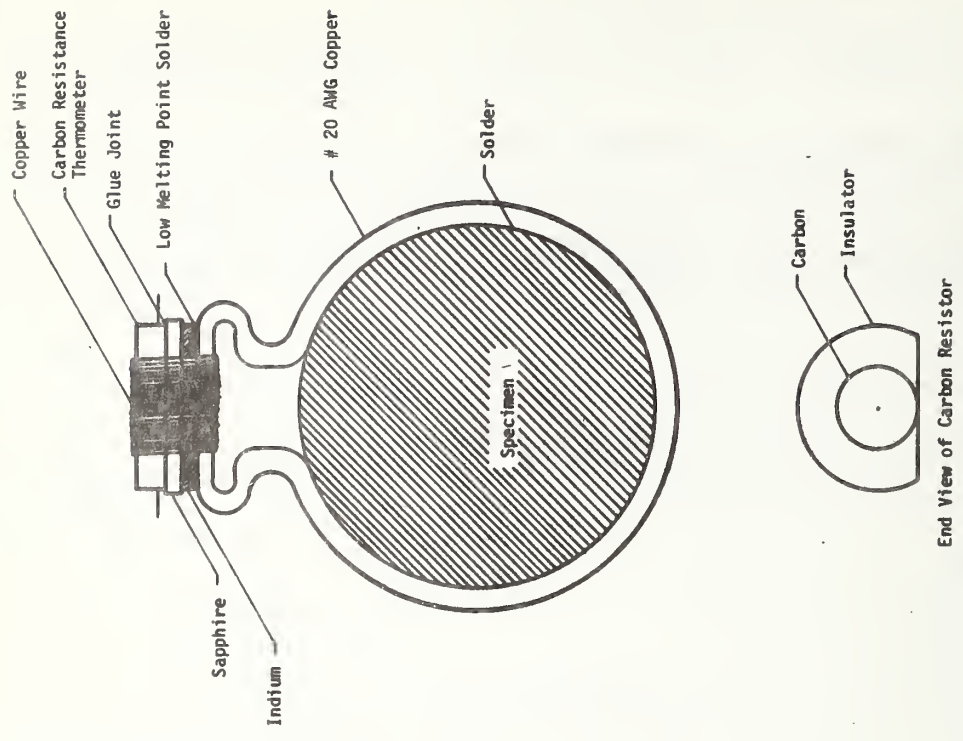


Figure 2. Modified method of attaching the carbon resistance thermometers to the specimen.

795-1992

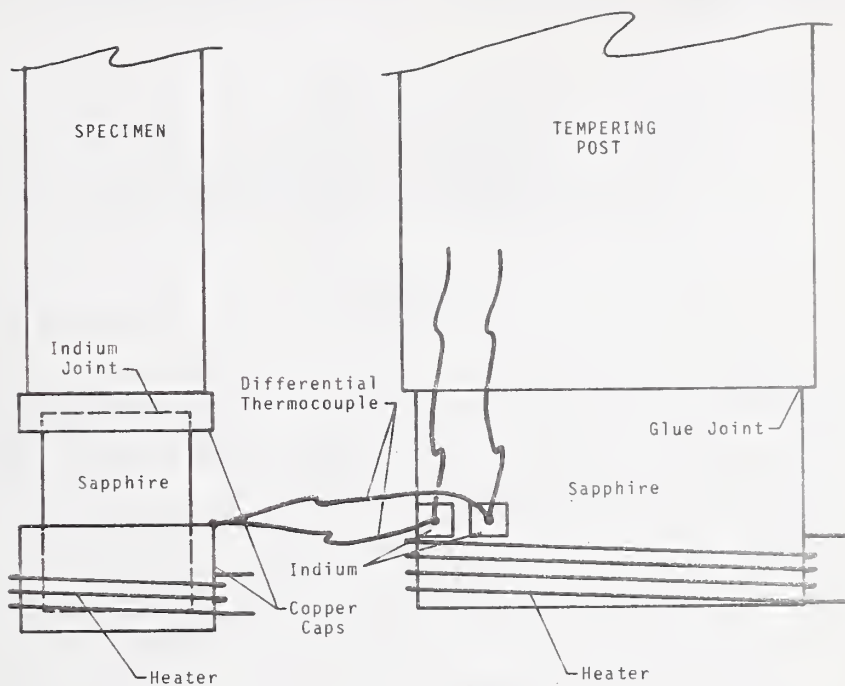


Figure 3. Modified method of making thermal contact with the differential thermocouple junctions.

76X 5103

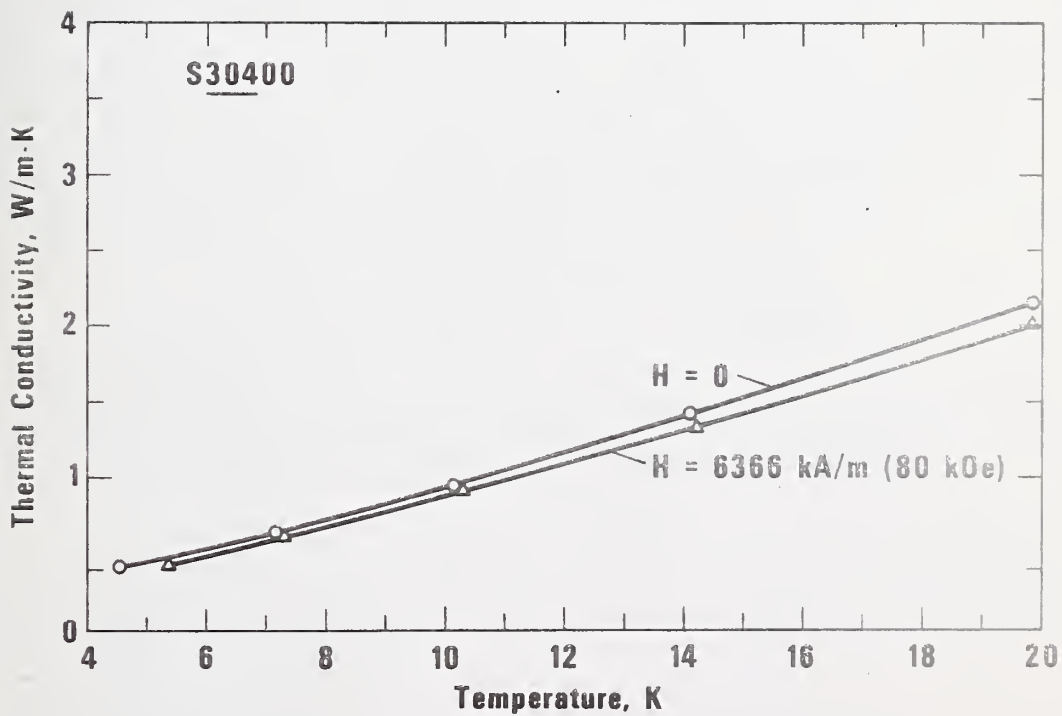


Figure 4. Thermal conductivity of S30400 stainless steel as a function of temperature for  $H = 0$  and  $6366 \text{ kA/m}$  ( $0$  and  $80 \text{ kOe}$  respectively).

# MAGNETOTHERMAL CONDUCTIVITY OF SELECTED PURE METALS AND ALLOYS

L. L. Sparks

Cryogenics Division  
NBS - Institute for Basic Standards  
Boulder, Colorado 80302

## ABSTRACT

The magnetothermal conductivity program was initiated to determine the effect of a magnetic field on the thermal resistance of technically important metals. The experiments are done in magnetic fields up to  $6366 \frac{\text{kA}}{\text{m}}$  (80 kOe) and cover the temperature range from 4 to 20 K. The results of this study are presented for a Ni-Cr-Fe alloy, AISI 310 stainless steel, oxygen-free copper, and a high purity copper specimen. A magnetic field typically increases the electronic thermal resistance and thus lowers the total thermal conductivity of a metal. The magnetic field effect at constant temperature is shown by the relative change in thermal resistance,  $\Delta W/W_{H=0}$ , where  $\Delta W$  is defined as  $W_{H \neq 0} - W_{H=0}$ . Our experimental data show that the effect of a  $6366 \text{ kA/m}$  (80 kOe) magnetic field on the Ni-Cr-Fe alloy is to increase  $\Delta W/W_{H=0}$  by 0.08 at 5 K and 0.03 at 19 K. The corresponding values for AISI 310 are 0.28 at 5 K and 0.10 at 19 K. The thermal resistivity of the better conductors was found to be affected more strongly. A  $6366 \text{ kA/m}$  (80 kOe) magnetic field causes  $\Delta W/W_{H=0}$  to increase to 1.3 at 5.5 K and 0.8 at 19 K for oxygen-free copper; for the high purity copper,  $\Delta W/W_{H=0}$  increases to 3.4 at 5.5 K and 2.7 at 20 K.

Key words: Copper; low temperature; magnetothermal conductivity; nickel alloy; stainless steel; thermal conductivity.

# MAGNETOTHERMAL CONDUCTIVITY OF SELECTED PURE METALS AND ALLOYS\*

L. L. Sparks

Cryogenics Division  
NBS - Institute for Basic Standards  
Boulder, Colorado 80302

## INTRODUCTION

The objective is to determine the effect of magnetic fields on the thermal conductivity of technically important metals. The need for this information arises from the development of rotating machinery operating at cryogenic temperatures. The existing literature on magnetothermal conductivity,  $\lambda(H)$ , is concerned almost exclusively with scientific materials, e.g., very pure materials and single crystals. A complete bibliography of magnetothermal conductivity was given by Sparks and Fickett.<sup>1</sup>

The materials studied in this program are being used or have potential use in superconducting motors and generators. Optimum design of these machines, which must operate at low temperatures while in magnetic fields, requires a detailed knowledge of how the thermal properties of the constituent materials are affected by a magnetic field. The broad material categories of interest include superconductor stabilizing materials such as copper and aluminum, and structural materials such as nickel alloys, stainless steels, and metallic composites.

## APPARATUS AND EXPERIMENTAL PROCEDURES

The experimental determination of the  $\lambda(H)$  of metals in high fields is complicated by the requirement that the specimen be contained in a region of homogeneous field. For magnets of reasonable size, this restriction necessitates small specimen lengths and resultant small temperature differences along the specimens. The  $\lambda(H)$  probe employed in this study was designed to be used in a superconducting solenoid with a 3.8 cm bore and a 2.5 cm homogeneous (1%) field sphere. Specimen lengths are therefore limited to approximately 2.5 cm.

---

\* Supported by the Advanced Research Projects Agency (ARPA); Department of Defense. ARPA Order No. 2569.

The principle components of the  $\lambda(H)$  system are shown in figure 1. A specimen is shown with its axis mounted parallel to the magnetic field. This configuration is used to determine the longitudinal  $\lambda(H)$ . Provisions for making transverse  $\lambda(H)$  measurements (heat flow perpendicular to the direction of the field) have been included in the system design.

The basic operation of the system involves balancing electrical power supplied to three heaters with the heat leak to the liquid helium bath via the THERMAL LINKS (capitalized parts refer to figure 1). The electrical heaters were wound, one each, on the TEMPERATURE CONTROLLED HEAT SINK (TCHS), the SPECIMEN, and the TEMPERING POST. The power supplied to the TCHS determines the approximate temperature of the specimen; the SPECIMEN HEATER is used to establish a temperature gradient along the specimen; and the TEMPERING POST HEATER is used to reduce the temperature difference between the specimen and the tempering post to less than  $\pm 5$  mK. The TEMPERING POST and TCHS heaters are automatically controlled during all tests while a constant current is supplied to the SPECIMEN HEATER.

The thermometers used in the probe are three 1/8 watt, 100 ohm Allen Bradley\* carbon resistors (CRT's) and a single calibrated germanium resistor (GRT). The CRT's are located, one each, in the TCHS, and the two THERMOMETER BLOCKS. The GRT is located in the TCHS and is used for zero-magnetic-field calibration of the CRT resistors. The effect of the magnetic field on the resistance of the CRT's is taken to be that published by Neuringer and Shapira<sup>2</sup>. Resistance measurements on the two specimen CRT's are made using a lock-in amplifier as both detector and power supply for an AC bridge. Both absolute and difference resistance measurements are possible using this system.

The thermal conductivity of a specimen is computed from the specimen geometry (Area/length), the specimen heater power ( $\dot{Q}$ ), and the measured temperature difference along the specimen ( $\Delta T$ ). The relationship of  $\lambda$  to these parameters is given by

$$\lambda = \frac{\dot{Q}}{\frac{A}{l} \Delta T} \quad (1)$$

\* The use of trade names of specific products is essential to a proper understanding of the work presented. Their use in no way implies any approval, endorsement, or recommendation by the National Bureau of Standards.

A series of measurements of  $\Delta T$  and  $\dot{Q}$  at various fields\* ( $0 \leq H \leq 6366$  kA/m or 80 kOe) and temperatures ( $4 < T < 20$  K) result in the data presented in this report.

## MATERIALS

A total of four materials have been tested--Ni-Cr-Fe alloy UNS-N07718, oxygen-free copper UNS-C10200, stainless steel UNS-S31000, and a high purity copper referred to as NBS-B stock 7. UNS-N07718 was tested in the age-hardened condition with a Rockwell hardness of C39 and an average grain diameter of 0.06 mm. The composition in weight percent for this material is: Ni = 54.57, Cr = 18.06, Fe = 17.08, Nb + Ta = 5.12, Mo = 3.18, Ti = 0.85, Al = 0.44, Mn = 0.29, Si = 0.24, Cu, C, and S < 0.1%; the residual resistance ratio ( $RRR = R_{273K}/R_{4K}$ ) is 1.06. The UNS-S31000 stainless steel was measured in the cold worked condition; its Rockwell hardness is B77 and its RRR = 1.27. The composition in weight percent for this material is: C = 0.13, Mn = 1.72, P = 0.016, S = 0.018, Si = 0.84, Cr = 24.47, Ni = 20.44, and Fe balance. Both polycrystalline copper specimens were vacuum annealed at 850°C for one hour. RRR for the UNS-C10200 copper specimen is 107. The electrical resistivity of the NBS-B stock 7 copper specimen was too low to be measured in the  $\lambda(H)$  system; however, extensive work by Fickett<sup>3</sup> on the electrical resistivity of this copper stock indicates that RRR = 1520 for heat treatments similar to that of our specimen.

## RESULTS

The effect of a magnetic field on the thermal conductivity of UNS-N07718 is shown as a function of temperature in figure 2. Data are shown only for 0 and 6366 kA/m (80 kOe) fields; curves for  $H = 796, 1592,$  and  $3183$  kA/m (10, 20, and 40 kOe respectively) fall between the two curves shown. The estimated 10% uncertainty of a single data point would indicate that the data at 0 and 6366 kA/m (80 kOe) are indistinguishable. However, the curves drawn through the data points indicate a definite trend to lower thermal conductivities at 6366 kA/m (80 kOe). The zero field data for UNS-N07718 is within 10% of the zero field data by Hust, et al.<sup>4</sup> for a similar Ni-Cr-Fe specimen.

Preliminary data for the thermal conductivity as a function of temperature for UNS-S31000 stainless steel are shown in figure 3. Again, only the 0 and 6366 kA/m (80 kOe) curves are shown.

\* The International System of Units (SI) designation for magnetic field strength is ampere per meter, and this unit is used throughout this paper. The more conventional unit of magnetic field strength, the oersted, is also given. Conversion of oersteds to amperes/meter is accomplished by multiplying oersteds by  $1000/4\pi$ .

The thermal conductivity and magnetic field effect are shown in figure 4 for UNS-C10200 copper. To my knowledge there are two other sources of zero field thermal conductivity data for similar copper in the literature. Powers, et al.<sup>5</sup> give no RRR for their specimen, which has a conductivity about 50% lower than these data at 20 K. Hust and Giarratano<sup>6</sup> find a conductivity about 90% higher than these data for a specimen whose RRR = 230. This range of results is indicative of the sensitivity of the thermal conductivity in this temperature range to trace impurities and heat treatment. Fevrier and Morize<sup>7</sup> measured the magnetothermal conductivity of two copper wires with RRR = 62 and 162 near 4 K. Our data fall generally between the curves for their two specimens as one would expect.

Data for NBS-B stock 7 copper are shown in figure 5. The experimental points at  $H = 0$  represent averages while the experimental points for  $H \neq 0$  are single data points. The extremely high conductivity at zero field is near the limit of what can be measured in the present system. Repeat runs and data averaging were used to increase the reliability of the zero field results. The source of the curve drawn through the  $H = 0$  data will be discussed later in this paper.

#### DISCUSSION

Our data indicate that a 6366 kA/m (80 kOe) magnetic field reduces the thermal conductivity of our UNS-N07718 specimen by 8% at 5.5 K and by 3% at 19.5 K. An estimate of the electronic contribution to the thermal conductivity of this alloy can be made using the Lorenz ratio ( $L = \rho\lambda/T$ ) given by Hust and Sparks,<sup>8</sup> and  $L_0 = 2.4 \times 10^{-8} \text{ V}^2/\text{K}^2$ . This estimate indicates that the electrons carry roughly 25% of the heat flow at 5 K and 18% at 19 K. The Lorenz numbers for stainless steels are typically lower than those for Ni-Cr-Fe alloys by approximately a factor of 2. This would suggest a larger electronic component in stainless steels, and consequently a larger field effect. The effect of a 6366 kA/m (80 kOe) field on the UNS-S31000 stainless steel specimen is to reduce the conductivity by 20% at 5.25 K and 11% at 19.5 K as determined at the extremes of temperature as shown in figure 3. At intermediate temperatures the field appears to have little effect on the thermal conductivity, i.e., the  $H = 0$  and  $H = 6366 \text{ kA/m}$  (80 kOe) data are the same within the stated experimental uncertainty. This behavior was unexpected and is unexplained at the present time. Further work on similar alloys should help to determine whether the observed behavior is due to some scattering phenomenon or possible experimental error.

The zero field thermal conductivity of the present data (figure 4) for UNS-C10200 copper exhibits a nearly linear decrease with decreasing temperature. This is the behavior expected for impurity scattering of electrons. The effect of the magnetic field is to reduce the thermal conductivity of our UNS-C10200 copper specimen by 45% at 6366 kA/m (80 kOe) and 19 K and by 60% at 6366 kA/m (80 kOe) and 5 K.

The very high thermal conductivity of the NBS-B stock 7 copper specimen causes experimental difficulties that result in lower accuracy in the zero field runs than was the case for the lower conductivity materials. The solid curve shown in figure 5 for  $H = 0$  was derived using the relationship<sup>9</sup>

$$1/\lambda = W = AT^n + B/T = 3.02 \times 10^{-8} T^{2.55} + 4.7 \times 10^{-4}/T. \quad (2)$$

This equation represents the experimental data within the experimental accuracy; the units of  $W$  are mK/W. The effect of a magnetic field is included in figure 5. The anomalous decrease shown in this figure for  $\lambda$  at 1592 kA/m (20 kOe) and high temperatures is probably not real; the single data point at 21 K appears to be bad, but no reason can be found to discard it. Figure 6 presents the relative change in thermal resistivity

$$\Delta W/W_{H=0} = (\lambda_{H=0} - \lambda_H)/\lambda_H \quad (3)$$

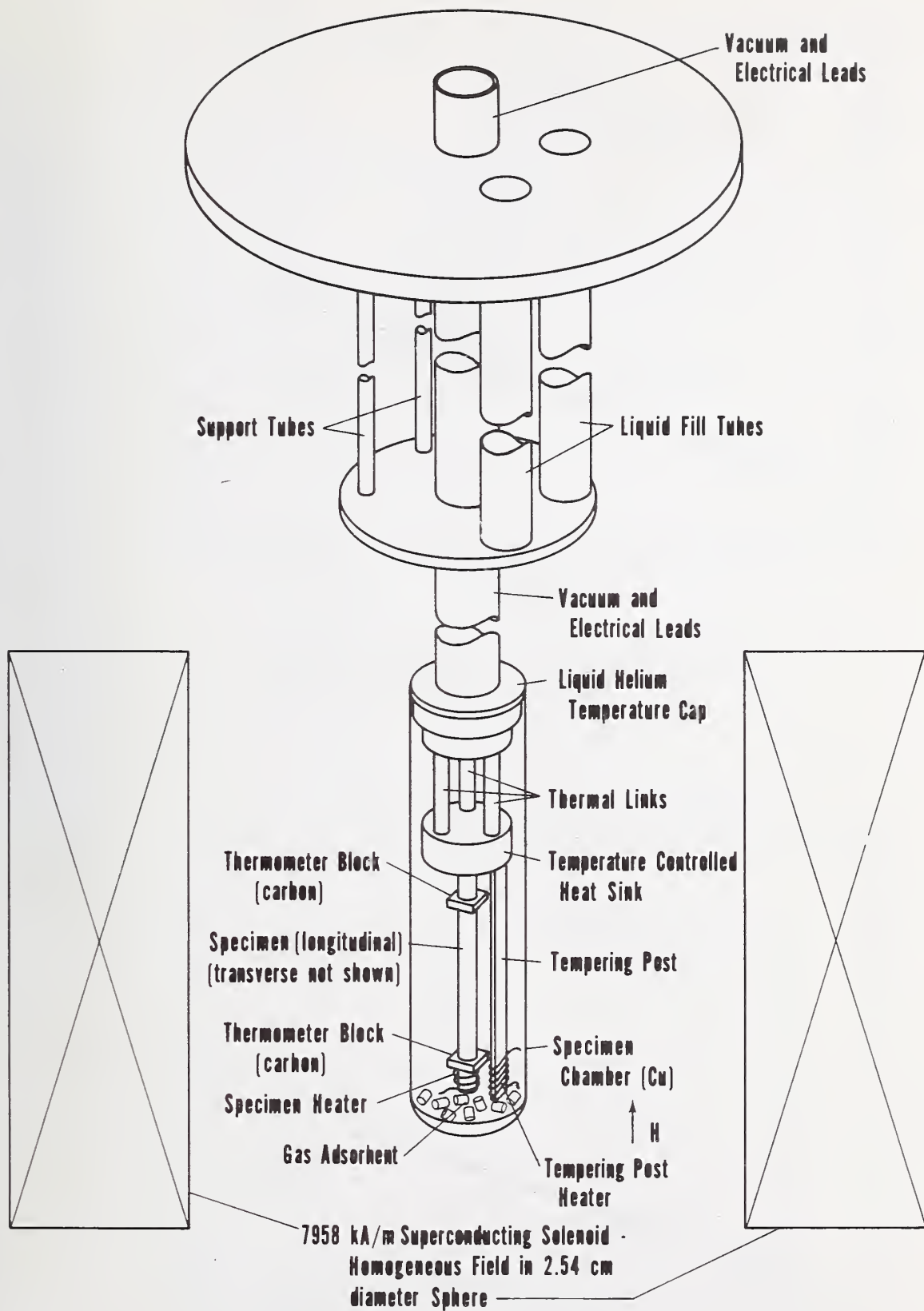
as a function of magnetic field. The high temperature, the 1592 kA/m (20 kOe) data have been ignored in this figure due to its anomalously low value.

The result is that, although the exact placement and shape of the knee is somewhat questionable, there is no doubt a rapid decrease in slope of  $\Delta W/W_{H=0}$  in the 796 to 3183 kA/m (10 to 40 kOe) range. A similar plot of  $\Delta W/W_{H=0}$  for UNS-C10200 copper is shown in figure 7; there is no rapid change in the slope of  $\Delta W/W_{H=0}$  for this material. A magnetic field should affect the electronic conductivity strongly whenever  $\omega\tau \geq 1$  where  $\omega$  is the angular frequency and  $\tau$  is the relaxation time.  $\omega$  is proportional to the magnetic field as indicated by the cyclotron relationship  $\omega = eH/mc$ . Further,  $\tau$  (high purity copper)  $>$   $\tau$  (low purity copper), so that with increasing fields  $\omega\tau$  becomes large for the high purity stock 7 copper before it does for the UNS-C10200 copper specimen; consequently, the effect of a magnetic field should be seen at lower fields for the stock 7 copper than for UNS-C10200 copper. A comparison of the data in figures 6 and 7 shows this to be the case.

In conclusion, the effect of a magnetic field on structural alloys, such as the Ni-Cr-Fe and stainless steel reported here, is relatively small. The results are not inconsistent with estimates of the possible field effects using Lorenz ratio data. Good conductors such as the two copper specimens show greater field effects which are to be expected due to the large electronic component of the thermal conductivity.

#### REFERENCES

1. L. L. Sparks and F. R. Fickett in: "Materials Research in Support of Superconducting Machinery," Nat. Bur. Stand. NBSIR-74-359 (March 1974). Available from NTIS, AD-780 596/3WM.
2. L. J. Neuringer and Y. Shapira, Rev. Sci. Instrum., 40(10): 1314 (1969).
3. F. R. Fickett, "A Preliminary Investigation of the Behavior of High Purity Copper in High Magnetic Fields," Annual Report to INCRA (August 1973).
4. J. G. Hust, D. H. Weitzel and R. L. Powell, J. Res. Nat. Bur. Stand. (U.S.), 75A(6): 269 (1971).
5. R. W. Powers, D. Schwartz and H. L. Johnston, "The Thermal Conductivity of Metals and Alloys at Low Temperatures I. Apparatus for Measurements between 25° and 300°K. Data on Pure Aluminum, OFHC Copper, and L Nickel," Ohio State University, TR 264-5 (1951).
6. J. G. Hust and P. J. Giarratano in "Materials Research in Support of Superconducting Machinery," Nat. Bur. Stand., NBSIR-74-393 (October 1974).
7. A. Fevrier and D. Morize, Cryogenics, 13: 603 (1973).
8. J. G. Hust and L. L. Sparks, Nat. Bur. Stand. (U.S.) Tech. Note 634, (February 1973).
9. H. M. Rosenberg, Low Temperature Solid State Physics, Oxford University Press, London (1963), p. 117.



76X 1969

Fig. 1. Magnetothermal conductivity probe and magnet.

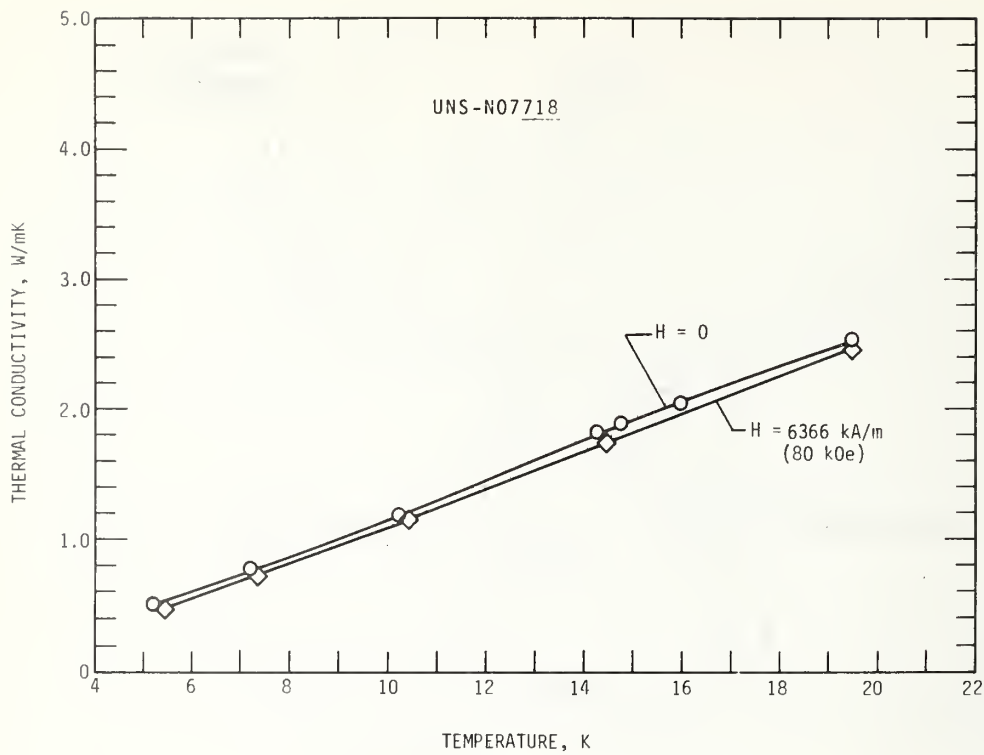


Fig. 2. Thermal conductivity of the Ni-Cr-Fe alloy UNS-N07718 as a function of temperature for H = 0 and 6366 kA/m (80 kOe).

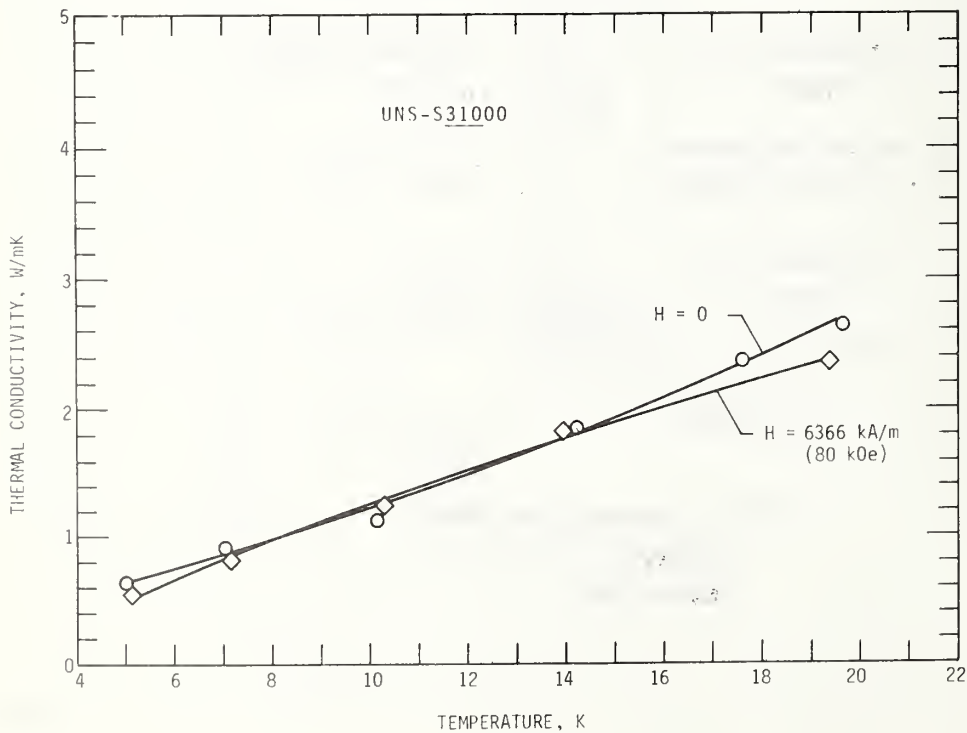


Fig. 3. Thermal conductivity of UNS-S31000 stainless steel as a function of temperature for H = 0 and 6366 kA/m (80 kOe).

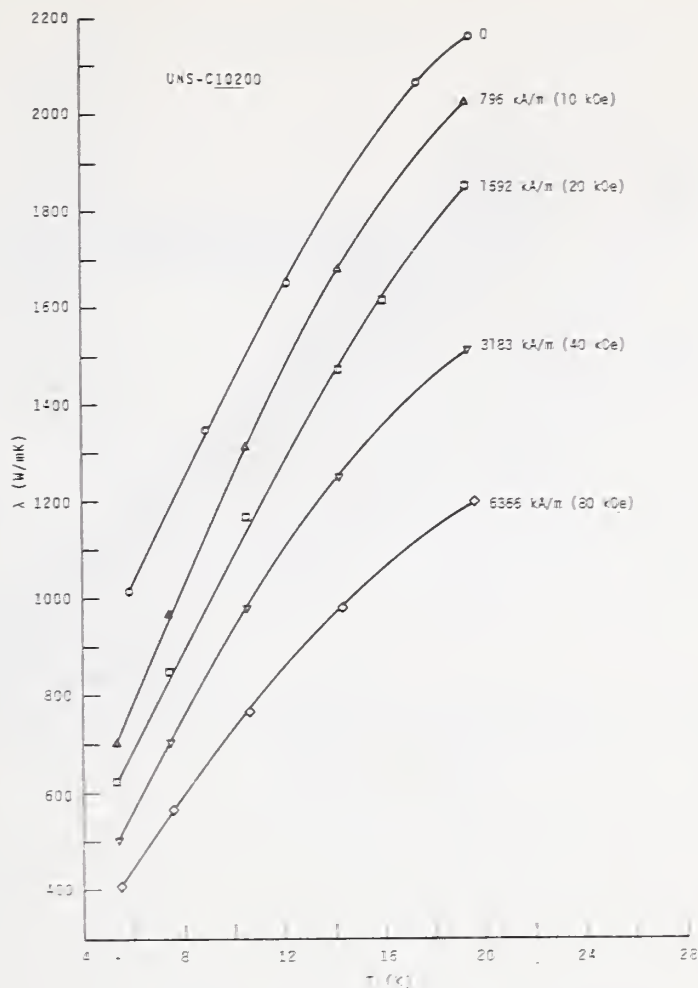


Fig. 4 Thermal conductivity of UNS-C10200 copper as a function of temperature for  $H = 0, 796, 1592, 3183, \text{ and } 6366$  kA/m (0, 10, 20, 40, and 80 kOe respectively).

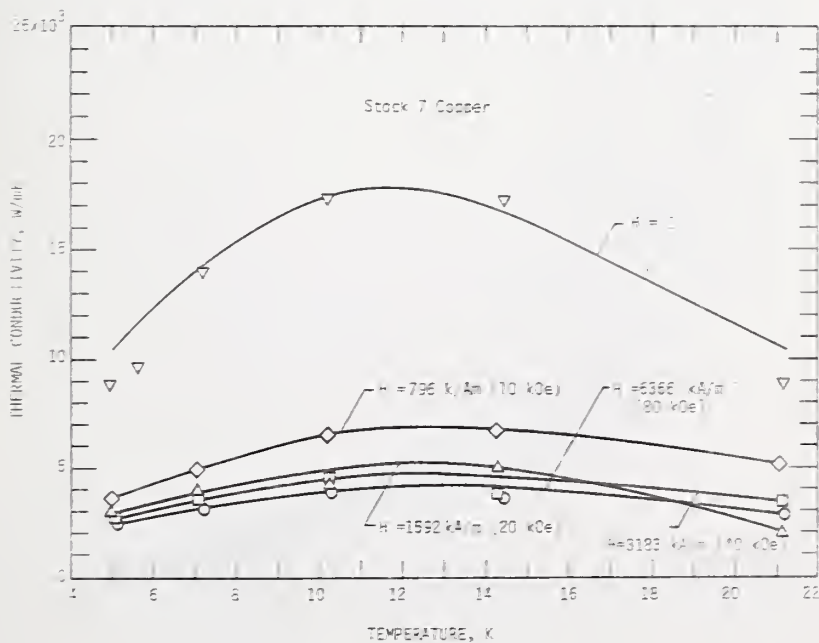


Fig. 5. Thermal conductivity of high purity copper (RRR = 1520) as a function of temperature for  $H = 0, 796, 1592, 3183, \text{ and } 6366$  kA/m (0, 10, 20, 40, and 80 kOe respectively).

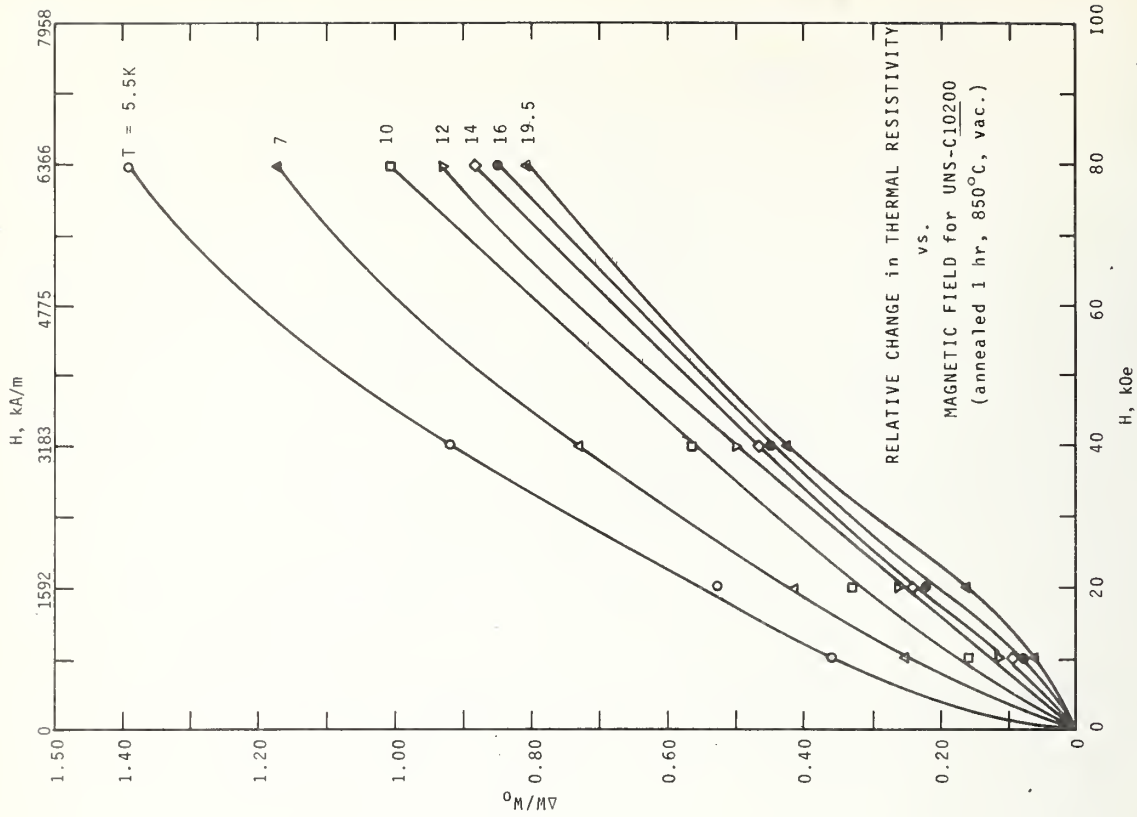


Fig. 7. Relative change in thermal resistance of UNS-C10200 copper as a function of magnetic field.

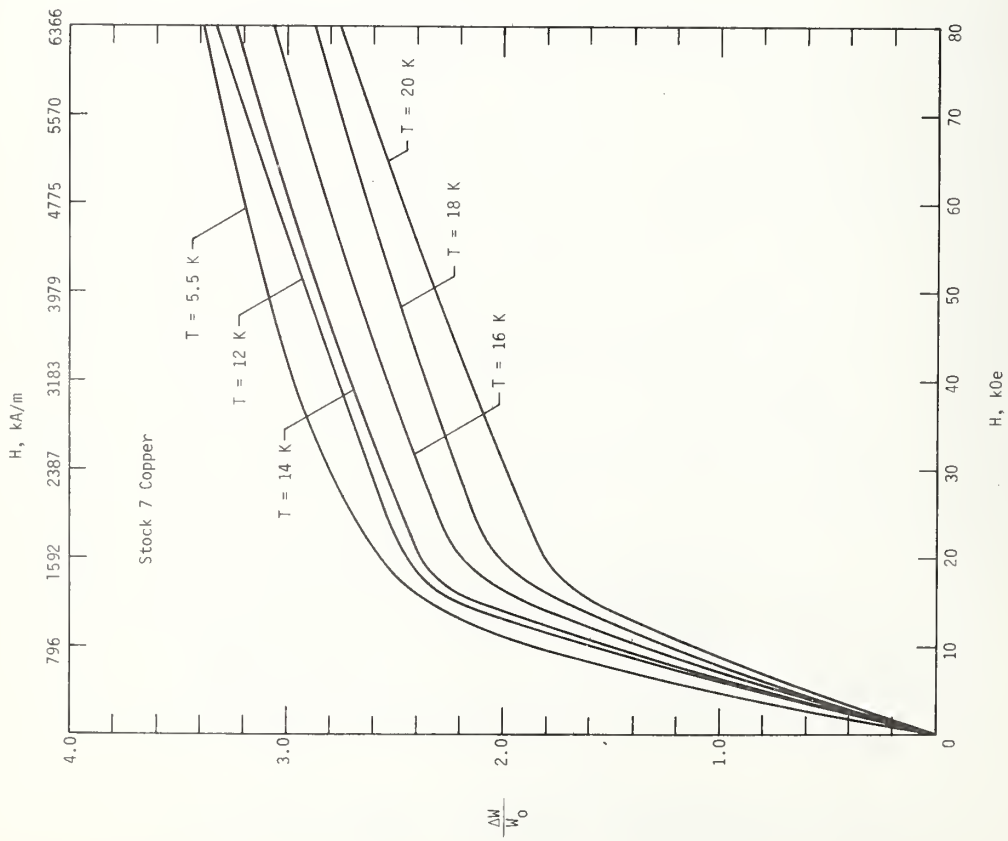


Fig. 6. Relative change in thermal resistance of high purity copper as a function of magnetic field.

NBSIR

SEMI-ANNUAL REPORT ON MATERIALS RESEARCH  
IN SUPPORT OF SUPERCONDUCTING MACHINERY

THERMAL CONDUCTIVITY

J. G. Hust

Cryogenics Division  
Institute for Basic Standards  
National Bureau of Standards  
Boulder, Colorado 80302

October 1975

Summary: Thermal Conductivity

Thermal conductivity data are reported for boron-epoxy composites. Comparisons are made with existing literature data and material variability is discussed.

# THERMAL CONDUCTIVITY

J. G. Hust

Cryogenics Division  
Institute for Basic Standards  
National Bureau of Standards  
Boulder, Colorado 80302

## 1. Introduction

At the request of Mike Jones for Watervliet Arsenal and in conjunction with the ARPA-NBS superconducting machinery program, the thermal conductivities of three specimens of boron-epoxy composite were measured. Both a transverse and a longitudinal specimen were measured using a fixed-point apparatus and a single longitudinal specimen was measured using a variable-temperature apparatus.

## 2. Apparatus and Specimen Characterization

A fixed-point thermal conductivity apparatus described by Hust [1,2] was used to measure transverse and longitudinal boron-epoxy composite specimens. The specimens were 2.54 cm in diameter and 3.56 cm in length. Thermal conductivity measurements with this apparatus are performed near the boiling point of helium (4 K) and nitrogen (76 K), the sublimation point of CO<sub>2</sub> (194 K), and the ice-point (273 K). The uncertainty of these measurements is estimated to be + 10%.

The specimens were fabricated from 5.6 mil boron-epoxy pre-impregnated tape. The boron volume fraction was about 48%. The void fraction is stated to be less than 2% by the supplier. A cursory examination of the material suggests that the void fraction is appreciably less than that.

A longitudinal specimen, with the same characteristics as above, was also measured in a variable-temperature apparatus. The specimen was 23 cm long and rectangular in cross-section (1.74 cm x 2.56 cm). The variable-temperature apparatus is designed to obtain data as a function of temperature from 4 to 300 K and is more accurate than the fixed point apparatus. This apparatus is described in detail by Hust et al. [3].

## 3. Results

Measurements were performed on a longitudinal specimen (i.e., in the direction of the boron fibers) of boron-epoxy composite at temperatures from 4 to 300 K using the variable-temperature apparatus. The experimental data are listed in table 1 and illustrated in figure 1. The following equation was least-squares fitted to these data using orthonormal fitting techniques:

$$\ln \lambda = \sum_{i=1}^n a_i [\ln T]^{i+1} \quad (1)$$

$\lambda$  is thermal conductivity in W·m<sup>-1</sup>·K<sup>-1</sup> and T is temperature in kelvin. The deviations of the experimental data from this representation are listed in table 2 and are illustrated in figure 2. The parameters obtained by least-squares fitting are listed in table 3. Tabular values of  $\lambda$  as computed from the above equation are listed in table 4 and illustrated in figure 3.

Measurements were conducted on both a longitudinal and a transverse specimen using the fixed-point apparatus. The resulting values of thermal conductivity are listed in table 5 and plotted in figure 3. The uncertainty of the smoothed data obtained with the variable-temperature apparatus is estimated at  $\pm 4\%$  and the uncertainty of the fixed-point apparatus data is estimated at  $\pm 10\%$ .

Literature data for similar composites have been compiled by Kasen [4]. These data [5,6] are included schematically in figure 3 for comparison to the data from this research. Reasonable agreement is observed between the literature data and the longitudinal specimen measured in the variable temperature apparatus and the transverse specimen. However, the longitudinal specimen measured in the fixed-point apparatus has a conductivity lower by about 50% than the other longitudinal specimen.

At ambient temperature the thermal conductivity of crystalline boron is  $20 \text{ W}\cdot\text{m}^{-1}\cdot\text{K}^{-1}$  and the thermal conductivity of epoxy is typically about  $0.2 \text{ W}\cdot\text{m}^{-1}\cdot\text{K}^{-1}$ . Since these composites are about 50% boron one would expect a conductivity near  $10 \text{ W}\cdot\text{m}^{-1}\cdot\text{K}^{-1}$  instead of  $1 - 2 \text{ W}\cdot\text{m}^{-1}\cdot\text{K}^{-1}$ . The observed results suggest the presence of strong phonon scattering in the boron fibers. These fibers are fabricated by vapor deposition of boron on a 0.5 mil diameter tungsten wire substrate. (See reference 7 for details). During the fabrication process compounds of tungsten and boron are formed at the center of the final filament and the major outer portion is reported to be pure amorphous or microcrystalline boron. The center portion has a lower thermal conductivity, but since it represents only a few percent of the cross section of the total filament, its effect on reducing conductivity can be neglected. If the outer boron portion of the filament is in a highly disordered or amorphous state, the thermal conductivity would be considerably reduced from that of crystalline boron. It is suggested in reference 7 that the boron is amorphous or microcrystalline structure with an effective crystal size of near  $20 \text{ \AA}$ . Boundary scattering of the heat carriers (phonons) from such small crystals is sufficient to reduce the thermal conductivity considerably since the phonon-phonon scattering mean free path at ambient temperature is near  $25 \text{ \AA}$ . The phonon-phonon mean free path,  $\lambda$ , is estimated from bulk boron thermal data and the classical equation  $\lambda = 1/3 C v \ell$ . It is likely that significant crystal size variations occur between different production runs of boron filaments. Thus, one would expect large batch-to-batch variations in thermal conductivity of the longitudinal specimens, which is consistent with the observed results.

In the transverse direction one can estimate the conductivity of the composite from a knowledge of the epoxy conductivity and the relative amount of epoxy present. From such considerations for this composite one obtains a value of conductivity of about 3 to 4 times greater than the conductivity of epoxy. This corresponds to  $0.6$  to  $0.8 \text{ W}\cdot\text{m}^{-1}\cdot\text{K}^{-1}$  at ambient temperature which is in reasonable agreement with the measured value of  $0.6 \text{ W}\cdot\text{m}^{-1}\cdot\text{K}^{-1}$ . Similar agreement is obtained at low temperature.

## References

1. J. G. Hust, Low temperature thermal conductivity measurements on longitudinal and transverse sections of a superconducting coil, *Cryogenics* 15, No. 1, 8-11 (1975).
2. J. G. Hust, Thermal conductivity fixed-point apparatus, NBS Laboratory Note 74-3, 9 pp. (1974).
3. J. G. Hust, R. L. Powell and D. H. Weitzel, Thermal conductivity standard reference materials from 4 to 300 K. I. Armco Iron: Including apparatus description and error analysis, *J. Res. Nat. Bur. Stand.* 74A, No. 5, 673-90 (1970).
4. M. B. Kasen, "Properties of filamentary-reinforced composites at cryogenic temperatures", *Composite Reliability*, ASTM STP 580 pp. 586-611 (1975).
5. J. Hertz, J. L. Christian and M. Varlas, "Advanced composite applications for spacecraft and missiles, Phase I final report, Volume II: Material development", AFML-TR 71-186, Vol. 2, March 1972 (AD 893 715L).
6. J. P. Gille, "Development of advanced materials for integrated tank insulation systems for long-term storage of cryogens in space", NASA CR-102 570 (Final) Sept. 1969 (N 70-23348).
7. *Modern Composite Materials*, edited by L. J. Broutman and R. H. Krock, Addison-Wesley Publishing Company, Reading, Mass. (1967).

NOTES RELATING TO TABLES

THE DATA LISTED ARE, IN PART, CARD IMAGES OF EXPERIMENTAL DATA AS READ INTO THE COMPUTER FOR DATA PROCESSING. THESE DATA ARE GENERALLY UNLABELLED. THE FOLLOWING IS A LINE BY LINE EXPLANATION OF THESE TABLES.

TABLE 1 (GRADIENT DATA)

- LINE 1- DATA IDENTIFICATION
- LINE 2- EMFS OF THERMOCOUPLES 1 THRU 8 (MICROVOLTS)
- LINE 3- PLATINUM RESISTANCE THERMOMETER CURRENT (MILLIAMPS), REFERENCE PLATINUM THERMOMETER VOLTAGE (MICROVOLTS), FLOATING SINK PLATINUM THERMOMETER VOLTAGE (MICROVOLTS), GERMANIUM THERMOMETER CURRENT (MICROAMPS), REFERENCE GERMANIUM THERMOMETER VOLTAGE (MICROVOLTS), FLOATING SINK GERMANIUM THERMOMETER (MICROVOLTS)
- LINE 4- SEEBECK EMF (MICROVOLTS), SPECIMEN VOLTAGE (MICROVOLTS), SPECIMEN CURRENT (MILLIAMPS), SPECIMEN HEATER VOLTAGE (VOLTS), SPECIMEN HEATER CURRENT (MILLIAMPS), CRYOGENIC BATH PRESSURE (MM OF HG), ROOM TEMPERATURE (DEGREES C), CRYOGENIC BATH CODE (1=LIQUID HELIUM, 2=LIQUID HYDROGEN, 3=LIQUID NITROGEN, 4=DRY ICE-ALCOHOL, 5=ICE WATER)

TABLE 2

THESE DATA ARE SEMI-PROCESSED COMPUTER OUTPUT. TEMPERATURE IS KELVIN, THERMAL CONDUCTIVITY IS IN WATTS PER METER PER KELVIN, ELECTRICAL RESISTANCE IS IN OHMS, AND THERMOVOLTAGE IS IN MICROVOLTS.

BORON-EPOXY (L1)

NUMBER OF CALIBRATION, ISOTHERMAL, AND GRADIENT RUNS, AND THERMOCOUPLES

66            -0            11            8

THERMOCOUPLE POSITIONS (CM)

0.0000    2.5400    5.0800    7.6200    10.1600    12.7000    15.2400    17.7800

SPECIMEN DIAMETERS BETWEEN THERMOCOUPLES (CM)

2.3815    2.3815    2.3815    2.3815    2.3815    2.3315    2.3815

TABLE 1. BASIC SEMI-PROCESSED TEMPERATURE GRADIENT DATA FOR BORON-EPOXY (L1)

THERMAL CONDUCTIVITY DATA FOR B-EPOXY(L1)								20MAY 75 1545	11
11.64	20.80	28.70	35.79	41.99	48.22	53.75	58.72		
2.0005	34.80	25.78	9.9880	9657.50	7598.50				
-0.00	-0.00	-0.00	.6740	3.3230	632.7	24.0	1.0		
REFERENCE TEMP		FLOATING SINK TEMP		SPECIMEN		HEATER			
PRT	GRT	PRT	GRT	RESISTANCE		POWER			
0.000	4.158	0.000	4.652	0.		.22431E-02			
THERMAL CONDUCTIVITY DATA FOR B-EPOXY(L1)								20MAY 75 1620	12
45.03	66.97	85.00	101.14	115.12	128.43	140.57	151.52		
-0.0000	-0.00	-0.00	9.9880	9505.50	4429.80				
-0.00	-0.00	-0.00	1.3560	6.6972	632.7	24.0	1.0		
REFERENCE TEMP		FLOATING SINK TEMP		SPECIMEN		HEATER			
PRT	GRT	PRT	GRT	RESISTANCE		POWER			
0.000	4.194	0.000	6.172	0.		.90814E-02			
THERMAL CONDUCTIVITY DATA FOR B-EPOXY(L1)								20MAY 75 1715	13
127.92	167.36	200.18	230.12	256.23	280.88	303.32	324.92		
2.0010	34.70	40.16	9.9880	9113.00	1529.50				
-0.00	-0.00	-0.00	2.4880	12.2820	635.0	24.0	1.0		
REFERENCE TEMP		FLOATING SINK TEMP		SPECIMEN		HEATER			
PRT	GRT	PRT	GRT	RESISTANCE		POWER			
0.000	4.289	0.000	10.313	0.		.30554E-01			
THERMAL CONDUCTIVITY DATA FOR B-EPOXY(L1)								20MAY 75 1740	14
265.04	340.28	403.64	463.67	517.90	569.72	620.66	669.33		
2.0010	34.6E	104.94	9.9880	8470.00	654.80				
-0.00	-0.00	-0.00	4.5140	22.2550	635.0	24.0	1.0		
REFERENCE TEMP		FLOATING SINK TEMP		SPECIMEN		HEATER			
PRT	GRT	PRT	GRT	RESISTANCE		POWER			
0.000	4.460	16.007	15.931	0.		.10046E+00			
THERMAL CONDUCTIVITY DATA FOR B-EPOXY(L1)								20MAY 75 1945	15
698.97	751.82	802.25	856.47	907.42	958.15	1010.30	1062.44		
2.0000	-0.00	2743.50	9.9880	7350.00	136.18				
-0.00	-0.00	-0.00	4.6560	22.9280	635.0	24.0	1.0		
REFERENCE TEMP		FLOATING SINK TEMP		SPECIMEN		HEATER			
PRT	GRT	PRT	GRT	RESISTANCE		POWER			
0.000	4.810	43.339	0.000	0.		.10670E+00			
THERMAL CONDUCTIVITY DATA FOR B-EPOXY(L1)								17 MAY 75 2215	7
113.31	163.22	211.24	262.72	312.72	361.91	413.10	461.69		
2.0020	9287.00	10280.00	-0.0000	-0.00	-0.00				
-0.00	-0.00	-0.00	4.3020	21.2100	633.5	25.0	3.0		
REFERENCE TEMP		FLOATING SINK TEMP		SPECIMEN		HEATER			
PRT	GRT	PRT	GRT	RESISTANCE		POWER			
75.905	0.000	80.332	0.000	0.		.91245E-01			

TABLE 1. (CONTINUED)

THERMAL CONDUCTIVITY DATA FOR B-EPOXY(L1) 20MAY 75 1040								10
1296.88	1464.36	1624.10	1797.40	1963.96	2124.40	2293.26	2450.64	
2.0010	9318.00	23035.00	-0.0000	-0.00	-0.00			
-0.00	-0.00	-0.00	7.2740	35.7000	634.5	23.8	3.0	
REFERENCE TEMP		FLOATING SINK TEMP		SPECIMEN		HEATER		
PRT	GRT	PRT	GRT	RESISTANCE		POWER		
76.067	0.000	138.550	0.000	0.		.25968E+00		
-----								
THERMAL CONDUCTIVITY DATA FOR B-EPOXY(L1) 18 MAY 75 1155								8
348.66	468.54	584.84	712.57	835.65	956.94	1083.82	1203.94	
2.0000	9290.20	12589.00	-0.0000	-0.00	-0.00			
-0.00	-0.00	-0.00	6.5260	32.0900	633.7	25.5	3.0	
REFERENCE TEMP		FLOATING SINK TEMP		SPECIMEN		HEATER		
PRT	GRT	PRT	GRT	RESISTANCE		POWER		
75.962	0.000	90.790	0.000	0.		.20942E+00		
-----								
THERMAL CONDUCTIVITY DATA FOR B-EPOXY(L1) 14 MAY 75 1345								3
126.50	195.80	263.20	334.80	403.80	469.70	537.00	600.20	
2.0025	34565.00	35520.00	-0.0000	-0.00	-0.00			
-0.00	-0.00	-0.00	4.5540	22.3600	-0.0	23.0	4.0	
REFERENCE TEMP		FLOATING SINK TEMP		SPECIMEN		HEATER		
PRT	GRT	PRT	GRT	RESISTANCE		POWER		
193.251	0.000	197.391	0.000	0.		.10183E+00		
-----								
THERMAL CONDUCTIVITY DATA FOR B-EPOXY(L1) 15 MAY 75 2140								5
591.89	776.83	956.91	1149.69	1335.47	1511.59	1692.39	1859.22	
2.0010	34720.00	39595.00	-0.0000	-0.00	-0.00			
-0.00	-0.00	-0.00	7.4000	36.3000	-0.0	23.0	4.0	
REFERENCE TEMP		FLOATING SINK TEMP		SPECIMEN		HEATER		
PRT	GRT	PRT	GRT	RESISTANCE		POWER		
194.118	0.000	217.087	0.000	0.		.26862E+00		
-----								
THERMAL CONDUCTIVITY DATA FOR B-EPOXY(L1) 7 MAY 75 835								1
48.78	102.73	153.90	208.29	260.50	310.31	360.70	407.00	
2.0000	51010.00	51420.00	-0.0000	-0.00	-0.00			
-0.00	-0.00	-0.00	3.9068	18.9450	-0.0	-0.0	5.0	
REFERENCE TEMP		FLOATING SINK TEMP		SPECIMEN		HEATER		
PRT	GRT	PRT	GRT	RESISTANCE		POWER		
273.474	0.000	274.735	0.000	0.		.74014E-01		
-----								

TABLE 2 THERMAL CONDUCTIVITY DEVIATIONS FOR BORON-EXY (L1)

THERMAL CONDUCTIVITY DATA FOR B-EPOXY(L1) 20MAY 75 1545					11
MEAN TEMPERATURE	TEMPERATURE DIFFERENCE	OBSERVED THERMAL CONDUCTIVITY	CALCULATED THERMAL CONDUCTIVITY	PERCENT DEVIATION	
5.522	.678	.189E+00	.191E+00	-1.1	
6.133	.546	.234E+00	.230E+00	1.9	
6.654	.495	.258E+00	.265E+00	-2.7	
7.112	.421	.304E+00	.297E+00	2.3	
7.518	.390	.328E+00	.325E+00	.9	
7.898	.370	.345E+00	.352E+00	-1.9	
8.243	.320	.400E+00	.376E+00	6.0	
-----					
THERMAL CONDUCTIVITY DATA FOR B-EPOXY(L1) 20MAY 75 1620					12
MEAN TEMPERATURE	TEMPERATURE DIFFERENCE	OBSERVED THERMAL CONDUCTIVITY	CALCULATED THERMAL CONDUCTIVITY	PERCENT DEVIATION	
8.240	1.417	.365E+00	.376E+00	-2.9	
9.510	1.122	.461E+00	.466E+00	-1.0	
10.576	1.009	.513E+00	.541E+00	-5.5	
11.506	.853	.607E+00	.607E+00	.1	
12.319	.773	.670E+00	.663E+00	1.0	
13.071	.731	.709E+00	.715E+00	-.9	
13.758	.644	.805E+00	.762E+00	5.3	
-----					
THERMAL CONDUCTIVITY DATA FOR B-EPOXY(L1) 20MAY 75 1715					13
MEAN TEMPERATURE	TEMPERATURE DIFFERENCE	OBSERVED THERMAL CONDUCTIVITY	CALCULATED THERMAL CONDUCTIVITY	PERCENT DEVIATION	
13.836	2.322	.750E+00	.771E+00	-2.7	
15.994	1.893	.920E+00	.912E+00	.9	
17.812	1.743	.999E+00	.103E+01	-2.9	
19.443	1.520	.115E+01	.113E+01	1.5	
20.904	1.401	.124E+01	.122E+01	2.2	
22.276	1.344	.130E+01	.129E+01	.3	
23.564	1.232	.141E+01	.136E+01	3.8	
-----					

TABLE 2 (CONTINUED)

THERMAL CONDUCTIVITY DATA FOR B-EPOXY(L1) 20MAY 75 1740					14
MEAN TEMPERATURE	TEMPERATURE DIFFERENCE	OBSERVED THERMAL CONDUCTIVITY	CALCULATED THERMAL CONDUCTIVITY	PERCENT DEVIATION	
22.996	4.390	.130E+01	.133E+01	-2.1	
27.058	3.734	.153E+01	.153E+01	.4	
30.714	3.578	.160E+01	.167E+01	-4.5	
34.132	3.257	.176E+01	.178E+01	-1.2	
37.304	3.088	.186E+01	.186E+01	-.2	
40.374	3.051	.188E+01	.192E+01	-2.1	
43.349	2.900	.198E+01	.196E+01	.8	
-----					
THERMAL CONDUCTIVITY DATA FOR B-EPOXY(L1) 20MAY 75 1945					15
MEAN TEMPERATURE	TEMPERATURE DIFFERENCE	OBSERVED THERMAL CONDUCTIVITY	CALCULATED THERMAL CONDUCTIVITY	PERCENT DEVIATION	
47.792	3.007	.202E+01	.200E+01	1.1	
50.825	3.058	.199E+01	.202E+01	-1.5	
53.739	2.771	.220E+01	.203E+01	7.6	
56.667	3.085	.197E+01	.204E+01	-3.2	
59.783	3.146	.193E+01	.204E+01	-5.3	
62.793	2.873	.212E+01	.203E+01	4.0	
65.688	2.918	.209E+01	.203E+01	2.7	
-----					
THERMAL CONDUCTIVITY DATA FOR B-EPOXY(L1) 17 MAY 75 2215					7
MEAN TEMPERATURE	TEMPERATURE DIFFERENCE	OBSERVED THERMAL CONDUCTIVITY	CALCULATED THERMAL CONDUCTIVITY	PERCENT DEVIATION	
83.469	2.702	.193E+01	.198E+01	-2.9	
86.118	2.595	.200E+01	.197E+01	1.5	
88.785	2.739	.190E+01	.197E+01	-3.6	
91.488	2.667	.195E+01	.196E+01	-.5	
94.126	2.610	.199E+01	.195E+01	2.0	
96.777	2.691	.193E+01	.195E+01	-.8	
99.393	2.542	.205E+01	.194E+01	5.1	
-----					

TABLE 2 (CONTINUED)

THERMAL CONDUCTIVITY DATA FOR B-EPOXY(L1) 20MAY 75 1040					10
MEAN TEMPERATURE	TEMPERATURE DIFFERENCE	OBSERVED THERMAL CONDUCTIVITY	CALCULATED THERMAL CONDUCTIVITY	PERCENT DEVIATION	
147.398	8.133	.182E+01	.189E+01	-4.0	
155.381	7.833	.189E+01	.189E+01	.1	
163.386	8.176	.181E+01	.189E+01	-4.1	
171.445	7.942	.186E+01	.188E+01	-.9	
179.281	7.731	.192E+01	.188E+01	2.0	
187.100	7.907	.187E+01	.187E+01	.0	
194.710	7.313	.202E+01	.187E+01	7.8	
-----					
THERMAL CONDUCTIVITY DATA FOR B-EPOXY(L1) 18 MAY 75 1155					8
MEAN TEMPERATURE	TEMPERATURE DIFFERENCE	OBSERVED THERMAL CONDUCTIVITY	CALCULATED THERMAL CONDUCTIVITY	PERCENT DEVIATION	
97.938	6.300	.190E+01	.195E+01	-2.6	
104.188	6.079	.196E+01	.193E+01	1.6	
110.488	6.522	.183E+01	.192E+01	-5.0	
116.885	6.272	.190E+01	.191E+01	-.6	
123.090	6.139	.195E+01	.191E+01	1.9	
129.324	6.330	.189E+01	.190E+01	-.9	
135.464	5.950	.201E+01	.190E+01	5.4	
-----					
THERMAL CONDUCTIVITY DATA FOR B-EPOXY(L1) 14 MAY 75 1345					3
MEAN TEMPERATURE	TEMPERATURE DIFFERENCE	OBSERVED THERMAL CONDUCTIVITY	CALCULATED THERMAL CONDUCTIVITY	PERCENT DEVIATION	
200.766	3.206	.181E+01	.186E+01	-2.9	
203.936	3.134	.185E+01	.186E+01	-.5	
207.164	3.321	.175E+01	.186E+01	-6.4	
210.412	3.175	.183E+01	.186E+01	-1.6	
213.525	3.050	.190E+01	.186E+01	2.3	
216.593	3.086	.188E+01	.185E+01	1.5	
219.583	2.895	.201E+01	.185E+01	7.7	
-----					

TABLE 2. (CONTINUED)

THERMAL CONDUCTIVITY DATA FOR B-EPOXY(L1) 15 MAY 75 2140					5
MEAN TEMPERATURE	TEMPERATURE DIFFERENCE	OBSERVED THERMAL CONDUCTIVITY	CALCULATED THERMAL CONDUCTIVITY	PERCENT DEVIATION	
225.745	8.433	.182E+01	.185E+01	-1.8	
234.104	8.285	.185E+01	.185E+01	.2	
242.656	8.819	.174E+01	.184E+01	-6.2	
251.275	8.418	.182E+01	.184E+01	-1.3	
259.512	8.056	.190E+01	.185E+01	2.9	
267.609	8.139	.188E+01	.185E+01	1.5	
275.382	7.407	.207E+01	.186E+01	10.0	
-----					
THERMAL CONDUCTIVITY DATA FOR B-EPOXY(L1) 7 MAY 75 835					1
MEAN TEMPERATURE	TEMPERATURE DIFFERENCE	OBSERVED THERMAL CONDUCTIVITY	CALCULATED THERMAL CONDUCTIVITY	PERCENT DEVIATION	
276.882	2.414	.175E+01	.186E+01	-6.7	
279.237	2.295	.184E+01	.187E+01	-1.6	
281.612	2.455	.172E+01	.187E+01	-8.9	
284.005	2.332	.181E+01	.188E+01	-3.7	
286.287	2.232	.189E+01	.189E+01	.5	
288.533	2.260	.187E+01	.189E+01	-1.0	
290.687	2.049	.206E+01	.189E+01	8.1	

TABLE 3. Parameters in equation 1 for a longitudinal boron-epoxy composite specimen

i	$a_i$
1	-17.065713
2	29.019209
3	-21.740071
4	9.1816220
5	- 2.3311507
6	0.35284329
7	- 0.029346836
8	0.001032607

TABLE 4. Thermal conductivity values of a longitudinal boron-epoxy composite specimen as calculated from equation 1

T (K)	$\lambda$ (W·m <sup>-1</sup> ·K <sup>-1</sup> )	T (K)	$\lambda$ (W·m <sup>-1</sup> ·K <sup>-1</sup> )
6	0.221	60	2.04
7	0.289	70	2.02
8	0.359	80	1.99
9	0.430	90	1.96
10	0.501	100	1.94
12	0.641	120	1.91
14	0.779	140	1.90
16	0.912	160	1.89
18	1.04	180	1.88
20	1.16	200	1.86
25	1.43	220	1.85
30	1.65	240	1.84
35	1.80	260	1.85
40	1.91	280	1.87
45	1.98		
50	2.02		

TABLE 5. Thermal conductivity values of a transverse and a longitudinal boron-epoxy composite specimen as measured using the fixed-point apparatus

T (K)	$\lambda$ (W·m <sup>-1</sup> ·K <sup>-1</sup> )	
7.83	0.178	} Longitudinal Specimen
82.0	0.913	
196	1.11	
280	1.02	
14.7	0.174	} Transverse Specimen
86.7	0.466	
200	0.553	
280	0.581	

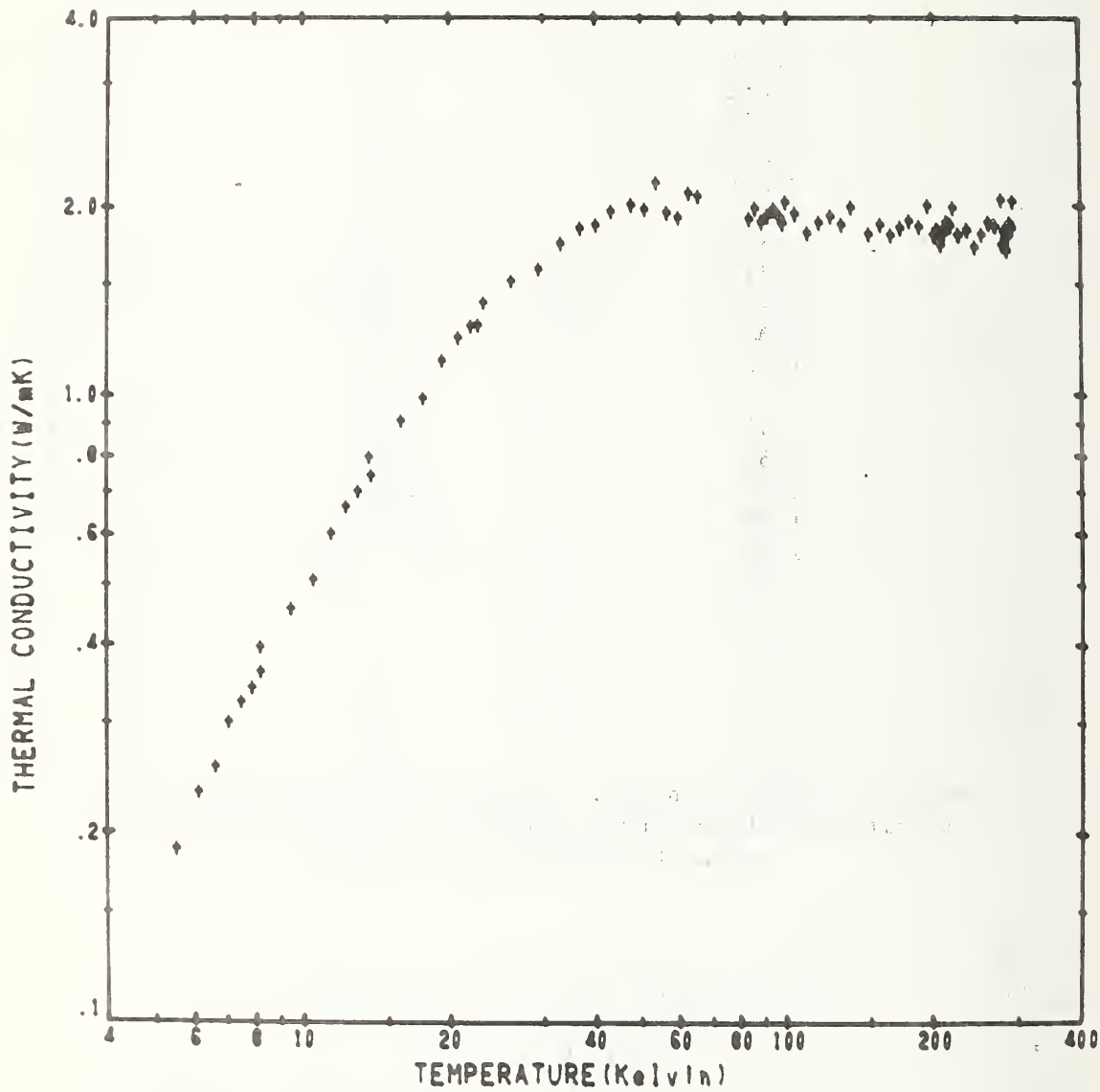


Figure 1 - Experimental data on longitudinal boron-epoxy composite specimen.

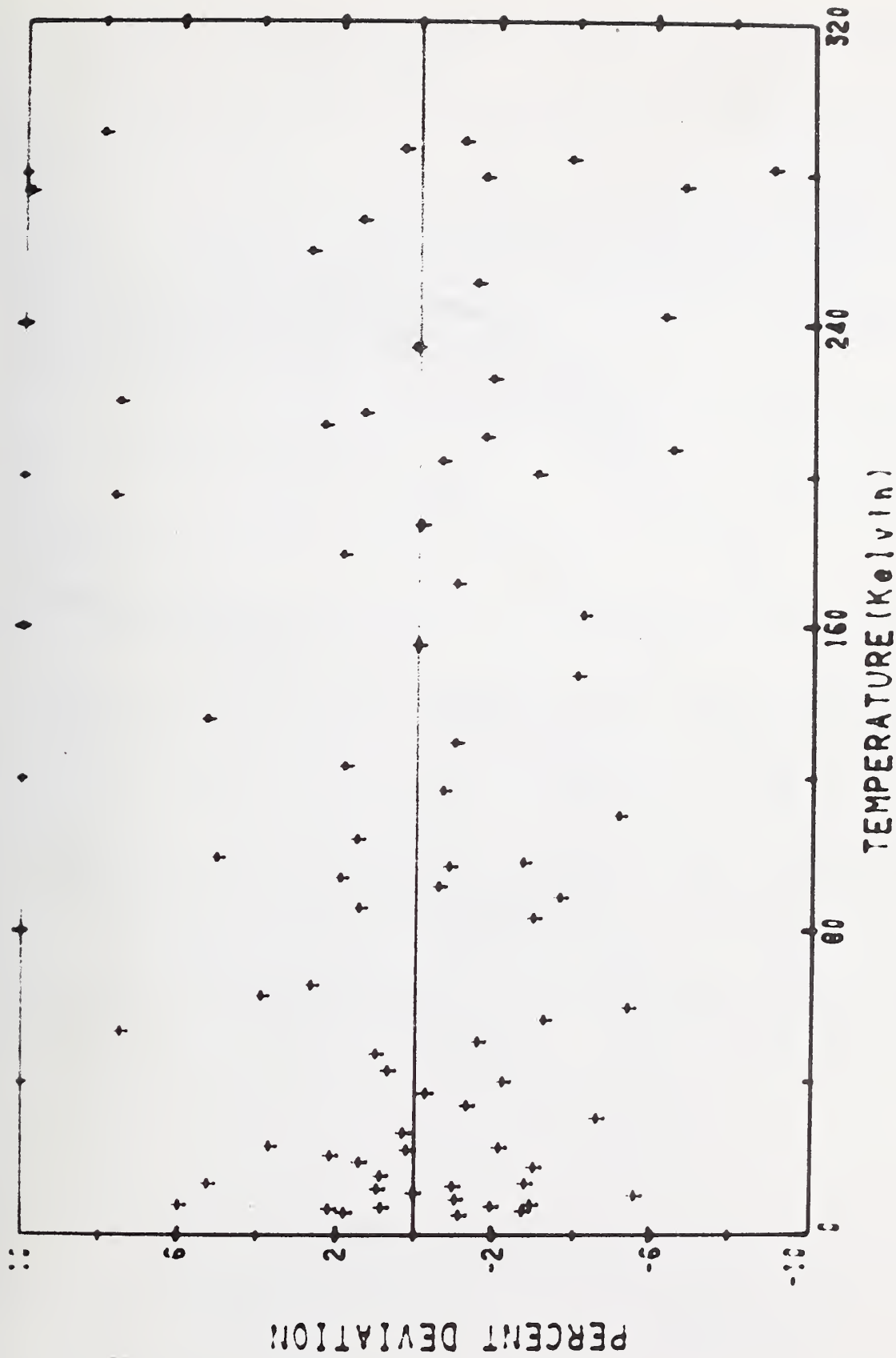


Figure 2 - Thermal conductivity deviations of experimental data from equation 1 for boron-epoxy composite.

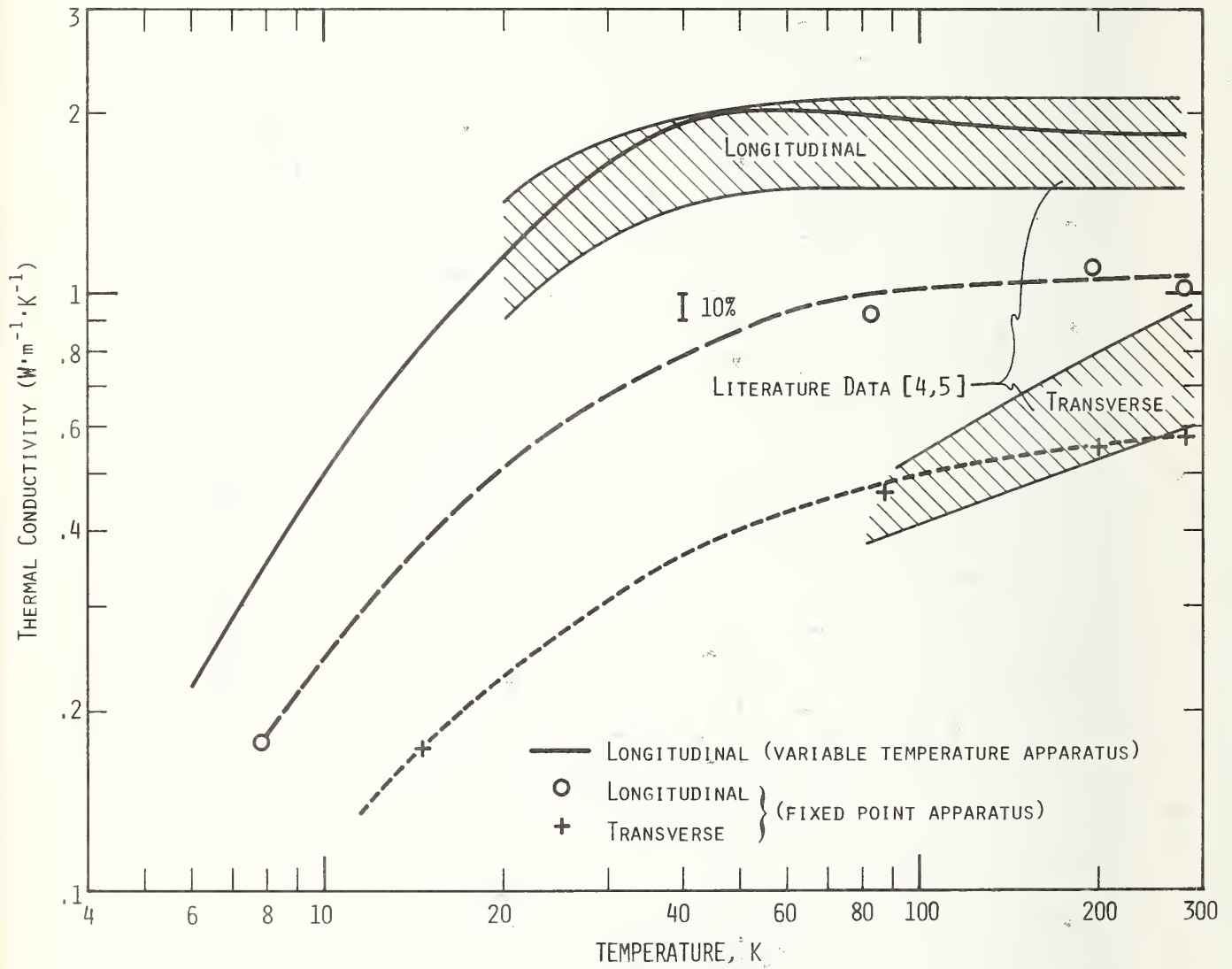


FIGURE 3 - Thermal conductivity of longitudinal and transverse boron-epoxy composite specimens.

U.S. DEPT. OF COMM. BIBLIOGRAPHIC DATA SHEET	1. PUBLICATION OR REPORT NO. NBSIR 75-828	2. Gov't Accession No.	3. Recipient's Accession No.
4. TITLE AND SUBTITLE Semi-Annual Report on Materials Research in Support of Superconducting Machinery		5. Publication Date January 1976 6. Performing Organization Code 275.03	
7. AUTHOR(S) R. P. Reed, J. G. Hust, M. B. Kasen, H. M. Ledbetter, E. R. Naimon, D. T. Read, R. E. Schramm, L. L. Sparks, R. L.		8. Performing Organ. Report No. NBSIR 75-828	
9. PERFORMING ORGANIZATION NAME AND ADDRESS NATIONAL BUREAU OF STANDARDS DEPARTMENT OF COMMERCE WASHINGTON, D.C. 20234		10. Project/Task/Work Unit No. 2756530 11. Contract/Grant No.	
12. Sponsoring Organization Name and Complete Address (Street, City, State, ZIP) Advanced Research Projects Agency (ARPA) 1400 Wilson Boulevard Arlington, Virginia 22209		13. Type of Report & Period Covered Interim April - September 1975 14. Sponsoring Agency Code	
15. SUPPLEMENTARY NOTES			
16. ABSTRACT (A 200-word or less factual summary of most significant information. If document includes a significant bibliography or literature survey, mention it here.)  Results are reported of a six-month study, March through August 1975, on candidate materials for superconducting machinery. The results cover five areas--advanced composites, elastic properties, fatigue resistance and fracture toughness, magnetothermal conductivity, and thermal conductivity. Material properties were studied over the temperature range 4 to 300 K. Materials studied include: oxygen-free copper; copper-nickel alloys; a precipitation-hardening copper alloy; invar; nickel-chromium-iron alloys; stainless steels; and the composite materials boron/aluminum, boron/epoxy, S-glass/epoxy, graphite/epoxy, and an organic-fiber/epoxy. Some notable results of the study are: the first 4 K fatigue data on a composite material; a ten-fold increase in the fatigue life of a uniaxial glass/epoxy composite between room temperature and liquid-helium temperature; the first 4 K fatigue fracture toughness studies on a nitrogen-strengthened chromium-nickel-manganese steel, which show this material has higher yield strength and adequate toughness compared to conventional stainless steels; room-temperature elastic properties of a copper-cadmium-chromium precipitation-hardening alloy, which are quite different from those of unalloyed copper and show a non-parallel behavior of the shear modulus and the bulk modulus; the thermal conductivity of 304 stainless steel may be reduced one third at 4 K by a 6 MA/m (80 kOe) magnetic field; the first systematic study of the tensile properties of fiber-reinforced composite materials between room temperature and liquid-helium temperature.  This work was supported by the Advanced Research Projects Agency of the U.S. Department of Defense.			
17. KEY WORDS (six to twelve entries; alphabetical order; capitalize only the first letter of the first key word unless a proper name; separated by semicolons) Composites; copper alloys; elastic properties; engineering materials; fatigue; fracture; iron alloys; cryogenic temperatures; mechanical properties; nickel alloys; superconducting machinery; thermal conductivity.			
18. AVAILABILITY <input checked="" type="checkbox"/> Unlimited  <input type="checkbox"/> For Official Distribution. Do Not Release to NTIS  <input type="checkbox"/> Order From Sup. of Doc., U.S. Government Printing Office Washington, D.C. 20402, SD Cat. No. C13  <input checked="" type="checkbox"/> Order From National Technical Information Service (NTIS) Springfield, Virginia 22151		19. SECURITY CLASS (THIS REPORT)  UNCLASSIFIED	21. NO. OF PAGES  193
		20. SECURITY CLASS (THIS PAGE)  UNCLASSIFIED	22. Price  \$7.00

